

Nanomaterials for antibacterial and tissue regeneration applications

A Thesis Submitted

In partial Fulfillment of the Requirements for the Degree of

DOCTOR OF PHILOSOPHY

by

Nahida Rasool

Entry No. 2017BMZ0007



to

**DEPARTMENT OF BIOMEDICAL ENGINEERING
INDIAN INSTITUTE OF TECHNOLOGY ROPAR**

Rupnagar

May 2024

Dedicated

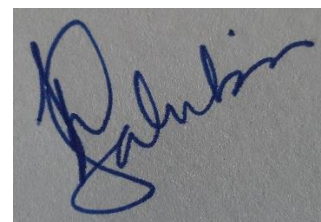
to

my

parents

Declaration of originality

I hereby declare that the work, which is being presented in the thesis, entitled “*Nanomaterials for antibacterial and tissue regeneration applications*”, has been solely authored by me. It presents the result of my own independent investigation/research conducted during the time period from January 2018 to February 2024 under the supervision of Dr. Yashveer Singh, Associate Faculty, Department of Biomedical Engineering, IIT Ropar, Rupnagar. To the best of my knowledge, it is an original work, both in terms of research content and narrative, and has not been submitted or accepted elsewhere, in parts or in full, for the award of any degree, diploma, fellowship, associateship, or similar title of any university or institution. Further, due credit has been attributed to the relevant state-of-the-art and collaborations with appropriate citations and acknowledgments, in line with the established ethical norms and practices. I also declare that any idea/data/fact/source stated in my thesis has not been fabricated/ falsified/ misrepresented. All the principles of academic honesty and integrity have been followed. I fully understand that if the thesis is found to be unoriginal, fabricated, or plagiarized, the institute reserves the right to withdraw the thesis from its archive and revoke the associated degree conferred. Additionally, the institute also reserves the right to appraise all concerned sections of the society of the matter for their information and necessary action. If accepted, I hereby consent for my thesis to be made available online in the Institute’s Open Access Repository, inter-library loan, and the title and abstract to be made available to outside organizations.



Signature

Name: Nahida Rasool

Entry Number: 2017BMZ0007

Program: PhD

Department: Biomedical Engineering

Indian Institute of Technology Ropar

Rupnagar, Punjab 140001

Date: 31-05-2024

Acknowledgments

They say research work is a team work, and no researcher can achieve his/her goals independently. This journey to success takes efforts of so many people at personal/ professional level. The completion of this work has been possible with the grace and divine help of Almighty Lord- I praise, glorify the Lord of Heavens, the Ever-Merciful for everything. He bestowed upon me His showering mercy. On the worldly side, I am extremely grateful to my PhD supervisor, **Dr. Yashveer Singh**, for providing me full support/opportunity to dwell in research world. Thank you, Sir, for pushing me out of comfort zone, having faith in me when I gave up on myself. I am immensely grateful for the patience showed with me, understanding my problems, and boosting my confidence. Your insightful feedback, constructive criticism, and scientific temperament was the driving force behind my humble progress in research. It is worthwhile to mention here that your style of supervision, and your great sense of sarcasm groomed a strong personality and independent researcher in me, with excellent sense of ethics. I feel privileged to be the part of your lab and being your student.

I offer sincerest gratitude to my Doctoral Committee members, **Dr. Srivatsava Naidu**, **Dr. Nagaraja C. M.**, **Dr. Durba Pal**, and **Dr. Puneet Goyal**, for timely monitoring the research progress, providing valuable suggestions, and their generous support towards me. I am thankful and have profound sense of regard to **Dr. Rajendra Srivastava** for always providing his expert opinion regarding material part. With the interdisciplinary nature of my research area, I was actively taking help for both instrumental and scientific advice from various labs, with special acknowledgement to **Prof. J. N. Agrewala** who provided me the access to his lab facilities. I am thankful to the Department for Biomedical Engineering and Department of Chemistry for providing generous access to the research facilities.

I would also like to acknowledge the past and present members of the lab for their support and motivation throughout this journey and providing a friendly environment at the workplace. I would like to thank Dr. Kamal Malhotra, Dr. Peeyush Sharma and Dr. Neelam Chauhan for insightful discussions and valuable feedback. In the overwhelming and competitive environment of research institute, it was a company of few that kept me sane and genuine- the mere presence of Dr. Aroof Aimen, Dr. Moumita Halder, and Dr. Irshad Majid was enough to strengthen me and face the personal and professional challenges. This thesis would have never seen the light of the day without the constant support of Deepa and Yashika. I would like to extend my deepest appreciation to my lab mates Soumyajit, Vatan, Prithviraj, Gurpreet, and friends including Dr. Sheetanshu Saproo, Dr. Rajesh Das, Dr. Sidhanta, Jaffar Abbas, Neha Mehani, and Bhavya for scientific and personal support, A heartfelt thanks to the likes of Bhavya, Ganesh, Dr. Debarun, Dr. Adeel Zafar, Dr. Sandeep Singh Dhankar, Dr. Rekha Dhiman, and Dr. Suman Dhingra.

At last, no amounts of words can express my gratitude to my family, my papa and mama for all the blessings and sacrifices you made on my behalf, my dearest husband Dr. Mir Zain, my beloved brothers Dr. Rahi Akhter Rasool and Sahil Sidheekh for being the pillars of faith and love and

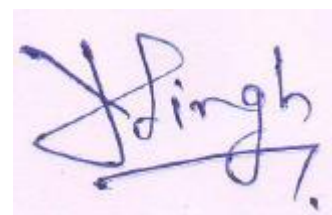
courage for me. A special mention to my darling son, Muhammad Humzah whose smile is enough to lighten my world.

Finally, I would like to acknowledge the financial assistance from the **Department of Biotechnology India** (grant # BT/PR40669/MED/32/761/2020) to my PhD supervisor and **IIT Ropar, Rupnagar** for the institute fellowship to me.

Certificate

This is to certify that the thesis, entitled “**Nanomaterials for antibacterial and tissue regeneration, applications**”, submitted by **Nahida Rasool (Entry # 2017BMZ0007)** for the award of the degree of **Doctor of Philosophy** of the Indian Institute of Technology Ropar, Rupnagar, is a record of original research work carried out under my guidance and supervision at the Department of Biomedical Engineering, IIT Ropar, Rupnagar. All other sources of information, material, and mentorship have been acknowledged at appropriate places in the thesis. To the best of my knowledge and belief, the work presented in this thesis is original and has not been submitted, either in part or full, for the award of any other degree, diploma, fellowship, associateship or similar title of any university or institution.

In my opinion, the thesis meets the requirements of the regulations relating to the award of PhD degree.



Signature of the Supervisor

Dr. Yashveer Singh

Department: Biomedical Engineering

Indian Institute of Technology Ropar

Rupnagar, Punjab 140001

Date: 31-05-2024

Lay summary

Nanomaterials are materials with at least one dimensions in the nanoscale (smaller than 100 nm). The nanomaterials have distinct shape, size, and flexible surface, which imparts unique biological properties to them. Nanoparticles have tunable surface chemistry that can be modulated to achieve desired effects. The nanomaterials loaded with drugs are likely to enhance the availability of drugs in the body and reduce side effects associated with the drug. They are often compatible to the living systems, disappear from the body (biodegradation) and do not elicit immune responses. Owing to their distinct physiochemical properties, nanomaterials are being investigated for applications, like drug delivery, wound healing, and tissue regeneration. In this thesis, we have developed bioactive nanomaterials (with inherent activity beneficial for the treatment) for bacterial infection in eyes, wounds that fail to heal, and bone regeneration in osteoporotic conditions. The chapter 1 provides the introduction of the topic, survey of earlier research done in this area, definition of the problem, and major goals of this study. The chapter 2 describes the development of ciprofloxacin-loaded chitosan/lecithin nanoparticles for treating eye infections caused by bacteria. The nanomaterials provided a prolonged drug release, excellent ability to kill bacteria, and were safe to cells. The chapter 3 reports the development of positively charged silica ceria nanocomposite. The nanocomposite showed ability to act as an antioxidant, kill different bacteria, and help with the stalled wound healing. The chapter 4 part reports the development of surface modified, mesoporous silica nanoparticles for bone regeneration in osteoporotic conditions. The nanoparticles showed promising antioxidant and bone regeneration properties. The final chapter 5 provides the summary of this thesis, its contribution to the field of research, and future perspectives. In this work, we have been able to develop multifunctional nanomaterial with improved therapeutic effects for various diseased conditions.

Abstract

Nanoparticulate systems have been employed for diagnostics, drug delivery, therapeutics, and tissue engineering applications. Nanoparticles with intrinsic antibacterial activity have shown promise in treating bacterial infections and combating the antimicrobial resistance (AMR) but the threat remains due to the ever-evolving biofilm. Ophthalmic drug delivery is challenging owing to the anatomical barriers present in eyes. Majority of marketed ophthalmic formulations are eye drops, which fail to overcome these barriers and, therefore, exhibit poor bioavailability. Altered wound healing is a major challenge faced by both developed and developing nations. Biofilm formation has been identified as one of the causative factors for the progression of chronic wounds as well as drug resistance. Osteoporosis is a chronic bone disorder characterized by the decreased bone mass, leading to brittle bones and fractures. Oxidative stress has been identified as the most profound trigger for the initiation and progression of osteoporosis. Current treatment strategies do not induce new bone formation and fail to address high level of reactive oxygen species (ROS). To overcome the challenges in the field, we have developed and evaluated nanomaterials to treat ocular bacterial infections, chronic wounds, and osteoporosis.

The present thesis is arranged into five chapters, where **Chapter 1** is introductory and includes the exhaustive literature survey, the definition of problem, and the specific objectives of this work. In **Chapter 2**, we have included the development and evaluation of ciprofloxacin-loaded polymeric nanoparticles of chitosan/lecithin for the treatment of ocular bacterial infections. The nanoparticles were prepared using ion gelation method and characterized, and their antibacterial properties were investigated against *P. aeruginosa* and *S. aureus* along with their cell compatible and mucoadhesive characteristics. The nanoparticles showed strong potential in treating ocular bacterial infections. **Chapter 3** discusses the fabrication and evaluation of functionalized, silica ceria nanocomposite, as an antibiotic-free system, to treat biofilms. The antioxidant activity, positive haloperoxidase-mimetic property, broad-spectrum antibacterial activities against *S. aureus* and *E. coli*, and antibiofilm activities were investigated along with its cytocompatibility (cell proliferative), hemocompatibility, and wound healing ability. The functionalized silica ceria nanocomposite showed a strong potential in chronic wound healing applications. In **Chapter 4**, we have investigated the potential of a thiolated, bioactive mesoporous silica nanoparticles to treat osteoporosis. The nanoparticles were fabricated and surface functionalized post-synthesis with thiol groups and its antioxidant activity, ability to neutralize reactive oxygen species formed in cells and provide protection against ROS-induced cell damage, cell compatibility, calcium deposition, and osteogenesis were investigated. The nanomaterial was found to be regenerative in nature, and it showed a strong potential as a complementary and an alternate treatment for osteoporosis along with the standard therapy. The conclusions, contribution to the field, and perspectives of this work has been discussed in **Chapter 5**.

List of publications

1. **Rasool, N.**; Negi, D.; Singh, Y. Thiol-functionalized, antioxidant, osteogenic mesoporous silica nanoparticles for osteoporosis. *ACS Biomater. Sci. Eng.* (chapter 3)
2. **Rasool, N.**; Srivastava, R.; Singh, Y. Cationized silica ceria nanocomposites to target biofilms in chronic wounds. *Biomater. Adv.* 2022, 138, 212939 (chapter 2).
3. Kumar, A., Singh, H., Kant, R., **Rasool, N.** Development of cold sprayed titanium/baghdadite composite coating for bio-implant applications. *J Therm Spray Tech.* 2021, 30, 2099–2116
4. Bhandari, M.; **Rasool, N.**; Singh, Y. Polymeric lipid nanoparticles for donepezil delivery. In Polymeric Biomaterials and Bioengineering; Gupta, B., Jawaid, M., Kaith, B. S., Rattan, S., Kalia, S., Eds.; *Lecture Notes in Bioengineering*; Springer Nature Singapore: Singapore, (2022). (Equal contributing authors)

Conferences

1. **Rasool, N.**, Negi, D., and Singh, Y., Thiolated mesoporous silica nanoparticles for treatment of oxidative stress-associated osteoporosis, *TERMIS AP 2022, Korean Tissue Engineering and Regenerative Medicine Society*, ICC, Jeju, South Korea, 5-8 October 2022 (**poster**)
2. **Rasool, N.**, Srivastava, R., and Singh, Y., Cationized silica-ceria composites to target biofilms in chronic wounds, *ACS Spring 2021*, American Chemical Society, 5-31 April, 2021 (virtual mode, **poster**)
3. **Rasool, N.**, Srivastava, R., and Singh, Y., Silicasome-based nanoparticulate system for tamoxifen delivery, *International Conference on Biomaterial-based Therapeutic Engineering and Regenerative Medicine (BioTERM 2019)*, Department of Biological Sciences and Bioengineering, Indian Institute of Technology Kanpur, Kanpur, 28 November-1 December 2019 (**poster**)

Table of contents

Declaration	v
Acknowledgements	vii
Certificate	ix
Lay Summary	xi
Abstract	xiii
List of Publications	xv
List of Conferences	xvii
List of Figures	xxi
List of Tables	xxiii
Notations and Abbreviations	xxv
Chapter 1: Introduction	1-34
1.1. Nanoparticles	3
1.1.1. Classification of nanoparticles	3
1.1.2. Physicochemical properties of nanoparticles	4
1.1.3. Preparation of nanoparticles	5
1.1.4. Characterization	5
1.1.5. Routes of administration	6
1.1.6. Pharmacokinetics of nanoparticles	6
1.1.7. Evolution of nanoparticles	7
1.2. Introduction to problem and literature survey	8
1.2.1. Drug delivery	8
1.2.1.1. Drug loading	8
1.2.1.2. Drug release	10
1.2.1.3. Ophthalmic drug delivery	11
1.2.2. Tissue Engineering and nanotechnology	14
1.2.2.1. Wound healing	15
1.2.2.2. Chronic wound healing	15
1.2.2.3. Rationale design of nanomaterials for biofilm infected wounds	17
1.2.3. Osteoporosis	18
1.2.3.1. Management of OP	20

1.3. Knowledge gaps in the field	22
1.4. Thesis objectives	23
1.5. Thesis outline	24
References	25-34
Chapter 2: Antibacterial lecithin chitosan nanoparticles for sustained release of Ciprofloxacin	35-55
2.1. Introduction	37
2.1.1. Ocular bacterial infections	37
2.1.2. Challenges	37
2.1.3. Research gap	37
2.2. Objectives	38
2.3. Experimental section	39
2.4. Results and discussions	42
2.5. Conclusions	49
References	51-55
Chapter 3: Cationized silica ceria nanocomposite to target biofilms in chronic wounds	57-88
3.1. Introduction	59
3.1.1. Wound healing	59
3.1.2. Challenges	59
3.1.3. Research gap	59
3.2. Objectives	60
3.3. Experimental section	62
3.4. Results and discussions	68
3.5. Conclusions	80
References	82-88
Chapter 4: Antioxidant and osteogenic thiolated mesoporous silica nanoparticles for osteoporosis	89-112
4.1. Introduction	91
4.1.1. Osteoporosis	91
4.1.2. Challenges	91
4.1.3. Research gap	91
4.2. Objectives	92
4.3. Experimental section	93
4.4. Results and discussions	96
4.5. Conclusions	106
References	108-112
Chapter 5: Conclusions and perspectives	113-117
5.1. Summary of the thesis	115
5.1.1. Contribution to the existing knowledge	116
5.1.2. Future perspectives	117
Appendix	119-135

List of figures

S. No.	Figure Caption	Page No.
1.1.	Routes of administration and pharmacokinetics of nanoparticles	6
1.2.	The timeline of clinically approved nanoparticulate-based drug delivery systems	7
1.3.	Overview of commercially available nanomedicines or those in clinical trials: (A) Current development status, and (B) Disease indications.	8
1.4.	The mechanisms of drug loading and release from nanomaterials	11
1.5.	Different routes of ocular administration	12
1.6.	Comparison in healing of normal wound vs altered healing in biofilm infected chronic wound	16
1.7.	The mechanisms of action of various nanoparticle-based treatments for biofilm infected chronic wounds	17
1.8.	Structure of bone and physiological process of bone remodeling	20
1.9.	Nanoparticles to target various therapeutics targets for treating bone defect	21
1.10.	Objectives of the thesis	24
2.1.	Preparation of Cipro-loaded, lecithin / chitosan (CLC) NPs	43
2.2.	FT-IR spectrum	43
2.3.	Thermogravimetric analysis of nanoparticles	44
2.4.	SEM micrograph	45
2.5.	Release profile of ciprofloxacin	46
2.6.	Antibacterial activity and live/dead assay	47
2.7.	Cell viability using MTT, CCK-8 assay, and live/dead assays	48
2.8.	Mucoadhesion analysis and in vitro percent hemolysis assay	49
3.1.	Preparation of cationized silica ceria nanocomposite (FSC) and HR-TEM images	61
3.2.	XPS spectra and elemental mapping	70
3.3.	ABTS assay and haloperoxidase assay	72
3.4.	Antibacterial assay and live dead assay	73
3.5.	HR-TEM images of bacterial cells	74
3.6.	Biofilm inhibition using crystal violet staining assay and live dead images	76
3.7.	Cell viability assay by MTT, CCK-8 assay, and live-dead staining	77
3.8.	Hemolysis assay and DCFH-DA assay	78

3.9.	Scratch assay	80
4.1.	Fabrication of thiolated mesoporous silica nanoparticles and HR-TEM images	97
4.2.	Physical and chemical characterization, particle size, FTIR, TGA, XRD and BET	98
4.3.	EDX mapping and XPS analysis	99
4.4.	Antioxidant assay, cell viability study by MTT assay and live-dead staining	101
4.5.	Osteogenic differentiation study by ALP and Ca deposition assay	102
4.6.	Gene expression of osteogenic genes using qRT-PCR	103
4.7.	Antioxidant activity by DCFDA assay	105
4.8.	Cytoskeletal staining of MC3T3 and scratch assay	106

List of tables

S. No	Table caption	Page No.
1.1	Some approved nanocarrier delivery system for ocular use	13
1.2	Some FDA approved antimicrobial nanoparticles	18
1.3	Some marketed nanomedicine-based preparation for bone disorders	22
2.1	Particle size distribution and zeta potential of LC and Cipro-loaded LC NPs	44
2.2	Zeta potential of free mucin, mucin / LC NPs, and Cipro-loaded LC NPs	49
3.1	Particle size distribution and zeta potential of MSN, CNP, FCNP, SC, and FSC	69
A1	Physical properties of nanoparticles (MSN, CNP) and nanocomposite (SC, FSC)	130
A2	Ratio of $\text{Ce}^{3+}/\text{Ce}^{4+}$ estimated using Ce 3d XPS spectrum of FSC	130
A3	Primer sequences used in real-time PCR	135

Notations and abbreviations

Acronym	Name
3D	Three Dimensional
ABTS	2,2'-azino-bis(3-ethylbenzothiazoline-6-sulfonic acid) diammonium
APTES	3-aminopropyl-triethoxysilane
ALP	Alkaline phosphatase
AFM	Atomic force microscope
ATR	Attenuated Total Reflectance
BBB	Blood-brain Barrier
BET	Brunauer-Emmett-Teller
BJH	Barrett-Joyner-Halenda
BMP	Bone morphogenetic protein
CS	Chitosan
CT	Computed topography
CCK	Cell counting kit
CLC	Ciprofloxacin lecithin chitosan
cDNA	Complementary deoxyribonucleic acid
CFU	Colony forming unit
CNP	Cerium oxide nanoparticles
CTAB	Cetrimonium bromide
DAPI	4',6-diamidino-2-phenylindole
DCFDA	2',7'-dichlorodihydrofluorescein diacetate
DNA	Deoxyribonucleic acid
DI	Deionized water
DIEA	N,N-diisopropylethylamine
DLS	Dynamic light scattering
DMEM	Dulbecco's modified eagle medium
DPBS	Dulbecco's Phosphate Buffered Saline
DMSO	Dimethyl sulfoxide
DNA	Deoxyribonucleic acid
DTNB	5,5'-dithiobis-2-nitrobenzoic acid
ECM	Extracellular matrix
EPR	Enhanced permeability and retention
EDTA	Ethylenediaminetetraacetic acid
EDX	Energy dispersive X-ray
EMA	European Medicine Agency
EPS	Extracellular polymeric substances
FSC	Functionalized silica ceria composite
FCNP	Functionalized cerium oxide nanoparticles
FBS	Fetal bovine serum
FDA	Food and Drug Administration
FESEM	Field emission scanning electron microscopy
FITC	Fluorescein isothiocyanate
FTIR	Fourier transform infrared
GAPDH	Glyceraldehyde-3-phosphate dehydrogenase
GSH	Glutathione

H ₂ O ₂	Hydrogen peroxide
HAp	Hydroxyapatite
HR-TEM	High resolution transmission electron microscope
LB	Luria-Bertani
LC	Lecithin chitosan
M-CSF	Macrophage colony-stimulating factor
MEM α	Minimum essential medium alpha
MAPK	Mitogen-activated protein kinase
MMP-2	Matrix metalloproteinase-2
MSN	Mesoporous silica nanoparticles
MRI	Magnetic resonance imaging
MTT	(3-(4,5-Dimethylthiazol-2-yl)-2,5-diphenyltetrazolium bromide
NaOH	Sodium hydroxide
NF- κ B	Nuclear factor
NP	Nanoparticle
ODDS	Ocular drug delivery system
OB	Osteoblast
OC	Osteoclast
OCN	Osteocalcin
OD	Optical density
OM	Osteogenic media
OP	Osteoporosis
OPN	Osteopontin
PEG	Poly ethylene glycol
PBS	Phosphate buffer saline
PI	Propidium iodide
PK	Pharmacokinetics
PLA	Poly lactic acid
PDLLA	Poly D,L-lactic acid
PLGA	Poly lactic-co-glycolic acid
pNPP	<i>para</i> -Nitrophenyl phosphate
PLA	Poly lactic acid
QS	Quorum sensing
RANKL	Receptor activator of nuclear factor kappa-B ligand
RBC	Red blood cells
ROS	Reactive oxygen species
rPTH	Recombinant human parathyroid hormone
RPM	Rotation per minute
RPMI	Roswell Park Memorial Institute
RUNX 2	Runt-related transcription factor 2
SC	Silica ceria nanocomposite
SD	Standard deviation
SEM	Scanning electron microscopy
SERM	Selective estrogen receptor modulators
Sr	Strontium
STF	Simulated tear fluid
SIRC	Staten's serum institute rabbit cornea
TEOS	Tetraethyl orthosilicate
TERM	Tissue engineering and regeneration
TPP	tripolyphosphate
TGA	Thermogravimetric analysis

TRAP	Tartrate-resistant acid phosphatase
UV	Ultra violet
USG	Ultra sonography
XPS	X-ray photoelectron spectroscopy
XRD	X-Ray diffraction

CHAPTER - 1

Introduction

1. Introduction

1.1 Nanoparticles

Nanoparticles as defined by the European Commission are “natural, incidental or manufactured materials containing particles, in an unbound state or as an aggregate or as an agglomerate and, where 50% or more of the particles in the number size distribution, one or more external dimensions are in the size range 1–100 nm. The concept of nanotechnology was introduced to the world by an American physicist and Nobel Laureate, Richard Feynman in 1959. Often considered as a modern-day scientific breakthrough, nanotechnology has garnered attention in numerous research areas for last two decades. It holds the potential to address longstanding challenges and fulfill unmet requirements through integrated platforms across various domains, including chemistry, physics, engineering, biotechnology, and medical sciences. Thus, nanotechnology broadens the horizons of current research, particularly in the realm of medicine.^{1,2} Nanoparticles can be classified into various types based on their chemical composition and applications.

1.1.1. Classification of nanoparticles

Based on the chemical composition, nanoparticles are broadly divided into following classes

(i) **Organic NPs:** These NPs are mainly made up of proteins, carbohydrates, lipids, polymers, or any other organic compounds, like dendrimers, liposomes, micelles, and protein complexes. They are typically biocompatible, bio-degradable in nature. Organic NPs find its uses mostly in targeted drug delivery and cancer therapy.³

(ii) **Inorganic NPs:** This class of NPs consist of metal NPs (iron, gold, copper, silver), metal oxide NPs (zinc oxide, silicon dioxide, titanium oxide), and ceramics (carbides, carbonates, oxides). These NPs have been used in catalysis, degradation of dyes, and photonics.⁴

(iii) **Carbon based NPs:** This class encompasses carbon-based nanomaterials and includes fullerenes, carbon nanotubes, graphene, and carbon quantum dots. These NPs have high thermal stability and are widely used in drug delivery, bioimaging, and biosensing.⁵

(iv) **Nanocomposites:** These are heterogeneous NPs, tailored by integrating two or more nanoscale components. These hybrid NPs exhibit improved and distinct properties in comparison to their individual components. These are employed in biomedicine and other applications as well. Typical examples are iron oxide-gold composite, silica ceria composite, and bioglass nanoparticles.⁴

On the basis of biomedical applications, nanoparticles can be broadly divided into four classes:

(i) **Bioactive / therapeutic nanoparticles:** Also known as nanomedicine, these are

pharmacologically active agents, which possess some intrinsic therapeutic value. Antibacterial nanoparticles, like zinc oxide, silver, chitosan exert biological activity owing to its nanotopography, surface property, and physical structure. Biomimetic nanoparticles /nano-enzymes are artificial enzymes. For example, cerium oxide nanoparticles act as catalysts to aid various enzymatic reactions.

(ii) Nanocarriers: Serves as carriers and are employed mainly for drug / gene / cell delivery. Nanoparticles ensure the sustained and prolonged release of drug and target tumors because of the enhanced permeability and retention (EPR) effect in tumors. They are mainly used in cancer targeted therapy. Most of the nanoparticles has tunable surface, which can be modified with ligand of choice to impart target-selective delivery.

(iii) Diagnostic nanoparticles: These are used for diagnostic purposes. For example, nanoparticles have been explored as contrast agents and biosensors in image-based diagnostic techniques, like MRI (magnetic resonance imaging), CT (computed tomography) and USG (ultrasonography). Nanoparticles can be used for multimode imaging. Magnetic nanoparticles, like iron oxide and semiconducting nanoparticles, like quantum dots serve as efficient diagnostic agents.

(iv) Nanoparticles for tissue engineering and regeneration (TERM): Nanoparticles, like ceramics, inorganic, metal, and natural polymers have found immense utilization in TERM due to their efficient spatiotemporal architect and mechanical strength. These nanoparticles provide niche for new growth and regeneration.

1.1.2. Physicochemical properties of nanoparticles

Nanoparticles, due to their small size and unique properties, interact with biological systems in distinct ways compared to larger particles. Some of the key properties of nanoparticles are listed below:

(i) Size and surface area: The small size of nanoparticles results in a high surface area to volume ratio, which makes them ideal carrier for high drug loading. The particle size plays important role in tissue distribution as well.

(ii) Shape: The shape of nanoparticles (spherical, rod-like, tubular, etc.) plays significant role in biological activity, such as antibacterial nanoparticles.

(iii) Surface chemistry: The chemical composition and functionalization of nanoparticle surface determines its solubility, stability, and interaction with biological molecules. Surface modifications can be used to target specific cells or tissues and to evade the immune system.

(iv) Charge: The surface charge of nanoparticles affects their interaction with cell membranes. Positively charged nanoparticles may have enhanced cellular uptake but can also be more toxic.

(v) Mechanical properties: Due to surface and quantum effects, NPs display different mechanical properties compared to bulk materials. Nanomaterials having good mechanical properties are good substitutes for composite filling for dental or orthopedic implants.

1.1.3. Preparation of nanoparticles

Nanoparticles are typically prepared using two approaches, as discussed below:

Top-down approach

(i) **Ball milling:** This is a mechanical method which involves grinding of bulk materials into nanoparticles using a ball mill. The process can be performed in dry or wet conditions. It is a simple and cost-effective method but might introduce impurities.

(ii) **Laser ablation:** In this technique, a high-energy laser is used to ablate material from a target, which then condenses into nanoparticles. This allows for the production of clean and well-defined nanoparticles but can be expensive.

(iii) **Etching:** This involves the removal of material from a larger bulk to create nanoparticles. The process can be done chemically or via ion beams, this method is precise but can be complex and costly.

Bottom-up approach

(i) **Sol-gel process:** This involves the transition of a solution (sol) into a solid (gel) phase. By controlling the process conditions, nanoparticles can be prepared. This method is versatile and relatively simple but can involve long processing times.

(ii) **Hydrothermal synthesis:** This involves reacting precursors in solvent at high temperatures and pressures. This process of synthesis is useful for producing crystalline nanoparticles but requires specialized equipment.

(iii) **Precipitation / solvent evaporation:** Nanoparticles are formed by the chemical reaction of precursors in solvent, leading to the precipitation of nanoparticles. This is a simple and widely used method but may require further processing to obtain the particle of desired size.

(iv) **Microemulsion:** This method uses a mixture of water, oil, and surfactants to create a microemulsion in which nanoparticles can form. It allows for the preparation of well-controlled nanoparticles but can be complex.

(v) **Biosynthesis:** This eco-friendly method uses biological organisms or extracts (like bacteria, fungi, or plant extracts) to synthesize nanoparticles. Biosynthesis is sustainable and can produce biocompatible nanoparticles but may offer less control over size and shape.^{3,6}

1.1.4. Characterization

Considering that the functions of nanomaterials are closely related to their properties, the characterization of nanomaterials and related evaluation of properties is vital and should be monitored first. The important characteristic properties, like charge, composition, aggregation state, size distribution, size, shape, surface chemistry, and surface area of nanoparticles are typically studied using various technique/instruments, like scanning electron microscope (SEM), high-resolution transmission electron microscope (HR-TEM), single particle inductively coupled plasma-mass spectrometer (spICP-MS), atomic force microscope (AFM), dynamic light scattering (DLS), zeta sizer, and ultraviolet-visible (UV-vis).⁴

1.1.5. Routes of administration

Nanoparticles are administered into body through various routes, such as oral administration, inhalation, transdermal, subcutaneous, and intramuscular injection. After administration, nanoparticles encounter and surpass various physiological barriers, like blood-brain barrier by paracellular route or receptor-mediated transport or gut mucosal barrier by changing the viscosity of mucus or tight junction relaxation. After effectively infiltrating the barriers, finally enter the systemic circulation or reach the target tissue upon local delivery. The choice of route of administration depends on the drug release kinetics, tissue to be targeted, and therapeutic goal.⁷

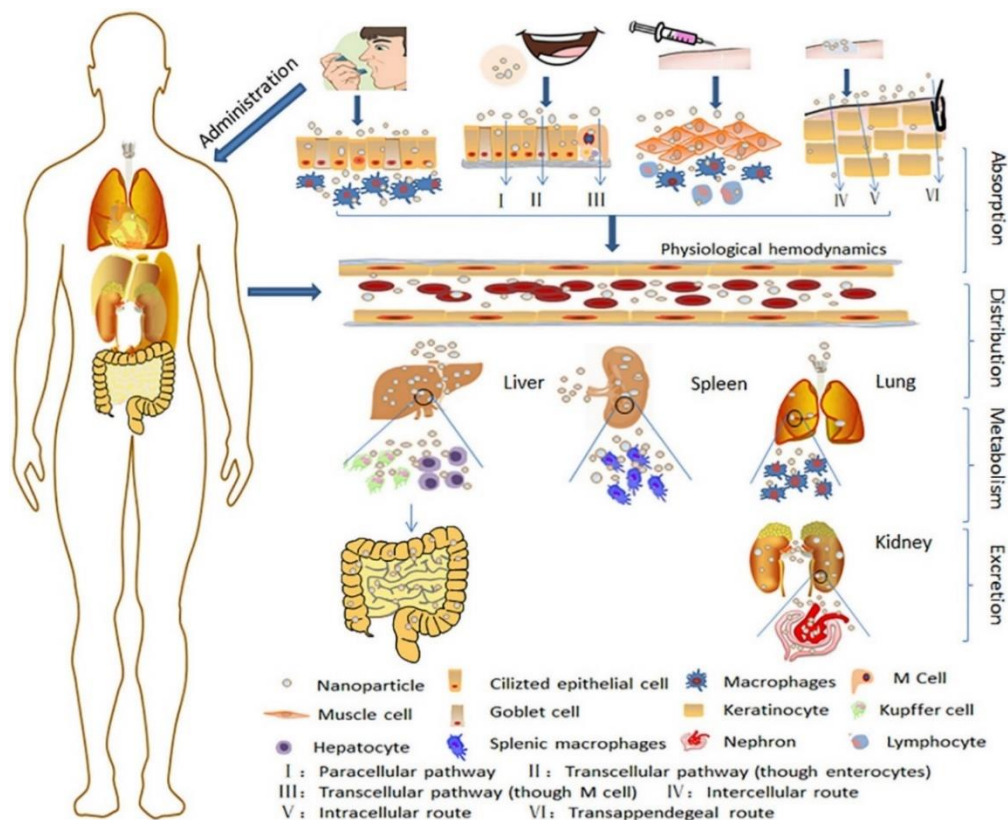


Figure 1.1. Routes of administration and pharmacokinetic pathway of nanoparticles in human body. Reproduced with kind permission from Zhang *et al.*, *Advances in colloid and Interface Science*, **2020**, 284, 102261 © 2020 Published by Elsevier B.V.

1.1.6. Pharmacokinetics (PK) of nanoparticles

The nanoparticles are absorbed and distribution throughout the body tissues occurs via blood circulation. The nanoparticles metabolized by liver and spleen, are finally excreted via intestines and kidneys as illustrated in **Figure 1.1**

(i) **Absorption:** On the basis of delivery system, administered nanoparticles are absorbed readily or in controlled manner and reach systemic circulation. Nanoparticles can be designed to efficiently pass through various biological barriers such as skin.

(ii) **Distribution:** Once in the bloodstream, based on size or surface characteristics,

nanoparticles exhibit characteristic distribution in tissues. Factors, like vascularity, permeability, and plasma content of tissue affect the distribution. Nanoparticles can be engineered to target specific tissues or cells, thus reducing systemic toxicity.

(iii) **Metabolism:** Nanoparticles are mainly metabolized in liver and spleen and release the active therapeutic agent upon degradation. Various release mechanism, like surface desorption, diffusion or enzymatic degradation or pH-based release.

(iv) **Excretion:** The excretion of nanoparticles can be slower than traditional drugs, thus increasing the drug residence time in body. The kidneys usually filter out smaller nanoparticles, while larger ones may be taken up by the liver.^{8,9}

1.1.7. Evolution of nanoparticles

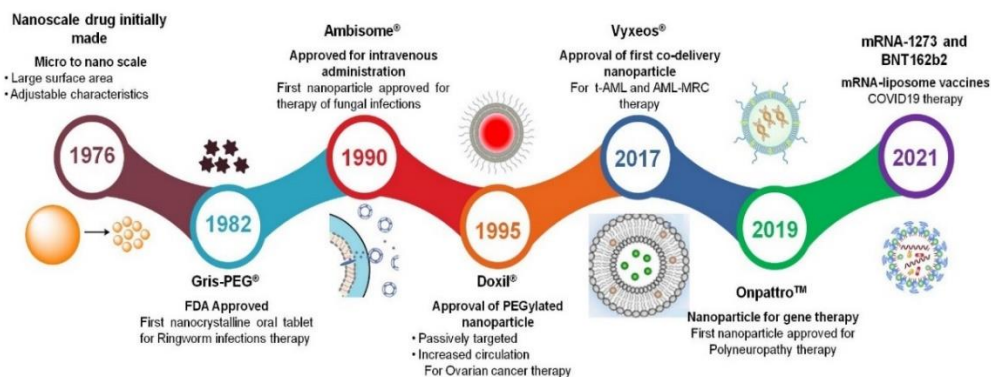


Figure 1.2. The timeline of clinically approved nanoparticulate-based drug delivery systems.

Since its inception in 1900s and decades of research in labs, nano-based systems have been successfully translated from bench to clinic, with as many as 100 formulations approved by regulatory authorities, like FDA and EMA, and the numbers are rising each year (**Figure 1.2**). For example, Doxil® (Baxter Healthcare) a doxorubicin loaded liposome is approved for ovarian cancer and multiple myeloma. Genexol PM® an anti-cancer medicine is paclitaxel mPEG-PDLLA micelle based on polymeric micelle technology developed by Lupin Ltd. Abraxane® (Eli Lilly) consists of paclitaxel-loaded albumin nanoparticles for metastatic cancer. Hensify® (hafnium oxide nanoparticles) developed by Nanobiotex are used for the treatment of advanced squamous cell carcinoma. NanOss®, a hydroxyapatite developed by RTI Surgical is used as bone substitute. There are plethora of nanomaterials under investigation or in clinical trials for various indications as therapeutics or vaccine development and promising ones are likely to hit the market soon (**Figure 1.3**)^{2,10,11}

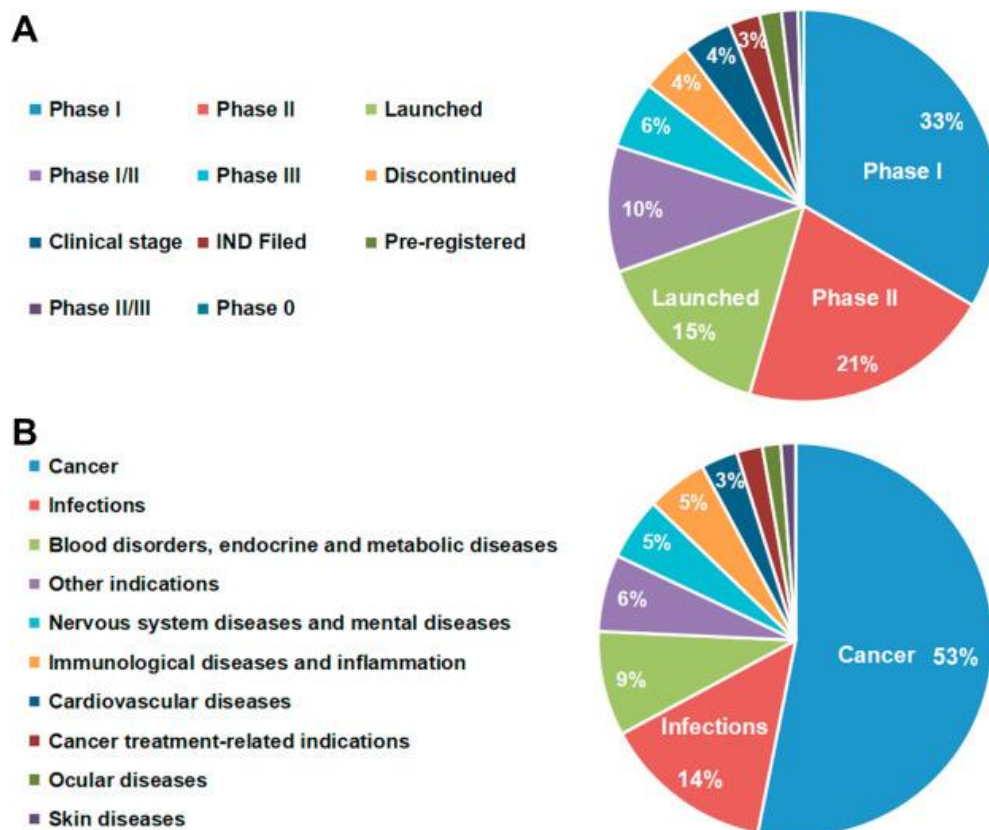


Figure 1.3. Overview of commercially available nanomedicines or those in clinical trials: (A) Current development status, and (B) Disease indications. Reproduced with kind permission from Shan *et al.*, *Acta Pharmaceutica Sinica B*, **2022**, 12, 3028-3048 © 2022 Elsevier B.V.

1.2. Introduction to the problem and literature survey

Although nanoparticles have wide array of applications, the current discussion is restricted to their applications in drug delivery and tissue engineering only as these are more relevant to the theme of this thesis.

1.2.1 Drug delivery

1.2.1.1. Drug loading

The drugs loading in nanoparticles occur due to several physical or chemical phenomena, such as physical entrapment, surface adsorption, covalent bonding, hydrogen bonding or electrostatic interactions. (**Figure 1.4**)

Encapsulation: Encapsulation within nanoparticles is one of the widely utilized drug loading technique as the hollow space inside nanoparticles help in the effective encapsulation of drug molecules. It can enhance solubility, improve drug stability, and help in the targeted delivery of drugs. Different nanoparticles are used as encapsulation vehicles, including inorganic nanoparticles, polymeric nanoparticles, lipid nanoparticles, and dendrimers¹² Aliabadi *et al.*, 2007 fabricated polymeric micelles of MePEO-*b*-PCL for the encapsulation of cyclosporine A.¹³ Gomez-gaete *et al.* encapsulated dexamethasone into biodegradable PLGA nanoparticles for ocular delivery.¹⁴ Lipid-based nanoparticles, like solid-lipid

nanoparticles and liposomes are also widely used as drug encapsulating vehicles. These liposomes help in encapsulating both hydrophilic and hydrophobic drugs. Okamoto Y *et al.* fabricated paclitaxel-loaded liposomes for the treatment of pancreatic cancer.¹⁵ However, in this method, the amount of drug loading is less, particularly with low solubility or high molecular weight drugs. Also, during encapsulation process, some drugs undergo physical /chemical changes, which results in the loss of activity.

Surface adsorption: Surface adsorption is also a well-known technique for drug loading. In this drug molecules get attached to surface of carrier material. This technique offers a simple and easy method to load drug molecules. Surface adsorption is used for drug loading in a number of carrier systems, such as nanoparticles, mesoporous materials, and porous structures.¹⁶ Zarkesh *et al.*, fabricated hyaluronan coated mesoporous silica nanoparticles for the delivery of cisplatin and the fabricated nanoparticle system provided a multifunctional pH-responsive approach for effective delivery of drugs.¹⁷ There are chances of drug desorption from surface, resulting in less loading capacity. There might be variance in drug release kinetics, the adsorbed drug molecules may not be uniformly distributed on the carrier surface, leading to inconsistent release profiles.

Covalent bonding: Covalent bonding can also be used to load drug into the nanoparticles. A high concentration of drug can be loaded into nanoparticle by means of the suitable functional groups present on its surface. Presence of large number of functional groups in nanoparticles is beneficial for the covalent conjugation of the drug to nanoparticles.¹⁸ For example, surface functionalization of nanoparticles with functional groups like thiol groups or amine groups help in the covalent conjugation of drugs through chemical reactions. Yan *et al.* fabricated mesoporous silica-based nanoparticles for anticancer drug delivery. In this system, paclitaxel drug was covalently attached to the doxorubicin-loaded mesoporous nanoparticle. The fabricated system provided nanoplatform for precision combination therapy that exhibited excellent cell-to-cancer selectivity.¹⁹ However, a major drawback of covalent bonding is the significant loss of activity that can occur after immobilization. This loss in activity is attributed to changes to the active sites of the drug.

Electrostatic interactions: The solubility of the hydrophobic drugs is enhanced by the nanoparticles containing functional groups, like amine and carboxyl groups. Due to presence of these functional groups, drug molecules electrostatically interact with nanoparticle system. For example, anti-inflammatory drugs, like ibuprofen and indomethacin were attached effectively with the nanoparticle system with the help of electrostatic interactions.²⁰ Meng *et al.*, 2010, fabricated mesoporous silica nanoparticles for the effective delivery of anticancer drugs to overcome drug resistance in cancer cell line.²¹ Electrostatic interactions are highly sensitive to environmental factors, such as pH, ionic strength, and solvent composition. Thus, any changes in these parameters can disrupt or weaken the electrostatic attraction between the drug and carrier, leading to inefficient loading or premature drug release under physiological

conditions.

Hydrogen bonding: Drug loading into nanoparticles can be done by hydrogen bonding, which is a non-covalent interaction between a hydrogen atom and an electronegative atom. Utilizing hydrogen bond formation between functional groups on the nanoparticle and functional groups on the drug molecules, loading can be accomplished. Ke *et al.*, 2019, fabricated curcumin-loaded nanoparticles using hydrogen bonding.²² The limitations of this method is that since hydrogen bindings are weak forces, there are chances of decreased loading capacity and immediate release of drugs.

1.2.1.2. Drug release

For efficient drug delivery, drug loading should be followed by sufficient release. Based on the size and chemical nature of nanoparticles, drug release occurs through various mechanisms as discussed below (**Figure 1.4**)

Diffusion: Diffusion controlled drug release is seen in the systems, where the drug is dispersed or dissolved in the core. The difference in concentration gradient across the membrane helps in the diffusion of drugs. For example, matrix type nanospheres, where the drug molecules are uniformly distributed in the polymer matrix, result in diffusion-controlled release.²³

Surface desorption: The term "surface desorption" describes the process by which drug molecules diffuse off the surface of nanoparticles and release the drug. This process is important for sustained and controlled release of drugs from nanoparticles.²⁴

Dissolution: One important process in the drug release from nanoparticles is dissolution. When drugs are loaded in the nanoparticles, they can release the drugs by dissolution upon contact with physiological fluids. This further leads to matrix disintegration or breakdown resulting in drug release.²⁵

Stimuli-responsive release: Nanoparticles can be made stimuli-responsive, which can respond to internal or external stimuli, such as temperature, pH, ionic strength, electric or magnetic fields, which will further regulate the release of drugs. This release mechanism is widely explored in targeted drug delivery.²⁶

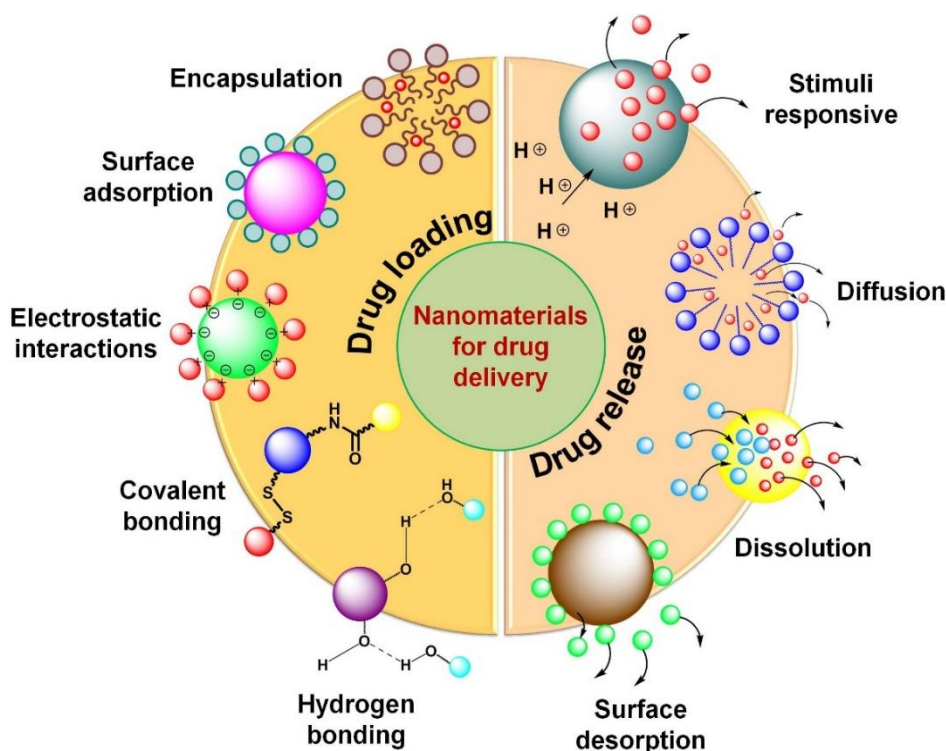


Figure 1.4. The mechanisms of drug loading and release from nanomaterials.

1.2.1.3. Ophthalmic drug delivery

Eye is one of most vulnerable organs due to the constant exposure to external world including the massive environmental bacterial load. The nature has designed the physiology in such a manner that eyes protect themselves but sometimes due to the malfunctioning of protective mechanisms, this defense fails to overcome the problems and ocular infections, trauma or infections occur. To treat the ocular disorders, drugs of choice are usually administered via invasive and non-invasive routes, such as intra cameral / vitreal injections (**Figure 1.5**). Topical application is most accepted route of administration.^{27,28} Delivering the drugs to target site without posing any risk to healthy issue is the goal of an ideal ocular drug delivery system (ODDS). Nanoparticles intended to be used in ODDS should typically exhibit following characteristics:

- (i) Be able to overcome both dynamic and static ocular barrier.
- (ii) Improve the drug stability.
- (iii) Increase the residence time of drug in tissue
- (iv) Exert minimal peripheral toxicity

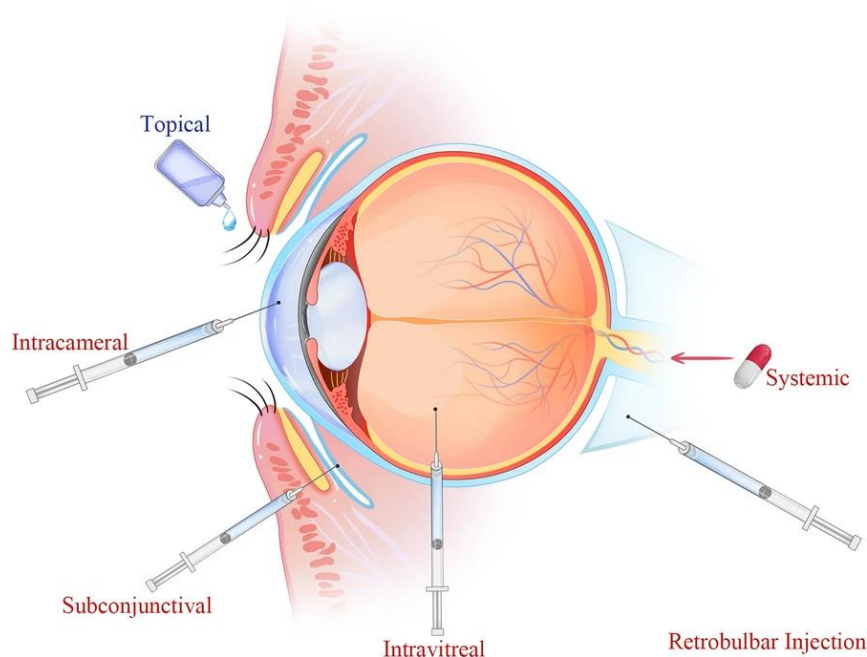


Figure 1.5. Different routes of ocular administration. Reproduced with kind permission from Li et al. *J Nanobiotechnol* **2023**, 21 (1), 232@ 2023 BMC.

The unique microenvironment and specialized physiological structures within the eye, such as the blood-retinal barrier, blood-aqueous barrier, and corneal barrier, pose significant challenges in developing safe and effective treatment. Several anatomical features and barriers in ocular tissue influence drug delivery. These are listed below:

Corneal barrier: The cornea is the outermost layer of eye and serves as a protective barrier. It consists of multiple layers of epithelial cells with tight junctions, which limit the penetration of drugs into the eye. However, the cornea is also highly vascularized, allowing for some drug absorption.

Conjunctival barrier: The conjunctiva lines the inner surface of eyelids and covers the sclera. It contains goblet cells that secrete mucin, forming a mucous layer that can trap and hinder drug penetration. The conjunctival epithelium also has tight junctions, which blocks the drug permeation.

Tear film: The tear film covers the ocular surface and serves as a protective barrier. It consists of aqueous, lipid, and mucin layers. The tear film can dilute drugs and wash them away from the ocular surface, reducing their bioavailability.

Blood-aqueous barrier: The blood-aqueous barrier separates the vascularized tissues of the iris and ciliary body from the aqueous humor in the anterior chamber of eye. This barrier restricts the passage of large molecules and cells from the bloodstream into the aqueous humor, affecting the distribution of systemically administered drugs.

Blood-retinal barrier: The blood-retinal barrier consists of tight junctions between endothelial cells of retinal blood vessels and the retinal pigment epithelium. It restricts the passage of substances from the bloodstream into the retina, limiting the efficacy of systemic drug delivery

for treating retinal diseases.

Ocular metabolism: Enzymes present in ocular tissues can metabolize drugs, reducing their bioavailability. For example, esterases in the cornea can hydrolyze ester prodrugs into active forms, affecting drug absorption and efficacy

Ocular clearance mechanisms: The eye has various clearance mechanisms, including tear turnover, lymphatic drainage, and systemic absorption through blood vessels in the conjunctiva and sclera. These mechanisms can rapidly remove drugs from the ocular surface, limiting their duration of action.^{29,30}

Understanding these anatomical features and barriers is crucial for designing effective ocular drug delivery systems that can overcome these challenges and improve drug penetration and bioavailability in ocular tissues. To address the existing limitations and design an efficient drug carrier, novel drug delivery systems made of polymers, lipids, inorganic nanoparticle developed in various delivery systems such as micelles, nanosuspensions, nanoemulsions, nanoparticles, liposomes, dendrimers, niosomes, cubosomes, and nanowafers have been investigated.^{31,32} Active research has been going on clinical translation of nanocarriers intended for ophthalmic drug delivery, with many formulation already approved by competent regulatory authorities, like FDA and EMA. Some of them have been listed below in **Table 1.1**.³³

Table 1.1. Some approved nanocarrier delivery system for ocular use.

Product	Nanocarrier	Drug	Indication	Reference
Ikervis [®]	Nanoemulsion	Cyclosporine A	Keratitis	Erighu et al ³⁴
Ozurde [®]	Polymer matrix	Dexamethasone	Post-operative ocular pain	Wentz et al ³⁵
Cequa [®]	Micelle	Cyclosporine A	Dry eye disease	Mandal et al ³⁶
Xelpros [®]	Nanoemulsion	Latanopros	Open-angle glaucoma	Kagkellaris et al ³⁷
Eysuvis [®]	Nanosuspension	Loteprednol etabonate	Dry eye diseases	Akhter et al ³⁸
Verkazia [®]	Nanoemulsion	Cyclosporine	Vernal keratoconjunctivitis	Gorantla et al ³²

Chitosan, a semi synthetic cationic polysaccharide, is derived from deacetylation of chitin. It finds various pharmaceutical applications, owing to its antimicrobial and

mucoadhesive properties. This polymer is easily available, cheap and biocompatible, and due to presence of functional groups can be easily modified to impart new properties. Chitosan has been developed in different kind of formulations like hydrogels, nanogels, nanoemulsions, and nanoparticles for various drug delivery, antibacterial and tissue engineering applications.^{39,40} Chitosan is one of most widely explored biomaterial for ocular drug delivery due to the favorable physiochemical characteristics. However, it poses some formulation challenges, like solubility, high viscosity, physical and chemical instability, and it needs stabilizing agent to be formulated into gels or nanoparticles.⁴¹ The degree of deacetylation and the molecular weight of chitosan affect its physico-mechanical properties. The degree of deacetylation affects its hydrophobicity, solubility, and toxicity. The molecular weight of chitosan affects its solubility and degradation. Chitosan with higher molecular weights show less solubility and lower degradation rate than the chitosan with lower molecular weight. Small sized particles provide larger surface areas for drug adsorption, thereby improving drug loading efficiency. Moreover, the particle size can also influence the release kinetics of the drug from the chitosan matrix.⁴² The protonation of amino groups in chitosan is highly dependent on pH and ionic strength. At lower pH or higher ionic strength, chitosan tends to become less soluble and less positively charged, which can affect drug loading and release behavior. Crosslinking chitosan with other molecules or through chemical modifications can alter its physicochemical properties, affecting drug loading capacity and release kinetics. Crosslinking can increase the mechanical strength of chitosan matrices, thereby controlling the release rate of drugs.⁴³ Use of anionic small molecules, such as sodium sulfate, sodium tripolyphosphate (TPP), or anionic polymers, like hyaluronic acid, alginates, chondroitin sulfate, and sodium cellulose sulfate, facilitate the formation of nanoparticles due to inter- and intramolecular crosslinking.⁴⁴ TPP as crosslinking/stabilizing agent for CS NPs was first investigated by Bodmeier *et al.*⁴⁵ Silva *et al.* developed erythropoietin loaded chitosan-hyaluronic acid nanoparticles by ionotropic gelation.⁴⁶ Chitosan has been combined with various synthetic polymers, such a PLA, PLGA, and PGA and shown some excellent results. In some recent advances, chitosan has been blended with liposomes, micelles, and solid lipidic NPs, which enhanced bioavailability, improved drug residence time, and provided sustained release of drugs.⁴⁷ Badran *et al.* prepared metoprolol-loaded liposomes coated with chitosan for ocular application.⁴⁸ The hybrid chitosan lipid nanoparticles were promising to explore and showed a sustained release of drug, antibacterial effect, mucoadhesiveness, and increased drug retention.

1.2.2. Tissue Engineering and nanotechnology

As defined by pioneers of field, Dr. Langer and Dr. Vacanti, tissue engineering is defined as “an interdisciplinary field that applies the principles of engineering and life sciences toward the development of biological substitutes that restore, maintain, or improve tissue function or a whole organ”. Nanotechnology paved its way into tissue engineering and extensive studies

have shown promising results, thus, qualifying nanoparticles as potential candidate in tissue engineering and regeneration. Several kinds of nanoparticles, such as metal oxide, inorganic, and polymeric nanoparticles have been explored in skin, bone, and cardiac tissue engineering.⁴⁹

1.2.2.1. Wound healing

Physiological wound healing is a complex but precise sequence of events triggered by injury/insult to tissue and ends with successful closure. It can be broadly divided into four overlapping stages:

(i) **Hemostasis/coagulation:** During this phase, vasoconstriction of blood vessels occurs to reduce the blood flow at the site of injury. This is followed by coagulation and blood clot formation.

(ii) **Inflammation:** Once hemostasis is achieved, the inflammatory phase begins. This stage is characterized by typical signs of inflammation, like redness, heat, swelling, and pain at the wound site. During this phase, various inflammatory cytokines enter the wound area to stave off infection by clearing bacteria and debris and preparing the wound bed for new tissue growth.

(iii) **Proliferation:** After the inflammation is settled, the process of wound repair is initiated. The new tissue regeneration begins with cell proliferation (keratinocyte) and formation of new blood vessels (neovascularization).

(iv) **Maturation/remodeling:** This is the final phase of wound healing. During the maturation phase, the newly formed tissue slowly gains strength and flexibility. Collagen fibers reorganize, and the new tissue gradually becomes more like the surrounding undamaged tissue. This phase can take a long time, sometimes years, depending on the severity of the wound.

Each phase of wound healing is crucial, and the process is highly regulated by various cellular and biochemical factors. Any disruption in this process can lead to impaired healing or complications like chronic wounds or scarring.^{50,51}

1.2.2.2. Chronic wound healing

The altered healing occurs due to various factors, such as impeding inflammation, hindered re-epithelialization, an increase in protease activity, impaired angiogenesis, and persisting infection (**Figure 1.6**). The global wound care market is projected to grow at a compound annual growth rate of 4.61% from 2023 to 2030. Chronic wounds impose significant expenses on healthcare systems and have severe effects on patients. Therefore, chronic non-healing wounds and excessive scarring represent a significant challenge for both patients and healthcare systems, prompting an increased focus on developing more effective treatment methods.^{52,53}

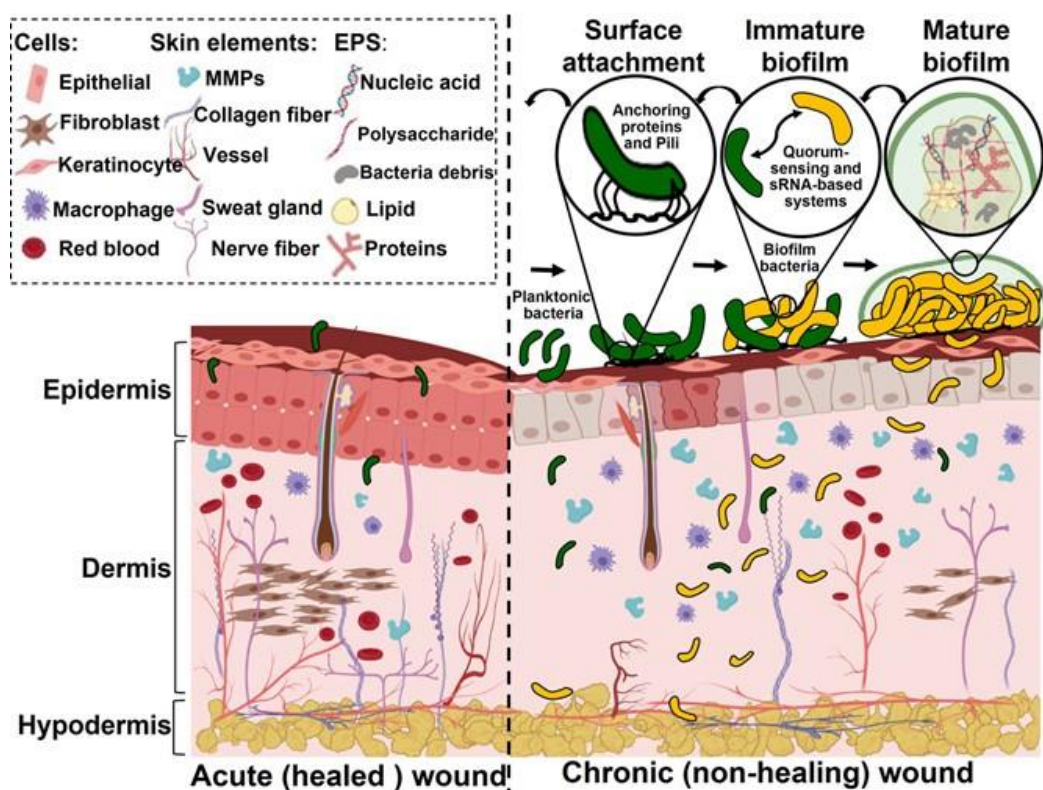


Figure 1.6. Comparison in healing of normal wound vs altered healing in biofilm infected chronic wound. Reproduced with kind permission from Darvishi et al, *Angew Chem Int Ed* **2022**, 61 (13), e202112218 © 2022 Wiley-VCH GmbH.

Role of biofilms in chronic wounds

Open wounds create conditions that allow microbes to invade and infect the wound site, resulting in activation of host immune system to combat these bacteria. Ischemic and necrotic tissues in ulcers increase the susceptibility of the wound to bacterial infection. These bacteria often develop biofilms, which are found in 60% of chronic wounds.⁵⁴ Biofilms are self-secretory matrix composed of heterogeneous bacterial population, polysaccharides, and extracellular DNA. This matrix offers a safe niche, enabling bacteria to withstand antibiotics or host environmental stress. As biofilms mature, they undergo dynamic phenotypic alterations. This results in antimicrobial resistance and the progression of wounds to a chronic state. Conventionally, biofilms are removed by physical aggressive debridement in severe cases or managed by using high doses and highly penetrating antibiotics. Unfortunately, these approaches fail to counter this problem, resulting in relapse of infection and immense side effects to host cells.

Nanomaterials for wound healing

Various types of antimicrobial nanoparticles have been explored for healing of these stalled wounds. Initially, nanotechnology was utilized to develop scaffolds for tissue engineering and

improvisation in traditional gauze dressing. With advancement in technology, focus has shifted to development of nanomaterials having intrinsic bioactivity, like antimicrobial, antioxidant, anti-inflammatory, antibiofilm properties (**Figure 1.7**). These properties are mainly due to the size, charge, shape, and presence of certain functional groups in nanomaterials.⁵⁵

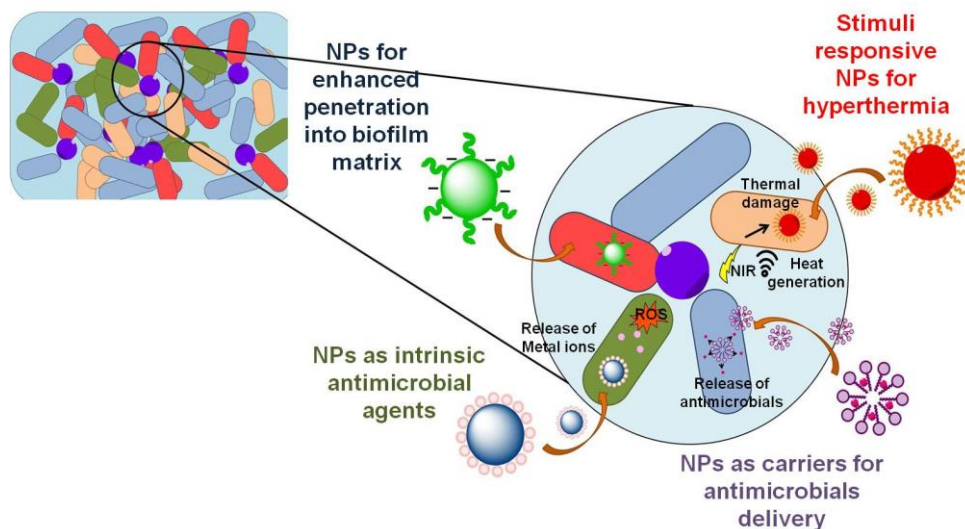


Figure 1.7. The mechanisms of action of various nanoparticle-based treatments for biofilm infected chronic wounds.

1.2.2.3. Rationale design of nanomaterials for the treatment of biofilm-infected chronic wounds

In order to develop effective strategies for prevention and treatment of biofilm infected wounds, it is imperative to understand the fundamental biology of biofilm formation. There are several stages which lead to an established biofilm

(i) **Surface attachment:** In this stage free flowing planktonic bacteria attach to both biotic and abiotic surfaces, via various forces like van der Waals, hydrophobic interactions or electrostatic interactions. Cell adhesion molecules play an important role at this stage.

(ii) **Formation of biofilm:** After successful adherence, these bacteria continue to divide rapidly and form micro colonies within the EPS matrix secreted by these cells itself.

(iii) **Biofilm maturation:** The existing microcolonies now grow in size and attain a 3D shape, thus providing structural stability to bacterial cells. This stage is crucial as antibiotics fail at to enter the biofilm.

(iv) **Dispersion of biofilm:** In final stage, some bacteria from mature biofilm starts detachment from substrate to relocate to different tissue and form new colonies there.

The lifecycle of biofilm thus heavily relies on adhesion molecules, EPS matrix and cell to cell communication also known as quorum sensing.⁵⁶⁻⁵⁸ Nanomaterial mainly act in two stages to counter biofilms, as briefed below:

(i) **Biofilm inhibition:** Most antimicrobial nanomaterials fall in this category. They inhibit

the initial attachment of planktonic cells to surfaces due to the excellent antibacterial properties and prevent proliferation of bacteria. Some nanomaterials, such as dextran-coated iron oxide particles developed by Naha *et al.*^{59,60} facilitate the generation of free radicals and thus kill bacteria. Metal nanoparticles, like Ag, Cu, and Au NPs act on the bacterial cell membrane and alter the permeability resulting in cell leakage and death. Goda *et al.*⁶¹ fabricated Ag NPs using pomegranate extract and observed that it possessed potent antibiofilm activity. Polymers, PVP and EC, stabilized Ag NP coating on urinary catheter, showed significant biofilm inhibition on clinical isolates in studies by Rugaie *et al.*⁶² Some nanomaterials hamper the bacterial cell to cell communication / quorum sensing (QS) through specific signaling pathways to inhibit the biofilm formation.⁶³ Elshaer *et al.* developed gold and selenium NPs to inhibit QS.⁶⁴ Similarly, functionalized chitosan showed QS inhibition property.⁶⁵

(ii) **Disruption of established biofilm:** The EPS matrix provides effective shield to protect the bacterial population within and it becomes very challenging to eradicate a mature biofilm. Ultrasmall nanoparticles due to their size can penetrate the EPS matrix and release the therapeutic agent and help in the disruption of biofilm as shown by Slomberg *et al.*⁶⁶ Cationic nanoparticles interact with anionic EPS matrix, and exert their bactericidal action.⁶⁷ Nanozymes, like cerium oxide due to DNase action cause matrix degradation of already established biofilm.⁶⁸

Many nanomaterials have been approved for clinical use by competent authorities as few have been listed in **Table 1.2**. The existing nanotechnology-based approaches are promising but new resistant species are emerging, which are capable of tolerating nanomedicine due to the dynamic evolution/selection pressure in bacterial population.⁶⁹ Therefore, new multifunctional nanomaterials are being explored and have lot of scope to act on multiple pathways to counter the chances of bacterial resistance.

Table 1.2. Some FDA approved antimicrobial nanoparticles.

Nanoparticles	Application	Approval	Reference
Ag NPs	Wound dressing	FDA	Burduşel <i>et al.</i> ⁷⁰
ZnO NPs	Antibacterial	FDA	Vassallo <i>et al.</i> ⁷¹
Au NPs	Photothermal therapy	FDA	Sibuyi et al. ⁷²
Dendrimer based NPs (VivaGel® BV)	Anti-infective for the prevention of recurrent bacterial vaginosis	FDA	Halwani <i>et al.</i> ⁷³

1.2.3. Osteoporosis

Osteoporosis is one of the most prevalent skeletal disorders, which is characterized by the reduced bone mineral density and higher risk of fractures.⁷⁴ The decreased bone mineral density results in mild symptoms in affected individuals until the onset of fragility fractures. Such fractures contribute to a cascade of adverse outcomes, such as persistent pain, disability, diminished quality of life, and elevated mortality. Bone is composed of hard tissue, which is essential for the body's many operations. The outermost layer of bone, known as the cortical or compact bone, bears the majority of the body's weight and has a great resistance to bending and twisting. Bone marrow is found in the highly vascularized trabecular or cancellous bone, which is the inner spongy portion. In a healthy person, osteoblasts produce bone while osteoclasts break it down, allowing for the efficient repair of any cracks or imperfections brought on by daily activities. But in an osteoporotic person, the trabecular area in particular loses bulk and osteoclast activity supersedes that of osteoblasts. The fewer connecting sites cause the bone to become more brittle, which is one of the main factors in the development of osteoporosis hormonal fluctuations along with age, particularly postmenopausal estrogen insufficiency in women and ageing.⁷⁵ The world's ageing population is causing osteoporosis to become a serious public health concern. Every year, over 9 million fragility fractures occur worldwide and approximately 200 million individuals are diagnosed with osteoporosis.⁷⁶ Primary osteoporosis and secondary osteoporosis are the two kinds of osteoporosis. Primary osteoporosis results from estrogen deficiency, commonly known as postmenopausal osteoporosis whereas type 2 osteoporosis affects both man and women and is commonly caused by ageing, it is also known as senile osteoporosis.⁷⁷

Bone formation

Bone is a connective tissue consisting of around 50% water and solid part consists of around 76% of calcium salt and 33% of cellular material. Bone cells including osteoblast, osteoclast, and chondrocytes. The maintenance of normal bone homeostasis depends on the balance between osteoblast and osteoclast activity. The primary cell type that forms bones is osteoblasts.^{78,79} Extracellular matrix proteins, like alkaline phosphatase, osteopontin, osteocalcin, and type I collagen are secreted by these cells. Multiple osteoblasts work together to form an osteon, which is a unit of bone. Large multinucleated cells called osteoclasts are primarily responsible for the resorption of bone. Originating from the hematopoietic lineage, these cells undergo differentiation into mature osteoclasts by the action of RANKL and macrophage colony-stimulating factor (M-CSF).⁸⁰ The skeleton receives structural support from the type I collagen and calcium deposited as hydroxyapatite. Bone formation process is called ossification or osteogenesis. After the formation of osteoblastic lines with progenitor cells, three phases of cell differentiation begin, which includes proliferation, matrix formation, and mineralization. The formation of bone is divided into two processes including intramembranous ossification and endochondral ossification.⁸¹ The bone remodeling is broadly

divided into four distinct phases known as resting phase, bone resorption, bone formation and bone mineralization, carried out in controlled manner by different cell types (**Figure 1.8**).

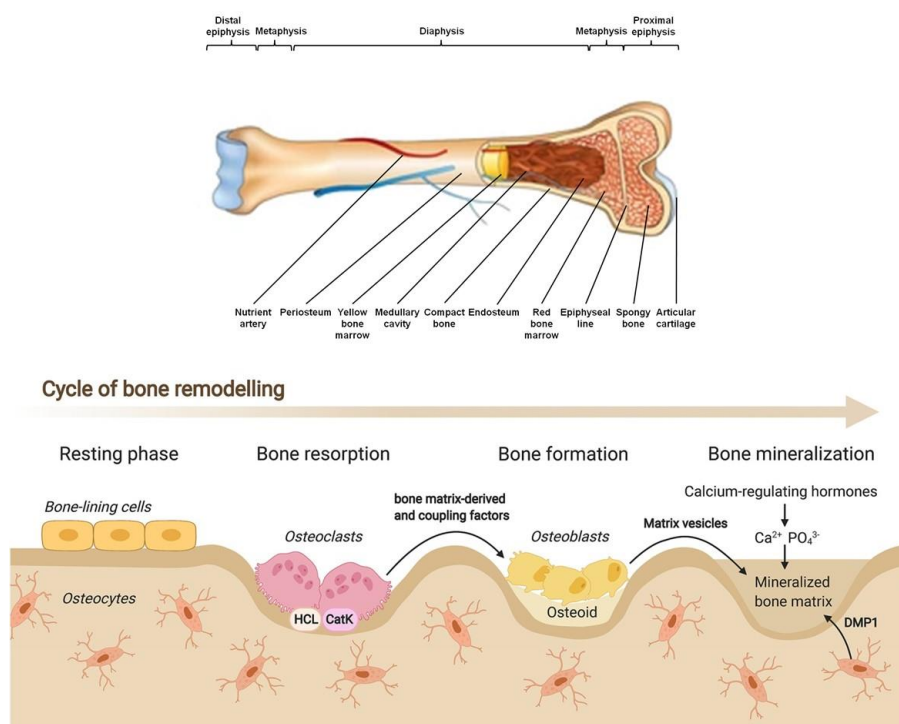


Figure 1.8. Structure of bone and physiological process of bone remodeling. Reproduced with kind permission from Winter *et al.*, *JBMR Plus*, **2021**, 5(10), 10504. ©2021Wiley.

1.2.3.1 Management of OP

Various drugs and therapeutic approaches have been effectively used for the treatment of osteoporosis. Most therapeutic efforts to prevent fracture and limit bone loss involve anti-resorptive medicines such as bisphosphonates, which target osteoclasts and enhance bone strength. Also, anabolic steroids, such as estrogens and recombinant human parathyroid hormone (rPTH) are used to inhibit apoptosis of osteoblast and aid the bone growth. Since the nature of this disease is such that it leads to the chronic use of these drugs, which results in severe side effects in patients.^{82,83} Thus, there is an urgent need to explore drug-free nanoparticulate systems to treat this bone disorder. Various nanomaterials have been explored for restoring the normal remodeling process and aid the bone tissue regeneration via different mechanism as discussed below (**Figure 1.9**).

Inhibition of bone resorption

Inhibition of bone resorption will prevent further bone loss. Various nanoparticles, such as gold, silver, hydroxyapatite and cerium NPs have been found to inhibit the bone resorption.^{84,85} Bai *et al.* reported the anti-resorption property of carboxylated gold nanoparticles.⁸⁶ Another study by Nah *et al.* showed inhibitory effect of vitamin D conjugated gold nanoparticles on osteoclast differentiation.⁸⁷ Silver nanoparticles have been found to have anti-resorptive property as investigated by Lee *et al.*⁸⁸

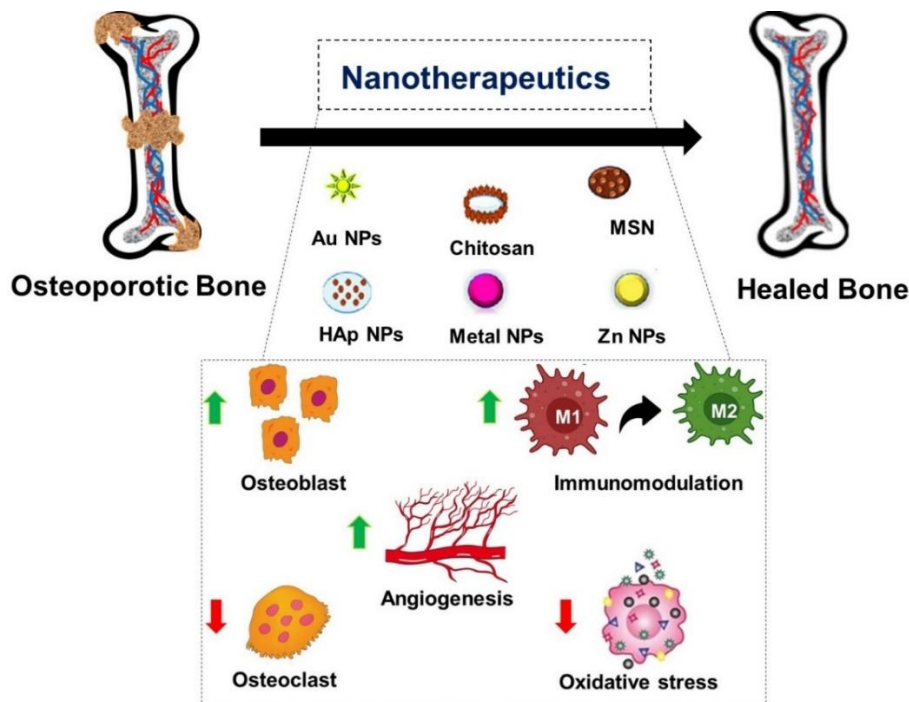


Figure 1.9. Nanoparticles to target various therapeutics targets for treating bone defects.

Stimulation of bone formation

Some organic and inorganic nanoparticles mediate osteoblast differentiation and promote bone growth, thus compensating the bone loss. Calcium phosphate-based material, like HAp, have been widely reported to have effect on osteoblast differentiation and enhance osteogenesis.⁷⁰ Silica nanoparticles have been found to have osteogenic potential as reported by multiple studies.^{89,90} Lee *et al.* demonstrated the osteogenic and biomineralization property of zinc oxide nanoparticles.⁹¹

Other factors playing a role in OP

Besides above-mentioned processes, there are some other factors, which play significant role in OP.

Mitigation of oxidative stress

Oxidative stress disrupts the bone remodeling process, creating an imbalance in hemostasis between osteoclasts and osteoblasts activity. This results in metabolic bone diseases and contribute to the development of skeletal system disorders, such as osteoporosis.^{92,93} There are reports, which suggest that inhibition of oxidative stress can positively augment bone mass. Shen *et al.* showed early osseointegration using Sr-doped titanium implants.⁹⁴ Similarly improved osteogenic activity was observed by Zheng *et al.* using antioxidant Ce-doped BG NPs.⁹⁵ Zhu *et al.* showed enhanced bone formation using antioxidant and osteogenic coated orthopedic implant.⁹⁶

Immune regulation

Immune cells play a critical role in bone tissue regeneration by regulating bone homeostasis.

The immune system is involved in both early stages of bone healing, including the inflammatory phase, and as well as in the later stages of bone remodeling.⁹⁷ Nanoparticles having immunomodulatory properties have been found to have positive impact on healing of bone defects.⁹⁸ Se-doped mesoporous bioglass promoted bone regeneration through immunomodulation as demonstrated by Chen *et al.*⁹⁹ Osteoinductive and immunomodulatory calcium nerveronate NPs facilitated bone healing as reported by Ma *et al.*¹⁰⁰ Yin *et al.* fabricated a biomimetic nanocapsule consisting of lipopolysaccharide treated macrophage encapsulated in Au cage, which induced M2 polarization and aided in bone tissue repair.¹⁰¹ Thus, it would be interesting to explore nanoparticles functionalized with certain chemical moieties to impart favorable properties and create a multifunctional nanomaterial for management of multifactorial disease such as osteoporosis.

Table 1.3. Some marketed nanomedicine-based preparation for bone disorders.

Nanosystem type	Product name	Active ingredient	Indication	Reference
Liposome	Liposome	Mifamurtide	High grade osteosarcoma	Frampton ¹⁰²
Polymer steroid mixture	Zilretta®	Triamcinolone acetonide	Knee osteoarthritis	Paik <i>et al.</i> ¹⁰³
Nanoparticle	BelOSTO	Hydroxyapatite	Bone substitute	Bhattacharyya <i>et al.</i> ¹⁰⁴

1.3. Knowledge gaps in the field

Nanoparticulate-based systems, mainly liposomes, have been widely explored for ocular drug delivery. There has been less focus on using bioactive nanomaterials as delivery vehicles. To address this gap, we have developed a nanoparticulate system from bioactive polymers having intrinsic antimicrobial and mucoadhesive properties, and loaded it with ciprofloxacin to treat bacterial ocular infections. In case of ocular bacterial infections, this approach not only assures efficient delivery but synergic/additive therapeutic value as well. Our nanoparticulate system exhibited high drug loading and sustained release, which resulted in excellent antibacterial properties. It also showed good mucoadhesive property, which is likely to enhance drug retention in eye.

New functional material having multiple actions are the need of hour to counter the antimicrobial resistance in biofilm. The existing nanomaterials can be modulated to impart new functions and promote wound healing in non-healing wounds. Composite nanomaterial offers the advantage of integrating two materials and creating a nanomaterial with improved and enhanced effects. We have developed a nanocomposite of cerium and silica nanoparticles

to address the challenge associated with their use

Oxidative stress is one of the major etiological factors responsible for disease progression in osteoporosis but existing therapeutics mainly focus on inhibiting bone resorption and improving bone mass, and effect of antioxidants are majorly ignored. Thus, the nanomaterial having antioxidant, osteogenic and angiogenic properties can be a promising alternative to ensure the treatment of bone defects and facilitate new bone formation.

1.4. Thesis objectives

Nanomaterials have gained immense attention and these are being actively explored for various biomedical application, like drug delivery, wound healing, and tissue engineering. The overall aim of this thesis was to explore new functional nanomaterials to address and overcome the existing challenges associated with current strategies (**Figure 1.10**). The specific thesis objectives are listed below:

- To develop nanocarrier having intrinsic antibacterial activity and mucoadhesive property to deliver and aid the sustained release of ciprofloxacin to treat ocular infections. Ocular drug delivery is challenging owing to the nature of ocular tissues and nanomaterials investigated for drug delivery to treat ocular infections are less effective due to risk of antimicrobial resistance.
- To fabricate cationic nanocomposite incorporating mesoporous silica nanoparticles with highly porous morphology and large surface area and bioactive cerium oxide nanoparticles to target the biofilm infected chronic wounds. Biofilms are the most common cause of chronic wound, and functional nanomaterials acting on multiple pathways are very much needed to restore the stalled healing.
- To explore antioxidant and osteogenic, thiolated silica mesoporous nanoparticles (MSN-SH) to prevent disease progression in osteoporosis. The improved osteogenic and antioxidant properties will promote new bone growth and reduce the course of the disease. Oxidative stress has been identified as major player for disease progression but nanomaterials having intrinsic osteogenic properties that are being currently explored often lack antioxidant capabilities.

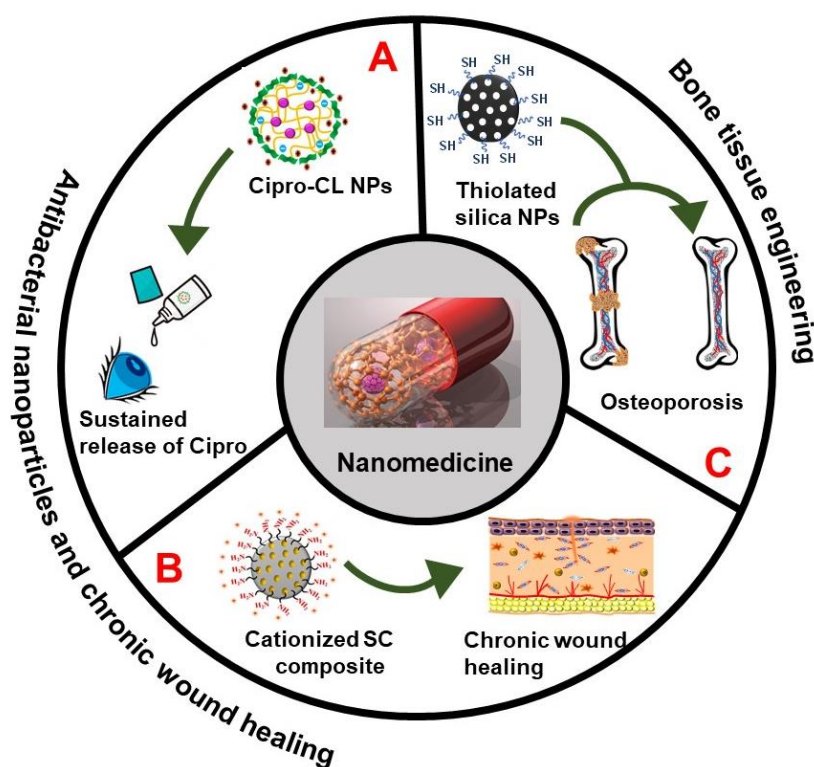


Figure 1.10. Objectives of the thesis- to develop functional nanomaterials for ocular infections, chronic wound healing, and osteoporosis.

1.5. Thesis outline

The aim of this thesis was to fabricate functional nanomaterials for ocular infections, wound healing, and osteoporosis. The chapter 1 includes an overview on nanomaterials used for biomedical applications, such as ophthalmic drug delivery, chronic wound healing, and osteoporosis. This chapter also provides a survey of work done in each area and identification of existing knowledge gaps along with the thesis objectives and outline of the thesis. In chapter 2, we have incorporated the development of antibacterial and mucoadhesive lecithin/chitosan nanoparticles for the sustained release of ciprofloxacin, to treat ocular bacterial infections. The chapter 3 describes the development of cationized silica ceria nanocomposite having antioxidant, antibacterial, and antibiofilm properties for restoring healing in biofilm stalled chronic wounds. The development of antioxidant and osteogenic, thiolated mesoporous silica nanoparticles for the treatment of osteoporosis has been discussed in chapter 4. The conclusions and prospectives of the thesis are presented in chapter 5.

References

- (1) Bayda, S.; Adeel, M.; Tuccinardi, T.; Cordani, M.; Rizzolio, F. The History of Nanoscience and Nanotechnology: From Chemical–Physical Applications to Nanomedicine. *Molecules* **2019**, *25* (1), 112. <https://doi.org/10.3390/molecules25010112>.
- (2) Thapa, R. K.; Kim, J. O. Nanomedicine-Based Commercial Formulations: Current Developments and Future Prospects. *J. Pharm. Investig.* **2023**, *53* (1), 19–33. <https://doi.org/10.1007/s40005-022-00607-6>.
- (3) Mekuye, B.; Abera, B. Nanomaterials: An Overview of Synthesis, Classification, Characterization, and Applications. *Nano Select* **2023**, *4* (8), 486–501. <https://doi.org/10.1002/nano.202300038>.
- (4) Joudeh, N.; Linke, D. Nanoparticle Classification, Physicochemical Properties, Characterization, and Applications: A Comprehensive Review for Biologists. *J Nanobiotechnol* **2022**, *20* (1), 262. <https://doi.org/10.1186/s12951-022-01477-8>.
- (5) Saha, S.; Bansal, S.; Khanuja, M. Classification of Nanomaterials and Their Physical and Chemical Nature. In *Nano-enabled Agrochemicals in Agriculture*; Elsevier, 2022; pp 7–34. <https://doi.org/10.1016/B978-0-323-91009-5.00001-X>.
- (6) Baig, N.; Kammakakam, I.; Falath, W. Nanomaterials: A Review of Synthesis Methods, Properties, Recent Progress, and Challenges. *Mater. Adv.* **2021**, *2* (6), 1821–1871. <https://doi.org/10.1039/D0MA00807A>.
- (7) Chenthamara, D.; Subramaniam, S.; Ramakrishnan, S. G.; Krishnaswamy, S.; Essa, M. M.; Lin, F.-H.; Qoronfleh, M. W. Therapeutic Efficacy of Nanoparticles and Routes of Administration. *Biomater Res* **2019**, *23* (1), 20. <https://doi.org/10.1186/s40824-019-0166-x>.
- (8) Li, S.-D.; Huang, L. Pharmacokinetics and Biodistribution of Nanoparticles. *Mol. Pharmaceutics* **2008**, *5* (4), 496–504. <https://doi.org/10.1021/mp800049w>.
- (9) Zhang, A.; Meng, K.; Liu, Y.; Pan, Y.; Qu, W.; Chen, D.; Xie, S. Absorption, Distribution, Metabolism, and Excretion of Nanocarriers in Vivo and Their Influences. *Advances in Colloid and Interface Science* **2020**, *284*, 102261. <https://doi.org/10.1016/j.cis.2020.102261>.
- (10) Shan, X.; Gong, X.; Li, J.; Wen, J.; Li, Y.; Zhang, Z. Current Approaches of Nanomedicines in the Market and Various Stage of Clinical Translation. *Acta Pharmaceutica Sinica B* **2022**, *12* (7), 3028–3048. <https://doi.org/10.1016/j.apsb.2022.02.025>.
- (11) Namiot, E. D.; Sokolov, A. V.; Chubarev, V. N.; Tarasov, V. V.; Schiöth, H. B. Nanoparticles in Clinical Trials: Analysis of Clinical Trials, FDA Approvals and Use for COVID-19 Vaccines. *IJMS* **2023**, *24* (1), 787. <https://doi.org/10.3390/ijms24010787>.

- (12) Chamundeeswari, M.; Jeslin, J.; Verma, M. L. Nanocarriers for Drug Delivery Applications. *Environ Chem Lett* **2019**, *17* (2), 849–865. <https://doi.org/10.1007/s10311-018-00841-1>.
- (13) Aliabadi, H.; Elhasi, S.; Mahmud, A.; Gulamhusein, R.; Mahdipoor, P.; Lavasanifar, A. Encapsulation of Hydrophobic Drugs in Polymeric Micelles through Co-Solvent Evaporation: The Effect of Solvent Composition on Micellar Properties and Drug Loading. *International Journal of Pharmaceutics* **2007**, *329* (1–2), 158–165. <https://doi.org/10.1016/j.ijpharm.2006.08.018>.
- (14) Gomezgaete, C.; Tsapis, N.; Besnard, M.; Bochot, A.; Fattal, E. Encapsulation of Dexamethasone into Biodegradable Polymeric Nanoparticles. *International Journal of Pharmaceutics* **2007**, *331* (2), 153–159. <https://doi.org/10.1016/j.ijpharm.2006.11.028>.
- (15) Okamoto, Y.; Taguchi, K.; Sakuragi, M.; Imoto, S.; Yamasaki, K.; Otagiri, M. Preparation, Characterization, and in Vitro/in Vivo Evaluation of Paclitaxel-Bound Albumin-Encapsulated Liposomes for the Treatment of Pancreatic Cancer. *ACS Omega* **2019**, *4* (5), 8693–8700. <https://doi.org/10.1021/acsomega.9b00537>.
- (16) Farzan, M.; Roth, R.; Schoelkopf, J.; Huwyler, J.; Puchkov, M. The Processes behind Drug Loading and Release in Porous Drug Delivery Systems. *European Journal of Pharmaceutics and Biopharmaceutics* **2023**, *189*, 133–151. <https://doi.org/10.1016/j.ejpb.2023.05.019>.
- (17) Zarkesh, K.; Heidari, R.; Iranpour, P.; Azarpira, N.; Ahmadi, F.; Mohammadi-Samani, S.; Farjadian, F. Theranostic Hyaluronan Coated EDTA Modified Magnetic Mesoporous Silica Nanoparticles for Targeted Delivery of Cisplatin. *SSRN Journal* **2022**. <https://doi.org/10.2139/ssrn.4186547>.
- (18) Liu, J.-M.; Zhang, D.-D.; Fang, G.-Z.; Wang, S. Erythrocyte Membrane Bioinspired Near-Infrared Persistent Luminescence Nanocarriers for in Vivo Long-Circulating Bioimaging and Drug Delivery. *Biomaterials* **2018**, *165*, 39–47. <https://doi.org/10.1016/j.biomaterials.2018.02.042>.
- (19) Yan, J.; Xu, X.; Zhou, J.; Liu, C.; Zhang, L.; Wang, D.; Yang, F.; Zhang, H. Fabrication of a pH/Redox-Triggered Mesoporous Silica-Based Nanoparticle with Microfluidics for Anticancer Drugs Doxorubicin and Paclitaxel Codelivery. *ACS Appl. Bio Mater.* **2020**, *3* (2), 1216–1225. <https://doi.org/10.1021/acsabm.9b01111>.
- (20) Kumari, A.; Singla, R.; Guliani, A.; Yadav, S. K. Nanoencapsulation for Drug Delivery. *EXCLI J* **2014**, *13*, 265–286.
- (21) Meng, H.; Liong, M.; Xia, T.; Li, Z.; Ji, Z.; Zink, J. I.; Nel, A. E. Engineered Design of Mesoporous Silica Nanoparticles to Deliver Doxorubicin and P-Glycoprotein siRNA to Overcome Drug Resistance in a Cancer Cell Line. *ACS Nano* **2010**, *4* (8), 4539–4550. <https://doi.org/10.1021/nn100690m>.

- (22) Ke, X.; Tang, H.; Mao, H.-Q. Effective Encapsulation of Curcumin in Nanoparticles Enabled by Hydrogen Bonding Using Flash Nanocomplexation. *International Journal of Pharmaceutics* **2019**, *564*, 273–280. <https://doi.org/10.1016/j.ijpharm.2019.04.053>.
- (23) Bermejo, M.; Sanchez-Dengra, B.; Gonzalez-Alvarez, M.; Gonzalez-Alvarez, I. Oral Controlled Release Dosage Forms: Dissolution versus Diffusion. *Expert Opinion on Drug Delivery* **2020**, *17* (6), 791–803. <https://doi.org/10.1080/17425247.2020.1750593>.
- (24) Kubo, T.; Tachibana, K.; Naito, T.; Mukai, S.; Akiyoshi, K.; Balachandran, J.; Otsuka, K. Magnetic Field Stimuli-Sensitive Drug Release Using a Magnetic Thermal Seed Coated with Thermal-Responsive Molecularly Imprinted Polymer. *ACS Biomater. Sci. Eng.* **2019**, *5* (2), 759–767. <https://doi.org/10.1021/acsbiomaterials.8b01401>.
- (25) Cao, Y.; Wang, B.; Wang, Y.; Lou, D. Dual Drug Release from Core–Shell Nanoparticles with Distinct Release Profiles. *Journal of Pharmaceutical Sciences* **2014**, *103* (10), 3205–3216. <https://doi.org/10.1002/jps.24116>.
- (26) Lee, J. H.; Yeo, Y. Controlled Drug Release from Pharmaceutical Nanocarriers. *Chem Eng Sci* **2015**, *125*, 75–84. <https://doi.org/10.1016/j.ces.2014.08.046>.
- (27) Deepthi, K. G.; Prabakaran, S. R. Ocular Bacterial Infections: Pathogenesis and Diagnosis. *Microbial Pathogenesis* **2020**, *145*, 104206. <https://doi.org/10.1016/j.micpath.2020.104206>.
- (28) Ahmed, S.; Amin, M. M.; Sayed, S. Ocular Drug Delivery: A Comprehensive Review. *AAPS PharmSciTech* **2023**, *24* (2), 66. <https://doi.org/10.1208/s12249-023-02516-9>.
- (29) Suri, R.; Beg, S.; Kohli, K. Target Strategies for Drug Delivery Bypassing Ocular Barriers. *Journal of Drug Delivery Science and Technology* **2020**, *55*, 101389. <https://doi.org/10.1016/j.jddst.2019.101389>.
- (30) Bachu, R.; Chowdhury, P.; Al-Saedi, Z.; Karla, P.; Boddu, S. Ocular Drug Delivery Barriers—Role of Nanocarriers in the Treatment of Anterior Segment Ocular Diseases. *Pharmaceutics* **2018**, *10* (1), 28. <https://doi.org/10.3390/pharmaceutics10010028>.
- (31) Onugwu, A. L.; Nwagwu, C. S.; Onugwu, O. S.; Echezona, A. C.; Agbo, C. P.; Ihim, S. A.; Emeh, P.; Nnamani, P. O.; Attama, A. A.; Khutoryanskiy, V. V. Nanotechnology Based Drug Delivery Systems for the Treatment of Anterior Segment Eye Diseases. *Journal of Controlled Release* **2023**, *354*, 465–488. <https://doi.org/10.1016/j.jconrel.2023.01.018>.
- (32) Gorantla, S.; Rapalli, V. K.; Waghule, T.; Singh, P. P.; Dubey, S. K.; Saha, R. N.; Singhvi, G. Nanocarriers for Ocular Drug Delivery: Current Status and Translational Opportunity. *RSC Adv.* **2020**, *10* (46), 27835–27855. <https://doi.org/10.1039/D0RA04971A>.

- (33) Li, S.; Chen, L.; Fu, Y. Nanotechnology-Based Ocular Drug Delivery Systems: Recent Advances and Future Prospects. *J Nanobiotechnol* **2023**, *21* (1), 232. <https://doi.org/10.1186/s12951-023-01992-2>.
- (34) Eroglu, Y. I. A Comparative Review of Haute Autorité de Santé and National Institute for Health and Care Excellence Health Technology Assessments of Ikervis® to Treat Severe Keratitis in Adult Patients with Dry Eye Disease Which Has Not Improved despite Treatment with Tear Substitutes. *Journal of Market Access & Health Policy* **2017**, *5* (1), 1336043. <https://doi.org/10.1080/20016689.2017.1336043>.
- (35) Wentz, S. M.; Price, F.; Harris, A.; Siesky, B.; Ciulla, T. Efficacy and Safety of Bromfenac 0.075% Formulated in DuraSite for Pain and Inflammation in Cataract Surgery. *Expert Opinion on Pharmacotherapy* **2019**, *20* (14), 1703–1709. <https://doi.org/10.1080/14656566.2019.1645834>.
- (36) Mandal, A.; Gote, V.; Pal, D.; Ogundele, A.; Mitra, A. K. Ocular Pharmacokinetics of a Topical Ophthalmic Nanomicellar Solution of Cyclosporine (Cequa®) for Dry Eye Disease. *Pharm Res* **2019**, *36* (2), 36. <https://doi.org/10.1007/s11095-018-2556-5>.
- (37) Kagkellaris, K.; Panayiotakopoulos, G.; Georgakopoulos, C. D. Nanotechnology-Based Formulations to Amplify Intraocular Bioavailability. *Ophthalmol Eye Dis* **2022**, *14*, 251584142211123. <https://doi.org/10.1177/25158414221112356>.
- (38) Akhter, M. H.; Ahmad, I.; Alshahrani, M. Y.; Al-Harbi, A. I.; Khalilullah, H.; Afzal, O.; Altamimi, A. S. A.; Najib Ullah, S. N. M.; Ojha, A.; Karim, S. Drug Delivery Challenges and Current Progress in Nanocarrier-Based Ocular Therapeutic System. *Gels* **2022**, *8* (2), 82. <https://doi.org/10.3390/gels8020082>.
- (39) Tsai, C.-H.; Wang, P.-Y.; Lin, I.-C.; Huang, H.; Liu, G.-S.; Tseng, C.-L. Ocular Drug Delivery: Role of Degradable Polymeric Nanocarriers for Ophthalmic Application. *IJMS* **2018**, *19* (9), 2830. <https://doi.org/10.3390/ijms19092830>.
- (40) Javed, S.; Abbas, G.; Shah, S.; Rasul, A.; Irfan, M.; Saleem, A.; Hosny, K. M.; Bukhary, S. M.; Safhi, A. Y.; Sabei, F. Y.; Majrashi, M. A.; Alkhalidi, H. M.; Alissa, M.; Khan, S. M.; Hanif, M. Tobramycin-Loaded Nanoparticles of Thiolated Chitosan for Ocular Drug Delivery: Preparation, Mucoadhesion and Pharmacokinetic Evaluation. *Heliyon* **2023**, *9* (9), e19877. <https://doi.org/10.1016/j.heliyon.2023.e19877>.
- (41) Sogias, I. A.; Williams, A. C.; Khutoryanskiy, V. V. Why Is Chitosan Mucoadhesive? *Biomacromolecules* **2008**, *9* (7), 1837–1842. <https://doi.org/10.1021/bm800276d>.
- (42) Herdiana, Y.; Wathoni, N.; Shamsuddin, S.; Muchtaridi, M. Drug Release Study of the Chitosan-Based Nanoparticles. *Heliyon* **2022**, *8* (1), e08674. <https://doi.org/10.1016/j.heliyon.2021.e08674>.

- (43) Aranaz, I.; Alcántara, A. R.; Civera, M. C.; Arias, C.; Elorza, B.; Heras Caballero, A.; Acosta, N. Chitosan: An Overview of Its Properties and Applications. *Polymers* **2021**, *13* (19), 3256. <https://doi.org/10.3390/polym13193256>.
- (44) Zamboulis, A.; Nanaki, S.; Michailidou, G.; Koumentakou, I.; Lazaridou, M.; Ainali, N. M.; Xanthopoulou, E.; Bikiaris, D. N. Chitosan and Its Derivatives for Ocular Delivery Formulations: Recent Advances and Developments. *Polymers* **2020**, *12* (7), 1519. <https://doi.org/10.3390/polym12071519>.
- (45) Bodmeier, R.; Chen, H.; Paeratakul, O. [No Title Found]. *Pharmaceutical Research* **1989**, *06* (5), 413–417. <https://doi.org/10.1023/A:1015987516796>.
- (46) Silva, N. C.; Silva, S.; Sarmento, B.; Pintado, M. Chitosan Nanoparticles for Daptomycin Delivery in Ocular Treatment of Bacterial Endophthalmitis. *Drug Delivery* **2015**, *22* (7), 885–893. <https://doi.org/10.3109/10717544.2013.858195>.
- (47) Das, B.; Nayak, A. K.; Mallick, S. Lipid-Based Nanocarriers for Ocular Drug Delivery: An Updated Review. *Journal of Drug Delivery Science and Technology* **2022**, *76*, 103780. <https://doi.org/10.1016/j.jddst.2022.103780>.
- (48) Badran, M. M.; Alomrani, A. H.; Almomen, A.; Bin Jordan, Y. A.; Abou El Ela, A. E. S. Novel Metoprolol-Loaded Chitosan-Coated Deformable Liposomes in Thermosensitive In Situ Gels for the Management of Glaucoma: A Repurposing Approach. *Gels* **2022**, *8* (10), 635. <https://doi.org/10.3390/gels8100635>.
- (49) Rajendran, A. K.; Kim, H. D.; Kim, J.-W.; Bae, J. W.; Hwang, N. S. Nanotechnology in Tissue Engineering and Regenerative Medicine. *Korean J. Chem. Eng.* **2023**, *40* (2), 286–301. <https://doi.org/10.1007/s11814-022-1363-1>.
- (50) Falanga, V.; Isseroff, R. R.; Soulika, A. M.; Romanelli, M.; Margolis, D.; Kapp, S.; Granick, M.; Harding, K. Chronic Wounds. *Nat Rev Dis Primers* **2022**, *8* (1), 50. <https://doi.org/10.1038/s41572-022-00377-3>.
- (51) Grubbs, H.; Manna, B. Wound Physiology. In *StatPearls*; StatPearls Publishing: Treasure Island (FL), 2023.
- (52) Barroso, A.; Mestre, H.; Ascenso, A.; Simões, S.; Reis, C. Nanomaterials in Wound Healing: From Material Sciences to Wound Healing Applications. *Nano Select* **2020**, *1* (5), 443–460. <https://doi.org/10.1002/nano.202000055>.
- (53) Solanki, D.; Vinchhi, P.; Patel, M. M. Design Considerations, Formulation Approaches, and Strategic Advances of Hydrogel Dressings for Chronic Wound Management. *ACS Omega* **2023**, *8* (9), 8172–8189. <https://doi.org/10.1021/acsomega.2c06806>.
- (54) Tan, M. L. L.; Chin, J. S.; Madden, L.; Becker, D. L. Challenges Faced in Developing an Ideal Chronic Wound Model. *Expert Opinion on Drug Discovery* **2023**, *18* (1), 99–114. <https://doi.org/10.1080/17460441.2023.2158809>.

- (55) Darvishi, S.; Tavakoli, S.; Kharaziha, M.; Girault, H. H.; Kaminski, C. F.; Mela, I. Advances in the Sensing and Treatment of Wound Biofilms. *Angew Chem Int Ed* **2022**, *61* (13), e202112218. <https://doi.org/10.1002/anie.202112218>.
- (56) Mukherjee, A.; Bose, S.; Shao, A.; Das, S. K. Nanotechnology Based Therapeutic Approaches: An Advanced Strategy to Target the Biofilm of ESKAPE Pathogens. *Mater. Adv.* **2023**, *4* (12), 2544–2572. <https://doi.org/10.1039/D2MA00846G>.
- (57) Sahli, C.; Moya, S. E.; Lomas, J. S.; Gravier-Pelletier, C.; Briandet, R.; Hémadi, M. Recent Advances in Nanotechnology for Eradicating Bacterial Biofilm. *Theranostics* **2022**, *12* (5), 2383–2405. <https://doi.org/10.7150/thno.67296>.
- (58) Kumar, L.; Bisen, M.; Harjai, K.; Chhibber, S.; Azizov, S.; Lalhlenmawia, H.; Kumar, D. Advances in Nanotechnology for Biofilm Inhibition. *ACS Omega* **2023**, *8* (24), 21391–21409. <https://doi.org/10.1021/acsomega.3c02239>.
- (59) Xiong, X.; Huang, Y.; Lin, C.; Liu, X. Y.; Lin, Y. Recent Advances in Nanoparticulate Biomimetic Catalysts for Combating Bacteria and Biofilms. *Nanoscale* **2019**, *11* (46), 22206–22215. <https://doi.org/10.1039/C9NR05054J>.
- (60) Naha, P. C.; Liu, Y.; Hwang, G.; Huang, Y.; Gubara, S.; Jonnakuti, V.; Simon-Soro, A.; Kim, D.; Gao, L.; Koo, H.; Cormode, D. P. Dextran-Coated Iron Oxide Nanoparticles as Biomimetic Catalysts for Localized and pH-Activated Biofilm Disruption. *ACS Nano* **2019**, *13* (5), 4960–4971. <https://doi.org/10.1021/acsnano.8b08702>.
- (61) Goda, R. M.; El-Baz, A. M.; Khalaf, E. M.; Alharbi, N. K.; Elkhooly, T. A.; Shohayeb, M. M. Combating Bacterial Biofilm Formation in Urinary Catheter by Green Silver Nanoparticle. *Antibiotics* **2022**, *11* (4), 495. <https://doi.org/10.3390/antibiotics11040495>.
- (62) Rugaie, O. A.; Abdellatif, A. A. H.; El-Mokhtar, M. A.; Sabet, M. A.; Abdelfattah, A.; Alsharidah, M.; Aldubaib, M.; Barakat, H.; Abudoleh, S. M.; Al-Regaiey, K. A.; Tawfeek, H. M. Retardation of Bacterial Biofilm Formation by Coating Urinary Catheters with Metal Nanoparticle-Stabilized Polymers. *Microorganisms* **2022**, *10* (7), 1297. <https://doi.org/10.3390/microorganisms10071297>.
- (63) Alghamdi, S.; Khandelwal, K.; Pandit, S.; Roy, A.; Ray, S.; Alsaiani, A. A.; Aljuaid, A.; Almeshmadi, M.; Allahyani, M.; Sharma, R.; Anand, J.; Alshareef, A. A. Application of Nanomaterials as Potential Quorum Quenchers for Disease: Recent Advances and Challenges. *Progress in Biophysics and Molecular Biology* **2023**, *184*, 13–31. <https://doi.org/10.1016/j.pbiomolbio.2023.08.005>.
- (64) Elshaer, S. L.; Shaaban, M. I. Inhibition of Quorum Sensing and Virulence Factors of *Pseudomonas Aeruginosa* by Biologically Synthesized Gold and Selenium Nanoparticles. *Antibiotics* **2021**, *10* (12), 1461. <https://doi.org/10.3390/antibiotics10121461>.

- (65) Nag, M.; Lahiri, D.; Mukherjee, D.; Banerjee, R.; Garai, S.; Sarkar, T.; Ghosh, S.; Dey, A.; Ghosh, S.; Pattnaik, S.; Edinur, H. A.; Kari, Z. A.; Pati, S.; Ray, R. R. Functionalized Chitosan Nanomaterials: A Jammer for Quorum Sensing. *Polymers* **2021**, *13* (15), 2533. <https://doi.org/10.3390/polym13152533>.
- (66) Slomberg, D. L.; Lu, Y.; Broadnax, A. D.; Hunter, R. A.; Carpenter, A. W.; Schoenfisch, M. H. Role of Size and Shape on Biofilm Eradication for Nitric Oxide-Releasing Silica Nanoparticles. *ACS Appl. Mater. Interfaces* **2013**, *5* (19), 9322–9329. <https://doi.org/10.1021/am402618w>.
- (67) Olmo, J. A.-D.; Ruiz-Rubio, L.; Pérez-Alvarez, L.; Sáez-Martínez, V.; Vilas-Vilela, J. L. Antibacterial Coatings for Improving the Performance of Biomaterials. *Coatings* **2020**, *10* (2), 139. <https://doi.org/10.3390/coatings10020139>.
- (68) Liu, Z.; Wang, F.; Ren, J.; Qu, X. A Series of MOF/Ce-Based Nanozymes with Dual Enzyme-like Activity Disrupting Biofilms and Hindering Recolonization of Bacteria. *Biomaterials* **2019**, *208*, 21–31. <https://doi.org/10.1016/j.biomaterials.2019.04.007>.
- (69) Duan, S.; Wu, R.; Xiong, Y.-H.; Ren, H.-M.; Lei, C.; Zhao, Y.-Q.; Zhang, X.-Y.; Xu, F.-J. Multifunctional Antimicrobial Materials: From Rational Design to Biomedical Applications. *Progress in Materials Science* **2022**, *125*, 100887. <https://doi.org/10.1016/j.pmatsci.2021.100887>.
- (70) Burduşel, A.-C.; Gherasim, O.; Andronescu, E.; Grumezescu, A. M.; Fica, A. Inorganic Nanoparticles in Bone Healing Applications. *Pharmaceutics* **2022**, *14* (4), 770. <https://doi.org/10.3390/pharmaceutics14040770>.
- (71) Vassallo, A.; Silletti, M. F.; Faraone, I.; Milella, L. Nanoparticulate Antibiotic Systems as Antibacterial Agents and Antibiotic Delivery Platforms to Fight Infections. *Journal of Nanomaterials* **2020**, *2020*, 1–31. <https://doi.org/10.1155/2020/6905631>.
- (72) Sibuyi, N. R. S.; Moabelo, K. L.; Fadaka, A. O.; Meyer, S.; Onani, M. O.; Madiehe, A. M.; Meyer, M. Multifunctional Gold Nanoparticles for Improved Diagnostic and Therapeutic Applications: A Review. *Nanoscale Res Lett* **2021**, *16* (1), 174. <https://doi.org/10.1186/s11671-021-03632-w>.
- (73) Halwani, A. A. Development of Pharmaceutical Nanomedicines: From the Bench to the Market. *Pharmaceutics* **2022**, *14* (1), 106. <https://doi.org/10.3390/pharmaceutics14010106>.
- (74) Yang, T.-L.; Shen, H.; Liu, A.; Dong, S.-S.; Zhang, L.; Deng, F.-Y.; Zhao, Q.; Deng, H.-W. A Road Map for Understanding Molecular and Genetic Determinants of Osteoporosis. *Nat Rev Endocrinol* **2020**, *16* (2), 91–103. <https://doi.org/10.1038/s41574-019-0282-7>.
- (75) Lei, C.; Song, J.; Li, S.; Zhu, Y.; Liu, M.; Wan, M.; Mu, Z.; Tay, F. R.; Niu, L. Advances in Materials-Based Therapeutic Strategies against Osteoporosis. *Biomaterials* **2023**, *296*, 122066. <https://doi.org/10.1016/j.biomaterials.2023.122066>.

- (76) Deng, Y.; Wei, W.; Tang, P. Applications of Calcium-Based Nanomaterials in Osteoporosis Treatment. *ACS Biomater. Sci. Eng.* **2022**, *8* (2), 424–443. <https://doi.org/10.1021/acsbiomaterials.1c01306>.
- (77) Patel, D.; Wairkar, S. Bone Regeneration in Osteoporosis: Opportunities and Challenges. *Drug Deliv. and Transl. Res.* **2023**, *13* (2), 419–432. <https://doi.org/10.1007/s13346-022-01222-6>.
- (78) Mallorie, A.; Shine, B. Normal Bone Physiology, Remodelling and Its Hormonal Regulation. *Surgery (Oxford)* **2022**, *40* (3), 163–168. <https://doi.org/10.1016/j.mpsur.2021.12.001>.
- (79) Winter, E. M.; Kooijman, S.; Appelman-Dijkstra, N. M.; Meijer, O. C.; Rensen, P. C.; Schilperoort, M. Chronobiology and Chronotherapy of Osteoporosis. *JBMR Plus* **2021**, *5* (10), e10504. <https://doi.org/10.1002/jbm4.10504>.
- (80) Salhotra, A.; Shah, H. N.; Levi, B.; Longaker, M. T. Mechanisms of Bone Development and Repair. *Nat Rev Mol Cell Biol* **2020**, *21* (11), 696–711. <https://doi.org/10.1038/s41580-020-00279-w>.
- (81) Berendsen, A. D.; Olsen, B. R. Bone Development. *Bone* **2015**, *80*, 14–18. <https://doi.org/10.1016/j.bone.2015.04.035>.
- (82) Barry, M.; Pearce, H.; Cross, L.; Tatullo, M.; Gaharwar, A. K. Advances in Nanotechnology for the Treatment of Osteoporosis. *Curr Osteoporos Rep* **2016**, *14* (3), 87–94. <https://doi.org/10.1007/s11914-016-0306-3>.
- (83) Yang, L.; Gao, C.; Wei, D.; Yang, H.; Chen, T. Nanotechnology for Treating Osteoporotic Vertebral Fractures. *IJN* **2015**, 5139. <https://doi.org/10.2147/IJN.S85037>.
- (84) Babuska, V.; Kasi, P. B.; Chocholata, P.; Wiesnerova, L.; Dvorakova, J.; Vrzakova, R.; Nekleionova, A.; Landsmann, L.; Kulda, V. Nanomaterials in Bone Regeneration. *Applied Sciences* **2022**, *12* (13), 6793. <https://doi.org/10.3390/app12136793>.
- (85) Rouco, H.; García-García, P.; Briffault, E.; Diaz-Rodriguez, P. Modulating Osteoclasts with Nanoparticles: A Path for Osteoporosis Management? *WIREs Nanomed Nanobiotechnol* **2023**, *15* (4), e1885. <https://doi.org/10.1002/wnan.1885>.
- (86) Bai, X.; Gao, Y.; Zhang, M.; Chang, Y.; Chen, K.; Li, J.; Zhang, J.; Liang, Y.; Kong, J.; Wang, Y.; Liang, W.; Xing, G.; Li, W.; Xing, G. Carboxylated Gold Nanoparticles Inhibit Bone Erosion by Disturbing the Acidification of an Osteoclast Absorption Microenvironment. *Nanoscale* **2020**, *12* (6), 3871–3878. <https://doi.org/10.1039/C9NR09698A>.
- (87) Nah, H.; Lee, D.; Lee, J. S.; Lee, S. J.; Heo, D. N.; Lee, Y.-H.; Bang, J. B.; Hwang, Y.-S.; Moon, H.-J.; Kwon, I. K. Strategy to Inhibit Effective Differentiation of RANKL-Induced Osteoclasts Using Vitamin D-Conjugated Gold Nanoparticles. *Applied Surface Science* **2020**, *527*, 146765. <https://doi.org/10.1016/j.apsusc.2020.146765>.

- (88) Lee, D.; Ko, W.-K.; Kim, S. J.; Han, I.-B.; Hong, J. B.; Sheen, S. H.; Sohn, S. Inhibitory Effects of Gold and Silver Nanoparticles on the Differentiation into Osteoclasts In Vitro. *Pharmaceutics* **2021**, *13* (4), 462. <https://doi.org/10.3390/pharmaceutics13040462>.
- (89) Liang, H.; Jin, C.; Ma, L.; Feng, X.; Deng, X.; Wu, S.; Liu, X.; Yang, C. Accelerated Bone Regeneration by Gold-Nanoparticle-Loaded Mesoporous Silica through Stimulating Immunomodulation. *ACS Appl. Mater. Interfaces* **2019**, *11* (44), 41758–41769. <https://doi.org/10.1021/acsami.9b16848>.
- (90) Pinna, A.; Torki Baghbaderani, M.; Vigil Hernández, V.; Naruphontjirakul, P.; Li, S.; McFarlane, T.; Hachim, D.; Stevens, M. M.; Porter, A. E.; Jones, J. R. Nanoceria Provides Antioxidant and Osteogenic Properties to Mesoporous Silica Nanoparticles for Osteoporosis Treatment. *Acta Biomaterialia* **2021**, *122*, 365–376. <https://doi.org/10.1016/j.actbio.2020.12.029>.
- (91) Tang, Y.; Rajendran, P.; Veeraraghavan, V. P.; Hussain, S.; Balakrishna, J. P.; Chinnathambi, A.; Alharbi, S. A.; Alahmadi, T. A.; Rengarajan, T.; Mohan, S. K. Osteogenic Differentiation and Mineralization Potential of Zinc Oxide Nanoparticles from *Scutellaria Baicalensis* on Human Osteoblast-like MG-63 Cells. *Materials Science and Engineering: C* **2021**, *119*, 111656. <https://doi.org/10.1016/j.msec.2020.111656>.
- (92) Domazetovic, V. Oxidative Stress in Bone Remodeling: Role of Antioxidants. *ccmbm* **2017**, *14* (2), 209. <https://doi.org/10.11138/ccmbm/2017.14.1.209>.
- (93) Sendur, O. F.; Turan, Y.; Tastaban, E.; Serter, M. Antioxidant Status in Patients with Osteoporosis: A Controlled Study. *Joint Bone Spine* **2009**, *76* (5), 514–518. <https://doi.org/10.1016/j.jbspin.2009.02.005>.
- (94) Shen, X.; Fang, K.; Ru Yie, K. H.; Zhou, Z.; Shen, Y.; Wu, S.; Zhu, Y.; Deng, Z.; Ma, P.; Ma, J.; Liu, J. High Proportion Strontium-Doped Micro-Arc Oxidation Coatings Enhance Early Osseointegration of Titanium in Osteoporosis by Anti-Oxidative Stress Pathway. *Bioactive Materials* **2022**, *10*, 405–419. <https://doi.org/10.1016/j.bioactmat.2021.08.031>.
- (95) Zheng, K.; Torre, E.; Bari, A.; Taccardi, N.; Cassinelli, C.; Morra, M.; Fiorilli, S.; Vitale-Brovarone, C.; Iviglia, G.; Boccaccini, A. R. Antioxidant Mesoporous Ce-Doped Bioactive Glass Nanoparticles with Anti-Inflammatory and pro-Osteogenic Activities. *Materials Today Bio* **2020**, *5*, 100041. <https://doi.org/10.1016/j.mtbio.2020.100041>.
- (96) Zhu, Y.; Zhou, D.; Zan, X.; Ye, Q.; Sheng, S. Engineering the Surfaces of Orthopedic Implants with Osteogenesis and Antioxidants to Enhance Bone Formation in Vitro and in Vivo. *Colloids and Surfaces B: Biointerfaces* **2022**, *212*, 112319. <https://doi.org/10.1016/j.colsurfb.2022.112319>.

- (97) Guder, C.; Gravius, S.; Burger, C.; Wirtz, D. C.; Schildberg, F. A. Osteoimmunology: A Current Update of the Interplay Between Bone and the Immune System. *Front. Immunol.* **2020**, *11*, 58. <https://doi.org/10.3389/fimmu.2020.00058>.
- (98) Cui, Y.; Li, H.; Li, Y.; Mao, L. Novel Insights into Nanomaterials for Immunomodulatory Bone Regeneration. *Nanoscale Adv.* **2022**, *4* (2), 334–352. <https://doi.org/10.1039/D1NA00741F>.
- (99) Chen, D.; Liang, Z.; Su, Z.; Huang, J.; Pi, Y.; Ouyang, Y.; Luo, T.; Guo, L. Selenium-Doped Mesoporous Bioactive Glass Regulates Macrophage Metabolism and Polarization by Scavenging ROS and Promotes Bone Regeneration *In Vivo*. *ACS Appl. Mater. Interfaces* **2023**, *15* (29), 34378–34396. <https://doi.org/10.1021/acsami.3c03446>.
- (100) Ma, W.; Wang, W.; Liu, F.; Kong, Y.; Xia, B.; Yang, H.; Zhao, H.; Wang, L.; Li, K.; Li, Y.; Sang, Y.; Liu, H.; Wang, X.; Qiu, J. Osteoinduction-Immunomodulation Dual-Functional Calcium Nervonate Nanoparticles for Promoting Bone Regeneration. *Composites Part B: Engineering* **2023**, *255*, 110612. <https://doi.org/10.1016/j.compositesb.2023.110612>.
- (101) Yin, C.; Zhao, Q.; Li, W.; Zhao, Z.; Wang, J.; Deng, T.; Zhang, P.; Shen, K.; Li, Z.; Zhang, Y. Biomimetic Anti-Inflammatory Nano-Capsule Serves as a Cytokine Blocker and M2 Polarization Inducer for Bone Tissue Repair. *Acta Biomaterialia* **2020**, *102*, 416–426. <https://doi.org/10.1016/j.actbio.2019.11.025>.
- (102) Frampton, J. E. Mifamurtide: A Review of Its Use in the Treatment of Osteosarcoma. *Pediatric Drugs* **2010**, *12* (3), 141–153. <https://doi.org/10.2165/11204910-000000000-00000>.
- (103) Paik, J.; Duggan, S. T.; Keam, S. J. Triamcinolone Acetonide Extended-Release: A Review in Osteoarthritis Pain of the Knee. *Drugs* **2019**, *79* (4), 455–462. <https://doi.org/10.1007/s40265-019-01083-3>.
- (104) Bhattacharyya, S.; Sandhu, K.; Chockalingam, S. Nanotechnology-Based Healthcare Engineering Products and Recent Patents—an Update. In *Emerging Nanotechnologies for Medical Applications*; Elsevier, 2023; pp 273–296. <https://doi.org/10.1016/B978-0-323-91182-5.00004-8>.

CHAPTER - 2

Antibacterial lecithin chitosan
nanoparticles for the sustained
release of ciprofloxacin

Antibacterial lecithin chitosan nanoparticles for the sustained ciprofloxacin release

2.1. Introduction

2.1.1. Ocular bacterial infections

Eye is one of the important and delicate anatomical structure in human body, which like skin faces external atmosphere. In normal physiological conditions, eye is self-protected by the secretion of antibacterial compounds in tears and aqueous fluids but sometimes this defense mechanism is overpassed by external factors. Out of all etiological factors, bacterial ones are most common cause for ocular infections.^{1,2} Major bacteria-induced eye diseases include conjunctivitis, keratitis, endophthalmitis, and orbital cellulitis. These infections if left unattended, can cause serious eye damage and even blindness. Conjunctivitis (also known as pink eye) being one of the most prevalent eye infections, is reported to affect 6 million people annually. It is actually inflammation of bulbar/palpebral conjunctival tissue, followed by swollen blood vessels and discharge of purulent discharge. The etiology of conjunctivitis can be infections like bacterial and viral, or noninfectious causes associated with systemic disease like metabolic syndromes, immune related disease, and vitamin A deficiency. Infectious conjunctivitis is the most prevalent one, and the bacteria identified to cause bacterial conjunctivitis are *Staphylococcus aureus*, *Staphylococcus epidermidis*, *Pseudomonas aeruginosa*, *Hemophilus*, and *Moraxella* species.³⁻⁵

2.1.2. Challenges

The bacterial conjunctivitis is generally managed by use of topical antibiotics like fluoroquinolone (ciprofloxacin, gatifloxacin, besifloxacin) and aminoglycosides like tobramycin and gentamicin in forms of ointment and eye drops. Ciprofloxacin hydrochloride is a broad spectrum, second generation, fluoroquinolone drug.³ It is effectively used to treat skin, bone and joint infections, besides respiratory and urinary tract infections. Ophthalmic ciprofloxacin in form of ointment or eye drops is the drug of choice to treat bacterial and allergic conjunctivitis. It mainly targets and inhibits DNA gyrase and DNA topoisomerase IV, two significant bacterial topoisomerase enzymes involved in DNA synthesis. Ciprofloxacin being hydrophilic drug has low ocular bioavailability, and commercially available ophthalmic solution require regular dosing, which results in high concentration followed by the precipitation of drug and ocular discomfort.⁶⁻⁷

2.1.3. Research gap

Ophthalmic drug delivery to anterior segment of eye is effectively achieved via topical or subconjunctival routes, and topical application being most commonly used route due to ease of

administration. However, anatomical barriers like efflux pumps and physiological ocular barriers like nasolacrimal drainage and reflux blinking pose challenges to ocular drug delivery. As a result, majority of marketed ophthalmic formulations fail to counter these barriers and exhibit bioavailability of less than 5%.^{8,9} Nanocarriers with particle size in range of 10-1000 nm and certain surface charge have been used for ophthalmic delivery.^{10,11} The positively charged nanoparticles interact with negatively charged cornea and conjunctiva, and this electrostatic interaction leads to retention of nanoparticles on ocular tissues. Nano formulations in the form of nanosuspensions, nanoemulsions, nanomicelles, polymeric nanoparticles, lipid carriers and nanogels have been investigated for efficient, sustained and controlled ocular delivery.^{12,13}

Polymeric system like chitosan nanoparticles, gelatin nanoparticles, PLGA nanoparticles, hyaluronic acid, albumin nanoparticles, and liposomes have been well documented in ophthalmic drug delivery.^{14,15} Chitosan is positively charged polysaccharide, synthesized by deacetylation of chitin. It is a natural, cheap and readily available polymer having excellent biocompatibility and is biodegradable in nature. Chitosan has been explored for various biomedical application due to its inherent antibacterial and mucoadhesive properties.⁴ Chitosan has been explored as excellent drug carrier for ocular delivery due to the ability to enhance the penetration of drugs across ocular tissues, prolong drug residence time in the eye, and improve drug bioavailability. Various formulation in from of nanoparticles, hydrogels and composites have been investigated.^{16,17}

Lipid-based systems have lately gained interest for the delivery of ocular drugs in preparation like liposomes, niosomes, solid lipid nanoparticles, and nanoemulsions. The lipidic nanocarriers exhibit prolonged residence and enhanced corneal permeability due to the interaction with lipid components of tear film. Lipid-based carriers in the size dimension of 50-500 nm are suitable for ocular administration.^{13,18} Lecithin are natural lipids consisting of mainly phospholipids, triglycerides, and glycolipids and it can be extracted from animal or plant source, like egg yolk, bovine or soybean. Lecithin extracted from soybean is more economical, stable, biocompatible and contains less polyunsaturated fatty acids. Being a lipophilic matrix, high drug loading and prolonged release, soy lecithin liposomes have been explored for various topical and transdermal drug delivery.^{19,20} polymeric and lipid carriers have been employed as carrier for drug delivery only, functional antimicrobial nanoparticles having therapeutic value is promising to be explored for drug cargo, this will result in synergic effect and effective treatment of bacterial infections.

2.2. Objectives

To address the existing challenges in the ophthalmic delivery of ciprofloxacin, we investigated the polymeric nanoparticles of lecithin and chitosan. Our aim was to develop antibacterial nanoparticles for the efficient delivery of ciprofloxacin and synergic/additive antibacterial

action. We fabricated the nanoparticles and loaded them with ciprofloxacin, and characterized its physical and chemical properties. Drug release was studied in buffer solution and simulated tear fluid (STF) and antibacterial properties were evaluated against both Gram-positive (*S. aureus*) and Gram-negative bacteria (*P. aeruginosa*). The mucoadhesiveness of nanoparticles was evaluated using Bradford assay and changes in zeta potential. Finally, the cytocompatibility was evaluated by investigating the hemolysis, and cell viability against fibroblast and rabbit corneal cell lines.

2.3. Experimental section

2.3.1. Materials

Ciprofloxacin HCl, chitosan ($\eta = 200\text{--}600$ mPas), soy lecithin, Luria broth, agar powder, glacial acetic acid, methanol, mucin (Type III from porcine stomach), sodium chloride, potassium chloride, sodium bicarbonate, calcium chloride, sodium citrate, Bradford reagents, and bacterial live-dead assay kit were procured from HiMedia and Thermo Fisher Scientific. The bacterial strains, *P. aeruginosa* and *S. aureus* (# MTCC 424 and MTCC 7443) were purchased from CSIR- IMTECH, Chandigarh. Mouse fibroblast cell line (L929) was a generous gift by Dr. Durba Pal, Assistant Professor, DBME, IIT Ropar and Staten's Serum Institute rabbit corneal cell line (SIRC) was procured from NCCS, Pune. Cell culture reagents and media, such as RPMI 1640, MEM (E), fetal bovine serum (FBS), pen-strep, 3-(4,5-dimethylthiazol-2-yl)-2,5-diphenyltetrazolium bromide (MTT) reagent and 0.25% trypsin/EDTA were purchased from Thermo Fisher Scientific. Live/dead and BacLight viability kits were obtained from Life Technologies Corp. Type I deionized (DI) water (Bio-Age) was used in all experiments. For assessment of hemocompatibility, blood was drawn from a healthy human donor, adhering to protocols sanctioned by the Institutional Biosafety Committee (# 07/2021-II/IIT/IEC).

2.3.2. Fabrication of lecithin chitosan nanoparticles

The blank lecithin chitosan nanoparticles were fabricated as reported, with slight modifications²¹. Chitosan solution (1%) was completely solubilized in water using glacial acetic acid (1% v/v) for overnight and 1 mL of this solution was diluted and volume made up to 23 mL. Soy lecithin was dissolved in methanol (2 mL) and sonicated to obtain a clear solution. Using a 5 mL syringe, lecithin solution was added carefully to the chitosan solution under vigorous shaking. The solution was immediately homogenized using probe sonicator in ice bath at a frequency of 80 Hz for 7 mins. The homogenized white precipitate was then centrifuged (30 min, 0 °C, 10,000 rpm/8385 \times g), and the pellet was washed twice with DI water to remove unreacted chitosan/lecithin. The nanoparticle pellet was dried in vacuum desiccator.

2.3.3. Fabrication of drug-loaded lecithin (LC) chitosan nanoparticles

Ciprofloxacin-loaded LC nanoparticles were fabricated in same manner as above, except that the ciprofloxacin was added in lecithin solution and dissolved completely. The drug/lecithin solution was added to the chitosan solution.

2.3.4. Characterization

DLS Microtrac/NanotracsFlex was used to calculate the particle size distribution and for zeta potential measurements. The FT-IR spectra of dry samples was recorded on Bruker ATR mode (400-4000 cm^{-1}). Thermogravimetric analysis (TA Instrument, USA, SDT-650) was done under flowing N_2 (100 mL/min), and samples were heated from room temperature to 800 $^{\circ}\text{C}$ (ramp rate of 5 $^{\circ}\text{C min}^{-1}$). The morphological characteristics of nanomaterial were analyzed using scanning electron microscope (SEM, JEOL JSM-6610LV) using drop casting method on copper grids.

2.3.5. Drug loading

The unloaded drug was separated from the CLC NPs using centrifugation (10000 rpm, 4 $^{\circ}\text{C}$). The concentration of free drug in the supernatant was estimated at the wavelength of 277 nm, using plate reader.²² The final drug loading in CLC NPs was calculated using following equation:

$$\text{Loading capacity (\%)} = \left[\frac{\text{Amount of drug loaded}}{\text{Weight of nanoparticles}} \right] \times 100 \quad \text{Equation 2.1}$$

where, amount of drug loaded = Total amount of drug used initially – unloaded amount of drug in supernatant.

2.3.6. Drug release in buffer

The release of drug from the nanoparticles system was studied.²³ A weighed amount of nanoparticles was suspended in PBS buffer of pH 7.4, and Tween X (0.5% w/v) was added to maintain the sink condition. The release media of 0.5 mL was withdrawn at each time interval of 4, 8, 12, 24, 48, and 72 h and replenished each time with the same volume of release media. The amount of drug released at each time interval was determined by measuring absorbance at 277 nm using a Tecan plate reader.

2.3.7. Drug release in simulated tear fluid (STF)

Artificial tear fluid was prepared by dissolving sodium chloride (6.78 g/L), potassium chloride (1.38 g/L), sodium bicarbonate (2.18 g/L), and calcium chloride (0.084 g/L) in DI water and pH was adjusted to 7.²⁴ The drug release was studied in same manner as described in section 2.3.6 above.

2.3.8. Antibacterial studies

Antibacterial studies were carried against Gram-negative (*P. aeruginosa*) and Gram-positive (*S. aureus*) strains. The antibacterial activity of blank and drug-loaded nanoparticles was evaluated using the absorbance method (OD).²⁵ The bacterial suspension of *P. aeruginosa* and *S. aureus* ($\text{OD}_{600\text{nm}} = 0.1$, 10^7 CFU/mL) was treated with ciprofloxacin, LC, and ciprofloxacin-

loaded LC NPs. The absorbance was recorded at 600 nm at specific time points of 24, 48, and 72 h.

$$\% \text{ Antibacterial activity} = \left[\frac{OD_c - OD_s}{OD_c} \right] \times 100 \quad \text{Equation 2.2}$$

where, OD_c indicates the absorbance of control (bacteria) and OD_s represents the absorbance of sample.

The antibacterial activity was further confirmed using bacterial lived dead staining.

2.3.9. Cell viability studies

To evaluate the toxicity profile of delivery system under consideration, cell studies using murine fibroblasts (L929) and rabbit cornea (SIRC) cells were carried out.²⁶

The cells were cultured in a cell culture treated T-25 flask, in complete RPMI media and MEM supplemented with 10% FBS and 1% antibiotic solution. The media was changed after 48 h, till the cells were 70% confluent. For MTT assay, cells (1×10^5 /mL) were seeded in cell culture treated 96 well plate. Both drug loaded and blank NPs were incubated in the media for 24 h. The conditioned media was passed through a 200 mm syringe filter to remove any kind of particulate. The cells were then incubated with conditioned media for 24 h. The untreated cells and ciprofloxacin (500 µg/mL) were taken as negative and positive controls. Next day, 20 µL of MTT solution was added to each well and further incubated for around 3 h at 37 °C. The purple-colored formazan crystals were dissolved in 100 µL of DMSO. The absorbance of plate was recorded using a Tecan plate reader at the wavelength of 570 nm. The percentage cell viability was calculated using following equation:

$$\% \text{ Cell viability} = \left[\frac{OD_c - OD_s}{OD_c} \right] \times 100 \quad \text{Equation 2.3}$$

OD_c is absorbance of control, and OD_s represents the absorbance of sample.

2.3.9.1. Live/Dead staining. The effect of NPs on cell viability was further confirmed by cell live dead assay using Invitrogen, LIVE/DEAD® Viability/Cytotoxicity Kit. A working dye solution was prepared by mixing 2 µM calcein AM and 4 µM ethidium homodimer 1-red in DPBS. The treated and untreated cells were thoroughly rinsed with DPBS buffer, and then incubated with 50 µL of working dye solution for 30 min. The cells were then visualized and images recorded using a fluorescence microscope according to manufacturer manual. Live cells were stained green, while red stain indicated dead cells.

2.3.10. Mucoadhesion studies

Porcine stomach mucin (Type III), which closely resembles the acidic nasal mucosa conditions, was used to test the mucoadhesive properties of both polymeric lipid NPs- LC and CLC. Briefly, the NP suspension (0.5 mL) was added with mucin solution (0.5 mL, 5 mg/mL), and the mixture was incubated in a shaker orbital at 37 °C (100 rpm, 1.5 h) for 15 min. The mixture was centrifuged at 10,000 rpm and the supernatant was collected and absorbance measured at 595 nm. The amount of free mucin was calculated using standard curve.²⁷ The mucoadhesion was further confirmed by zeta potential analysis, by measuring the change in

zeta potential after the incubation along with mucin dispersion.²⁸ Briefly, 0.1% w/v mucin dispersion was mixed with an equal volume of CLC NPs, and the mixture was incubated in a water bath at 37 °C. Meanwhile, blank mucin dispersion, LC and CLC NPs were also incubated in water bath. After 2 h, samples from blank mucin, LC, CLC, and the dispersion of mucin and CLC were withdrawn and zeta potential was recorded.

2.3.11. Hemocompatibility

The effect of NPs on red blood cells (RBCs) was investigated using hemolysis assay. RBCs were separated from whole blood using centrifugation for 20 min at 4 °C and 1500 rpm. The resulting pellet was washed with PBS (1x) until a clear suspension was achieved. For the working solution, 1 mL of RBC suspension was diluted to 10 mL and about 1 mL of this solution was added to each sample, and it was centrifuged for 10 min at 10,000 rpm after being incubated for 4 h at 37 °C. Using a plate reader, the absorbance of each supernatant was measured at 394 nm. Triton X (1%) was chosen as the positive control and PBS was utilised as the negative control.²⁹ Following equation was used to determine percentage hemolysis:

$$\% \text{ Hemolysis} = \frac{OD_s - OD_{neg}}{OD_{pos} - OD_{neg}} \times 100 \quad \text{Equation 2.4}$$

where, OD_s is absorbance of sample, OD_{neg} is absorbance of PBS, and OD_{pos} is absorbance of Triton X.

2.3.12. Statistical analysis

The statistical analysis was carried out using Student's t-test and data were presented as average values and standard deviations from the mean value. *p values less than 0.05 were regarded as significant and ns indicates non-significant difference between the control and samples.

2.4. Results and discussion

The aim of this study was to develop an antibacterial, mucoadhesive polymeric nanocarriers of chitosan lecithin for the sustained release of ciprofloxacin to treat bacterial ocular infections. The LC NPs were prepared and characterized. Presence of chitosan imparts antibacterial and mucoadhesive property to the system, while lecithin works as surfactant to aid drug permeation across ocular tissue. We believe that chitosan shell degrades and lecithin core is exposed. Lecithin is mucoadhesive in nature and it will slowly permeate through cell membrane and provide prolonged release. Thus, these self-assembled lecithin chitosan nanoparticles possess integrated effect to enhance drug retention time and drug penetration.

2.4.1. Fabrication and characterization of chitosan lecithin NPs / nanoemulsion

The chitosan lecithin NPs were prepared using the ionic gelation method, and resulting emulsion was homogenized and centrifuged to form solid NPs (**Figure 2.1**). This nanoemulsion formation occurs due to the self-interaction between the lecithin and chitosan.

The organic solution of lecithin/ciprofloxacin was added to the aq. chitosan solution to initiate the electrostatic interaction between the positively charged chitosan (protonated amine group) and negatively charged lecithin (phosphate group), leading to the formation of internal core of lecithin / ciprofloxacin encapsulated by outer hydrophilic layer of chitosan. Hydrogen bonding and hydrophobic interaction also contribute to the complex formation.³⁰

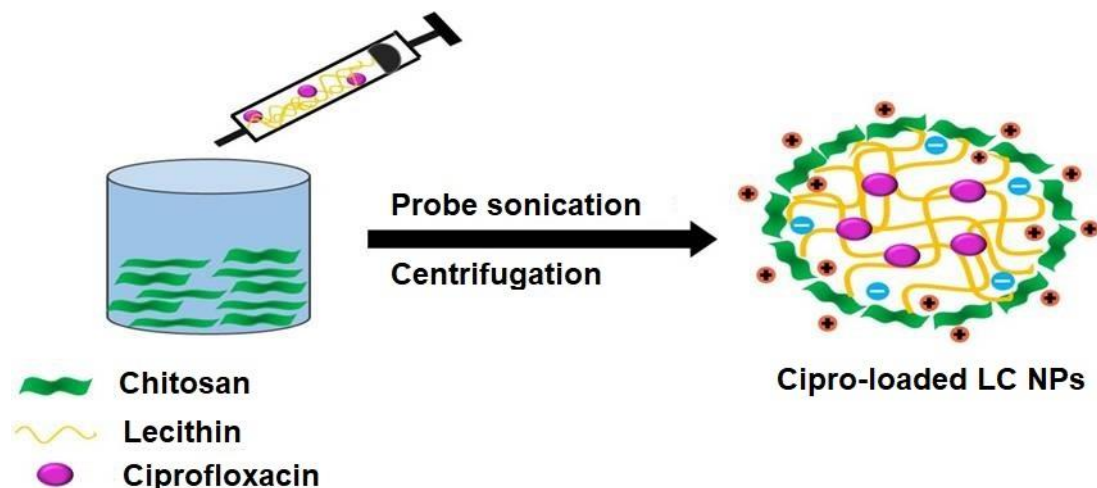


Figure 2.1. Preparation of Cipro-loaded Lecithin Chitosan (CLC) NPs.

2.4.2. Physical and chemical characterization

The NPs were characterized by various spectrometric techniques. FT-IR spectra of CL NPs revealed characteristics peak at 1061 cm^{-1} and 1730 cm^{-1} corresponding to C-O-C and N-H bands. The presence of peak at 1156 cm^{-1} can be attributed to P-O stretching, indicating the ionic bond between amino group of chitosan and phosphate group of lecithin.^{30,31} The drug loading in case of Cipro-loaded LC NPs was confirmed by the peaks at 2680 cm^{-1} and 2451 cm^{-1} . Rest of the spectra was similar to unloaded nanoparticles (**Figure 2.2.a, b**).

The thermal analysis was done using TGA technique and an initial weight loss ($\sim 2.75\%$) was observed from temperature 25 to $97\text{ }^{\circ}\text{C}$, corresponding to the loss of moisture. In the unloaded chitosan lecithin NPs, the weight loss ($\sim 33.84\%$) from 278 to $390\text{ }^{\circ}\text{C}$ was due to the degradation of chitosan, whereas in the ciprofloxacin-loaded NPs, the sharp decrease in the weight loss ($\sim 49.29\%$) in the range of $250\text{ }^{\circ}\text{C}$ and $332\text{ }^{\circ}\text{C}$ can be attributed to the degradation of ciprofloxacin (melting point $\sim 270\text{ }^{\circ}\text{C}$) and chitosan (**Figure 2.3.a**)^{32,33}. Higher weight loss for loaded NPs indicates the presence of the drug in NPs.

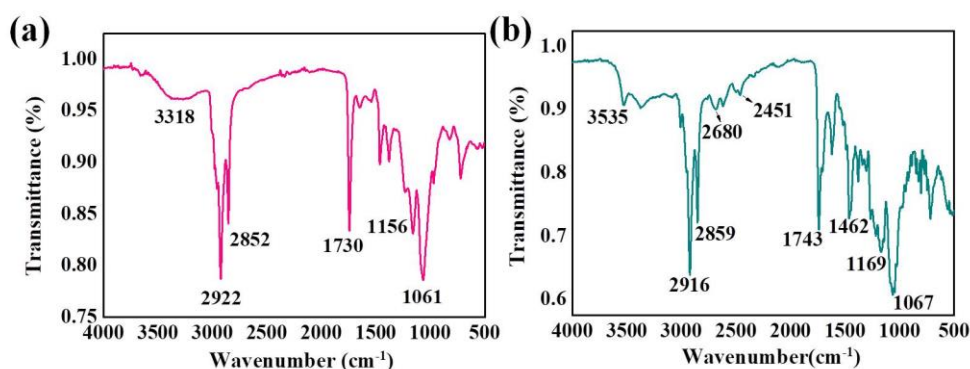


Figure 2.2. FT-IR spectra: (a) lecithin chitosan (LC) NPs, and (b) Cipro-loaded lecithin chitosan NPs (CLC).

The particle size and zeta potential were analyzed- CL NPs exhibited average size of 209 ± 9.6 nm and ciprofloxacin-loaded NPs revealed particle size of 226 ± 23 nm. An increase in particle size occurs due to the drug loading (Figure 2.3 b, c). The particle size of less than 400 nm is desirable in nanoparticles intended for use in ocular drug delivery.¹⁰ The zeta potential is defined as the electrical potential that exists in the hydrodynamic shear plane around a charged particle and very important parameter to determine the stability of colloidal solutions/suspensions. The zeta potential of LC and drug-loaded LC NPs was found to be 25.67 ± 0.41 mV and 29.1 ± 0.92 mV. Even though lecithin is negatively charged, the zeta potential of system mainly remained positive due to high chitosan to lecithin ratio and outer layer of chitosan.^{28,34} In case of ciprofloxacin-loaded LC NPs, there was a slight decrease in zeta potential.

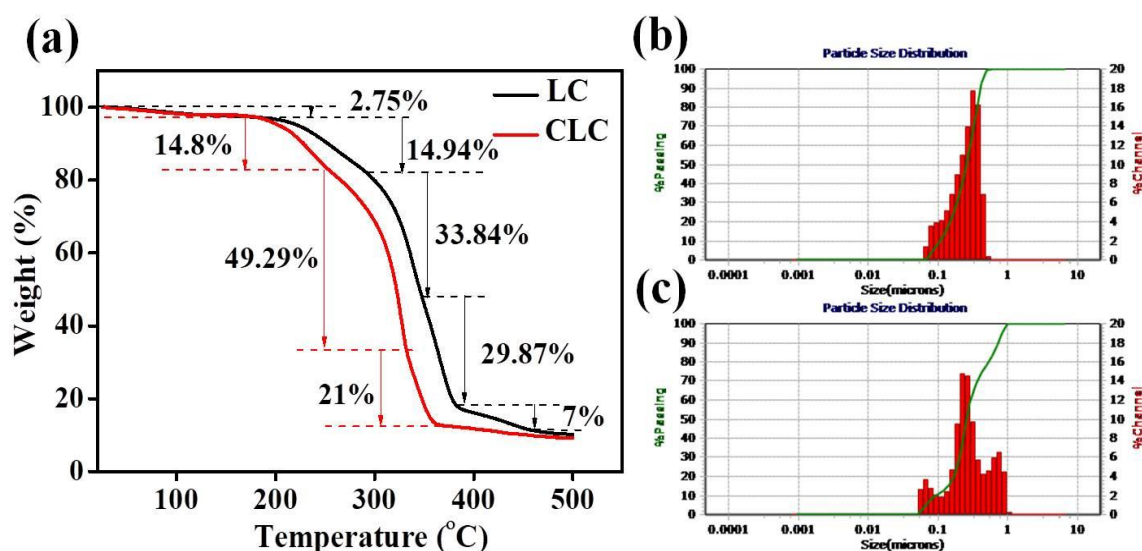


Figure 2.3. (a) Thermogravimetric analysis of nanoparticles. (b, c) Particle size analysis of LC and Cipro-loaded LC NPs.

Table 2.1. Particle size distribution and zeta potential of LC and Cipro-loaded LC NPs.

Sample	LC NPs	Cipro-loaded LC NPs
Particle Size (nm)	209 ± 9.6	226 ± 23.8
PDI	0.13	0.8
Zeta Potential (mV)	25.67 ± 4.4	29.3 ± 0.92

Morphological features were studied using SEM (**Figure 2.4.**). The results revealed the spherical shape of chitosan lecithin NPs due to the super-molecular self-organizing interaction between lecithin and chitosan.³⁰ There was no noticeable change in morphology between blank and drug-loaded LC NPs.

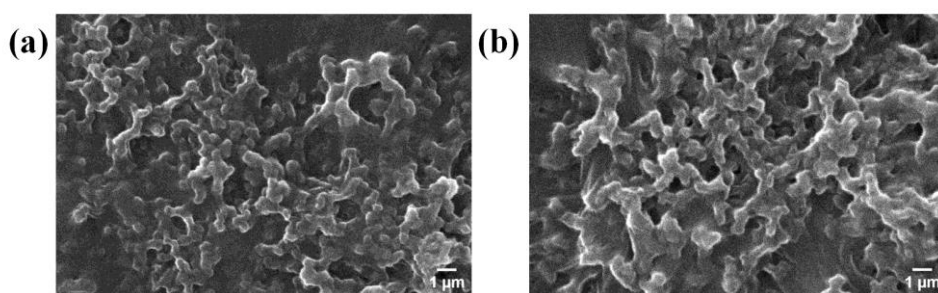


Figure 2.4. SEM micrograph of: (a) LC NPs. (b) Cipro-loaded LC NPs. Scale bar: 1 μ m.

2.4.3. Drug loading and release

The percentage of drug loaded in CLC NPs was calculated to be around 37%. The % loading of drug was found to be better than chitosan-coated sodium alginate-chitosan nanoparticles studied by Nagarwal *et al*³⁵ and comparable to chitosan nanoparticles reported by Silva *et al*³⁶. The drug release from polymer matrix is mainly influenced by factors like polymer swelling / erosion rate, degree of diffusion, solubility of drug, and polymer drug interaction. In the ocular aqueous environment, lipid polymer matrix hydrates, swells and degrades slowly and drug diffusion occurs. The rates at which polymer hydrates, swells, or erodes is usually governed by the molecular weight of polymer used. Almost 96% of the drug was released in 72 h in a biphasic manner, with a slow release within first 4 h, followed by burst release, and then nearly sustained release up to 72 h (**Figure 2.5**). Lecithin core will be shielded initially but will be gradually exposed after the dissolution of chitosan layer. The aim of this system was to have sustained release system, wherein positively charged chitosan will be taken up cells, causing the initial burst release of drugs, followed by slow infiltration of negatively charged lecithin, which will provide prolonged release of drugs over the period of time. The initial quick release can be beneficial for quickly attaining a therapeutic level, with the subsequent steady release helping to maintain the level. The release data was plotted using various models

and showed best fit with Higuchi model with good regression coefficient value ($R^2 = 0.94$). This indicates that release of drug occurs due to swelling, diffusion, and erosion of polymer matrix. Similar release profile of drug from chitosan lecithin nanoparticles have been demonstrated by Ilk et al., 2017²² and Alomrani et al., 2019.³⁴ The sustained release of the drug from the nanoparticles could be maintained for 72 h, which is significantly higher than chitosan-based nanoparticles reported by Zhao *et al.*³⁷ and Nagarwal *et al.*³⁵

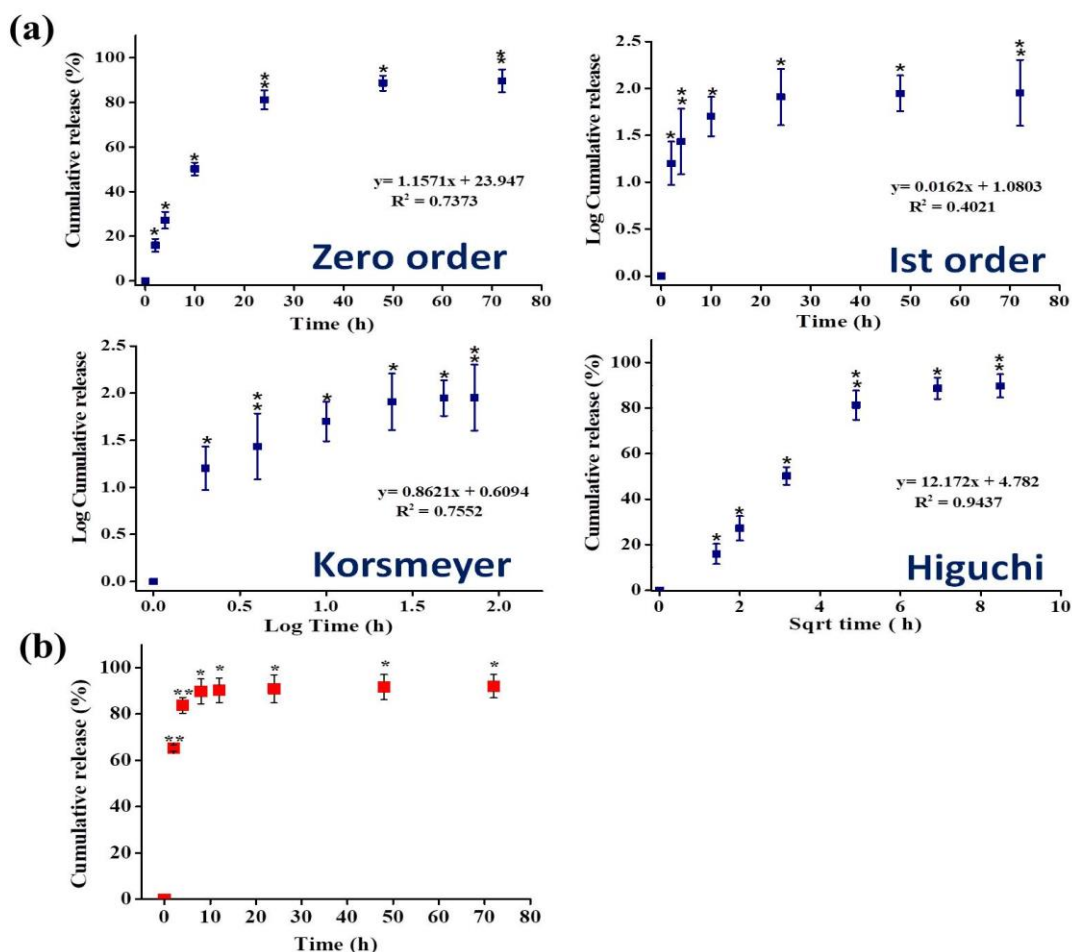


Figure 2.5. Release profile of ciprofloxacin from NPs. (a) PBS. (b) Simulated tear fluid. * $p < 0.05$ represents the statistically significant difference and ns the non-significant difference.

2.4.4. Antibacterial studies

The antimicrobial effect was studied against both Gram-positive and Gram-negative bacteria, using OD method. CLC NPs showed activity of 72% against *P. aeruginosa* and around 96% killing was observed in case of *S. aureus* in 72 h. Ciprofloxacin, a broad-spectrum antibiotic, inhibits the cell division by binding with DNA gyrase. It was highly effective against *S. aureus* with almost 100% inhibition, and also showed inhibitory activity of 78% against *P. aeruginosa*.³⁸ LC NPs owing to the presence of chitosan, exhibited intrinsic antimicrobial property of 45% and 59% against *P. aeruginosa* and *S. aureus*. Depending on the structure of each bacterial cell membrane, chitosan in its polycationic form exhibits antibacterial action against both Gram-positive and Gram-negative bacteria. Chitosan interacts with anionic

surface components of Gram-negative bacteria, including proteins, and lipopolysaccharides, while it directly interacts with the negatively charged peptidoglycan and teichoic acid layer of Gram-positive bacteria's cell wall.³⁹ Thus CLC NPs have pronounced and additive antimicrobial activity from ciprofloxacin and LC NPs (**Figure 2.6.a**). The live dead assay was used to confirm the antibacterial effect of NPs. Similar observations were observed as above (**Figure 2.6 b**). The results obtained were comparable to those reported by Garhwal *et al*⁴⁰ and Yu *et al.*⁴¹

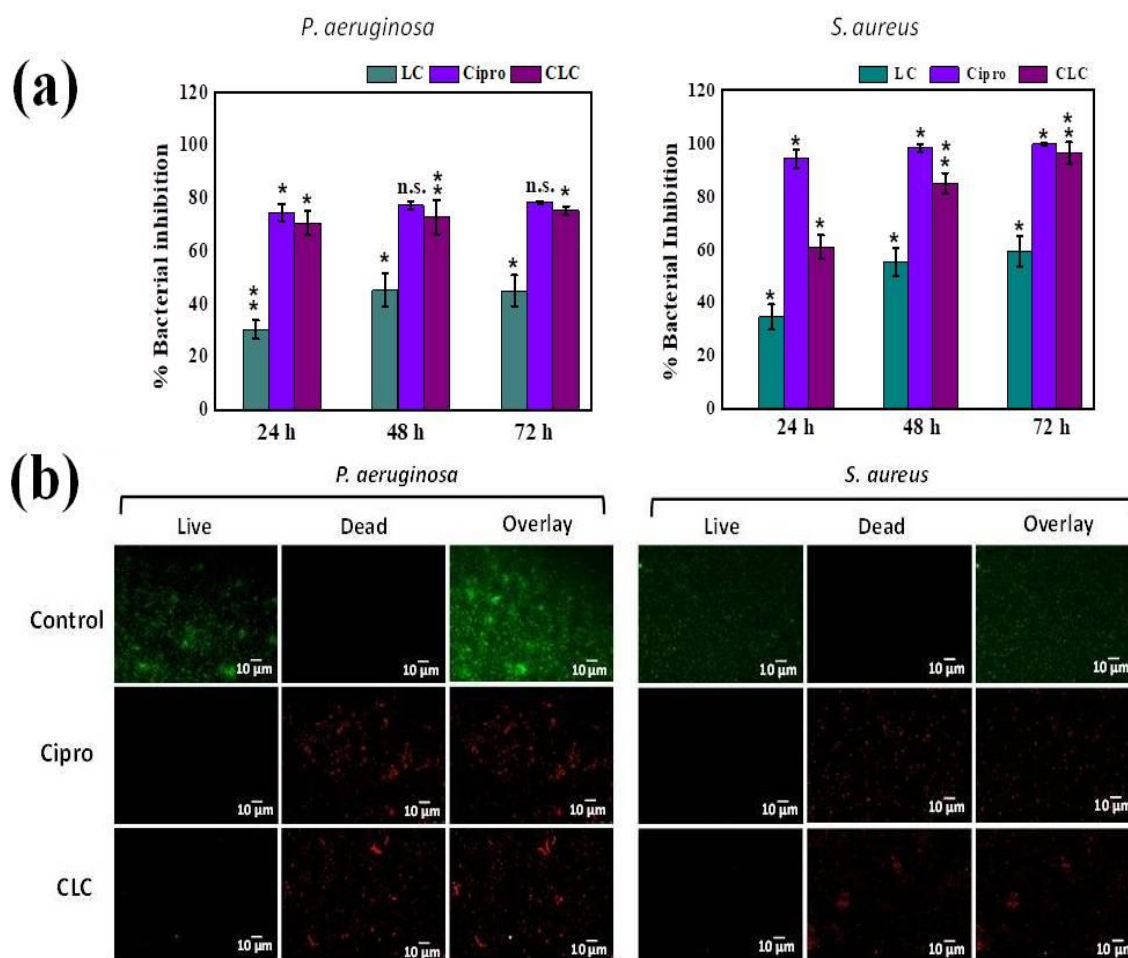


Figure 2.6. Antibacterial activity and live/dead assay. (a) Inhibition of bacterial growth of *P. aeruginosa* and *S. aureus* after 24, 48, and 72 h. *p < 0.05 represents the statistically significant difference and ns the non-significant difference. (b) Fluorescent images of untreated, Cipro, and Cipro-loaded LC NP-treated bacterial suspension of *P. aeruginosa* and *S. aureus*. Scale bar: 10 μ m.

2.4.5. Cell viability studies

MTT, a rapid colorimetric assay was used to measure the metabolic activity of cells. The conversion of MTT into purple colored formazan crystals by living cells is indicator of cell viability or toxicity. The results demonstrated that in L929 cells, ciprofloxacin HCl exhibited toxicity, with cell viability of 60%. Ciprofloxacin is reported to induce the oxidative stress in

fibroblast cells.⁴² Both CL and CLC were found to be safe with cell viability of 100 and 82% (**Figure 2.7.a, c.**). In case of SIRC cells, LC NPs were found to cell proliferative in nature with 110% cell viability, while as drug-loaded CLC NP-treated cells exhibited around 93% cell viability (**Figure.2.7.b.**).⁴³ Our material was cytocompatible similar to materials reported by Lin *et al*⁴⁴ and Asasutjarit *et al.*⁴⁵

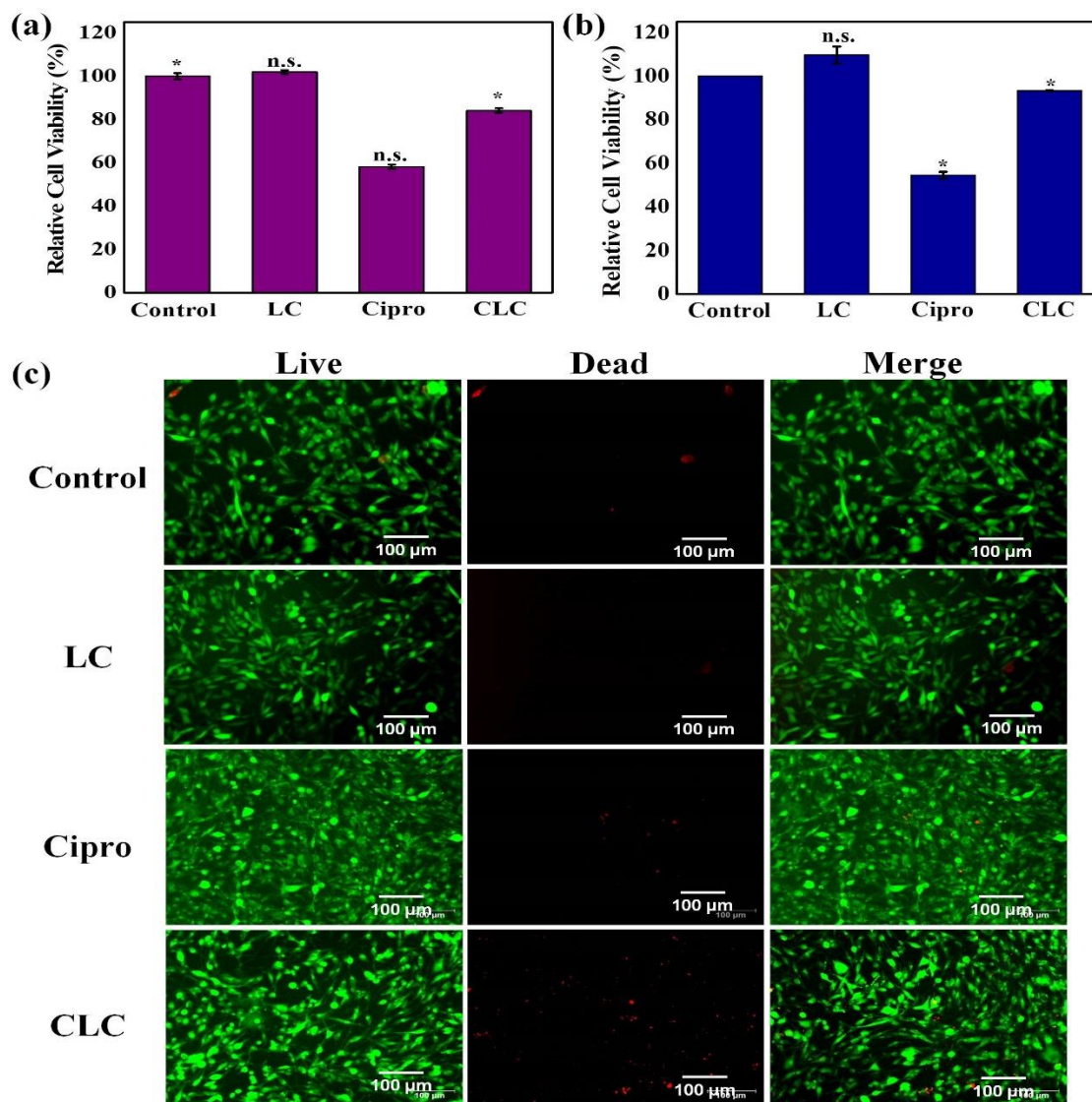


Figure 2.7. Cell viability and live/dead assays of blank (untreated), LC NPs, Cipro, and Cipro-loaded LC NP extracts-treated L929 and SIRC cells after 24 h. (a, b) MTT assay. * $p < 0.05$ represents the statistically significant difference and ns the non-significant difference. (c) Fluorescence images of untreated cells (control) and cells treated with LC NPs, Cipro, and Cipro-loaded LC NP conditioned media. Scale bar: 100 μm .

2.4.6. Mucoadhesive property

The mucoadhesiveness was studied using two methods- Bradford assay and change in zeta potential. The decrease in zeta potential was observed in both mucin, LC and mucin CLC. This is due to the adsorption of negatively charged mucin on positively charged LC and CLC NPs (**Table 2.2**). Besides electrostatic interaction, physical entanglement between chitosan

and mucin is also involved.^{46,47} Similar observation was made in Bradford assay- the amount of free mucin was significantly less in the supernatant of LC and CLC NPs (**Figure 2.8 a**). Both results indicate that CLC NPs are mucoadhesive in nature, which ensures longer residence time and, thus, prolonged drug delivery. The amount of mucin adsorbed by nanoparticles was found to be significantly higher than chitosan-coated polylactic acid nanoparticles reported by Mahaling *et al*⁴⁸ and similar to dexamethasone–glycol chitosan conjugates studied by Yu *et al*.⁴⁹

2.4.7. Hemocompatibility

As the NPs are to be administered in the eye, they might enter the vascular layer via choroid and come in contact with the erythrocytes. To ensure the safety of the eye, hemocompatibility of the NPs was assessed using hemolysis assay. The supernatant of samples (0.5 mg/mL) showed minimal hemolysis (<4%) which makes it clinically safe. The drug-loaded NPs (CLC) showed relatively lower hemolysis in comparison to ciprofloxacin itself (**Figure 2.8 b**). The system was relatively more hemocompatible than cipro-loaded Au NPs reported by Nawaz *et al*.⁵⁰

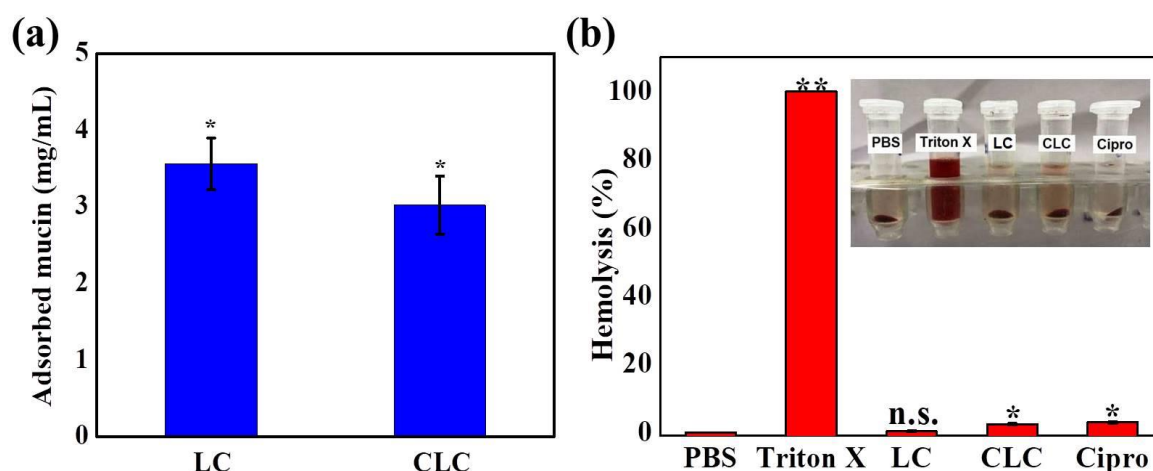


Figure 2.8. (a) Mucoadhesion analysis of LC and Cipro-loaded LC NPs using Bradford assay. (b) In vitro percent hemolysis of untreated, Triton X, LC, Cipro-loaded CL NPs, and ciprofloxacin. **p < 0.01, *p < 0.05 represents the statistically significant difference and ns the non-significant difference.

Table 2.2. Zeta potential of free mucin, mucin bound with LC NPs, and Cipro-loaded LC NPs.

Sample	Mucin	Mucin / LC	Mucin / CLC
Zeta Potential (mV)	-20	1.14	3.72

2.5. Conclusions

To conclude, we have fabricated lecithin chitosan nanoparticles for the sustained release of ciprofloxacin to treat bacterial ocular infections. The nanoparticles were characterized by FT-IR, SEM, DLS, zeta potential, and TGA. About 37% of drug loading was observed and subsequently drug release kinetics were studied in PBS and simulated tear fluid. The lecithin chitosan nanoparticles showed a Fickian diffusion, with Higuchi model being the best fit. The release of ciprofloxacin was sustained for up to 72 h. The nanomaterial was evaluated for antibacterial properties against both Gram-positive (*P. aeruginosa*) and Gram-negative bacteria (*S. aureus*) and found to exhibit antimicrobial properties for prolonged time against both strains. The cell viability in fibroblast and rabbit corneal cell lines showed that nanomaterials developed are cytocompatible. The hemolysis assay using red blood cells revealed their non-hemolytic characteristics. The nanomaterials have amphiphilic nature and demonstrated promising mucoadhesiveness, which is required to increase its retention time in the eye and decrease the frequency of dosage. Thus, lecithin chitosan nanoparticles can be regarded as promising candidate for the ocular bacterial infections. The intrinsic antimicrobial and mucoadhesive nature of chitosan and lecithin along with the antimicrobial activity of ciprofloxacin results in accentuated and improved antibacterial activity.

References

- (1) Hashmi, M. F.; Gurnani, B.; Benson, S. Conjunctivitis. In *StatPearls*; StatPearls Publishing: Treasure Island (FL), **2022**.
- (2) Kowalski, R. P.; Dhaliwal, D. K. Ocular Bacterial Infections: Current and Future Treatment Options. *Expert Rev. Anti Infect. Ther.* **2005**, *3* (1), 131–139. <https://doi.org/10.1586/14787210.3.1.131>.
- (3) Hutnik, C.; Cheema. Bacterial Conjunctivitis. *Clin. Ophthalmol.* **2010**, *4*, 1451. <https://doi.org/10.2147/OPHTH.S10162>.
- (4) Deepthi, K. G.; Prabakaran, S. R. Ocular Bacterial Infections: Pathogenesis and Diagnosis. *Microb. Pathog.* **2020**, *145*, 104206. <https://doi.org/10.1016/j.micpath.2020.104206>.
- (5) Teweldemedhin, M.; Gebreyesus, H.; Atsbaha, A. H.; Asgedom, S. W.; Saravanan, M. Bacterial Profile of Ocular Infections: A Systematic Review. *BMC Ophthalmol.* **2017**, *17* (1), 212. <https://doi.org/10.1186/s12886-017-0612-2>.
- (6) Jacinto, T. A.; Oliveira, B.; Miguel, S. P.; Ribeiro, M. P.; Coutinho, P. Ciprofloxacin-Loaded Zein/Hyaluronic Acid Nanoparticles for Ocular Mucosa Delivery. *Pharmaceutics* **2022**, *14* (8), 1557. <https://doi.org/10.3390/pharmaceutics14081557>.
- (7) Hashemikia, S.; Farhangpazhouh, F.; Parsa, M.; Hasan, M.; Hassanzadeh, A.; Hamidi, M. Fabrication of Ciprofloxacin-Loaded Chitosan/Polyethylene Oxide/Silica Nanofibers for Wound Dressing Application: In Vitro and in Vivo Evaluations. *Int. J. Pharm.* **2021**, *597*, 120313. <https://doi.org/10.1016/j.ijpharm.2021.120313>.
- (8) Onugwu, A. L.; Nwagwu, C. S.; Onugwu, O. S.; Echezona, A. C.; Agbo, C. P.; Ihim, S. A.; Emeh, P.; Nnamani, P. O.; Attama, A. A.; Khutoryanskiy, V. V. Nanotechnology Based Drug Delivery Systems for the Treatment of Anterior Segment Eye Diseases. *J. Controlled Release* **2023**, *354*, 465–488. <https://doi.org/10.1016/j.jconrel.2023.01.018>.
- (9) Urtti, A. Challenges and Obstacles of Ocular Pharmacokinetics and Drug Delivery. *Adv. Drug Deliv. Rev.* **2006**, *58* (11), 1131–1135. <https://doi.org/10.1016/j.addr.2006.07.027>.
- (10) Gorantla, S.; Rapalli, V. K.; Waghule, T.; Singh, P. P.; Dubey, S. K.; Saha, R. N.; Singhvi, G. Nanocarriers for Ocular Drug Delivery: Current Status and Translational

- Opportunity. *RSC Adv.* **2020**, *10* (46), 27835–27855. <https://doi.org/10.1039/D0RA04971A>.
- (11) Xie, G.; Lin, S.; Wu, F.; Liu, J. Nanomaterial-Based Ophthalmic Drug Delivery. *Adv. Drug Deliv. Rev.* **2023**, *200*, 115004. <https://doi.org/10.1016/j.addr.2023.115004>.
 - (12) Tsai, C.-H.; Wang, P.-Y.; Lin, I.-C.; Huang, H.; Liu, G.-S.; Tseng, C.-L. Ocular Drug Delivery: Role of Degradable Polymeric Nanocarriers for Ophthalmic Application. *Int. J. Mol. Sci.* **2018**, *19* (9), 2830. <https://doi.org/10.3390/ijms19092830>.
 - (13) Das, B.; Nayak, A. K.; Mallick, S. Lipid-Based Nanocarriers for Ocular Drug Delivery: An Updated Review. *J. Drug Deliv. Sci. Technol.* **2022**, *76*, 103780. <https://doi.org/10.1016/j.jddst.2022.103780>.
 - (14) Javed, S.; Abbas, G.; Shah, S.; Rasul, A.; Irfan, M.; Saleem, A.; Hosny, K. M.; Bukhary, S. M.; Safhi, A. Y.; Sabei, F. Y.; Majrashi, M. A.; Alkhalidi, H. M.; Alissa, M.; Khan, S. M.; Hanif, M. Tobramycin-Loaded Nanoparticles of Thiolated Chitosan for Ocular Drug Delivery: Preparation, Mucoadhesion and Pharmacokinetic Evaluation. *Heliyon* **2023**, *9* (9), e19877. <https://doi.org/10.1016/j.heliyon.2023.e19877>.
 - (15) Han, H.; Li, S.; Xu, M.; Zhong, Y.; Fan, W.; Xu, J.; Zhou, T.; Ji, J.; Ye, J.; Yao, K. Polymer- and Lipid-Based Nanocarriers for Ocular Drug Delivery: Current Status and Future Perspectives. *Adv. Drug Deliv. Rev.* **2023**, *196*, 114770. <https://doi.org/10.1016/j.addr.2023.114770>.
 - (16) Jurišić Dukovski, B.; Juretić, M.; Bračko, D.; Randjelović, D.; Savić, S.; Crespo Moral, M.; Diebold, Y.; Filipović-Grčić, J.; Pepić, I.; Lovrić, J. Functional Ibuprofen-Loaded Cationic Nanoemulsion: Development and Optimization for Dry Eye Disease Treatment. *Int. J. Pharm.* **2020**, *576*, 118979. <https://doi.org/10.1016/j.ijpharm.2019.118979>.
 - (17) Sanchez Armengol, E.; Grassiri, B.; Piras, A. M.; Zambito, Y.; Fabiano, A.; Laffleur, F. Ocular Antibacterial Chitosan-Maleic Acid Hydrogels: In Vitro and in Vivo Studies for a Promising Approach with Enhanced Mucoadhesion. *Int. J. Biol. Macromol.* **2024**, *254*, 127939. <https://doi.org/10.1016/j.ijbiomac.2023.127939>.
 - (18) Battaglia, L.; Serpe, L.; Foglietta, F.; Muntoni, E.; Gallarate, M.; Del Pozo Rodriguez, A.; Solinis, M. A. Application of Lipid Nanoparticles to Ocular Drug Delivery. *Expert Opin. Drug Deliv.* **2016**, *13* (12), 1743–1757. <https://doi.org/10.1080/17425247.2016.1201059>.
 - (19) Chan, J. M.; Zhang, L.; Yuet, K. P.; Liao, G.; Rhee, J.-W.; Langer, R.; Farokhzad, O. C. PLGA–Lecithin–PEG Core–Shell Nanoparticles for Controlled Drug Delivery. *Biomaterials* **2009**, *30* (8), 1627–1634. <https://doi.org/10.1016/j.biomaterials.2008.12.013>.

- (20) Ahmed, S.; Amin, M. M.; Sayed, S. Ocular Drug Delivery: A Comprehensive Review. *AAPS PharmSciTech* **2023**, *24* (2), 66. <https://doi.org/10.1208/s12249-023-02516-9>.
- (21) Saha, M.; Saha, D. R.; Ulhosna, T.; Sharkar, S. M.; Shohag, M. H.; Islam, M. S.; Ray, S. K.; Rahman, G. M. S.; Reza, H. M. QbD Based Development of Resveratrol-Loaded Mucoadhesive Lecithin/Chitosan Nanoparticles for Prolonged Ocular Drug Delivery. *J. Drug Deliv. Sci. Technol.* **2021**, *63*, 102480. <https://doi.org/10.1016/j.jddst.2021.102480>.
- (22) Jalal, R. R.; Ways, T. M. M.; Abu Elella, M. H.; Hassan, D. A.; Khutoryanskiy, V. V. Preparation of Mucoadhesive Methacrylated Chitosan Nanoparticles for Delivery of Ciprofloxacin. *Int. J. Biol. Macromol.* **2023**, *242*, 124980. <https://doi.org/10.1016/j.ijbiomac.2023.124980>.
- (23) Bhandari, M.; Rasool, N.; Singh, Y. Polymeric Lipid Nanoparticles for Donepezil Delivery. In *Polymeric Biomaterials and Bioengineering*; Gupta, B., Jawaid, M., Kaith, B. S., Rattan, S., Kalia, S., Eds.; Lecture Notes in Bioengineering; Springer Nature Singapore: Singapore, 2022; pp 51–63. https://doi.org/10.1007/978-981-19-1084-5_5.
- (24) Liu, C.; Tai, L.; Zhang, W.; Wei, G.; Pan, W.; Lu, W. Penetratin, a Potentially Powerful Absorption Enhancer for Noninvasive Intraocular Drug Delivery. *Mol. Pharm.* **2014**, *11* (4), 1218–1227. <https://doi.org/10.1021/mp400681n>.
- (25) Chauhan, N.; Singh, Y. Self-Assembled Fmoc-Arg-Phe-Phe Peptide Gels with Highly Potent Bactericidal Activities. *ACS Biomater. Sci. Eng.* **2020**, *6* (10), 5507–5518. <https://doi.org/10.1021/acsbiomaterials.0c00660>.
- (26) Rasool, N.; Srivastava, R.; Singh, Y. Cationized Silica Ceria Nanocomposites to Target Biofilms in Chronic Wounds. *Biomater. Adv.* **2022**, *138*, 212939. <https://doi.org/10.1016/j.bioadv.2022.212939>.
- (27) Lee, J.-S.; Suh, J. W.; Kim, E. S.; Lee, H. G. Preparation and Characterization of Mucoadhesive Nanoparticles for Enhancing Cellular Uptake of Coenzyme Q10. *J. Agric. Food Chem.* **2017**, *65* (40), 8930–8937. <https://doi.org/10.1021/acs.jafc.7b03300>.
- (28) Chhonker, Y. S.; Prasad, Y. D.; Chandasana, H.; Vishvkarma, A.; Mitra, K.; Shukla, P. K.; Bhatta, R. S. Amphotericin-B Entrapped Lecithin/Chitosan Nanoparticles for Prolonged Ocular Application. *Int. J. Biol. Macromol.* **2015**, *72*, 1451–1458. <https://doi.org/10.1016/j.ijbiomac.2014.10.014>.
- (29) Liu, L.; Ma, Q.; Wang, S.; Gao, Y.; Zhu, C.; Zhao, W.; Sun, W.; Ma, H.; Sun, Y. Efficient Epidermal Delivery of Antibiotics by Self-Assembled Lecithin/Chitosan Nanoparticles for Enhanced Therapy on Epidermal Bacterial Infections. *Int. J. Biol. Macromol.* **2022**, *218*, 568–579. <https://doi.org/10.1016/j.ijbiomac.2022.07.165>.
- (30) Mahmood, S.; Kiong, K. C.; Tham, C. S.; Chien, T. C.; Hilles, A. R.; Venugopal, J. R. PEGylated Lipid Polymeric Nanoparticle–Encapsulated Acyclovir for In Vitro

- Controlled Release and Ex Vivo Gut Sac Permeation. *AAPS PharmSciTech* **2020**, *21* (7), 285. <https://doi.org/10.1208/s12249-020-01810-0>.
- (31) Zewail, M. B.; El-Gizawy, S. A.; Asaad, G. F.; El-Dakrouy, W. A. Development of Famotidine-Loaded Lecithin-Chitosan Nanoparticles for Prolonged and Efficient Anti-Gastric Ulcer Activity. *J. Drug Deliv. Sci. Technol.* **2024**, *91*, 105196. <https://doi.org/10.1016/j.jddst.2023.105196>.
 - (32) Valencia, M. S.; Silva Júnior, M. F. da; Xavier-Júnior, F. H.; Veras, B. de O.; Albuquerque, P. B. S. de; Borba, E. F. de O.; Silva, T. G. da; Xavier, V. L.; Souza, M. P. de; Carneiro-da-Cunha, M. das G. Characterization of Curcumin-Loaded Lecithin-Chitosan Bioactive Nanoparticles. *Carbohydr. Polym. Technol. Appl.* **2021**, *2*, 100119. <https://doi.org/10.1016/j.carpta.2021.100119>.
 - (33) Mesallati, H.; Umerska, A.; Paluch, K. J.; Tajber, L. Amorphous Polymeric Drug Salts as Ionic Solid Dispersion Forms of Ciprofloxacin. *Mol. Pharm.* **2017**, *14* (7), 2209–2223. <https://doi.org/10.1021/acs.molpharmaceut.7b00039>.
 - (34) Murthy, A.; Ravi, P. R.; Kathuria, H.; Vats, R. Self-Assembled Lecithin-Chitosan Nanoparticles Improve the Oral Bioavailability and Alter the Pharmacokinetics of Raloxifene. *Int. J. Pharm.* **2020**, *588*, 119731. <https://doi.org/10.1016/j.ijpharm.2020.119731>.
 - (35) Nagarwal, R. C.; Kumar, R.; Pandit, J. K. Chitosan Coated Sodium Alginate–Chitosan Nanoparticles Loaded with 5-FU for Ocular Delivery: In Vitro Characterization and in Vivo Study in Rabbit Eye. *European Journal of Pharmaceutical Sciences* **2012**, *47* (4), 678–685. <https://doi.org/10.1016/j.ejps.2012.08.008>.
 - (36) Silva, N. C.; Silva, S.; Sarmiento, B.; Pintado, M. Chitosan Nanoparticles for Daptomycin Delivery in Ocular Treatment of Bacterial Endophthalmitis. *Drug Delivery* **2015**, *22* (7), 885–893. <https://doi.org/10.3109/10717544.2013.858195>.
 - (37) Zhao, R.; Li, J.; Wang, J.; Yin, Z.; Zhu, Y.; Liu, W. Development of Timolol-Loaded Galactosylated Chitosan Nanoparticles and Evaluation of Their Potential for Ocular Drug Delivery. *AAPS PharmSciTech* **2017**, *18* (4), 997–1008. <https://doi.org/10.1208/s12249-016-0669-x>.
 - (38) Campoli-Richards, D. M.; Monk, J. P.; Price, A.; Benfield, P.; Todd, P. A.; Ward, A. Ciprofloxacin: A Review of Its Antibacterial Activity, Pharmacokinetic Properties and Therapeutic Use. *Drugs* **1988**, *35* (4), 373–447. <https://doi.org/10.2165/00003495-198835040-00003>.
 - (39) Guarnieri, A.; Triunfo, M.; Scieuzo, C.; Ianniciello, D.; Tafi, E.; Hahn, T.; Zibek, S.; Salvia, R.; De Bonis, A.; Falabella, P. Antimicrobial Properties of Chitosan from Different Developmental Stages of the Bioconverter Insect *Hermetia Illucens*. *Sci. Rep.* **2022**, *12* (1), 8084. <https://doi.org/10.1038/s41598-022-12150-3>.
 - (40) Garhwal, R.; Shady, S. F.; Ellis, E. J.; Ellis, J. Y.; Leahy, C. D.; McCarthy, S. P.;

- Crawford, K. S.; Gaines, P. Sustained Ocular Delivery of Ciprofloxacin Using Nanospheres and Conventional Contact Lens Materials. *Invest. Ophthalmol. Vis. Sci.* **2012**, *53* (3), 1341. <https://doi.org/10.1167/iov.11-8215>.
- (41) Yu, A.; Hu, Y.; Ma, X.; Mo, L.; Pan, M.; Bi, X.; Wu, Y.; Wang, J.; Li, X. Sequential Drug Release of Co-Assembled Supramolecular Hydrogel as Synergistic Therapy against Staphylococcus Aureus Endophthalmitis. *Chemical Engineering Journal* **2022**, *427*, 130979. <https://doi.org/10.1016/j.cej.2021.130979>.
 - (42) Gürbay, A.; Garrel, C.; Osman, M.; Richard, M.-J.; Favier, A.; Hincal, F. Cytotoxicity in Ciprofloxacin-Treated Human Fibroblast Cells and Protection by Vitamin E. *Hum. Exp. Toxicol.* **2002**, *21* (12), 635–641. <https://doi.org/10.1191/0960327102ht305oa>.
 - (43) Jain, D.; Carvalho, E.; Banthia, A. K.; Banerjee, R. Development of Polyvinyl Alcohol–Gelatin Membranes for Antibiotic Delivery in the Eye. *Drug Dev. Ind. Pharm.* **2011**, *37* (2), 167–177. <https://doi.org/10.3109/03639045.2010.502533>.
 - (44) Lin, P.-H.; Jian, H.-J.; Li, Y.-J.; Huang, Y.-F.; Anand, A.; Huang, C.-C.; Lin, H.-J.; Lai, J.-Y. Alleviation of Dry Eye Syndrome with One Dose of Antioxidant, Anti-Inflammatory, and Mucoadhesive Lysine-Carbonized Nanogels. *Acta Biomaterialia* **2022**, *141*, 140–150. <https://doi.org/10.1016/j.actbio.2022.01.044>.
 - (45) Asasutjarit, R.; Theerachayanan, T.; Kewsuwan, P.; Veeranondha, S.; Fuongfuchat, A.; Ritthidej, G. C. Gamma Sterilization of Diclofenac Sodium Loaded- N-Trimethyl Chitosan Nanoparticles for Ophthalmic Use. *Carbohydrate Polymers* **2017**, *157*, 603–612. <https://doi.org/10.1016/j.carbpol.2016.10.029>.
 - (46) Bhatta, R. S.; Chandasana, H.; Chhonker, Y. S.; Rathi, C.; Kumar, D.; Mitra, K.; Shukla, P. K. Mucoadhesive Nanoparticles for Prolonged Ocular Delivery of Natamycin: In Vitro and Pharmacokinetics Studies. *Int. J. Pharm.* **2012**, *432* (1–2), 105–112. <https://doi.org/10.1016/j.ijpharm.2012.04.060>.
 - (47) Sogias, I. A.; Williams, A. C.; Khutoryanskiy, V. V. Why Is Chitosan Mucoadhesive? *Biomacromolecules* **2008**, *9* (7), 1837–1842. <https://doi.org/10.1021/bm800276d>.
 - (48) Mahaling, B.; Baruah, N.; Ahamad, N.; Maisha, N.; Lavik, E.; Katti, D. S. A Non-Invasive Nanoparticle-Based Sustained Dual-Drug Delivery System as an Eyedrop for Endophthalmitis. *International Journal of Pharmaceutics* **2021**, *606*, 120900. <https://doi.org/10.1016/j.ijpharm.2021.120900>.
 - (49) Yu, A.; Shi, H.; Liu, H.; Bao, Z.; Dai, M.; Lin, D.; Lin, D.; Xu, X.; Li, X.; Wang, Y. Mucoadhesive Dexamethasone-Glycol Chitosan Nanoparticles for Ophthalmic Drug Delivery. *International Journal of Pharmaceutics* **2020**, *575*, 118943. <https://doi.org/10.1016/j.ijpharm.2019.118943>.
 - (50) Nawaz, A.; Ali, S. M.; Rana, N. F.; Tanweer, T.; Batool, A.; Webster, T. J.; Menaa, F.; Riaz, S.; Rehman, Z.; Batool, F.; Fatima, M.; Maryam, T.; Shafique, I.; Saleem, A.; Iqbal, A. Ciprofloxacin-Loaded Gold Nanoparticles against Antimicrobial Resistance:

An In Vivo Assessment. *Nanomaterials* **2021**, *11* (11), 3152.
<https://doi.org/10.3390/nano11113152>.

CHAPTER - 3

Cationized silica ceria
nanocomposite to target biofilms in
chronic wounds

Cationized silica ceria nanocomposite to target biofilms in chronic wounds

3.1. Introduction

3.1.1. Wound healing

Wound healing is an intricate, multistep biological mechanism orchestrated by various cells, including platelets, neutrophils, macrophages, and fibroblasts, operating in a synchronized fashion.^{1,2} Disruptions or anomalies in any phase can induce malfunctions, culminating in persistent, non-healing wounds that hinder proper wound closure. The global ramifications of impaired wound healing are substantial, with associated costs reaching approximately \$25 billion annually on a global scale.³ The incidence of chronic wounds is surging up, primarily driven by the rising prevalence of conditions, like diabetes and obesity. It's projected that 1–2% of individuals in industrialized nations will confront the challenges of impaired wound healing at some point in their lives.^{4,5} One predominant factor impeding wound healing is bacterial infections leading to chronic wounds. These bacteria, within biofilm structures at the wound site, produce toxins and virulence factors that impede healing, resulting in chronic wound conditions.⁶ Biofilms are self-secretory matrices encompassing a diverse bacterial population, lipopolysaccharides, and extracellular DNA. This matrix offers a safeguarded environment, enabling bacteria to withstand antibiotics or adverse cellular conditions. As biofilms mature, they undergo dynamic phenotypic alterations. Their presence often results in antimicrobial resistance and the progression of wounds to a chronic state.^{7,8}

3.1.2. Challenges

While aggressive antibiotic regimens have been explored to counteract biofilm-associated infections, they often worsen the situation. This is especially true when biofilms form on living tissues (like, chronic wound sites), further aggravating the pre-existing inflammatory state of the wounds.⁹ Numerous methodologies have been explored to counteract biofilm and its associated complications. Nanomaterials have emerged to prominence as potent antimicrobial agents. Their diverse attributes and tunable chemistry make them ideal candidates for devising robust strategies to both prevent and eliminate biofilms.¹⁰⁻¹² Metal nanoparticles, lanthanide elements, carbon nanotubes, graphene oxide nanoparticles, and nanocomposites have been extensively explored to combat bacterial and biofilm-related infections. However, addressing biofilm-induced wound complications remains a formidable challenge.¹³

3.1.3. Research gap

Given the dynamic nature of biofilms, which adapt their phenotype in response to therapeutic agents, a multifaceted approach targeting the diverse aspects of wounds is needed to enhance the efficacy and circumvent resistance. We have addressed this gap by designing a hybrid nanocomposite (FSC) of mesoporous silica nanoparticles (MSNs) and cerium oxide nanoparticles (CNPs) to exhibit robust bactericidal and anti-biofilm property while maintaining the biocompatibility on biofilm-covered biological surfaces in order to restore the compromised wound healing processes.

3.1.4. Nanomaterials for antimicrobial property

Cerium oxide, a multifunctional enzyme-mimetic lanthanide metal, is recognized for its antibacterial and antioxidant properties. The catalytic activity of cerium oxide is mostly attributed to the ability of cerium to self-regenerate redox states between Ce^{4+} and Ce^{3+} .¹⁴ This catalytic activity is intrinsically size-dependent and the effect becomes more pronounced with the decrease in nanoparticle dimensions.^{15,16} Cerium oxide exhibits both antibacterial and anti-biofilm property by instigating the hydrolysis of extracellular DNA through nucleophilic attack on the organophosphate backbone. Numerous studies have identified cerium oxide as a DNA-mimetic enzyme, which triggers the lysis of extracellular DNA present in biofilm.^{17,18} Additionally, cerium oxide demonstrates tissue regenerative properties, promotes wound healing, and helps in scavenging reactive oxygen species (ROS).¹⁹ Nonetheless, cerium oxide nanoparticles face challenges, such as limited colloidal stability and dispersity in aqueous solutions, alongside size-dependent behavior. To address these limitations, various surface modification techniques have been explored to stabilize these nanoparticles.²⁰

Mesoporous silica nanoparticles (MSNs) have emerged as excellent carrier in the biomedical realm due to their expansive surface area, biocompatibility, and inherent porosity. This robust framework facilitates adaptable surface functionalization while preserving its porosity for encapsulating guest substances.²¹ While MSNs lack inherent bactericidal properties, they have proven to be potent drug delivery vehicles and foundational substrates for composite materials, and thus expanding their potential in wound healing applications.²² Cationic surfaces or polymers manifest pronounced antibacterial effects, and their propensity to induce drug resistance is minimal.²³ These positively charged entities adhere to the anionic bacterial membrane, leading to the disruption of membrane constituents and subsequent cellular death. The effect is equally potent against both Gram-positive and Gram-negative bacterial strains.²⁴

3.2. Objectives

The objective of this work was to fabricate and characterize a cationic nanocomposite (FSC) incorporating mesoporous silica nanoparticles (MSNs) and cerium oxide nanoparticles (CNPs)

with the objective of mitigating the presence of biofilm in persistent wounds (**Figure 3.1**). The nanocomposite has been designed to take advantage of the expansive surface area of MSNs serving as a scaffold for the homogenous distribution of CNPs and enhanced surface functionalization. This cationized nanocomposite exhibit more positive charge density, which is complemented by the inherent antibacterial and anti-biofilm attributes of CNPs, thereby increasing its antimicrobial potency. Comprehensive characterization of the nanocomposite was done along with the evaluation of its antioxidant, haloperoxidase-mimetic, and antibacterial activities against both Gram-positive and Gram-negative bacterial strains. Its effect on preventing biofilm generation and eradicating pre-established biofilm was investigated. Subsequent studies included its cytocompatibility towards mouse fibroblast cell line, proficiency in protecting cells from ROS-induced oxidative stress, and hemocompatibility with human blood samples. Conclusively, the nanocomposite's capability in facilitating wound closure in cell cultures was assessed. Overall, this nanocomposite demonstrated a strong potential in counteracting biofilm proliferation within chronic wound environments.

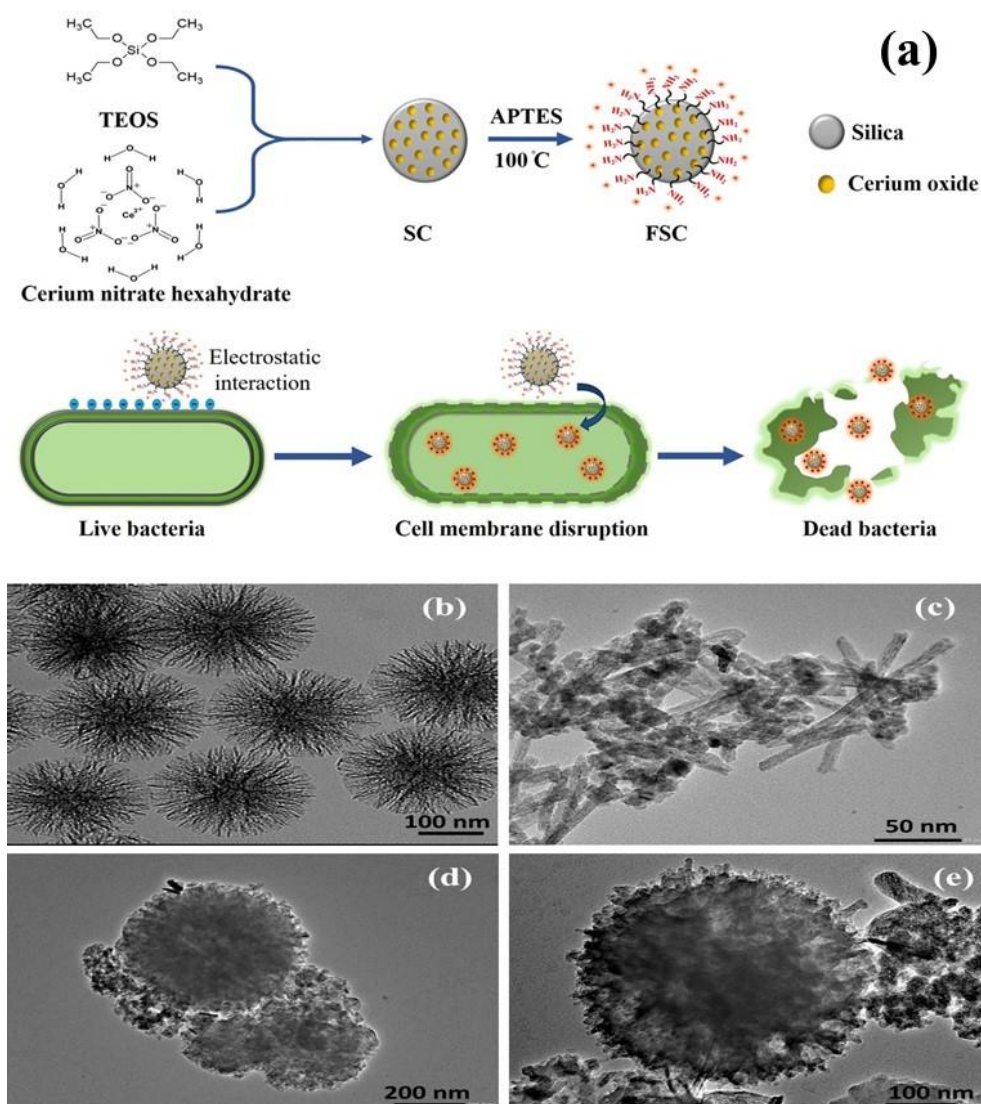


Figure. 3.1. (a) Preparation of cationized silica ceria nanocomposite (FSC) and its activity on bacteria. (b-e) HR-TEM images. (b) MSN. (c) CNP. (d) SC. (e) FSC. Scale bar: (b, e) 100 nm. (c) 50 nm. (d) 200 nm.

3.3. Experimental section

3.3.1. Materials

Tetraethyl orthosilicate (TEOS), 3-aminopropyl-triethoxysilane (APTES), 2,2'-azino-bis-(3-ethylbenzothiazoline-6-sulfonic acid) (ABTS), ethanol, potassium bromide, crystal violet, and potassium persulfate, were sourced from Sigma-Aldrich. Additional reagents, including ascorbic acid, bacteriological agar powder, cetrimonium bromide (CTAB), gentamicin, Luria broth, phosphate-buffered saline (PBS), and urea, were procured from HiMedia. Ammonia (30%) and phenol red were supplied by Avra, whereas glacial acetic acid, hydrogen peroxide, sodium hydroxide, and p-xylene were obtained from Merck. DMSO, pentanol, and toluene were acquired from Spectrochem, and cerium nitrate hexahydrate (99.9% AR) was sourced from Loba Chemie. All reagents were utilized as received, without additional refinement. Bacterial strains *S. aureus*, and *E. coli* bearing accession numbers MTCC 7433 and MTCC 1687 were obtained from CSIR- IMTECH, Chandigarh. The bacterial live-dead assay kit was sourced from Thermo Fisher. The L929 cell line was generous gift by Dr. Durba Pal from DBME, IIT Ropar. Other materials, including CCK 8 reagent, 2',7'-dichlorodihydrofluorescein diacetate (DCFDA), fetal bovine serum (FBS), MTT reagent, penstrep, RPMI 1640, and 0.25% trypsin/EDTA were procured either from Thermo Fisher or Sigma. All experiments were carried out in Type I deionized (DI) water (Bioage). For the assessment of hemocompatibility, blood was drawn from a healthy human donor by adhering to the protocol approved by the Institutional Biosafety Committee (# 07/2021-II/IIT/IEC).

3.3.2. Fabrication of mesoporous silica nanoparticles (MSN)

Mesoporous silica nanoparticles (MSNs) were fabricated using a method reported in literature.²⁵ Initially, CTAB (0.2 g, 0.54 mmol) and urea (0.24 g, 3.99 mmol) were solubilized in 10 mL of DI water, and agitated at 1000 rpm for 15 min. Further, TEOS (1 mL, 4.8 mmol) was added to 10 mL of p-xylene and was subsequently added to CTAB-urea mixture, with continuous stirring maintained for an additional 20 min. Next, dropwise addition of pentanol (0.6 mL) was done to the reaction mixture, and the system was subjected to intense agitation for 30 min. The colloidal solution was then subjected to reflux conditions at 140 °C for a span of 2 h. The resulting slurry was washed several times with water and ethanol. The isolated white nanoparticulate matter was then subjected to calcination at 550 °C for 6 h in air in order to remove CTAB.

3.3.3. Fabrication of cerium oxide nanoparticles (CNPs)

Cerium oxide nanoparticles were fabricated using hydrothermal technique.²⁶ Cerium nitrate hexahydrate (0.4 g, 1 mmol) was solubilized in 4 M NaOH (60 mL) and vigorously stirred for

30 min. This resultant suspension was then transferred to a 100 mL Teflon-coated stainless-steel autoclave and subsequently incubated in an oven at 100 °C for a 24 h period. CNPs were obtained as dark yellow powder by centrifuging the reaction mixture and subsequently washing them with water and ethanol (10,000 rpm, 4°C).

3.3.4. In situ fabrication of silica ceria nanocomposite (SC)

According to a standardized procedure, CTAB (0.1 g, 0.3 mmol) was solubilized in water (20 mL). A combined solution of 30% ammonia (25 mL) and ethanol (35 mL) was added to ensure alkaline conditions. The resulting mixture was stirred for a span of 30 min and TEOS (0.54 mL, 2.6 mmol) was added, and the reaction mixture was further stirred for another 30 min, leading to the formation of a white suspension. Cerium nitrate hexahydrate (0.6 g, 1.3 mmol) was then introduced to this suspension. The entire reaction assembly was stirred under ambient conditions for an hour, post which it was transferred to a Teflon-coated stainless-steel autoclave and incubated in the oven at 100 °C overnight. The resultant suspension was then centrifuged and subjected to a washing sequence using both ethanol and water. The isolated nanoparticles underwent calcination at 550 °C for 5 h, yielding CTAB-free, characteristic yellow-hued nanocomposite.²⁷

3.3.5. Amine functionalization

Following the fabrication, surface modification was performed using previously established method.²⁸ The composite was kept in vacuum desiccator overnight at 50 °C to remove the moisture. Subsequently, the dehydrated powder was dispersed in toluene, followed by sonication for a period ranging between 40 to 50 min. APTES (0.8 mmol, 0.17 mL) was then introduced to this dispersion, and the reaction mixture was subjected to reflux conditions at 110 °C for an overnight period. The resultant suspension was centrifuged, followed by a washing sequence using toluene to eliminate any residual, unreacted APTES. The sample, denoted as FSC, was then air-dried at 50 °C. An analogous procedure was employed for the functionalization of CNPs, yielding the product termed as FCNP.

3.3.6. Characterization

The nanoparticles were comprehensively characterization via multiple analytical techniques. The morphological attributes of the nanomaterials were elucidated using a High-Resolution Transmission Electron Microscope (HR-TEM JEM-2100 Plus, 200 kV) employing the drop-casting technique. Fourier Transform Infrared (FT-IR) spectra of desiccated samples were acquired on a Bruker spectrophotometer, utilizing the Attenuated Total Reflectance (ATR) mode spanning a wavenumber range of 400 to 4000 cm⁻¹. The crystalline nature of the materials was ascertained by X-ray Diffraction (XRD) on a RIGAKU Mini-flex diffractometer, with scanning angles between 10° and 80° and Cu K α radiation (λ = 0.154 nm). Band gap energy estimations for both CNPs and nanocomposites were conducted on a Shimadzu spectrophotometer, employing BaSO₄ as a reference standard. Surface attributes of the materials were probed through N₂-adsorption analysis. Prior to analysis, samples were

degassed at 200 °C for 5 h to eliminate surface-bound adsorbates. The Brunauer-Emmett-Teller (BET) equation was employed to determine specific surface areas within a relative pressure range of 0.05 to 0.3. Pore distribution was deduced utilizing the Barrett-Joyner-Halenda (BJH) methodology on a Quantachrome instrument. Dynamic Light Scattering (DLS) on a Microtrac/Nanotrac Flex apparatus facilitated the assessment of particle size distribution and zeta potential. X-ray Photoelectron Spectroscopy (XPS) analysis, conducted on a Thermo Fisher Scientific K Alpha instrument provided insights into the elemental composition and oxidation states of the nanocomposites. Lastly, Energy Dispersive X-ray (EDX) studies, executed on a BrukerSplash 6130, facilitated the exploration of elemental mapping and the spatial distribution of integral elements within the nanocomposite.

3.3.7. Antioxidant assay

ABTS (7 mM) and potassium persulfate (2.45 mM) solutions were formulated using DI water.²⁹ These solutions were mixed in equimolar proportions and incubated overnight under ambient conditions in the absence of light, facilitating the generation of free radicals. Subsequently, the resultant solution was diluted with phosphate-buffered saline (PBS) until an absorbance value of 0.8 units at 734 nm was achieved. Individual samples were exposed to the optimized ABTS solution for an hour. This was followed by centrifugation, leading to the isolation of supernatants. The absorbance of these supernatants was then quantified, and the radical scavenging efficiency was computed, using ascorbic acid (1%) as the standard control.

$$\% \text{ Antioxidant Activity} = \left[\frac{A_c - A_s}{A_c} \right] \times 100 \quad \text{Equation 3.1}$$

where, A_c is the absorbance of the control and A_s is the absorbance of the sample.

3.3.8. Haloperoxidase-mimicking properties

The haloperoxidase activity was assessed based on a previously documented method, albeit with minor alterations.³⁰ Phenol red (50 µM) and potassium bromide (25 µM) were solubilized in water. This was succeeded by the incorporation of hydrogen peroxide (300 µM). The pH of the solution was adjusted between 5 to 6. Subsequently, individual samples (concentration: 2 mg/mL) were incubated with the reactant mixture for a span of 5 h under ambient conditions. Absorbance values at wavelengths of 432 nm and 590 nm were periodically captured at 30 min intervals over the 5 h duration, utilizing a UV-Vis spectrophotometer.

3.3.9. Antibacterial assay

The antibacterial efficacy was evaluated against bacterial strains *E. coli* and *S. aureus*. These bacteria were propagated in Luria broth until they reached the mid-logarithmic growth phase at 37 °C in an orbital shaker incubator operating at 100 rpm. The bacterial cultures were diluted to achieve a concentration of 1×10^7 CFU/mL.³¹ Sample suspensions at varying concentrations (0.5, 1, 2 mg/mL) were exposed to both *S. aureus* and *E. coli* for durations of 12 and 24 h, while maintaining a consistent agitation speed of 100 rpm. At designated intervals, aliquots (100 µL) of the bacterial mixture were subjected to serial dilution and

subsequently plated on Luria agar media. These plates were incubated for a period ranging between 6 to 8 h until countable bacterial colonies could be recognized. The degree of bacterial growth inhibition was quantified relative to a control group of untreated bacteria. For reference, gentamicin (0.1 mg/mL) and untreated bacterial cultures were employed as positive and negative controls. To assess the impact of nanoparticle dimensions on antibacterial performance, FSCs of different sizes (257, 450, and 911 nm) were fabricated by modulating specific reaction parameters, like rate of addition of TEOS and reaction time during the fabrication process. The antibacterial activities of these varied-sized FSCs were assessed against *E. coli* and *S. aureus* by employing the optical density (OD) technique.

3.3.10. Inhibition of biofilm formation

Overnight cultured *S. aureus* was diluted in fresh Luria Broth (LB) media to achieve a concentration of 1×10^7 CFU/mL. Subsequently, 500 μ L of this bacterial suspension was introduced to each sample (concentration: 2 mg/mL) in a 48-well plate and incubated at 37 °C for a duration of 48 h.³² Post-incubation, the well contents were discarded and each well underwent a triple washing sequence with phosphate-buffered saline (PBS) to eliminate any free-floating (planktonic) bacterial cells. The adherent bacteria were fixed using absolute ethanol for a 15 min period. Staining was achieved by treating the fixed bacteria with a 0.1% crystal violet solution for a time span ranging between 5 to 10 min and excess stain was rinsed off with water. To solubilize the biofilm-bound dye, 10% glacial acetic acid was added to each well. The absorbance of resultant solution was measured at a wavelength of 590 nm.

3.3.11. Disruption of established biofilm

To assess the efficacy of the nanocomposite against pre-formed biofilm, a suspension of *S. aureus* (concentration: 1×10^7 CFU/mL) was inoculated into a tissue culture-treated 48-well plate. This setup was incubated at 37 °C for 48 h to facilitate biofilm development.³³ Post-incubation, each well was rinsed with phosphate-buffered saline (PBS) to eliminate any non-adherent bacterial entities. Subsequently, each sample solution (concentration: 2 mg/mL) in Luria Broth (LB) media was added to the wells. The plate underwent an additional incubation period of 24 h. The quantification of biofilm biomass was executed utilizing the crystal violet staining protocol.

3.3.12. Live/dead bacterial staining

A working dye solution was formulated by mixing SYTO 9 and propidium iodide (PI) in equimolar proportions using sterile water. Both treated and untreated bacterial samples were exposed to this dye mixture and incubated for 30 min under ambient conditions, shielded from light. Post-incubation, the stained bacterial entities were immobilized onto glass slides and visualized employing a Leica DMI8 fluorescence microscope. For bacteria within mature biofilms, a similar staining protocol was adopted. Biofilms were cultivated for a 48 h period within a treated 48-well plate and exposed to the sample solutions for an additional 24 h. Following a washing sequence with PBS, the dye mixture was introduced and allowed to

interact with the biofilm for 15 min. After discarding the dye solution, the biofilm-laden wells were examined under the fluorescence microscope.

3.3.13. HR-TEM imaging

The influence of FSC on bacterial structural integrity was determined with the help of HR-TEM (model: JEM-2100 Plus, operating at 200 kV). Bacterial strains, *E. coli* and *S. aureus*, were cultivated as described previously and exposed to FSC for time intervals of 12 and 24 h. Post-treatment, both treated and control bacterial samples were centrifuged (4 °C). The resultant pellet was subjected to a triple washing sequence using PBS (pH 7.4). The bacterial cells were fixed overnight using a 2.5% glutaraldehyde solution, followed by a 30 min treatment with 1% osmium tetroxide. A systematic dehydration of the pellet was executed using an ethanol gradient, progressing from concentrations of 30% to 90%. The final pellet was reconstituted in absolute ethanol. A 5 µL aliquot of this bacterial suspension was drop-casted onto a carbon-coated copper grid (with a mesh size of 300). Imaging was performed using the HR-TEM.³⁴

3.3.14. In vitro cell viability

The viability and proliferation of cells were assessed using the mouse fibroblast (L929) cell line. These cells were cultivated in RPMI media, supplemented with 10% Fetal Bovine Serum (FBS) and 1% antibiotic, within a tissue culture-treated flask (T-25).³⁵ Upon achieving 70–80% confluence, the cells were trypsinized. The detached cells were seeded into a 48-well plate at a density of 1×10^4 cells/mL and incubated in a CO₂-rich environment for 24 h. Various concentrations (0.5, 1, and 2 mg/mL) of each sample were incubated in the media at 37 °C for 24 h. Subsequent to this incubation, the samples were filtered using a 0.2 µm syringe filter to eliminate any particulate contaminants. The original media in the wells was substituted with this conditioned media, and the cells underwent further incubation for periods of 24 and 72 h. The viability of cells at the 24 h and 72 h was determined using the following methods:

3.3.14.1. MTT assay. A 30 µL aliquot of MTT solution (concentration: 5 mg/mL) was introduced to each well, followed by an incubation period of 3.5 h at 37 °C. The emergent formazan crystals were solubilized using 100 µL of dimethyl sulfoxide (DMSO). Absorbance was taken at a wavelength of 570 nm utilizing a Tecan Infinite M Plex plate reader. Cell viability percentages were deduced by juxtaposing the absorbance values of treated cells against those of the untreated control.

$$\% \text{ Cell Viability} = \frac{\text{Absorbance of sample}}{\text{Absorbance of control}} \times 100 \quad \text{Equation 3.2}$$

3.3.14.2. CCK 8 assay. To each well of a 48-well plate, 20 µL of CCK 8 dye was introduced, followed by an incubation period of 3.5 h at 37 °C. Absorbance readings were subsequently recorded at a wavelength of 450 nm utilizing a plate reader.

3.3.14.3. Live/dead staining. Post 24 h incubation period, cellular staining was executed using the LIVE/DEAD® Viability/Cytotoxicity Kit for mammalian cells (sourced from Invitrogen) by adhering to the manufacturer's guidelines. A working dye solution was formulated, comprising of 2 µM calcein AM and 4µM ethidium homodimer 1-red, dissolved in DPBS. Prior to staining, cells underwent a meticulous washing process using DPBS buffer. Subsequently, they were exposed to 50 µL of the prepared dye solution and incubated for 30 min. Cellular imaging was accomplished utilizing a fluorescence microscope.

3.3.15. Hemolysis assay

The compatibility of the samples with human blood, termed hemocompatibility, was assessed.³⁶ Erythrocytes, or red blood cells (RBCs), were procured via centrifugation at a speed of 1500 rpm for duration of 20 min. The RBCs underwent three washing cycles with 1× PBS. A working RBC solution was formulated by diluting a 1 mL erythrocyte pellet in 9 mL of PBS. Each sample was supplemented with 1 mL of this working solution and subjected to incubation at 37 °C for a span of 4 h. This was followed by a centrifugation at 10,000 rpm for 10 min. The absorbance of the supernatant from each sample was measured at 394 nm using a plate reader. For reference, PBS served as the negative control, while 1% Triton X served as the positive control. The percentage of hemolysis was determined using the following equation:

$$\% \text{ Hemolysis} = \left[\frac{OD_{\text{sample}} - OD_{\text{negative}}}{OD_{\text{positive}} - OD_{\text{negative}}} \right] \times 100 \quad \text{Equation 3.3}$$

3.3.16. In vitro ROS/oxidative stress

In this study, L929 cells were cultured at a density of 1×10^4 cells/mL in a 48-well plate and allowed to incubate for 24 h at 37 °C.³⁷ Cells were exposed to 50 mM of H₂O₂ for an hour. The medium was replaced with sample extracts and the incubation continued for an additional 24 h. To assess intracellular reactive oxygen species (ROS) generation, cells were treated with DCFDA dye (25 µM) and kept in the dark for 30 min. Post-incubation, the wells were washed with 200 µL of PBS and the fluorescence from ROS-bound DCFDA was visualized using a fluorescence microscope. To determine the protective effect of the nanocomposite against oxidative stress, cell viability in the presence of H₂O₂ was evaluated.⁴² Cells were cultured at a density of 1×10^4 cells/mL in a 48-well plate and incubated for 24 h. The culture medium was replaced with conditioned medium containing the nanocomposite, followed by the introduction of 50 mM H₂O₂. After 24 h incubation, cell viability was assessed using the MTT assay, as described previously. Control groups, both exposed and unexposed to H₂O₂, served as positive and negative controls.

3.3.17. In vitro scratch assay

The wound healing potential of the nanomaterials was evaluated using an in vitro scratch assay, as previously described.³⁸ L929 cells were cultured at a density of 1×10^4 cells/mL in a treated 6-well plate until they reached full confluence. A sterile 200 µL pipette tip was used to

create a straight-line scratch on the monolayer of cells. After removing cell debris by washing with DPBS, conditioned media was added to each well, and the plate was incubated at 37 °C. Wound healing progression was monitored at 6, 12, and 24 h intervals, with images captured using an inverted microscope (Evos XL core, Invitrogen). The healing percentage, in terms of area covered, was quantified using ImageJ software. The calculation was based on the following formula:

$$\% \text{ Healing} = \left[\frac{Area_{t_0} - Area_{t_i}}{Area_{t_0}} \right] \times 100 \quad \text{Equation 3.4}$$

where, $t_0 = 0$ h, $t_i = 6, 12$, and 24 h.

3.3.18. Statistical analysis

Statistical analysis was done using the student's t-test and the data were presented as mean values \pm standard deviations. A p-value below 0.05 was considered statistically significant (*), while "ns" denotes no significant difference between the control and tested samples.

3.4. Results and discussion

Cerium oxide nanoparticles (CNPs) are recognized as enzyme-mimetic nanomaterials with antibacterial, antioxidant, and tissue regeneration capabilities.³⁹ The efficacy of cerium-based nanoparticles in antibacterial applications often depends on factors, like size, morphology, and pH. This research aimed to improve the antibacterial potential of CNPs, irrespective of their geometric attributes, by employing mesoporous silica nanoparticles (MSNs) as a matrix. This matrix encapsulated the cerium oxide, forming a silica-ceria nanocomposite (SC). Subsequent cationic functionalization of this composite (FSC) was pursued to enhance its performance against bacterial entities and biofilms (**Figure. 3.1**).

3.4.1. Fabrication and characterization of silica/ceria nanocomposite

The fabrication of MSNs was executed using a straightforward reflux approach in a round-bottom-flask, where TEOS underwent hydrolysis in an alkaline setting utilizing CTAB as a template to guide the formation of silica nanoparticles. The CNPs were fabricated via a hydrothermal technique, employing a cerium precursor and undergoing precipitation in an alkaline milieu at an elevated temperature of 100 °C. The porous SC nanocomposite powder was derived through a template-driven hydrothermal process involving both cerium and silica precursors (**Figure 3.1**). Post-synthesis, CNP and SC underwent surface modification using APTES. This functionalization was confirmed by FT-IR analysis and a shift in zeta potential from negative to positive values. The resultant nanomaterials were thoroughly characterized to ascertain their physicochemical attributes. The average particle size and zeta potential measurements are shown in **Table 3.1** and **Figure A1, A2 (Appendix)**.

Table 3.1. Particle size distribution and zeta potential of MSN, CNP, FCNP, SC, and FSC.

Sample	Average particle size (nm)	PDI	Zeta potential (mV)
MSN	236 ± 18	0.1	-18.9 ± 2
CNP	85 ± 12	0.1	-1.8 ± 1
FCNP	103 ± 12	0.1	10.7 ± 1
SC	480 ± 30	0.2	-17.9 ± 2
FSC	449 ± 9	0.1	21.6 ± 1

TEM imaging disclosed that CNPs possess a rod-like structure, whereas MSNs display a dendritic form (**Figure 3.1, b-e**). Both nanocomposites, namely SC and FSC, showed a spherical, dendritic morphology. FT-IR spectra showed distinctive peaks representing various functional groups (**Figure A3, Appendix**). Notably, a peak at 1624 cm⁻¹ was attributed to the δ (OH) mode, while another at 3397 cm⁻¹ was linked to the ν (O-H) mode of hydrogen-bonded water molecules. Bands around 800 and 1000 cm⁻¹ were associated with ν_s Si-O-Si and ν_{as} Si-O-Si vibrations.³⁰ The spectral peaks for pure silica and silica nanocomposite remained largely consistent. However, the emergence of an NH bending band at 1556 cm⁻¹ in FCNP and FSC indicated the presence of an amine group, thus confirming successful APTES-based functionalization.⁴⁰ CNPs displayed characteristic CH₂ stretching peaks at 2928 cm⁻¹, while FCNP exhibited a peak near 1553 cm⁻¹, attributed to its amine-functionalized surface.⁴¹ XRD profiles for silica, ceria, and their nanocomposites can be found in **Figure A4 (Appendix)**. CNPs exhibited distinct sharp peaks at angles 28.55, 33.22, 47.47, and 56.33°, corresponding to the 111, 200, 220, and 311 planes, indicating a fluorite-like crystalline structure as per JCPDS file no. 34-0394. In contrast, MSNs displayed a typical amorphous characteristic.⁴² The PXRD pattern for the nanocomposite mirrored that of ceria but the peak intensity decreased due to its incorporation with amorphous silica.

Band gap energies were ascertained using solid-state UV-Vis spectroscopy. The band gap of 2.7 eV was noted for both pure CNPs and SC. FCNP and FSC exhibited energy values of 2.84 eV and 2.99 eV (**Figure A4, Appendix**). The diminished band gap energy can be linked to the elevated oxygen vacancies and the Ce⁴⁺ oxidation state. Prior studies have highlighted the profound influence of oxygen vacancy on haloperoxidase properties.³⁰ BET

surface area analysis showed a type IV isotherm for MSN, while CNPs, SC, and FSC displayed a type II isotherm. Specific surface area and pore volume metrics for each material can be found in **Table A1 (Appendix)**. Additionally, N₂-isotherms and pore size distribution graphs are presented in **Figure A5 and A6, Appendix**.

The oxidation state of elements within the nanocomposite was determined from XPS spectra (**Figure 3.2, A7 Appendix**). The high-resolution Ce 3d spectrum for FSC displayed peaks associated with spin–orbit coupling, specifically for Ce 3d 3/2 and Ce 3d 5/2. Peaks at II (885.13 eV), IV (898.19 eV), and VI (903.65 eV) are indicative of the Ce³⁺ oxidation state. The peaks at I (882.34 eV), III (888.49 eV), V (900.80 eV), VII (907.68 eV), and VIII (916.71 eV) represent the Ce⁴⁺ oxidation state. The Ce³⁺ to Ce⁴⁺ ratio was calculated to be 0.94 (**Table A2, Appendix**). Oxygen vacancy in the material was found using the formula: $\text{Ce}^{3+}/(\text{Ce}^{3+} + \text{Ce}^{4+}) \times 100$, resulting in a value of 48%.³⁸ FSCs, with an oxygen vacancy of 48%, are anticipated to showcase potent catalytic activity as such activity is bolstered by the presence of oxygen vacancies. Elemental distribution within samples was examined using EDX mapping. The distribution map for SC highlighted the presence of Ce and O elements. The composite map revealed a uniform distribution of Ce within the silica ceria nanocomposite (**Figure A8, Appendix**).³⁹

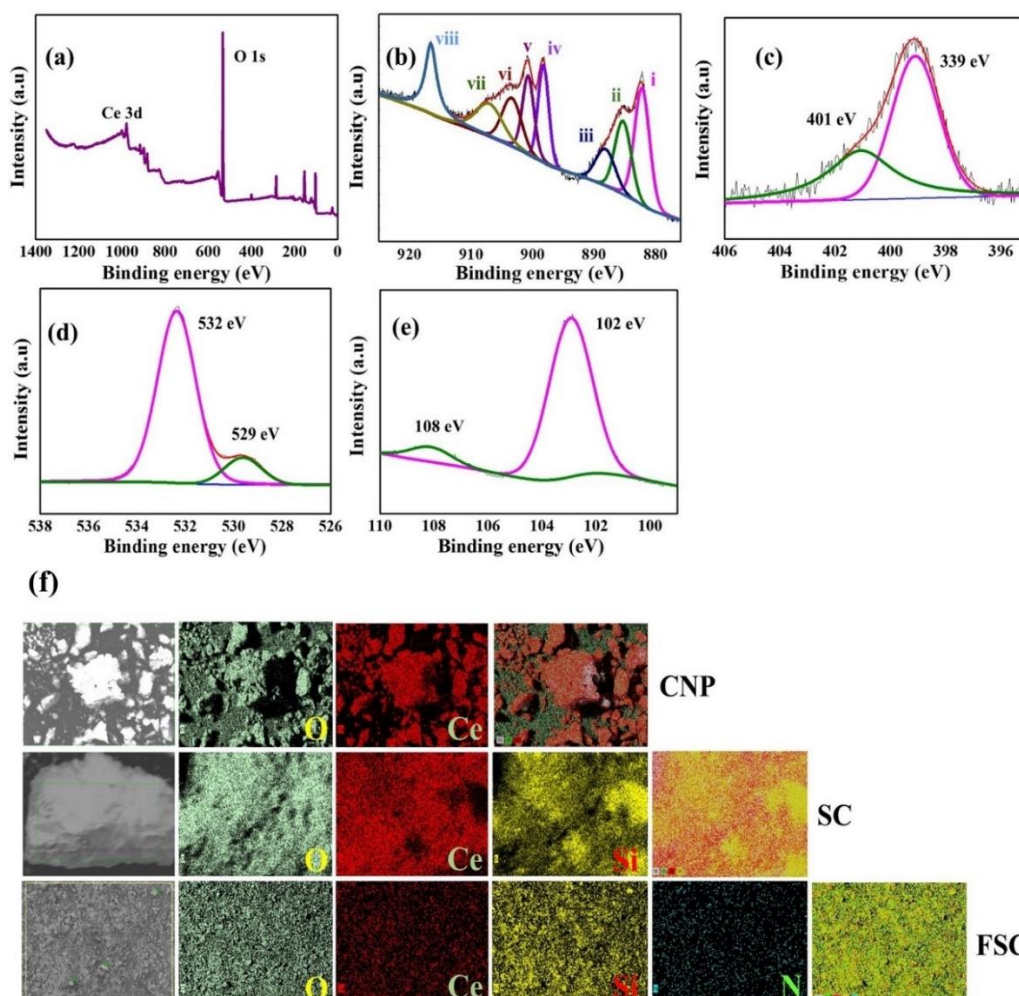


Figure 3.2. XPS spectra of FSC. (a) Surface survey spectrum (b) Ce 3d. (c) N 1s. (d) O 1s. (e) Si 2p. (f) Elemental mapping of CNP, SC, and FSC.

3.4.2. Antioxidant activity

Overproduction of free radicals at wound locations can induce oxidative stress, further exacerbating wound chronicity. For a material to be effective in wound healing, it should inherently possess antioxidant capabilities.⁴³ The antioxidant potential of our nanomaterial was validated using the ABTS assay. In the presence of free radicals, ABTS undergoes oxidation, resulting in the formation of a green-colored radical cation, $\text{ABTS}^{+\cdot}$, which exhibits absorbance at 734 nm. Antioxidants counteract this oxidation by neutralizing these radicals, preventing the formation of the colored compound. While CNPs are recognized as effective radical scavengers, their activity is size-dependent. Our results indicated that amine-functionalized materials, namely FSC and FCNP, demonstrated superior scavenging capacities of 86% and 70%, compared to CNP and SC, which only achieved 33% and 13% scavenging (**Figure. 3a**). As expected, MSN showed no significant activity, while ascorbic acid (serving as a positive control) at a concentration of 10 $\mu\text{g/mL}$ displayed an activity of 87%. The introduction of the $-\text{NH}_2$ functional group amplified the antioxidant potential of the material because of the amine group's enhanced electron-donating capacity and its proficiency in neutralizing free radicals.⁴⁴ The antioxidant activity presented in this study surpasses the 68% achieved by the cerium oxide hydrogel composite discussed by Augustine *et al.*⁴⁵ and is on par with the 80-89% results from biosynthesized cerium reported by Nezhad *et al.*⁴⁶ and Saravanakumar *et al.*⁴⁷

3.4.3. Haloperoxidase-mimicking activity

Haloperoxidases are a subset of peroxidase enzymes responsible for catalyzing halide oxidation. The enzyme-mimetic activity of our material was assessed using the phenol red bromination assay (**Figure 3.3b**). MSN and SC displayed no activity, while CNPs exhibited some activity. However, the functionalized variants, FCNP and FSC, demonstrated enzyme-like behaviors, as evident by a spectral shift from 590 nm to 560 nm (**Figure 3.3c**). This shift can be attributed to the inherent basicity of these materials.⁴⁸ In the presence of a haloperoxidase-mimicking catalyst, phenol red undergoes bromination to produce bromophenol blue when halide ions and peroxide are available. A decrease in phenol red concentration (λ_{max} at 432 nm) coupled with a rise in bromophenol blue concentration (λ_{max} at 590 nm) indicates a successful reaction.³⁰ The decomposition of H_2O_2 on cerium oxide's crystalline facets initiates the oxidation of a Ce^{3+} site to a Ce^{4+} site. This transition results in the creation of two ligands: a hydroxyl anion (OH^-) and a hydroxyl radical (OH^\cdot). The OH^\cdot radical subsequently reacts with the bromide anion, leading to the production of hypobromite and regeneration of Ce^{3+} site. This surface-mediated interaction facilitates the generation of hypohalous acid, a compound known to inhibit bacterial quorum sensing, which is a crucial

communication system for modulating factors that influence biofilm formation. The haloperoxidase activity will enhance its antibacterial efficacy.³⁹

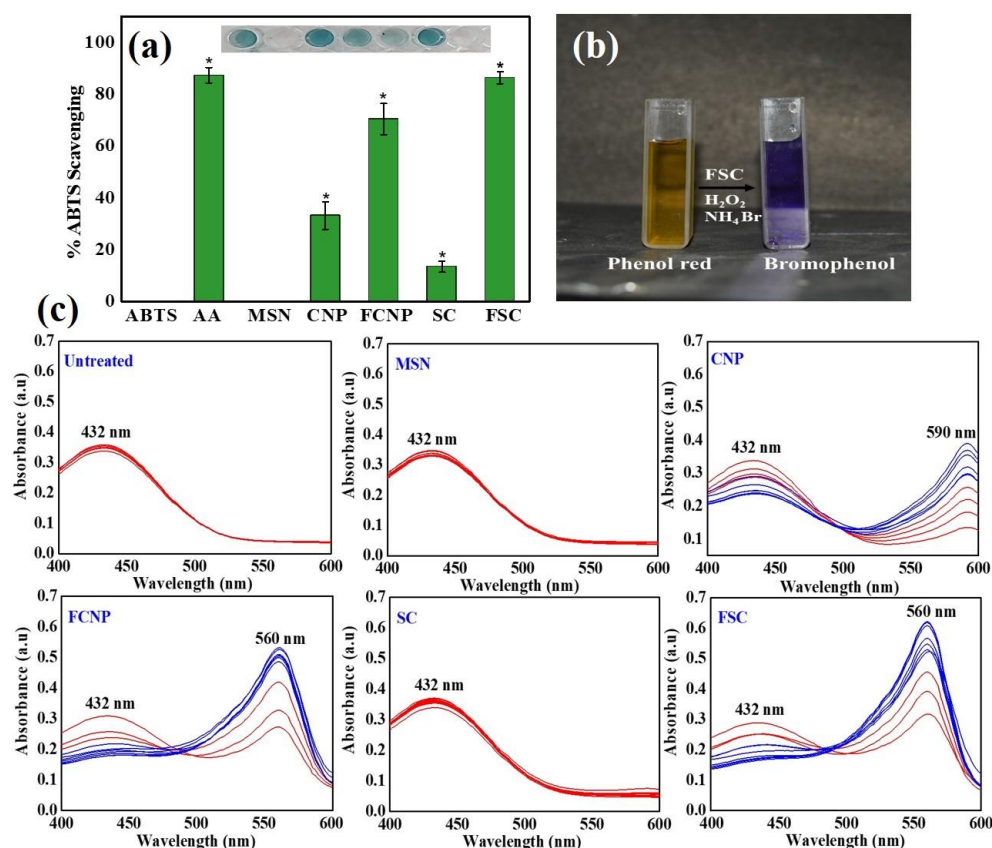


Figure 3.3 (a) ABTS assay of untreated ABTS⁺ and treated with ascorbic acid, MSN, CNP, FCNP, SC, and FSC. *p < 0.05 represents the statistically significant difference. (b) Bromination of phenol red to bromophenol catalyzed by FSC (haloperoxidase-mimicking activity) in presence of ammonium bromide and hydrogen peroxide. (c) UV-Vis spectra of untreated ABTS⁺ and treated with MSN, CNP, FCNP, SC, and FSC over a duration of 5 h, indicating the conversion of phenol red to bromophenol.

3.4.4. Antibacterial activity

The antimicrobial spectrum of the material in question was evaluated against both Gram-negative (*E. coli*) and Gram-positive (*S. aureus*) bacteria by using the broth dilution technique (**Figure 3.4**). When tested against *E. coli*, the unmodified samples of MSN, CNP, and SC (2 mg/mL) demonstrated activities of 6%, 62%, and 42% over a 24 h period. In contrast, the functionalized samples, FCNP and FSC, exhibited enhanced activities of 73% and 82% (**Figure 3.4a**). Given the prevalence of *S. aureus* in chronic wound infections, its inhibition is of particular interest. Remarkably, FSC achieved near-total inhibition (99.9%) within 12 h, while FCNP showed 71% inhibition. The non-functionalized nanoparticles, MSN, CNP, and SC, showed inhibitions of 5%, 61%, and 51% (**Figure 3.4b**). The inhibition rates of *E. coli* at 12 hours and *S. aureus* at 6 h are presented in **Figure A9 (Appendix)**. In comparison to

previously reported cerium nanocomposites, FSC demonstrated superior antibacterial properties.^{49,50}

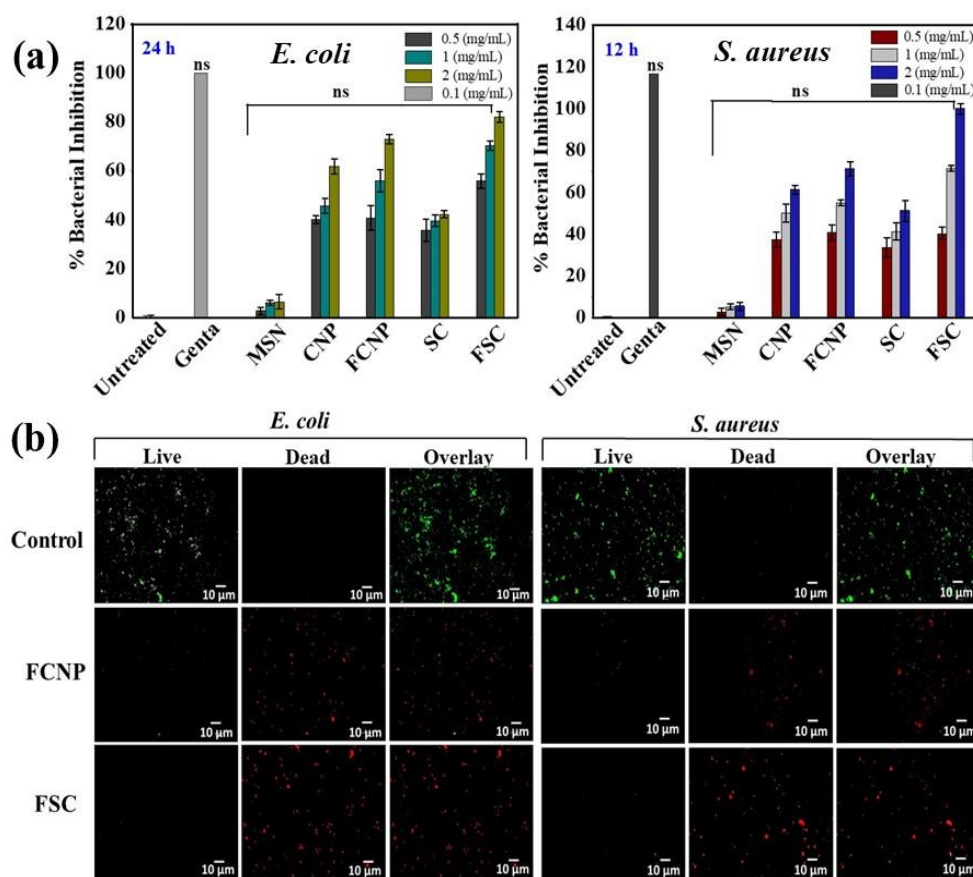


Figure 3.4. Antibacterial activity and live/dead assay. (a) Inhibition of bacterial growth of *E. coli* (24 h) and *S. aureus* (12 h). * $p < 0.05$ represents the statistically significant difference and ns the non-significant difference. (b) Fluorescent images of untreated and FCNP and FSC-treated bacterial suspension of *E. coli* and *S. aureus*. Scale bar: 10 μm .

The primary mechanism of action for cationic surfaces is bacterial membrane penetration and disruption. Given the negative charge of bacterial membranes, there's an electrostatic attraction to positively charged nanoparticles.^{51,52} A highly cationic nature promotes bacterial adhesion, leading to significant membrane alterations and subsequent cell death. The inherent activity of cerium oxide, combined with the functionalized silica surface, contributes to its effectiveness. The material displayed robust activity against both bacterial types but was notably more effective against *S. aureus*. This could be attributed to the inherent resistance of Gram-negative bacteria due to their double-membrane structure.^{23,53} To further understand the influence of FSC particle size on antibacterial activity, nanocomposites of varying sizes (257 nm, 450 nm, and 911 nm) were fabricated and tested against *E. coli* and *S. aureus* (**Figure A10, Appendix**). While increasing the particle size to 450 nm didn't significantly impact antibacterial activity but a substantial reduction was observed when the size was further increased to 911 nm (**Figure A11, Appendix**).

To evaluate the impact of nanoparticles on bacterial cell membrane integrity, a live/dead viability assay was employed on both *E. coli* and *S. aureus*. This assay utilizes two fluorescent nucleic acid stains: SYTO 9, which can permeate both live and dead bacterial cells and emits a green fluorescence at 485 nm, and propidium iodide (PI), which enters only bacteria with damaged membranes, emitting a red fluorescence. Post-dye incubation, the bacterial cells were fixed and observed under a fluorescence microscope. Healthy bacteria with intact membranes fluoresce green, while those with damaged membranes appear red. As depicted in **Figure 3.4b**, the majority of bacterial cells treated with the functionalized nanoparticles, FCNP and FSC, were predominantly dead. The results of the live/dead assay for bacteria treated with gentamicin (a positive control), MSN, CNP, and SC are provided in the appendix (**Figure A12 and A13**). To further validate the interaction between FSC and bacterial cell membranes, leading to bacterial cell death, HR-TEM was employed (**Figure 3.5**). Untreated bacterial cells displayed a well-preserved morphology, including intact membranes and cytoplasm. In contrast, bacteria treated with FSC showed signs of membrane disruption and overall cellular damage, underscoring the bactericidal properties of FSC on the cell surface.

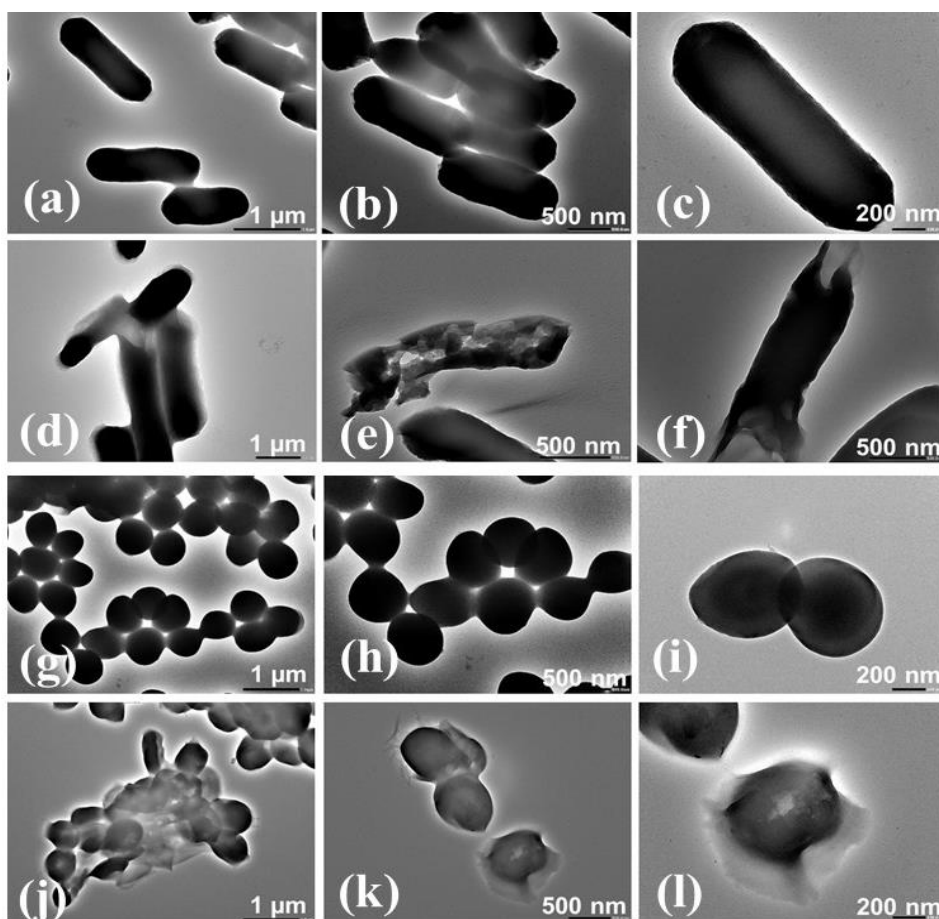


Figure 3.5 HR-TEM images of bacterial cells. (a, b, c) Untreated *E. coli*. (d, e, f) *E. coli* treated with FSC. (g, h, i) Untreated *S. aureus*. (j, k, l) *S. aureus* treated with FSC. Scale bar: (a, d, g, j) 1 μ m. (b, e, h, k) 500 nm. (c, f, i, l) 200 nm.

3. 4.5. Biofilm inhibition

The nanocomposite's ability to inhibit biofilm formation was assessed using the crystal violet staining technique, as depicted in **Figure 3.6a**. *S. aureus*, a prevalent pathogen in chronic wounds, was selected for this experiment and was exposed to the samples for duration of 48 h. At a bacterial concentration of 2 mg/mL, FSC demonstrated an 80% reduction in biofilm formation, while SC achieved only a 35% reduction. CNP and FCNP displayed antibiofilm activities of 41% and 51%, whereas MSN had minimal effect. The nanomaterials' impact on biofilm development can be linked to their antibacterial properties- effective bacterial eradication naturally hinders biofilm establishment. The positively charged surface of the nanomaterials adheres to the negatively charged bacterial surface, neutralizing the bacteria and obstructing both cell-to-cell adhesion and subsequent biofilm development.^{26,49} Consequently, the suppression of biofilm growth is directly related to the inhibition of bacterial proliferation. Following the biofilm inhibition, our focus shifted to the impact of composite material on established biofilms. A bacterial concentration of 1×10^7 CFU/mL was incubated to allow biofilm formation over 48 h. The medium was substituted with FSC (2 mg/mL) and further incubated for 24 h. The biofilm's mass was quantified via crystal violet staining, as illustrated in **Figure 3.6b**. FSC inhibited 77% of biofilm growth, whereas the SC composite only managed a 40% reduction. Notably, pure cerium oxide (CNP) demonstrated a slightly superior activity (83%) against the mature biofilm, likely due to its DNase-like properties. The functionalized cerium (FCNP) achieved a 62% reduction, while MSN exhibited no significant effect. The cationic groups present interact and form crosslinks with the biofilm's extracellular DNA. The combination of this cationic charge and cerium's inherent DNase activity leads to the disruption of the mature biofilm.⁵⁵

Previous research has shown that naturally produced cerium oxide nanoparticles inhibited 70% of *S. aureus* biofilm,⁵⁶ while Sn-doped cerium oxide nanoparticles achieved approximately 65% biofilm inhibition.⁵⁷ Other studies, such as those by Qin *et al.*⁵⁸ and Kumar *et al.*⁵⁹ reported 85% and 80% biofilm disruption using different cerium oxide nanoparticle formulations. Our nanocomposite not only inhibited biofilm formation but also demonstrated a disruptive effect on mature biofilms. To assess the viability of bacteria within the biofilm, wells were rinsed to eliminate non-adherent bacteria. This was followed by a staining process using a bacterial viability kit (**Figure 3.6c**). In the untreated sample, a significant number of live cells were observed. In contrast, CNP and FSC-treated samples predominantly contained dead cells with a minimal presence of live cells.

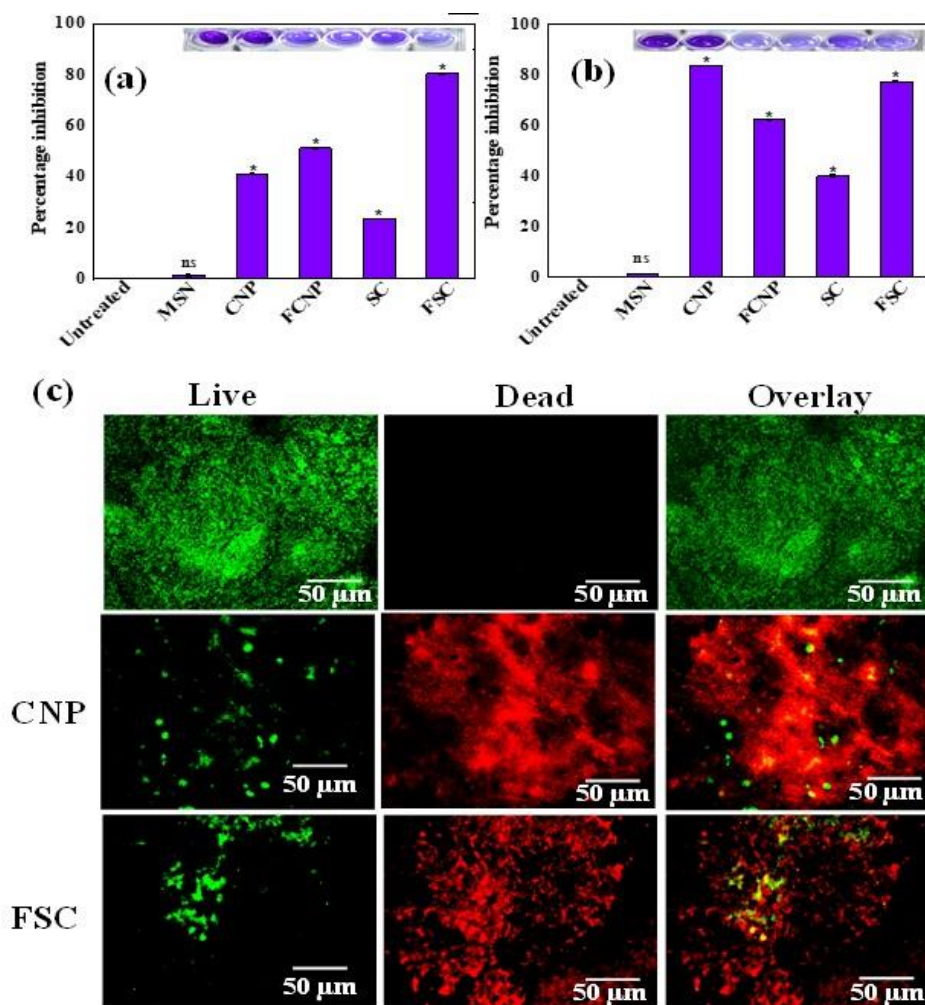


Figure 3.6. Inhibition of biofilm. (a) Inhibition of the biofilm formation by MSN, CNP, FCNP, SC, and FSC. (b) Disruptive effect of MSN, CNP, FCNP, SC, and FSC on the established biofilm. * $p < 0.05$ represents the statistically significant difference and ns the non-significant difference. (c) Fluorescence microscopic live/dead stained images of untreated, and CNP- and FSC-treated biofilm. Scale bar: 50 μm .

3.4.6. Cell viability

For biomaterials designed for wound healing applications, promoting cell proliferation is crucial to facilitate wound closure.⁶⁰ The cell viability of materials was evaluated using two assays: MTT and CCK 8, spanning a period of 72 h (**Figure 3.7** and **Figure A14, Appendix**).

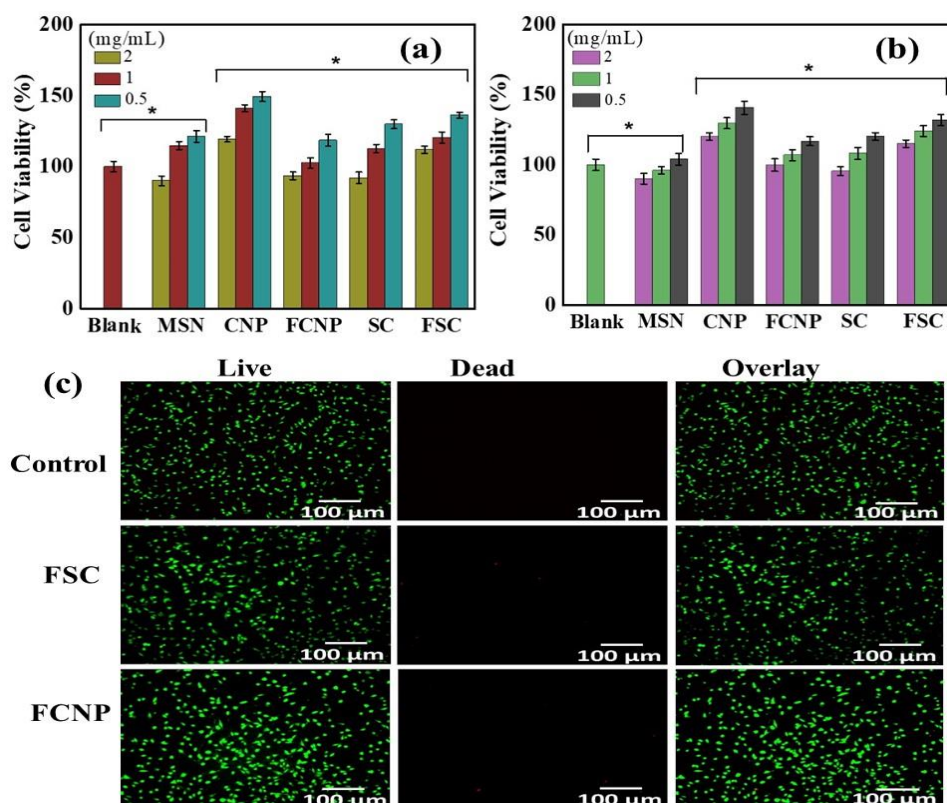


Figure 3.7. Cell viability assays and live/dead cell staining of blank (untreated) and MSN, CNP, FCNP, SC, and FSC extract-treated L929 cells for 24 h. (a) MTT. (b) CCK 8. * $p < 0.05$ represents the statistically significant difference and ns the non-significant difference. (c) Fluorescence images of untreated cells (control) and cells treated with FCNP and FSC conditioned media. Scale bar: 100 μm .

Observations indicated that all tested samples were compatible with mouse fibroblast cells (L929). It was observed that with an increase in nanomaterial concentration led to a decrease in cell viability. After 24 h incubation with a concentration of 2 mg/mL, both bare MSNPs and CNPs exhibited cell viability of around 90% and slightly above 100%. As both FCNP and FSC composites demonstrated over 100% viability, it implies that they have proliferative properties. In the CCK 8 assay, all samples up to a concentration of 2 mg/mL were deemed non-toxic. CNP, FCNP, and FSC displayed over 100% cell viability against L929 cells, while MSN and SC recorded 90% and 95% viability. By 72 h, an increase in cell viability was observed, suggesting the non-toxic nature of nanomaterials (**Figure 14, Appendix**). The slight discrepancy between the two assay results might stem from the inherent sensitivity differences between the assays. Notably, the functionalized surfaces of CNP and SC were less proliferative compared to pure cerium oxide, likely due to their cationic properties. Nevertheless, both materials maintained substantial cell proliferation capabilities, which makes them potential candidates for wound healing applications. The material's cytotoxicity and its impact on cellular membrane integrity were further validated using a live/dead cell staining kit. The resulting images highlighted proliferation in CNP, FCNP, and

FSC samples compared to the control (**Figure 3.7c**), which aligns with the cell viability data. Comparable outcomes were observed for MSN, SC, and CNP when exposed to conditioned media-treated L929 cells (**Figure 15, Appendix**). The functionalized nanomaterial, FSC, exhibited superior proliferative properties when juxtaposed with previously reported cerium hydrogel composites and pure cerium oxide nanoparticles.^{45,53}

3.4.7. Hemolysis

All samples underwent hemocompatibility testing by exposure to a red blood cell (RBC) solution in PBS. The results indicated that the samples were non-hemolytic (**Figure 3.8a**). Supernatants from all nanomaterial-treated samples (at a concentration of 2 mg/mL) appeared almost transparent, indicating less than 4% hemolysis, which is clinically acceptable. Notably, the amine-functionalized samples, FCNP and FSC, exhibited hemolysis percentages approximately twice that of their non-functionalized counterparts. Triton X, serving as a positive control, demonstrated complete (100%) lysis, while PBS (used as a negative control) showed no lysis. The reduced hemolytic activity observed in MSNs and CNPs can be attributed to their negative charge, which may deter interactions with RBCs.⁶¹ In contrast, positively charged nanomaterials, such as FCNPs and SCs, exhibited pronounced electrostatic interactions with RBC membranes, potentially leading to membrane disruption³⁶, as suggested by Uppal *et al.*⁶² and More *et al.*⁶³

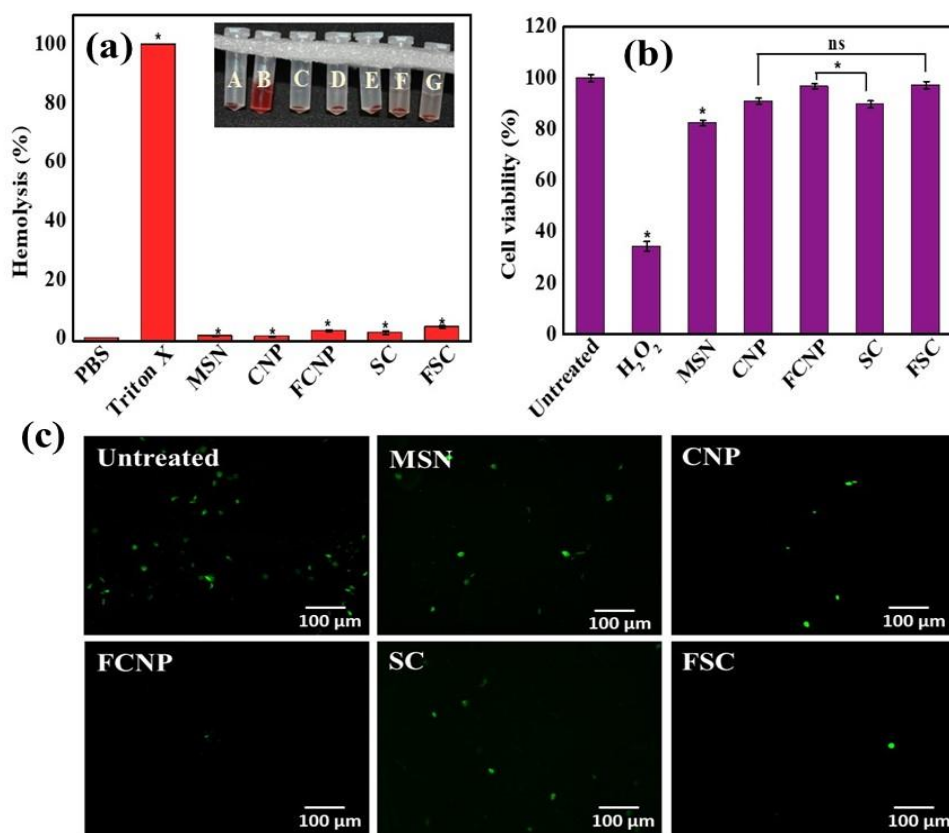


Figure 3.8. (a) *In vitro* percent hemolysis of untreated and triton X, MSN, CNP, FCNP, SC, and FSC-treated RBCs. (b) Viability of L929 cells in the presence of oxidative stress in untreated cells (control) and MSN, CNP, FCNP, SC and FSC-treated cells. *p < 0.05

represents the statistically significant difference and ns the non-significant difference. (c) Reactive oxygen species (ROS) scavenging in L929 cells. Scale bar: 100 μ m.

3.4.8. Reactive oxygen species (ROS) scavenging

To assess cell viability under oxidative stress conditions, H_2O_2 was employed to instigate oxidative stress and prompt radical formation within cells. L929 cells were exposed to H_2O_2 alone (serving as a positive control) and the conditioned media of samples, MSN, CNP, FCNP, SC, and FSC (2 mg/mL). Untreated cells acted as a negative control. The antioxidant capabilities of FSC and FCNP effectively neutralized the radicals, thereby safeguarding cells from oxidative stress-induced damage and mortality (**Figure 3.8b**). Cells subjected to these cationic materials, namely FSC and FCNP, exhibited cell viabilities of 97% and 96%. These figures align closely with the 91% viability observed in CNP-treated cells.²⁹ Intriguingly, MSN and SC, despite their limited antioxidant ability in the ABTS chemical assay, still demonstrated cell viabilities of 82% and 89%. Compared to CNPs (91 %), FSC and FCNP displayed cell viability of 97 and 96%.²⁹ We can deduce that the antioxidant property of FSC's is giving its protection against oxidative stress.

Oxidative stress in wounded tissues, primarily induced due to ROS, can culminate in cellular death, thereby hampering the healing process.⁵⁶ Consequently, for a biomaterial earmarked for wound healing applications, the ability to scavenge ROS is crucial. In our experiment, H_2O_2 was utilized to induce ROS production in L929 cells. The fluorogenic dye, DCFDA, was employed to stain ROS species. Upon cellular uptake, DCFH-DA undergoes deacetylation by intracellular esterases, transforming into a non-fluorescent compound. This compound is subsequently oxidized to 2'-7' dichlorofluorescein (DCF) by ROS. Hence, a higher intracellular radical presence would yield more DCF.⁶⁴ Both FCNP and FSC showcased superior ROS scavenging capabilities compared to CNPs, as depicted in **Figure 3.8c**. This can be attributed to their enhanced antioxidant properties. While SC and MSN exhibited modest activity, their performance was notably improved when compared with the ABTS antioxidant data. These findings are consistent with previously published research.^{41, 60}

3.4.9. Scratch assay

The nanocomposite's influence on cell migration during in vitro wound healing was checked using the scratch assay (**Figure 3.9**). Both cell migration and proliferation are instrumental in tissue restoration during the wound healing process. Post the creation of scratch on the cell monolayer, the cells were exposed to conditioned media, and the subsequent healing was monitored. For cells treated with FSC, cellular migration commenced by the 6 h, with notable healing evident by 12 h, culminating in complete wound closure by the 24 h. This healing trajectory can be ascribed to the composite's inherent proliferative attributes and the chemotactic properties of cerium oxide. Both CNPs and FCNPs achieved 100% healing, while SC and MSN achieved wound closures of 81% and 71%. In contrast, the untreated control

group exhibited 56% wound closure (**Figure A16, Appendix**). Wound areas at each time interval were quantified utilizing the ImageJ software. FSC possesses healing properties, which makes it a viable candidate for wound healing applications. These findings align with the outcomes observed for the electrospun cerium hydrogel nanocomposite reported by More *et al.*⁶³

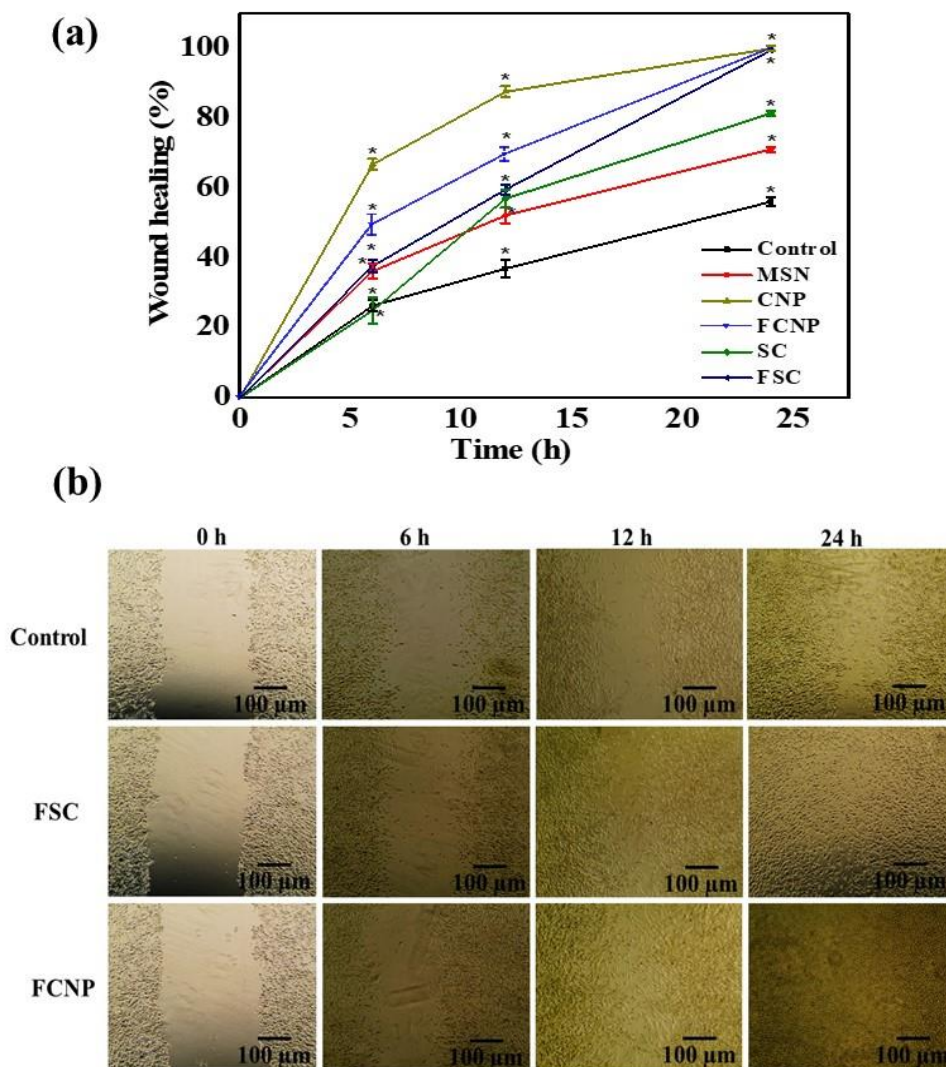


Figure 3.9. (a) Percentage wound healing of untreated and MSN, CNP, FCNP, SC, and FSC-treated L929 cells. * $p < 0.05$ represents the statistically significant difference and ns the non-significant difference. (b) Microscopic images of untreated and FSC and FCNP-treated L929 cells at 0, 6, 12, and 24 h. Scale bar: 100 μ m.

3.5 Conclusions

In essence, we've engineered and meticulously analyzed a highly cationic silica ceria nanocomposite, derived from mesoporous silica nanoparticles and cerium oxide nanoparticles, with the objective of enhancing the antibacterial and wound healing capabilities of cerium oxide nanoparticles. The mesoporous silica nanoparticles offer an expansive surface area, facilitating the even distribution of cerium oxide

nanoparticles and enabling surface functionalization. Concurrently, the cerium oxide nanoparticles impart antibacterial and anti-biofilm attributes. This nanocomposite demonstrated formidable antibacterial activity against *E. coli* and *S. aureus*, prevented biofilm genesis, and disrupted pre-established *S. aureus* biofilms. It manifested antioxidant capabilities and shielded cells from oxidative stress induced by reactive oxygen species. Cytocompatibility tests revealed the nanocomposite's safety towards mouse fibroblast cells, and it was found to foster cell proliferation. Moreover, the nanocomposite facilitated the healing of wounds in mouse fibroblast cells. A salient feature of this nanocomposite is its antibiotic-free nature, relying solely on the inherent activities of its constituents for its effects. While the results are encouraging, it's imperative to assess this nanomaterial against clinical strains of wound-related bacteria and gauge its effectiveness against resistant variants. This nanocomposite holds significant promise in the realm of wound healing, particularly in rejuvenating healing processes hindered by biofilms.

References

- (1) Menke, N. B.; Ward, K. R.; Witten, T. M.; Bonchev, D. G.; Diegelmann, R. F. Impaired Wound Healing. *Clin. Dermatol.* **2007**, *25* (1), 19–25. <https://doi.org/10.1016/j.clindermatol.2006.12.005>.
- (2) Falanga, V.; Isseroff, R. R.; Soulika, A. M.; Romanelli, M.; Margolis, D.; Kapp, S.; Granick, M.; Harding, K. Chronic Wounds. *Nat. Rev. Dis. Primer* **2022**, *8* (1), 50. <https://doi.org/10.1038/s41572-022-00377-3>.
- (3) Sen, C. K. Human Wounds and Its Burden: An Updated Compendium of Estimates. *Adv. Wound Care* **2019**, *8* (2), 39–48. <https://doi.org/10.1089/wound.2019.0946>.
- (4) Wolcott, R. D.; Rhoads, D. D.; Dowd, S. E. Biofilms and Chronic Wound Inflammation. *J. Wound Care* **2008**, *17* (8), 333–341. <https://doi.org/10.12968/jowc.2008.17.8.30796>.
- (5) Jiang, L.; Loo, S. C. J. Intelligent Nanoparticle-Based Dressings for Bacterial Wound Infections. *ACS Appl. Bio Mater.* **2021**, *4* (5), 3849–3862. <https://doi.org/10.1021/acsabm.0c01168>.
- (6) Wang, J.; Chen, X.-Y.; Zhao, Y.; Yang, Y.; Wang, W.; Wu, C.; Yang, B.; Zhang, Z.; Zhang, L.; Liu, Y.; Du, X.; Li, W.; Qiu, L.; Jiang, P.; Mou, X.-Z.; Li, Y.-Q. pH-Switchable Antimicrobial Nanofiber Networks of Hydrogel Eradicate Biofilm and Rescue Stalled Healing in Chronic Wounds. *ACS Nano* **2019**, *13* (10), 11686–11697. <https://doi.org/10.1021/acs.nano.9b05608>.
- (7) Bjarnsholt, T. The Role of Bacterial Biofilms in Chronic Infections. *APMIS* **2013**, *121*, 1–58. <https://doi.org/10.1111/apm.12099>.
- (8) Negi, D.; Singh, Y. Gallium Oxide Nanoparticle-Loaded, Quaternized Chitosan-Oxidized Sodium Alginate Hydrogels for Treatment of Bacteria-Infected Wounds. *ACS Appl. Nano Mater.* **2023**, *6* (14), 13616–13628. <https://doi.org/10.1021/acsanm.3c02266>.
- (9) Sharma, D.; Misba, L.; Khan, A. U. Antibiotics versus Biofilm: An Emerging Battleground in Microbial Communities. *Antimicrob. Resist. Infect. Control* **2019**, *8* (1), 76. <https://doi.org/10.1186/s13756-019-0533-3>.
- (10) Xiong, X.; Huang, Y.; Lin, C.; Liu, X. Y.; Lin, Y. Recent Advances in Nanoparticulate Biomimetic Catalysts for Combating Bacteria and Biofilms. *Nanoscale* **2019**, *11* (46), 22206–22215. <https://doi.org/10.1039/C9NR05054J>.
- (11) Karnwal, A.; Kumar, G.; Pant, G.; Hossain, K.; Ahmad, A.; Alshammari, M. B. Perspectives on Usage of Functional Nanomaterials in Antimicrobial Therapy for Antibiotic-Resistant Bacterial Infections. *ACS Omega* **2023**, *8* (15), 13492–13508. <https://doi.org/10.1021/acsomega.3c00110>.

- (12) Jiang, T.; Li, Q.; Qiu, J.; Chen, J.; Du, S.; Xu, X.; Wu, Z.; Yang, X.; Chen, Z.; Chen, T. Nanobiotechnology: Applications in Chronic Wound Healing. *Int. J. Nanomedicine* **2022**, Volume 17, 3125–3145. <https://doi.org/10.2147/IJN.S372211>.
- (13) Han, C.; Romero, N.; Fischer, S.; Dookran, J.; Berger, A.; Doiron, A. L. Recent Developments in the Use of Nanoparticles for Treatment of Biofilms. *Nanotechnol. Rev.* **2017**, 6 (5), 383–404. <https://doi.org/10.1515/ntrev-2016-0054>.
- (14) Liu, Z.; Wang, F.; Ren, J.; Qu, X. A Series of MOF/Ce-Based Nanozymes with Dual Enzyme-like Activity Disrupting Biofilms and Hindering Recolonization of Bacteria. *Biomaterials* **2019**, 208, 21–31. <https://doi.org/10.1016/j.biomaterials.2019.04.007>.
- (15) Lee, S. S.; Song, W.; Cho, M.; Puppala, H. L.; Nguyen, P.; Zhu, H.; Segatori, L.; Colvin, V. L. Antioxidant Properties of Cerium Oxide Nanocrystals as a Function of Nanocrystal Diameter and Surface Coating. *ACS Nano* **2013**, 7 (11), 9693–9703. <https://doi.org/10.1021/nn4026806>.
- (16) Alpaslan, E.; Geilich, B. M.; Yazici, H.; Webster, T. J. pH-Controlled Cerium Oxide Nanoparticle Inhibition of Both Gram-Positive and Gram-Negative Bacteria Growth. *Sci. Rep.* **2017**, 7 (1), 45859. <https://doi.org/10.1038/srep45859>.
- (17) Chen, Z.; Ji, H.; Liu, C.; Bing, W.; Wang, Z.; Qu, X. A Multinuclear Metal Complex Based DNase-Mimetic Artificial Enzyme: Matrix Cleavage for Combating Bacterial Biofilms. *Angew. Chem.* **2016**, 128 (36), 10890–10894. <https://doi.org/10.1002/ange.201605296>.
- (18) Khulbe, K.; Karmakar, K.; Ghosh, S.; Chandra, K.; Muges, G. Nanoceria-Based Phospholipase-Mimetic Cell Membrane Disruptive Anti-Biofilm Agents. 30.
- (19) Xu, Z.; Han, S.; Gu, Z.; Wu, J. Advances and Impact of Antioxidant Hydrogel in Chronic Wound Healing. *Adv. Healthc. Mater.* **2020**, 9 (5), 1901502. <https://doi.org/10.1002/adhm.201901502>.
- (20) Ju, X.; Fučíková, A.; Šmíd, B.; Nováková, J.; Matolínová, I.; Matolín, V.; Janata, M.; Bělinová, T.; Hubálek Kalbáčová, M. Colloidal Stability and Catalytic Activity of Cerium Oxide Nanoparticles in Cell Culture Media. *RSC Adv.* **2020**, 10 (65), 39373–39384. <https://doi.org/10.1039/D0RA08063B>.
- (21) Tasia, W.; Lei, C.; Cao, Y.; Ye, Q.; He, Y.; Xu, C. Enhanced Eradication of Bacterial Biofilms with DNase I-Loaded Silver-Doped Mesoporous Silica Nanoparticles. *Nanoscale* **2020**, 12 (4), 2328–2332. <https://doi.org/10.1039/C9NR08467C>.
- (22) He, Y.; Liang, S.; Long, M.; Xu, H. Mesoporous Silica Nanoparticles as Potential Carriers for Enhanced Drug Solubility of Paclitaxel. *Mater. Sci. Eng. C* **2017**, 78, 12–17. <https://doi.org/10.1016/j.msec.2017.04.049>.
- (23) Yang, Y.; Cai, Z.; Huang, Z.; Tang, X.; Zhang, X. Antimicrobial Cationic Polymers: From Structural Design to Functional Control. *Polym. J.* **2018**, 50 (1), 33–44. <https://doi.org/10.1038/pj.2017.72>.

- (24) Hoque, J.; Ghosh, S.; Paramanandham, K.; Haldar, J. Charge-Switchable Polymeric Coating Kills Bacteria and Prevents Biofilm Formation in Vivo. *ACS Appl. Mater. Interfaces* **2019**, *11* (42), 39150–39162. <https://doi.org/10.1021/acsami.9b11453>.
- (25) Maity, A.; Polshettiwar, V. Scalable and Sustainable Synthesis of Size-Controlled Monodisperse Dendritic Fibrous Nanosilica Quantified by E-Factor. *ACS Appl. Nano Mater.* **2018**, *1* (7), 3636–3643. <https://doi.org/10.1021/acsanm.8b00761>.
- (26) Trenque, I.; Magnano, G. C.; Bolzinger, M. A.; Roiban, L.; Chaput, F.; Pitault, I.; Briançon, S.; Devers, T.; Masenelli-Varlot, K.; Bugnet, M.; Amans, D. Shape-Selective Synthesis of Nanoceria for Degradation of Paraoxon as a Chemical Warfare Simulant. *Phys. Chem. Chem. Phys.* **2019**, *21* (10), 5455–5465. <https://doi.org/10.1039/C9CP00179D>.
- (27) Cho, E.-B.; Yim, S.; Kim, D.; Jaroniec, M. Surfactant-Assisted Synthesis of Mesoporous Silica/Ceria–Silica Composites with High Cerium Content under Basic Conditions. *J. Mater. Chem. A* **2013**, *1* (40), 12595. <https://doi.org/10.1039/c3ta12482g>.
- (28) Soto-Cantu, E.; Cueto, R.; Koch, J.; Russo, P. S. Synthesis and Rapid Characterization of Amine-Functionalized Silica. *Langmuir* **2012**, *28* (13), 5562–5569. <https://doi.org/10.1021/la204981b>.
- (29) Davoodbasha, M. A.; Saravanakumar, K.; Abdulkader, A. M.; Lee, S.-Y.; Kim, J.-W. Synthesis of Biocompatible Cellulose-Coated Nanoceria with pH-Dependent Antioxidant Property. *ACS Appl. Bio Mater.* **2019**, *2* (5), 1792–1801. <https://doi.org/10.1021/acsabm.8b00647>.
- (30) He, X.; Tian, F.; Chang, J.; Bai, X.; Yuan, C.; Wang, C.; Neville, A. Haloperoxidase Mimicry by CeO₂-x Nanorods of Different Aspect Ratios for Antibacterial Performance. *ACS Sustain. Chem. Eng.* **2020**, *8* (17), 6744–6752. <https://doi.org/10.1021/acssuschemeng.0c01113>.
- (31) Ivanova, A.; Ivanova, K.; Hoyo, J.; Heinze, T.; Sanchez-Gomez, S.; Tzanov, T. Layer-By-Layer Decorated Nanoparticles with Tunable Antibacterial and Antibiofilm Properties against Both Gram-Positive and Gram-Negative Bacteria. *ACS Appl. Mater. Interfaces* **2018**, *10* (4), 3314–3323. <https://doi.org/10.1021/acsami.7b16508>.
- (32) Kong, C.; Chee, C.-F.; Richter, K.; Thomas, N.; Abd. Rahman, N.; Nathan, S. Suppression of Staphylococcus Aureus Biofilm Formation and Virulence by a Benzimidazole Derivative, UM-C162. *Sci. Rep.* **2018**, *8* (1), 2758. <https://doi.org/10.1038/s41598-018-21141-2>.
- (33) Zhang, P.; Li, S.; Chen, H.; Wang, X.; Liu, L.; Lv, F.; Wang, S. Biofilm Inhibition and Elimination Regulated by Cationic Conjugated Polymers. *ACS Appl. Mater. Interfaces* **2017**, *9* (20), 16933–16938. <https://doi.org/10.1021/acsami.7b05227>.

- (34) Chauhan, N.; Singh, Y. Self-Assembled Fmoc-Arg-Phe-Phe Peptide Gels with Highly Potent Bactericidal Activities. *ACS Biomater. Sci. Eng.* **2020**, *6* (10), 5507–5518. <https://doi.org/10.1021/acsbiomaterials.0c00660>.
- (35) Malhotra, K.; Shankar, S.; Rai, R.; Singh, Y. Broad-Spectrum Antibacterial Activity of Proteolytically Stable Self-Assembled A γ -Hybrid Peptide Gels. *Biomacromolecules* **2018**, *19* (3), 782–792. <https://doi.org/10.1021/acs.biomac.7b01582>.
- (36) Yin, M.; Wan, S.; Ren, X.; Chu, C.-C. Development of Inherently Antibacterial, Biodegradable, and Biologically Active Chitosan/Pseudo-Protein Hybrid Hydrogels as Biofunctional Wound Dressings. *ACS Appl. Mater. Interfaces* **2021**, *13* (12), 14688–14699. <https://doi.org/10.1021/acsami.0c21680>.
- (37) Li, Y.; Sun, M.; Liu, Y.; Liang, J.; Wang, T.; Zhang, Z. Gymnemic Acid Alleviates Type 2 Diabetes Mellitus and Suppresses Endoplasmic Reticulum Stress *in Vivo* and *in Vitro*. *J. Agric. Food Chem.* **2019**, *67* (13), 3662–3669. <https://doi.org/10.1021/acs.jafc.9b00431>.
- (38) Liang, C.-C.; Park, A. Y.; Guan, J.-L. In Vitro Scratch Assay: A Convenient and Inexpensive Method for Analysis of Cell Migration in Vitro. *Nat. Protoc.* **2007**, *2* (2), 329–333. <https://doi.org/10.1038/nprot.2007.30>.
- (39) Hu, M.; Korschelt, K.; Viel, M.; Wiesmann, N.; Kappl, M.; Brieger, J.; Landfester, K.; Thérien-Aubin, H.; Tremel, W. Nanozymes in Nanofibrous Mats with Haloperoxidase-like Activity To Combat Biofouling. *ACS Appl. Mater. Interfaces* **2018**, *10* (51), 44722–44730. <https://doi.org/10.1021/acsami.8b16307>.
- (40) Miao, W.; Zhang, C.; Cai, Y.; Zhang, Y.; Lu, H. Fast Solid-Phase Extraction of N-Linked Glycopeptides by Amine-Functionalized Mesoporous Silica Nanoparticles. *The Analyst* **2016**, *141* (8), 2435–2440. <https://doi.org/10.1039/C6AN00285D>.
- (41) Rojas, S.; Gispert, J. D.; Abad, S.; Buaki-Sogo, M.; Victor, V. M.; Garcia, H.; Herance, J. R. In Vivo Biodistribution of Amino-Functionalized Ceria Nanoparticles in Rats Using Positron Emission Tomography. *Mol. Pharm.* **2012**, *9* (12), 3543–3550. <https://doi.org/10.1021/mp300382n>.
- (42) Sreeremya, T. S.; Thulasi, K. M.; Krishnan, A.; Ghosh, S. A Novel Aqueous Route To Fabricate Ultrasmall Monodisperse Lipophilic Cerium Oxide Nanoparticles. *Ind. Eng. Chem. Res.* **2012**, *51* (1), 318–326. <https://doi.org/10.1021/ie2019646>.
- (43) Kim, J. H.; Yang, B.; Tedesco, A.; Lebig, E. G. D.; Ruegger, P. M.; Xu, K.; Borneman, J.; Martins-Green, M. High Levels of Oxidative Stress and Skin Microbiome Are Critical for Initiation and Development of Chronic Wounds in Diabetic Mice. *Sci. Rep.* **2019**, *9* (1), 19318. <https://doi.org/10.1038/s41598-019-55644-3>.
- (44) Wang, L.; Yang, F.; Zhao, X.; Li, Y. Effects of Nitro- and Amino-Group on the Antioxidant Activity of Genistein: A Theoretical Study. *Food Chem.* **2019**, *275*, 339–345. <https://doi.org/10.1016/j.foodchem.2018.09.108>.

- (45) Augustine, R.; Zahid, A. A.; Hasan, A.; Dalvi, Y. B.; Jacob, J. Cerium Oxide Nanoparticle-Loaded Gelatin Methacryloyl Hydrogel Wound-Healing Patch with Free Radical Scavenging Activity. *ACS Biomater. Sci. Eng.* **2021**, *7* (1), 279–290. <https://doi.org/10.1021/acsbiomaterials.0c01138>.
- (46) Aseyd Nezhad, S.; Es-haghi, A.; Tabrizi, M. H. Green Synthesis of Cerium Oxide Nanoparticle Using *ORIGANUM MAJORANA* L. Leaf Extract, Its Characterization and Biological Activities. *Appl. Organomet. Chem.* **2020**, *34* (2). <https://doi.org/10.1002/aoc.5314>.
- (47) Saravanakumar, K.; Sathiyaseelan, A.; Mariadoss, A. V. A.; Wang, M.-H. Antioxidant and Antidiabetic Properties of Biocompatible Ceria Oxide (CeO₂) Nanoparticles in Mouse Fibroblast NIH3T3 and Insulin Resistant HepG2 Cells. *Ceram. Int.* **2021**, *47* (6), 8618–8626. <https://doi.org/10.1016/j.ceramint.2020.11.230>.
- (48) Schornack, P. A.; Gillies, R. J. Contributions of Cell Metabolism and H⁺ Diffusion to the Acidic pH of Tumors. *Neoplasia* **2003**, *5* (2), 135–145. [https://doi.org/10.1016/S1476-5586\(03\)80005-2](https://doi.org/10.1016/S1476-5586(03)80005-2).
- (49) Şen Karaman, D.; Kietz, C.; Govardhanam, P.; Slita, A.; Manea, A.; Pamukçu, A.; Meinander, A.; Rosenholm, J. M. Core@shell Structured Ceria@mesoporous Silica Nanoantibiotics Restrains Bacterial Growth in Vitro and in Vivo. *Mater. Sci. Eng. C* **2021**, 112607. <https://doi.org/10.1016/j.msec.2021.112607>.
- (50) Kalaycıoğlu, Z.; Kahya, N.; Adımcılar, V.; Kaygusuz, H.; Torlak, E.; Akın-Evingür, G.; Erim, F. B. Antibacterial Nano Cerium Oxide/Chitosan/Cellulose Acetate Composite Films as Potential Wound Dressing. *Eur. Polym. J.* **2020**, *133*, 109777. <https://doi.org/10.1016/j.eurpolymj.2020.109777>.
- (51) Bassous, N. J.; Garcia, C. B.; Webster, T. J. A Study of the Chemistries, Growth Mechanisms, and Antibacterial Properties of Cerium- and Yttrium-Containing Nanoparticles. *ACS Biomater. Sci. Eng.* **2021**, *7* (5), 1787–1807. <https://doi.org/10.1021/acsbiomaterials.0c00776>.
- (52) Lang, S.; Chen, C.; Xiang, J.; Liu, Y.; Li, K.; Hu, Q.; Liu, G. Facile and Robust Antibacterial Functionalization of Medical Cotton Gauze with Gallic Acids to Accelerate Wound Healing. *Ind. Eng. Chem. Res.* **2021**, *60* (28), 10225–10234. <https://doi.org/10.1021/acs.iecr.1c01833>.
- (53) de la Fuente-Núñez, C.; Korolik, V.; Bains, M.; Nguyen, U.; Breidenstein, E. B. M.; Horsman, S.; Lewenza, S.; Burrows, L.; Hancock, R. E. W. Inhibition of Bacterial Biofilm Formation and Swarming Motility by a Small Synthetic Cationic Peptide. *Antimicrob. Agents Chemother.* **2012**, *56* (5), 2696–2704. <https://doi.org/10.1128/AAC.00064-12>.
- (54) Takahashi, H.; Nades, E. T.; Kuroda, K. Cationic Amphiphilic Polymers with Antimicrobial Activity for Oral Care Applications: Eradication of *S. Mutans* Biofilm.

<https://doi.org/10.1021/acs.biomac.6b01598>.

- (55) Jennings, L. K.; Storek, K. M.; Ledvina, H. E.; Coulon, C.; Marmont, L. S.; Sadovskaya, I.; Secor, P. R.; Tseng, B. S.; Scian, M.; Filloux, A.; Wozniak, D. J.; Howell, P. L.; Parsek, M. R. Pel Is a Cationic Exopolysaccharide That Cross-Links Extracellular DNA in the *Pseudomonas Aeruginosa* Biofilm Matrix. *Proc. Natl. Acad. Sci.* **2015**, *112* (36), 11353–11358. <https://doi.org/10.1073/pnas.1503058112>.
- (56) Altaf, M.; Manoharadas, S.; Zeyad, M. T. Green Synthesis of Cerium Oxide Nanoparticles Using *ACORUS CALAMUS* Extract and Their Antibiofilm Activity against Bacterial Pathogens. *Microsc. Res. Tech.* **2021**, *84* (8), 1638–1648. <https://doi.org/10.1002/jemt.23724>.
- (57) Naidi, S. N.; Khan, F.; Tan, A. L.; Harunsani, M. H.; Kim, Y.-M.; Khan, M. M. Photoantioxidant and Antibiofilm Studies of Green Synthesized Sn-Doped CeO₂ Nanoparticles Using Aqueous Leaf Extracts of *Pometia Pinnata*. *New J. Chem.* **2021**, *45* (17), 7816–7829. <https://doi.org/10.1039/D1NJ00416F>.
- (58) Qin, J.; Feng, Y.; Cheng, D.; Liu, B.; Wang, Z.; Zhao, Y.; Wei, J. Construction of a Mesoporous Ceria Hollow Sphere/Enzyme Nanoreactor for Enhanced Cascade Catalytic Antibacterial Therapy. *ACS Appl. Mater. Interfaces* **2021**, *13* (34), 40302–40314. <https://doi.org/10.1021/acsami.1c10821>.
- (59) Kumar, S.; Ahmed, F.; Shaalan, N. M.; Saber, O. Biosynthesis of CeO₂ Nanoparticles Using Egg White and Their Antibacterial and Antibiofilm Properties on Clinical Isolates. *Crystals* **2021**, *11* (6), 584. <https://doi.org/10.3390/cryst11060584>.
- (60) Liu, S.; Jiang, T.; Guo, R.; Li, C.; Lu, C.; Yang, G.; Nie, J.; Wang, F.; Yang, X.; Chen, Z. Injectable and Degradable PEG Hydrogel with Antibacterial Performance for Promoting Wound Healing. *ACS Appl. Bio Mater.* **2021**, *4* (3), 2769–2780. <https://doi.org/10.1021/acsabm.1c00004>.
- (61) Singh, N.; Sahoo, S. K.; Kumar, R. Hemolysis Tendency of Anticancer Nanoparticles Changes with Type of Blood Group Antigen: An Insight into Blood Nanoparticle Interactions. *Mater. Sci. Eng. C* **2020**, *109*, 110645. <https://doi.org/10.1016/j.msec.2020.110645>.
- (62) Uppal, S.; Aashima; Kumar, R.; Sareen, S.; Kaur, K.; Mehta, S. K. Biofabrication of Cerium Oxide Nanoparticles Using Emulsification for an Efficient Delivery of Benzyl Isothiocyanate. *Appl. Surf. Sci.* **2020**, *510*, 145011. <https://doi.org/10.1016/j.apsusc.2019.145011>.
- (63) More, N.; Ranglani, D.; Kharche, S.; Kapusetti, G. Electrospun Mat of Thermal-treatment-induced Nanocomposite Hydrogel of Polyvinyl Alcohol and Cerium Oxide for Biomedical Applications. *J. Appl. Polym. Sci.* **2020**, *137* (46), 49426. <https://doi.org/10.1002/app.49426>.

- (64) Jie, G.; Lin, Z.; Zhang, L.; Lv, H.; He, P.; Zhao, B. Free Radical Scavenging Effect of Pu-Erh Tea Extracts and Their Protective Effect on Oxidative Damage in Human Fibroblast Cells. *J. Agric. Food Chem.* **2006**, *54* (21), 8058–8064. <https://doi.org/10.1021/jf061663o>.
- (65) Jain, A.; Behera, M.; Mahapatra, C.; Sundaresan, N. R.; Chatterjee, K. Nanostructured Polymer Scaffold Decorated with Cerium Oxide Nanoparticles toward Engineering an Antioxidant and Anti-Hypertrophic Cardiac Patch. *Mater. Sci. Eng. C* **2021**, *118*, 111416. <https://doi.org/10.1016/j.msec.2020.111416>.

CHAPTER - 4

Antioxidant and osteogenic,
thiolated mesoporous silica
nanoparticles for osteoporosis

Antioxidant and osteogenic, thiol-functionalized mesoporous silica nanoparticles for osteoporosis

4.1. Introduction

4.1.1. Osteoporosis

Osteoporosis (OP) is a leading cause of bone defects, contributing to approximately 8.9 million osteoporotic fractures reported worldwide. Osteoporotic fractures are expected to continue to rise in the future, making them one of the leading causes of illness worldwide.^{1,2} Osteoporosis involves loss of bone mass, which can lead to fractures and brittle bones. It is broadly divided into primary and secondary OP. Primary OP predominantly affects ageing populations, such as post-menopausal women and men over 70 years, while secondary OP occurs in individuals having endocrine malfunction, autoimmune disorders, tumors, or systemic disorders.^{3,4} One of the main contributing factors to the development and course of post-menopausal OP is known to be the oxidative stress. Under normal physiological conditions, reactive oxygen species (ROS) play an important role in regulating intracellular levels of MAPK and Ca^{2+} thus maintain bone tissue resorption. However, high ROS levels disturb bone homeostasis, resulting in increased osteoblast death and increased osteoclast production. Reduced bone density and a rise in calcified tissues are the outcomes of this imbalance.^{5,6}

4.1.2. Challenges

Conventionally the treatment for OP is based on two approaches- use of anabolic drugs (like teriparatide) and anti-resorptive agents (like SERM and bisphosphonates). While these are effective in preventing further bone loss and maintaining bone density, these drugs are associated with significant side effects, such as tissue necrosis and nephrotoxicity.⁷ Newer treatment strategies include growth factors, such as BMP-2, which are expensive and might cause serious side effects if used frequently.⁸ Even though the role of oxidative stress is well defined, both conventional and recent treatment approaches fail to address the high ROS levels in osteoporotic tissues.

4.1.3. Research gap

The rise of nanotechnology has led to the development of bioactive materials, like silica, hydroxyapatite and calcium phosphate for bone tissue regeneration.^{9,10} Mesoporous silica nanoparticles (MSNs) have garnered attention in bone tissue engineering due to their innate osteogenic properties and effectiveness as a carrier for osteoinductive drugs and growth factors.^{11,12} These biocompatible inorganic materials offer a tunable surface area with adjustable surfaces for chemical modifications and drug attachment. While the release of Si ions in bodily fluids causes the formation of carbonated apatite, which binds to bone and promotes bone matrix mineralization and osteoblast development, it also has a beneficial

effect on osteoprogenitor cells and favors osteogenic differentiation.¹³ Composites like Au/mesoporous silica have shown the ability to hasten bone regeneration through immunomodulation.¹⁴ BMP-2 loaded hollow MSNs facilitate sustained delivery for bone regeneration,¹⁵ while dexamethasone-peptide loaded biodegradable MSNs enhance angiogenesis in bone regeneration.¹⁶ However, MSNs lack an inherent antioxidant property crucial for such applications, an area that requires further exploration.¹⁷

Thiol groups (–SH) serve as scavengers for reactive oxygen species (ROS), neutralizing the harmful effects of oxidative stress by reacting with ROS to form disulfide bonds (–S–S–). Thiols are believed to control inflammation through the NF-κB pathway. Previous research has shown that thiol-based antioxidants can lessen the consequences of oxidative stress.^{18,19} Reports indicate reduced thiol/glutathione levels and a thiol/disulfide imbalance in osteoporotic females.^{20,21,22} Due to their mucoadhesive nature and cell permeation ability, thiolated polymers and nanoparticles have been used in different delivery systems like nasal, vaginal and ophthalmic.^{23,24} Previous research highlights tissue regeneration and wound healing potential of thiolated systems. Researchers like Lingli et al. and Lin et al. investigated thiolated gelatin and histatin-modified chitosan hydrogel, respectively, for wound repair and tissue engineering applications.^{25,26} Beyond their role as natural antioxidants, thiols aid in the proliferation of cells and cell adhesion. Thiol-ene hydrogels have been employed in the localized delivery of parathyroid hormone and enhanced bone regeneration.²⁷ Hegedus et al. have studied the effect of free thiol groups on cell viability, morphology, and differentiation in tooth progenitor cells²⁸ but the effect of thiols has not been explored in osteoblast cells according to our knowledge.

4.2. Objectives

To overcome the limitations in existing therapeutics, we have developed and investigated thiolated silica nanoparticles (MSN-SH) based on the hypothesis that adding thiols to the surface of MSNs will provide a bioactive, biocompatible system with improved osteogenic and antioxidant properties, which will promote new bone growth and reduce the course of the disease. A major aim of this work is to impart antioxidant properties to MSNs by thiolation and investigate its osteogenic potential in cell culture. We have synthesized MSNs, functionalized them with thiol groups to obtain MSN-SH, and conducted a comprehensive analysis of their physical and chemical properties. Evaluation of the antioxidant activity, cell viability, and osteogenic potential of MSN-SH was performed in murine bone osteoblast precursor cells (MC3T3) by measuring various osteogenic markers and proteins and assessing its ability to inhibit osteoclastogenesis. Wound healing capabilities were assessed in the same cell line using a scratch assay, while its impact on human umbilical vein endothelial cells (HUVEC) was studied via MTT and migration assays.

4.3. Experimental section

4.3.1. Materials

Cetrimonium bromide (CTAB), ascorbic acid, urea, propanol, tetraethyl orthosilicate (TEOS), 2,2'-azino-bis-(3-ethylbenzothiazoline-6-sulfonic acid (ABTS), Triton X, cyclohexane, and cetylpyridinium chloride (CPC) were purchased from HiMedia. HUVECs EGMTM-2 and EGM 2 endothelial cell growth medium-2 Bullet Kit™ were acquired from Lonza, while ATCC provided the MC3T3-E1 cells (CRL-2593, subclone-4). RAW 264.7 (mouse leukemic monocyte macrophage) cell line was a kind gift from Prof. Javed N Agrewala, DBME, IIT Ropar. Corning USA provided the cell culture inserts, while PROSPEC supplied the recombinant mouse soluble RANK ligand protein (RANKL). The iScript™ cDNA synthesis kit was sourced from Bio-Rad. Additional materials, including RPMI 1640, Pen-strep, fetal bovine serum (FBS), SYBR™ Green Master Mix, 0.25% trypsin/EDTA, MTT reagent, 2',7'-dichlorodihydrofluorescein diacetate (DCFDA), Alexa Fluor phalloidin 488, and trizol, were acquired from Thermo Fisher Scientific. Furthermore, cetylpyridinium chloride (CPC), alizarin red S, 4',6-diamidino-2-phenylindole (DAPI), were obtained from Sigma-Aldrich, while 3-mercaptopropyl trimethoxysilane (MPTMS), 5,5'-dithiobis-2-nitrobenzoic acid (DTNB), dexamethasone, 4-nitrophenyl phosphate (pNPP), were purchased from TCI Chemicals. Hydrogen peroxide, toluene and sodium acetate were procured from Merck. Type I deionized (DI) water (Bioage) was utilized in all experiments.

4.3.2. Fabrication of mesoporous silica nanoparticles (MSNs)

A previously published method was used to fabricate MSNs.¹⁴ The process involved dissolving 0.42 g of CTAB in 200 mL of DI water, which was stirred at 50 °C. The temperature was then raised to 80 °C, and 1 mL of 4M NaOH was added to maintain basic conditions. After 2 h of vigorous shaking, a solution of TEOS in methanol (1:5) was gradually added to the mixture and stirred. The mixture was then centrifuged, and the resultant nanoparticles were cleaned with ethanol and water. To successfully remove CTAB, the nanoparticles were air-dried at 60 °C for an entire night and then calcined at 550 °C.

4.3.3. Post-synthesis thiol functionalization (MSN-SH)

Surface modification was carried out post-synthesis according to already published protocol.²⁹ The material was dehydrated at 80 °C for a whole night to activate the MSN surface. The MSN (150 mg) was ultrasonically sonicated for 30 min after being suspended in 30 mL of toluene in a round-bottom flask. After adding 0.2 mL of MPTMS, the solution was refluxed at 110 °C for the entire night. Thiolated mesoporous silica nanoparticles (MSN-SH) were obtained by centrifugation, air drying at 50 °C for an overnight period, and washing the resultant nanoparticles with ethanol and toluene.

4.3.4. Characterization

Physical and chemical characterization of material was performed by various spectroscopic and microscopic techniques.

Chemical Properties. FT-IR spectra were performed in the 400–4000 cm⁻¹ range on Bruker in ATR mode. By using Cu K α (λ = 0.154 nm) radiation in the 10-80 nm range, X-ray diffraction (XRD) was performed with a RIGAKU Mini-flex Diffractometer to assess the material's crystallinity. The electronic states and elemental distribution were investigated using XPS (Thermo Fisher Scientific K Alpha) and EDX (Bruker Splash 6130) studies. Thermogravimetric analysis (TGA) was performed using TA Instrument, USA, SDT-650.

Physical Properties. DLS Microtrac/Nanotrac Flex were used to determine particle size distribution and zeta potential. The morphological characteristics of nanoparticles were analyzed by HR-TEM (High-Resolution Transmission Electron Microscope (HR-TEM JEM-2100 Plus, 200kV). Surface area and pore size analysis utilized N₂-adsorption analysis (Quantachrome) following sample degassing at 120 °C before the analysis. The pore size distribution was assessed using the Barrett-Joyner-Halenda (BJH) method on a Quantachrome instrument, while surface area was determined via the Brunauer-Emmett-Teller (BET) method.

4.3.5. Ellman's assay

Thiol functionalization quantification was performed using Ellman's assay.²⁹ About 4 mg of DTNB and 20.5 mg of sodium acetate were dissolved in 5 mL distilled water to prepare a working solution of DTNB. A 2.5 mL of tris buffer (1 M, pH 8) was mixed with 50 μ L of Ellman's reagent to make a blank solution. After adding each sample (250 μ L, 1 mg/mL) to the blank, it was incubated at room temperature for 15 min and the absorbance was recorded at 412 nm. The reagent's extinction coefficient (13600 M⁻¹ cm⁻¹) was used to calculate the quantity of thiol groups grafted on MSN.

4.3.6. Anti-oxidant assay

ABTS (7 mM) and potassium persulfate (2.45 mM) solutions were prepared and mixed in equal proportions to generate free radicals overnight. The working solution was then prepared from the stock, diluted using PBS, and the absorbance at 734 nm was adjusted to 0.8-0.9 units. The ABTS solution was added to each sample and incubated in the dark for 1 h. The resulting suspension was centrifuged, and the absorbance of the collected supernatant was measured using a UV-Vis spectrophotometer. The percent antioxidant activity was calculated using the following equation, and ascorbic acid (1%) was used as a positive control.³⁰

$$\% \text{ Antioxidant Activity} = \left[\frac{A_c - A_s}{A_c} \right] \times 100 \quad \text{Equation 4.1}$$

where A_c indicates the absorbance of the control and A_s represents the absorbance of the sample.

4.3.7. Cell culture studies

MC3T3-E1, a murine osteoblast precursor cell line was used. The T-25 flask was used to cultivate the cells in full MEM- α media, with frequent media changes every 48 h to maintain cell confluence at roughly 70%. In order to conduct cell viability assays, MC3T3 cells were

sown in a 96-well plate treated with cell culture at a density of 1×10^5 cells/mL. For three days, the cells were treated with a suspension of nanoparticles weighing 50, 100, 250, and 500 μg . Complete MEM- α was the negative control, while osteogenic media (OM) was the positive control.

MTT Assay. MTT assay was conducted on days 1 and 3 to evaluate cell viability. 0.5 mL of MTT reagent was added to each well and incubated for 4 h, the resulting formazan crystals were dissolved in DMSO. After complete solubilization the absorbance at 570 nm was measured. The cell viability was compared to the negative control. The cell viability of MSN and MSN-SH on HUVECs cells was also assessed using an MTT assay for 24 h.

Live/Dead Staining. Cells were stained with the LIVE/DEAD® Viability/Cytotoxicity Kit. A 2 μM of calcein AM and 4 μM ethidium homodimer 1-red were mixed to prepare a working solution in DPBS. After 3 days of incubation, cells were stained and imaged using a fluorescence microscope.³¹

4.3.8. In vitro osteogenic activity

The osteogenic potential of nanomaterials was evaluated by analyzing the ALP activity, calcium deposition, and gene expression. Cells were treated with MSN and MSN-SH (100 μg) in basal α -MEM media and incubated for 7 and 14 days.

Alkaline Phosphatase Assay (ALP). On days 7 and 14, ALP activity was assessed by measuring absorbance at 405 nm after incubating cell lysates with p-nitrophenyl phosphate solution. By normalizing the OD values at $\lambda = 405$ nm (ALP assay) with the OD values at $\lambda = 570$ nm obtained from the MTT assay, the relative ALP activity was determined.

Calcium Deposition. Alizarin red S staining was used to assess the amount of calcium deposited in the cells. Cells were completely washed with PBS on days 7 and 14, and then they were fixed for 15 min with a paraformaldehyde (4%) solution. The cells were rinsed once again, 500 μL of alizarin red solution was added, and the mixture was incubated for 60 min in the dark. Mineral nodes were observed under a microscope after removing the extra dye. The calcium concentration was evaluated by dissolving the mineralized nodules in 10% cetylpyridinium, taking an aliquot of 100 μL from each well, and measuring the absorbance at 562 nm.

Gene Analysis. The gene expression of osteogenic markers, including runt-related transcription factor 2 (RUNX2), alkaline phosphatase (ALP), osteocalcin (OCN), and osteopontin (OPN), were assessed using RT-PCR analysis. Cells were cultured in a 6-well plate with the nanoparticle suspension for 14 days, and RNA was isolated on days 7 and 14. RT-PCR was employed to quantify gene expression levels using GAPDH as a housekeeping gene for normalization.

4.3.9. Effect of MSN-SH on osteoclastic resorption

RAW267.4 cells were seeded at a concentration of 25,000 cells/well in a 12-well plate with MC3T3-E1 cells. Differentiating RAW267.4 cells were induced into osteoclasts by RANKL

protein. MSN and MSN-SH suspension were added to MC3T3 cells. Gene expression levels of RANKL and TRAP were evaluated in MC3T3-E1 and differentiating RAW267.4 cells on day 7 using RT-PCR.³²

4.3.10. In vitro ROS scavenging assay

Cellular oxidative stress was induced by H₂O₂, and the effect of nanoparticles on ROS levels was studied. Cells were seeded in a 96-well plate and exposed to H₂O₂. The cellular ROS was quantified using DCFDA dye solution and imaged under a fluorescence microscope. Cell viability was assessed using MTT assay. Ascorbic acid was used as a positive control and untreated cells served as the negative control.¹⁷

4.3.11. In vitro scratch assay

To evaluate the regenerative properties of nanomaterials, a scratch assay was performed on MC3T3 cells.³³ The migration was monitored and images were captured at various time intervals. The effect of nanomaterial on the migration of HUVECs cells was also studied using the same scratch assay methodology. Wound healing was quantified using Image J software.

$$\% \text{ Healing} = \left[\frac{\text{Area}_{t_0} - \text{Area}_{t_i}}{\text{Area}_{t_0}} \right] \times 100 \quad \text{Equation 4.2}$$

where, $t_0 = 0$ h, $t_i = 12$ and 24 h.

4.3.12. Cytoskeletal staining

Cell morphology was assessed by growing cells on coverslips, which were stained with Alexa Fluor Phalloidin for F-actin and DAPI for nuclei. Imaging was conducted using a Leica fluorescence microscope.³⁴

4.3.13. Statistical analysis

The statistical analysis involved a student's t-test and the data were presented as mean values along with the standard deviations (*p values less than 0.05 were considered significant, and 'ns' indicated a non-significant difference between the control and samples).

4.4. Results and discussion

The primary objective of this research was to develop a functional, bioactive nanomaterial intended for the prevention and treatment of OP. This study involved the development of thiolated, mesoporous silica nanoparticles (MSN-SH) designed to possess antioxidant and osteogenic properties for regenerating bone in OP conditions. While silica nanoparticles naturally encourage the formation of new bone and blood vessels, the inclusion of thiol (–SH) groups provides antioxidant capabilities, potentially halting disease progression. This study represents the first investigation into the role of free thiols in bone differentiation within osteoblast precursor cells, to the best of our knowledge.

4.4.1. Fabrication of MSN

The fabrication of MSN nanoparticles was done using the Stöber method. It involves the hydrolysis of a silica precursor (TEOS) in the presence of a surface directing template

(CTAB). Post-synthesis, the surface was modified using the saline derivative, MPTMS, resulting in MSN-SH, where 11% of the surface was grafted with thiol groups (**Figure 4.1**). Examination through HR-TEM revealed a typical ordered mesoporous structure, with hexagonal-shaped nanoparticles displaying uniformity in their structure. Despite the functionalization, the nanoparticles retained their original morphology similar to MSN.

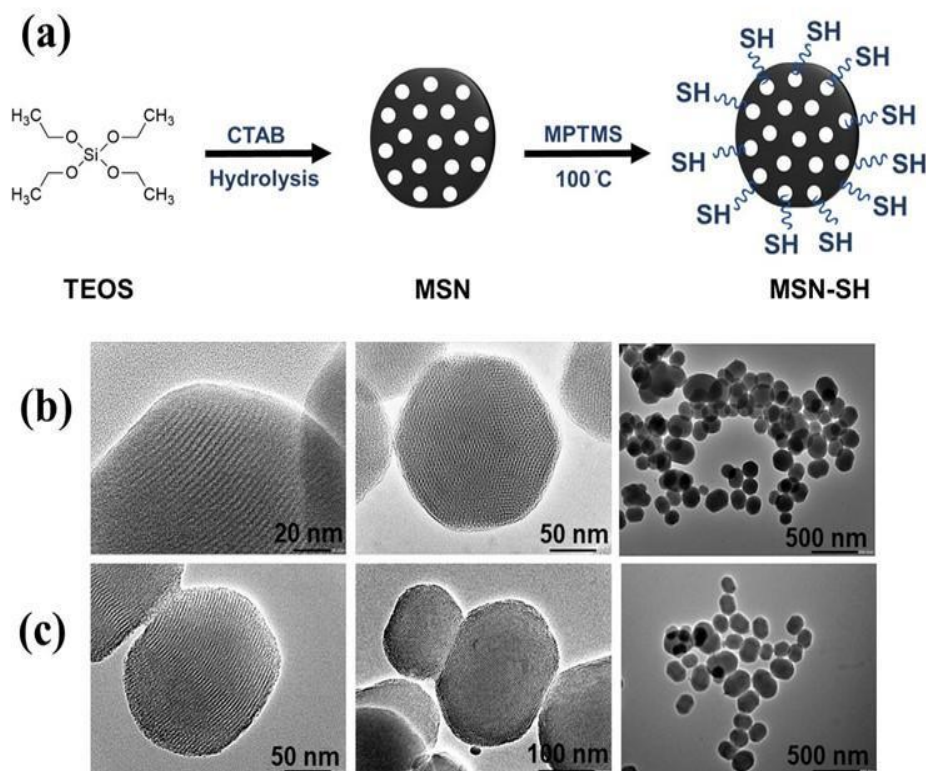


Figure 4.1. (a) Fabrication of thiolated mesoporous silica nanoparticles (MSN-SH). (b, c) HR-TEM images: (b) MSN. (c) MSN-SH. Scale bar: (b) 20, 50, and 500 nm. (c) 50, 100, and 500 nm.

4.4.2. Characterization of nanoparticles

Both the chemical and physical properties of the nanoparticles were extensively characterized (**Figure 4.2, 4.3**). The particle size of MSN was found to be 280 ± 20.23 nm and MSN-SH was found to be 330 ± 15.77 nm and zeta potential was found to be -31.6 ± 5.11 and -47.0 ± 4.83 (**Figure A17, Appendix**). FTIR spectra of both MSN and MSN-SH displayed characteristic peaks at 800 and 1066 cm^{-1} , representing Si–O and Si–O–Si stretching, while an additional peak at 2976 cm^{-1} specifically in MSN-SH indicated the presence of thiol groups³². The grafted thiol groups were quantified using Ellman’s assay, and found to be 5.20×10^{-4} M/20.8 molar per mg.

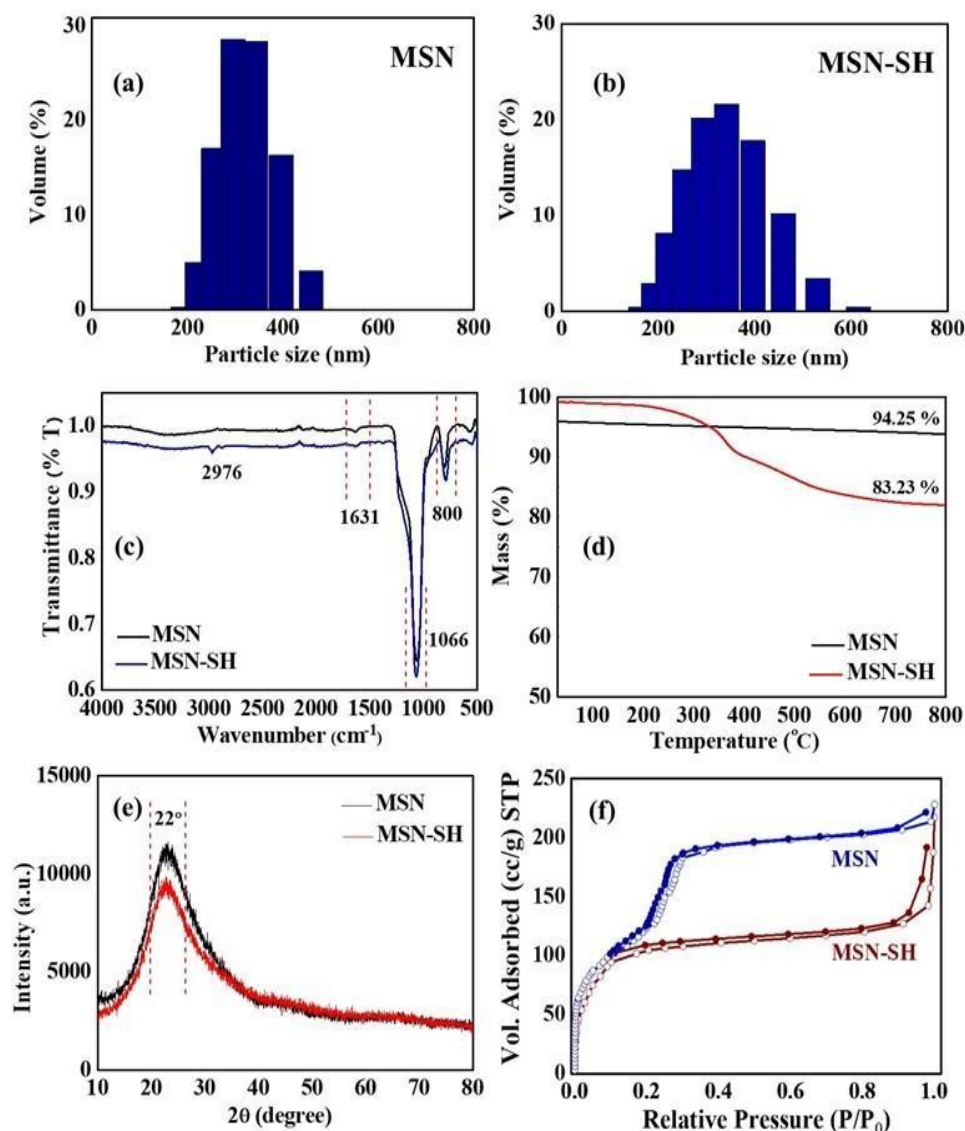


Figure 4.2. Physical and chemical characterization of MSN and MSN-SH. (a, b) Particle size distribution. (c) FT-IR spectra. (d) TGA curves. (e) XRD spectra. (f) N₂ adsorption-desorption isotherms. $n = 3$, mean \pm SD.

The successful thiolation of MSN-SH was further confirmed by TGA studies, which showed an approximate 11% weight loss due to the degradation of MPTMS. XRD spectra demonstrated the typical amorphous nature of MSN and MSN-SH, where no sharp peaks but a broad peak at 22° (2θ) was observed.¹⁴ The reduction in peak intensity of MSN-SH was likely due to the presence of functional groups. Nitrogen sorption studies highlighted the mesoporous nature of both MSN and MSN-SH, displaying type IV isotherms (**Figure A18, Appendix**). The total surface area was determined as 1080 and 338 cm³ g⁻¹ for MSN and MSN-SH, with pore sizes measured as 2.24 and 2.03 nm. The reduction in surface area and pore size of MSN-SH indicates effective functionalization.

The results of the EDX analysis revealed a uniform element distribution in the nanomaterials and the presence of the sulfur element in the case of thiolated MSNs (**Figure 4.3**). The EDX spectra of MSN and MSN-SH is included in the **Appendix (Figure A19)**. XPS

was employed to analyze the elemental composition and functional groups present in the nanomaterial. The functionalization of MSN-SH is demonstrated in a figure, where peaks at 163 and 164 eV correspond to S 2p_{1/2} and S 2p_{3/2}.^{35,36} Additionally, the peaks at 533 and 103.5 eV correspond to SiO₂ and O₂ in the case of MSN and MSN-SH. The XPS spectrum of MSN is provided in **Figure 20, Appendix**. The findings from EDX and XPS analyses were in accordance with the other characterization data.

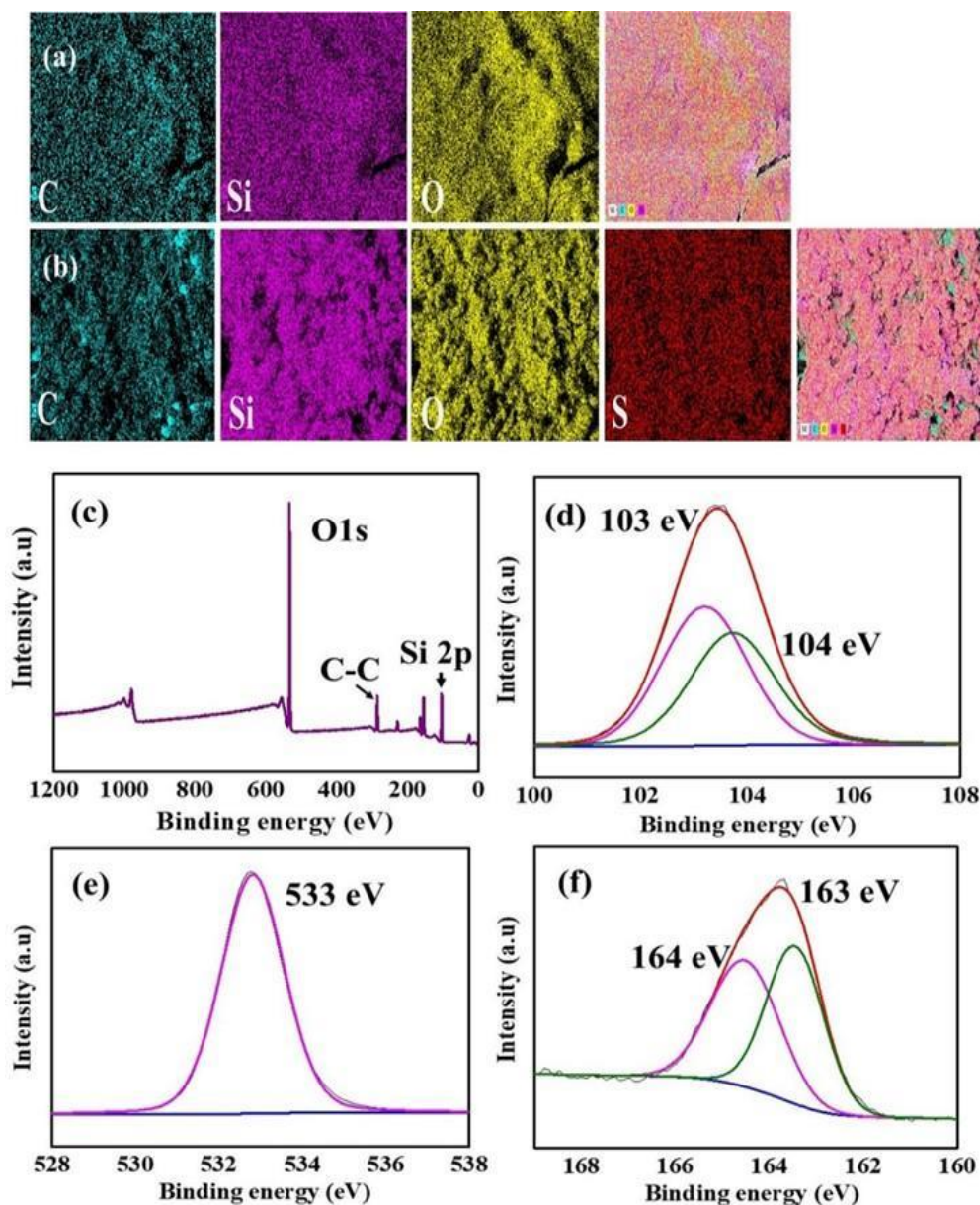


Figure 4.3. (a, b) EDX mapping of elements in nanomaterials: (a) MSN. (b) MSN-SH. (c-f) XPS spectra of MSN-SH: (c) Survey scan. (d) Si 2p. (e) O 1s. (f) S 2p. n = 3, mean \pm SD.

4.4.3. Antioxidant studies

An ABTS assay was conducted to assess the antioxidant activity of the nanoparticles. When ROS species are present, ABTS is oxidized, resulting in the formation of the green-colored ABTS^{•+} cation with a peak absorbance at 734 nm. As shown in **Figure 4.4**, MSN alone displayed minimal antioxidant properties, while MSN-SH exhibited over 90% antioxidant

activity even at concentrations of up to 500 $\mu\text{g/mL}$. At a concentration of 100 $\mu\text{g/mL}$, ascorbic acid demonstrated around 93% activity. This enhanced activity is attributed to the presence of thiol groups on the surface of MSNs. Thiols naturally act as radical scavengers, working as cellular redox buffers by oxidizing themselves and counteracting free radicals by accepting unpaired electrons.¹⁸ The antioxidant behavior of MSN-SH is potentially beneficial for managing the oxidative stress found in osteoporotic tissues and safeguarding cells from damage caused by radical species. The antioxidant performance of our nanomaterial exceeded that of MSN-curcumin nanoparticles as reported by Abouatah et al.³⁷

4.4.4. Cell viability studies

The impact of the nanoparticles on cell viability was analyzed using MTT and live/dead assays in murine osteoblast precursor cells (MC3T3). In the MTT assay, cells were exposed to the nanoparticle suspension for up to 3 days, and cell viability was determined by comparing the absorbance relative to untreated cells (control). Both MSN and MSN-SH exhibited cytocompatibility and enhanced cell proliferation in a time-dependent manner (**Figure 4.4.**). Cells treated with osteogenic media showed 110% viability on day 3, while cells treated with MSN and MSN-SH at a concentration of 100 $\mu\text{g/mL}$ displayed viabilities of 108% and 140%, within 72 h.

At higher concentrations, both MSN and MSN-SH displayed reduced viability and were toxic to cells at 500 $\mu\text{g/mL}$. The increased proliferation of MSN-SH can be attributed to the thiol groups on its surface, which facilitate cell adhesion and promote the proliferation of cells responsible for hard tissue generation, such as osteoblasts. The interaction between the thiol groups of MSN-SH and the free -SH groups of L-cysteine, present on the cell surfaces, aids in cell adhesion.²⁸ The cytocompatibility of these nanoparticles was further confirmed using live/dead staining, and the outcomes were consistent with the MTT assay. The live/dead stained images of OM and MSN-treated cells are provided in **Figure A21, Appendix**. The effect of MSN-SH on cell viability were in accord with the results of previously reported composite nanomaterials by Liang et al. (110%)¹⁴ and Pinna et al. (100%).³²

During the process of bone remodeling, osteogenesis doesn't act in isolation but is intricately linked with angiogenesis, as proper vascularization is crucial for the formation of new bones³⁸. The compatibility of MSN-SH with HUVECs cells was also assessed using the MTT assay (**Figure A22 Appendix**). The results showed that both MSN and MSN-SH were non-toxic to HUVECs cells, with MSN-SH treated cells exhibiting 102% cell viability within 48 h, while cells treated with MSN showed 100% cell viability within the same period, indicating their cell-proliferative nature. The similar cell viability displayed by both nanomaterials may be attributed to the release of Si ions that stimulate angiogenesis.³⁹

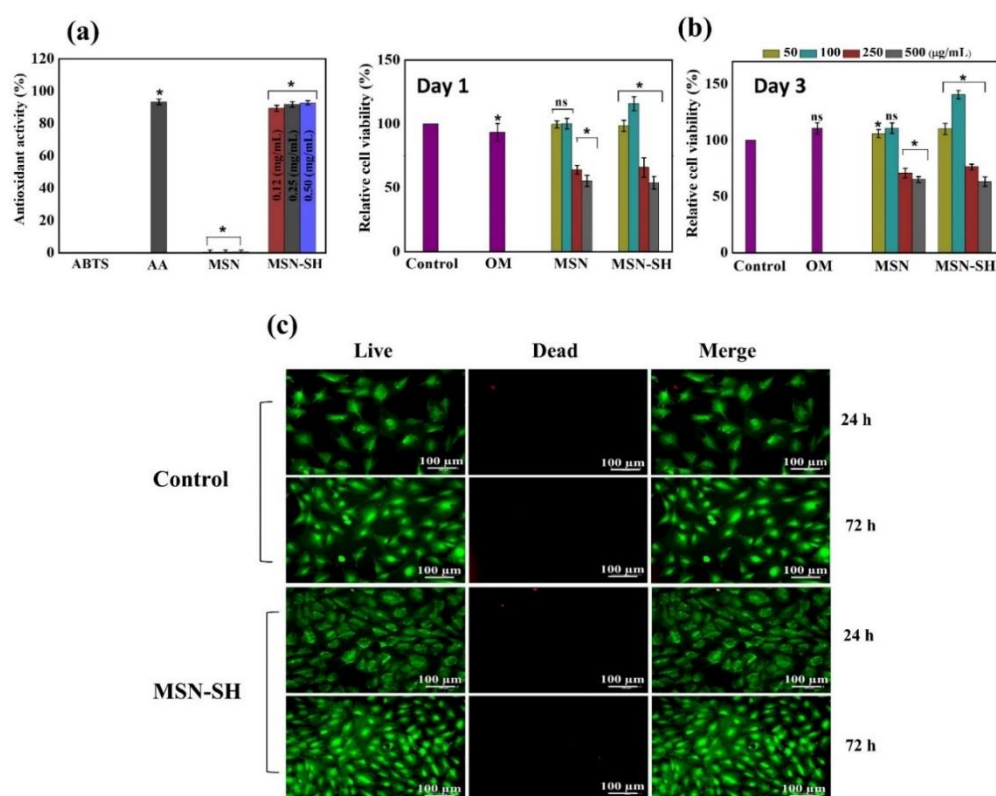


Figure 4.4. Antioxidant and cell viability studies. (a) Antioxidant activities of nanomaterials using ABTS assay. ABTS was used as a negative control, whereas ascorbic acid (AA) was used as a positive control. (b) Cell viability studies in murine osteoblast precursor cells (MC3T3) by MTT assay. Cells were treated with osteogenic media, MSN, and MSN-SH, and untreated cells were taken as a control. $n = 3$, mean \pm SD, * $p < 0.05$ represents the statistical significance and ns represents the non-significant difference. (c) Live/dead assay. Fluorescence images of untreated MC3T3 cells (control) and cells treated with MSN-SH. Scale bar: 100 μm .

4.4.5. In Vitro assessment of osteogenic and osteoclastogenic activity

The osteogenic potential of the nanomaterial was studied using ALP activity, calcium deposition assays, and gene expression analysis. MC3T3 cells were cultured for 14 days in a nanoparticle suspension of MEM- α and evaluated for ALP levels and calcium deposition at intervals of 7 and 14 days. The ALP activity of cells treated with MSN-SH was notably higher compared to those treated with basal MEM media, MSN, and osteogenic media, as shown in **Figure 4.5**. The ALP activity of MSN-SH surpassed that of the osteogenic media, indicating the potency of the developed osteogenic nanomaterial. This increased activity can be linked to the upregulated expression of the ALP gene, as confirmed by RT-PCR analysis. The impact of MSN and MSN-SH on bone mineralization was also observed through the calcium deposition assay. Cells treated with MSN-SH nanoparticles exhibited dense calcium deposits, while MSN and OM-treated cells showed similar calcium deposition (**Figure 4.5**). The augmented

biomineralization in the presence of MSN-SH could be attributed to the negatively charged –SH groups on the nanoparticles. It has been reported that negatively charged groups, such as PO_4^{3-} , $-\text{COOH}$, and $-\text{OH}$, induce bone mineralization by hydroxyapatite nucleation^{40,41}. Furthermore, the enhanced mineral deposition can be explained by MSN-SH inducing a higher expression level of the osteopontin gene, which is known to stimulate and regulate the bone mineralization process. The osteogenic potential of the drug-free nanomaterial, MSN-SH, presented here is comparable to BMP-2 loaded mesoporous silica nanoparticles by Cui et al.¹⁵ and dexamethasone-MSN conjugate reported by Qiu et al.⁴²

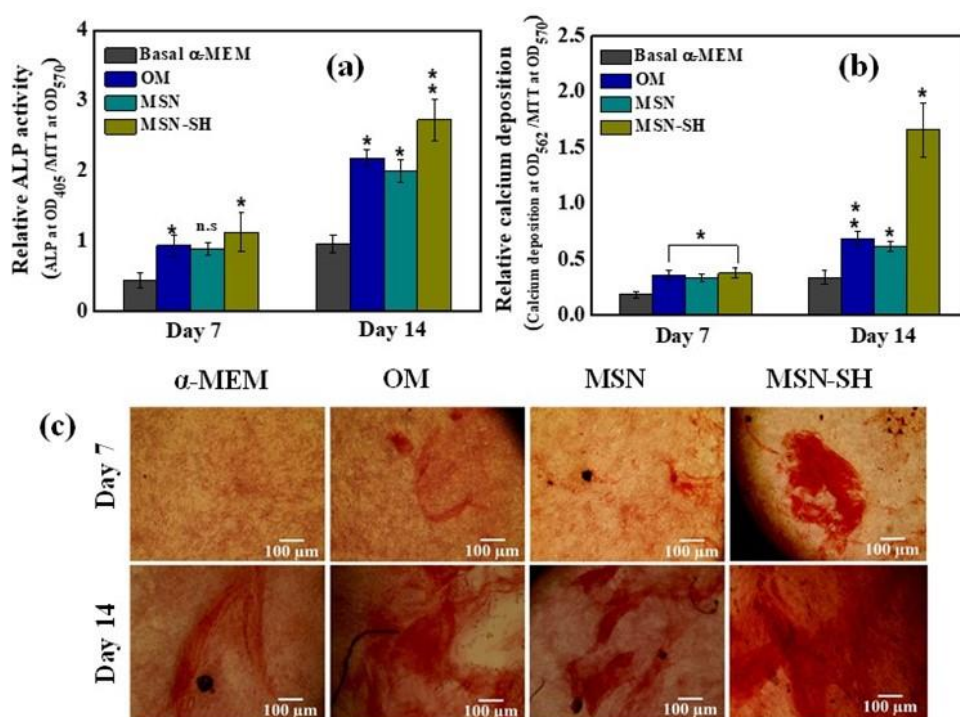


Figure 4.5. In vitro differentiation of murine osteoblast precursor cells (MC3T3). (a) Relative ALP activity. (b, c) Calcium deposition in cells treated with basal MEM- α media, osteogenic media (OM), MSN, and MSN-SH. $n = 3$, mean \pm SD, * $p < 0.05$, ** $p < 0.01$ represents the statistical significance. Scale bar: 100 μm .

By assessing the expression of common osteogenic gene markers by RT-PCR at intervals of 7 and 14 days, the osteoblast differentiation in the presence of basal α -media, osteogenic media, MSN, and MSN-SH was further validated (**Figure 4.6**). Many different kinds of genes, including RUNX 2, ALP, OCN, and OPN, influence bone development.¹⁴ RUNX 2 belongs to the Runt-related transcription family and is primarily responsible for skeletal morphogenesis and osteoblast differentiation. One indicator of osteoblast cells in the development stage is alkaline phosphate (ALP). The primary non-collagenous protein, osteopontin, controls bone mineralization and stimulates osteogenesis. The osteocalcin gene encodes a protein that is strongly expressed by developing osteoblasts and responsible for bone remodeling and metabolism. All four gene expressions were expressed at higher levels in cells treated with OM and MSN-SH, and at lower levels in cells treated with MSN. It was

found that the expression levels were time-dependent, with higher expressions being seen as the incubation period increased. The outcomes supported a previous MSN composite study published by Liang et al.¹⁴

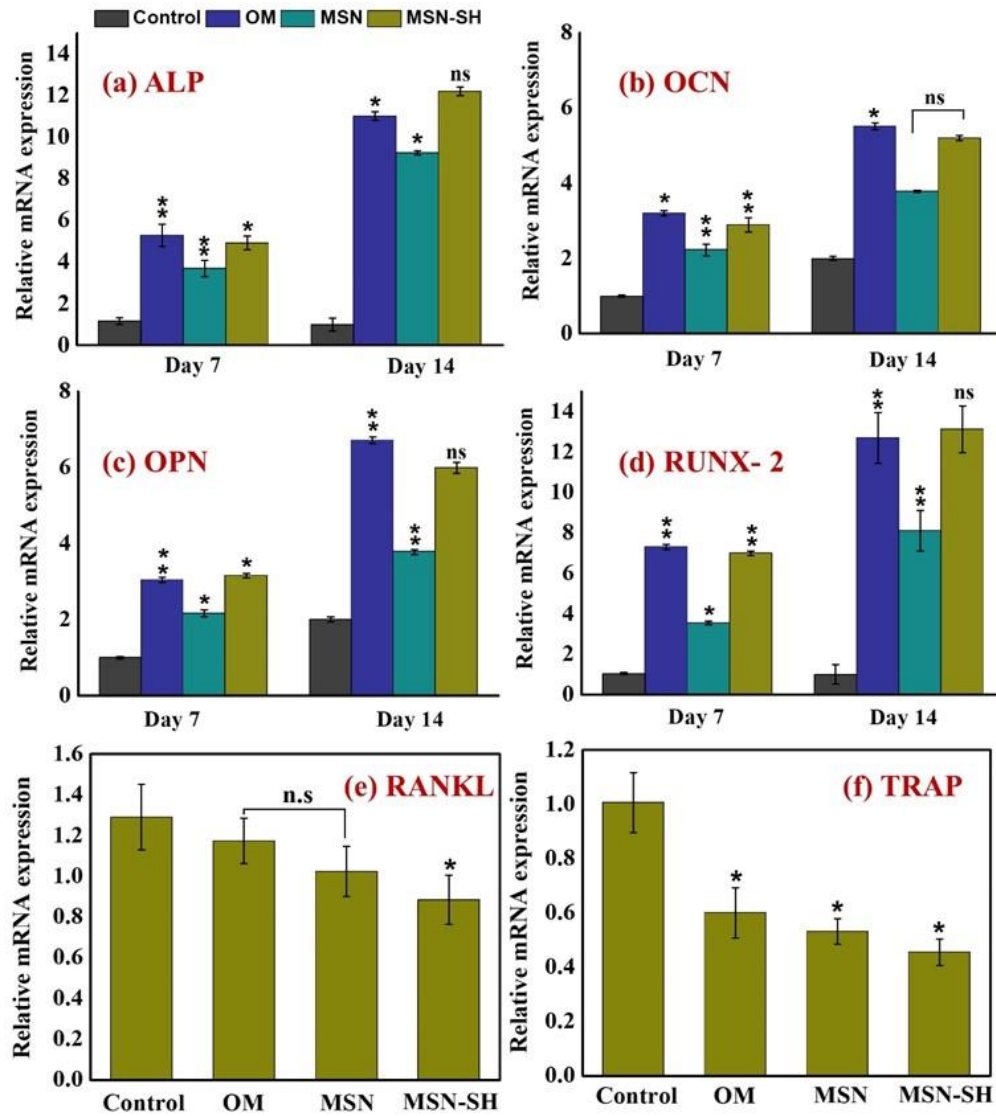


Figure 4.6. RT-PCR analysis of various gene expressions in untreated (control) murine osteoblast precursor cells (MC3T3-E1) and cells treated with osteogenic media (OM), MSN, and MSN-SH. (a) Alkaline phosphatase (ALP). (b) Osteocalcin (OCN). (c) Osteopontin (OPN). (d) Runt-related transcription factor-2 (RUNX-2). (e) RANKL. (f) TRAP. $n = 3$, mean \pm SD, * $p < 0.05$, ** $p < 0.01$ represents the statistical significance and ns represents the non-significant difference.

RANKL, secreted by osteoblasts, plays a significant role in osteoclastogenesis. To investigate the impact of MSN-SH on osteoclast formation, we examined RANKL expression in preosteoblast (MC3T3-E1) and TRAP expression in differentiating macrophage (RAW 267.4) cells (**Figure 4.6**). After seven days of culture, a considerable decrease in RANKL expression was observed in cells treated with MSN-SH (**Figure 4.6**). This inhibitory effect on RANKL expression hinders osteoclast differentiation, potentially impeding bone resorption.

These findings align with earlier studies.^{43–45} TRAP is an important gene linked with osteoclast differentiation. The expression level of TRAP was investigated in differentiated RAW 267.4 cells. The results demonstrated that both MSN and MSN-SH led to decreased expression levels of TRAP (**Figure 4.6**).^{45–47} Therefore, MSN-SH promotes osteogenesis by upregulating osteogenic genes, such as ALP, RUNX-2, OCN, and OPN, while simultaneously inhibiting osteoclastogenesis by downregulating osteoclastic gene expressions, like RANKL and TRAP.

4.4.6. In Vitro ROS scavenging

Elevated levels of ROS in bone cells contribute to osteoporosis, resulting in cell damage and skeletal fragility. Therefore, it's crucial to neutralize radicals and restore them to physiological levels for effective healing. We assessed the nanomaterials capacity for anti-ROS activity and their protective effects against ROS-induced damage in MC3T3 cells (**Figure 4.7**). Cell viabilities were determined using the MTT assay in the presence of ROS induced by hydrogen peroxide (H₂O₂). Treatment with H₂O₂ and ascorbic acid (AA, 100 µg/mL) led to a significant reduction in viability to 39% and 50%. Since hydrogen peroxide is an endogenous inducer of oxidative stress, it is toxic to cells. Interestingly, ascorbic acid, despite being an antioxidant, was found to be toxic, possibly due to its high concentration. Cells treated with OM (containing 50 µg/mL ascorbic acid) displayed 61% cell viability, whereas cells treated with MSN-SH showed 78% viability compared to MSN-treated cells, which exhibited only 42% cell viability. Thus, MSN-SH exhibited a protective effect against H₂O₂-induced cell damage, likely attributed to its antioxidant nature, which neutralizes radical species. Using the DCF-DA method, cells were imaged for fluorescence. Both MSN-SH and ascorbic acid (positive control) exhibited antioxidant activity, effectively neutralizing ROS species, while MSN and OM showed negligible ROS scavenging properties. The ROS scavenging ability and protection against oxidative stress offered by our material exceed that of the MSN-cerium composite reported by Pinna et al.³²

4.4.7. Cell morphology and scratch assay

The impact of the samples on cell morphology was assessed using phalloidin and DAPI staining, and there were no evident differences in cell morphology between the control (MEM- α basal media) and MSN-SH treated cells (**Figure 4.8**). For effective bone remodeling and repair, the migration of osteoblastic cells is crucial. To investigate the regenerative potential of nanomaterials, an in vitro scratch and migration assays were performed in MC3T3 cells.⁴⁸ After wound formation, cells were treated with samples for 24 h, and complete wound closure (100%) due to cell migration and proliferation was observed in MSN-SH treated cells within 24 h, while MSN treated cells also exhibited cell migration (93%).

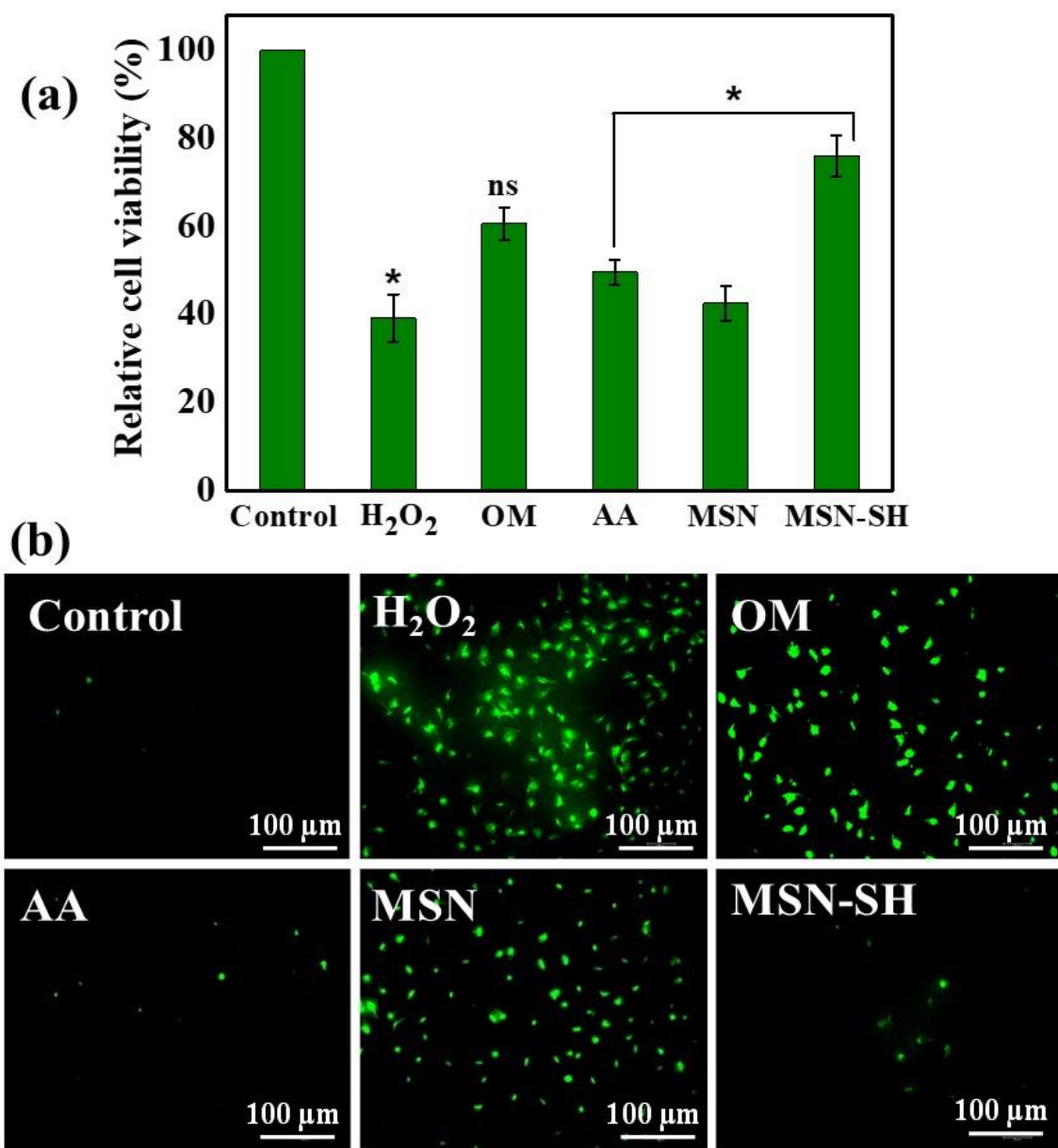


Figure 4.7. Nanomaterials effect on oxidative stress in murine osteoblast precursor cells (MC3T3). (a) Cell viabilities using MTT assay without H₂O₂, with H₂O₂ (negative control), osteogenic media (OM), ascorbic acid (AA, positive control), MSN, and MSN-SH. $n = 3$, mean \pm SD, * $p < 0.05$ represents the statistically significant difference and ns represents the non-significant difference. (b) Fluorescence images of DCF-DA stained cells treated with following: (i) Negative Control (without H₂O₂), (ii) H₂O₂ (iii) osteogenic media (OM), (iv) ascorbic acid (AA, positive control), (v) mesoporous silica nanoparticles (MSN), and (vi) thiolated mesoporous silica nanoparticles (MSN-SH). Scale bar: 100 μ m.

Consequently, MSN-SH stimulates cell migration, showcasing its regenerative potential, and can be effectively employed in bone tissue engineering. The migration assays of cells treated with osteogenic media and MSN are provided as **Figure A23, Appendix**. The proliferation and directed migration of endothelial cells (HUVEC) are essential for angiogenesis. Various cues control this motile process, including chemotactic, hepatotactic, and mechanotactic cues, which are essential for the breakdown of the extracellular matrix

(ECM) to facilitate cell migration.⁴⁹ To assess the impact of nanomaterials on HUVECs cell migration, a scratch assay was conducted. The results indicated that both MSN and MSN-SH promote migration and wound closure of 96 and 100% within 48 h, which can be attributed to the release of Si from nanoparticles that facilitates the proliferation and migration of HUVECs cells³⁹ (**Figure A24, Appendix**). The capability to enhance osteoblast and endothelial cell migration suggests that MSN-SH can contribute to new tissue/bone formation, and our findings align with a previous study by Sun et al., who investigated angiogenic peptide and dexamethasone-loaded MSNs to enhance angiogenesis in bone regeneration.¹⁶

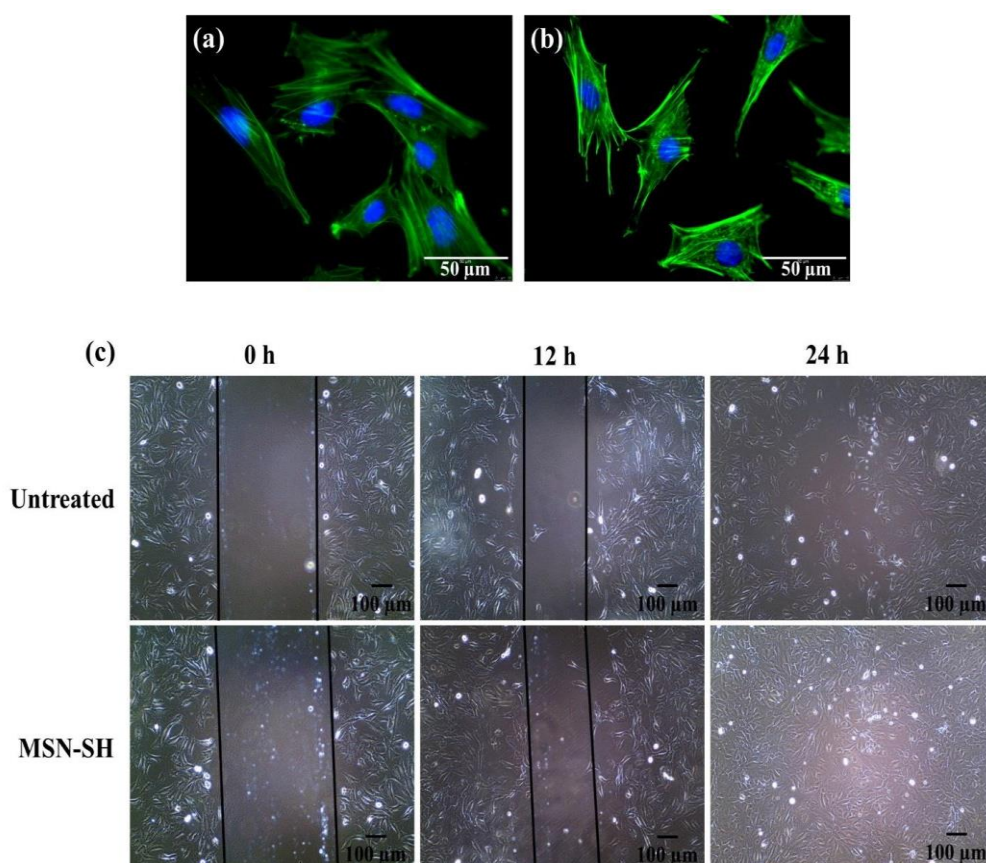


Figure 4.8. (a, b) Cytoskeletal staining of MC3T3 cells, where phalloidin (green) shows actin and DAPI (blue) shows nucleus. (a) Untreated cells (control). (b) Thiolated mesoporous silica nanoparticle (MSN-SH)-treated cells. Scale bar: 50 μm . (c) Migration assay in untreated and MSN-SH treated cells. Scale bar: 100 μm . $n = 3$, mean \pm SD.

4.5. Conclusions

We have effectively synthesized and characterized thiolated mesoporous silica nanoparticles, exploring their antioxidant and osteogenic capabilities in cell culture for preventing the advancement of osteoporosis. Through surface modification, we obtained uniformly ordered, negatively charged thiolated mesoporous silica nanoparticles, characterized via SEM, DLS, Zeta potential, FT-IR, TGA, EDX, XPS, and XRD. The nanomaterial exhibited potent antioxidant properties, effectively neutralizing radical species and protecting murine osteoblast precursor cells (MC3T3) from reactive oxygen species (ROS)-induced damage and cell death.

Demonstrating promising osteogenic potential, the nanomaterial notably increases alkaline phosphatase (ALP) activity and calcium deposition, while upregulating the expression of osteogenic genes (ALP, OCN, OPN, and RUNX 2) in precursor cells and downregulating osteoclastic genes (RANKL, TRAP) in differentiating osteoclasts. Moreover, the nanomaterial was found to be cytocompatible, promoting cell migration and proliferation in both murine osteoblast precursor cells and endothelial cells (HUVEC), crucial for new bone formation, as well as facilitating rapid wound closure. In summary, our developed nanomaterial not only hinders disease progression but also stimulates new bone generation in osteoporotic conditions. The unexplored antioxidant and osteogenic potential of thiolated mesoporous silica nanoparticles positions it as a promising adjunct treatment to conventional therapies.

References

- (1) Wu, A.-M.; Bisignano, C.; James, S. L.; Abady, G. G.; Abedi, A.; Abu-Gharbieh, E.; Alhassan, R. K.; Alipour, V.; Arabloo, J.; Asaad, M.; Asmare, W. N.; Awedew, A. F.; Banach, M.; Banerjee, S. K.; Bijani, A.; Birhanu, T. T. M.; Bolla, S. R.; Cámara, L. A.; Chang, J.-C.; Cho, D. Y.; Chung, M. T.; Couto, R. A. S.; Dai, X.; Dandona, L.; Dandona, R.; Farzadfar, F.; Filip, I.; Fischer, F.; Fomenkov, A. A.; Gill, T. K.; Gupta, B.; Haagsma, J. A.; Haj-Mirzaian, A.; Hamidi, S.; Hay, S. I.; Ilic, I. M.; Ilic, M. D.; Ivers, R. Q.; Jürisson, M.; Kalhor, R.; Kanchan, T.; Kavetsky, T.; Khalilov, R.; Khan, E. A.; Khan, M.; Kneib, C. J.; Krishnamoorthy, V.; Kumar, G. A.; Kumar, N.; Laloo, R.; Lasrado, S.; Lim, S. S.; Liu, Z.; Manafi, A.; Manafi, N.; Menezes, R. G.; Meretoja, T. J.; Miazgowski, B.; Miller, T. R.; Mohammad, Y.; Mohammadian-Hafshejani, A.; Mokdad, A. H.; Murray, C. J. L.; Naderi, M.; Naimzada, M. D.; Nayak, V. C.; Nguyen, C. T.; Nikbakhsh, R.; Olagunju, A. T.; Otstavnov, N.; Otstavnov, S. S.; Padubidri, J. R.; Pereira, J.; Pham, H. Q.; Pinheiro, M.; Polinder, S.; Pourchamani, H.; Rabiee, N.; Radfar, A.; Rahman, M. H. U.; Rawaf, D. L.; Rawaf, S.; Saeb, M. R.; Samy, A. M.; Sanchez Riera, L.; Schwebel, D. C.; Shahabi, S.; Shaikh, M. A.; Soheili, A.; Tabarés-Seisdedos, R.; Tovani-Palone, M. R.; Tran, B. X.; Travillian, R. S.; Valdez, P. R.; Vasankari, T. J.; Velazquez, D. Z.; Venketasubramanian, N.; Vu, G. T.; Zhang, Z.-J.; Vos, T. Global, Regional, and National Burden of Bone Fractures in 204 Countries and Territories, 1990–2019: A Systematic Analysis from the Global Burden of Disease Study 2019. *Lancet Healthy Longev.* **2021**, 2 (9), e580–e592. [https://doi.org/10.1016/S2666-7568\(21\)00172-0](https://doi.org/10.1016/S2666-7568(21)00172-0).
- (2) Reginster, J.-Y.; Burlet, N. Osteoporosis: A Still Increasing Prevalence. *Fight. Osteoporos. Two Fronts* **2006**, 38 (2, Supplement 1), 4–9. <https://doi.org/10.1016/j.bone.2005.11.024>.
- (3) Raisz, L. G. Pathogenesis of Osteoporosis: Concepts, Conflicts, and Prospects. *J. Clin. Invest.* **2005**, 115 (12), 3318–3325. <https://doi.org/10.1172/JCI27071>.
- (4) Sozen, T.; Ozisik, L.; Calik Basaran, N. An Overview and Management of Osteoporosis. *Eur. J. Rheumatol.* **2017**, 4 (1), 46–56. <https://doi.org/10.5152/eurjrheum.2016.048>.
- (5) Domazetovic, V. Oxidative Stress in Bone Remodeling: Role of Antioxidants. *Clin. Cases Miner. Bone Metab.* **2017**, 14 (2), 209. <https://doi.org/10.11138/ccmbm/2017.14.1.209>.
- (6) Zhu, Y.; Zhou, D.; Zan, X.; Ye, Q.; Sheng, S. Engineering the Surfaces of Orthopedic Implants with Osteogenesis and Antioxidants to Enhance Bone Formation in Vitro and in Vivo. *Colloids Surf. B Biointerfaces* **2022**, 212, 112319. <https://doi.org/10.1016/j.colsurfb.2022.112319>.
- (7) Khosla, S.; Hofbauer, L. C. Osteoporosis Treatment: Recent Developments and Ongoing Challenges. *Lancet Diabetes Endocrinol.* **2017**, 5 (11), 898–907. [https://doi.org/10.1016/S2213-8587\(17\)30188-2](https://doi.org/10.1016/S2213-8587(17)30188-2).

- (8) James, A. W.; LaChaud, G.; Shen, J.; Asatrian, G.; Nguyen, V.; Zhang, X.; Ting, K.; Soo, C. A Review of the Clinical Side Effects of Bone Morphogenetic Protein-2. *Tissue Eng. Part B Rev.* **2016**, *22* (4), 284–297. <https://doi.org/10.1089/ten.teb.2015.0357>.
- (9) Barry, M.; Pearce, H.; Cross, L.; Tatullo, M.; Gaharwar, A. K. Advances in Nanotechnology for the Treatment of Osteoporosis. *Curr. Osteoporos. Rep.* **2016**, *14* (3), 87–94. <https://doi.org/10.1007/s11914-016-0306-3>.
- (10) Gao, C.; Wei, D.; Yang, H.; Chen, T.; Yang, L. Nanotechnology for Treating Osteoporotic Vertebral Fractures. *Int. J. Nanomedicine* **2015**, *10*, 5139–5157. <https://doi.org/10.2147/IJN.S85037>.
- (11) Vallet-Regí, M.; Schüth, F.; Lozano, D.; Colilla, M.; Manzano, M. Engineering Mesoporous Silica Nanoparticles for Drug Delivery: Where Are We after Two Decades? *Chem. Soc. Rev.* **2022**, 10.1039.D1CS00659B. <https://doi.org/10.1039/D1CS00659B>.
- (12) Chen, L.; Zhou, X.; He, C. Mesoporous Silica Nanoparticles for Tissue-Engineering Applications. *WIREs Nanomedicine Nanobiotechnology* **2019**, *11* (6), e1573. <https://doi.org/10.1002/wnan.1573>.
- (13) Luo, Z.; Deng, Y.; Zhang, R.; Wang, M.; Bai, Y.; Zhao, Q.; Lyu, Y.; Wei, J.; Wei, S. Peptide-Laden Mesoporous Silica Nanoparticles with Promoted Bioactivity and Osteo-Differentiation Ability for Bone Tissue Engineering. *Colloids Surf. B Biointerfaces* **2015**, *131*, 73–82. <https://doi.org/10.1016/j.colsurfb.2015.04.043>.
- (14) Liang, H.; Jin, C.; Ma, L.; Feng, X.; Deng, X.; Wu, S.; Liu, X.; Yang, C. Accelerated Bone Regeneration by Gold-Nanoparticle-Loaded Mesoporous Silica through Stimulating Immunomodulation. *ACS Appl. Mater. Interfaces* **2019**, *11* (44), 41758–41769. <https://doi.org/10.1021/acsami.9b16848>.
- (15) Cui, W.; Liu, Q.; Yang, L.; Wang, K.; Sun, T.; Ji, Y.; Liu, L.; Yu, W.; Qu, Y.; Wang, J.; Zhao, Z.; Zhu, J.; Guo, X. Sustained Delivery of BMP-2-Related Peptide from the True Bone Ceramics/Hollow Mesoporous Silica Nanoparticles Scaffold for Bone Tissue Regeneration. *ACS Biomater. Sci. Eng.* **2018**, *4* (1), 211–221. <https://doi.org/10.1021/acsbiomaterials.7b00506>.
- (16) Sun, P.; Zhang, Q.; Nie, W.; Zhou, X.; Chen, L.; Du, H.; Yang, S.; You, Z.; He, J.; He, C. Biodegradable Mesoporous Silica Nanocarrier Bearing Angiogenic QK Peptide and Dexamethasone for Accelerating Angiogenesis in Bone Regeneration. *ACS Biomater. Sci. Eng.* **2019**, *5* (12), 6766–6778. <https://doi.org/10.1021/acsbiomaterials.9b01521>.
- (17) Rasool, N.; Srivastava, R.; Singh, Y. Cationized Silica Ceria Nanocomposites to Target Biofilms in Chronic Wounds. *Biomater. Adv.* **2022**, *138*, 212939. <https://doi.org/10.1016/j.bioadv.2022.212939>.
- (18) Baba, S. P.; Bhatnagar, A. Role of Thiols in Oxidative Stress. *Curr. Opin. Toxicol.* **2018**, *7*, 133–139. <https://doi.org/10.1016/j.cotox.2018.03.005>.
- (19) Cazzola, M.; Rogliani, P.; Salvi, S. S.; Ora, J.; Matera, M. G. Use of Thiols in the

- Treatment of COVID-19: Current Evidence. *Lung* **2021**, *199* (4), 335–343. <https://doi.org/10.1007/s00408-021-00465-3>.
- (20) Lean, J. M.; Davies, J. T.; Fuller, K.; Jagger, C. J.; Kirstein, B.; Partington, G. A.; Urry, Z. L.; Chambers, T. J. A Crucial Role for Thiol Antioxidants in Estrogen-Deficiency Bone Loss. *J. Clin. Invest.* **2003**, *112* (6), 915–923. <https://doi.org/10.1172/JCI200318859>.
- (21) Sendur, O. F.; Turan, Y.; Tastaban, E.; Serter, M. Antioxidant Status in Patients with Osteoporosis: A Controlled Study. *Joint Bone Spine* **2009**, *76* (5), 514–518. <https://doi.org/10.1016/j.jbspin.2009.02.005>.
- (22) Korkmaz, V.; Kurdoglu, Z.; Alisik, M.; Turgut, E.; Sezgin, O. O.; Korkmaz, H.; Ergun, Y.; Erel, O. Thiol/Disulfide Homeostasis in Postmenopausal Osteoporosis. *J. Endocrinol. Invest.* **2017**, *40* (4), 431–435. <https://doi.org/10.1007/s40618-016-0585-7>.
- (23) Summonte, S.; Racaniello, G. F.; Lopodota, A.; Denora, N.; Bernkop-Schnürch, A. Thiolated Polymeric Hydrogels for Biomedical Application: Cross-Linking Mechanisms. *J. Controlled Release* **2021**, *330*, 470–482. <https://doi.org/10.1016/j.jconrel.2020.12.037>.
- (24) Hock, N.; Racaniello, G. F.; Aspinall, S.; Denora, N.; Khutoryanskiy, V. V.; Bernkop-Schnürch, A. Thiolated Nanoparticles for Biomedical Applications: Mimicking the Workhorses of Our Body. *Adv. Sci.* **2022**, *9* (1), 2102451. <https://doi.org/10.1002/advs.202102451>.
- (25) Li, L.; Lu, C.; Wang, L.; Chen, M.; White, J.; Hao, X.; McLean, K. M.; Chen, H.; Hughes, T. C. Gelatin-Based Photocurable Hydrogels for Corneal Wound Repair. *ACS Appl. Mater. Interfaces* **2018**, *10* (16), 13283–13292. <https://doi.org/10.1021/acsami.7b17054>.
- (26) Lin, Z.; Li, R.; Liu, Y.; Zhao, Y.; Ao, N.; Wang, J.; Li, L.; Wu, G. Histatin1-Modified Thiolated Chitosan Hydrogels Enhance Wound Healing by Accelerating Cell Adhesion, Migration and Angiogenesis. *Carbohydr. Polym.* **2020**, *230*, 115710. <https://doi.org/10.1016/j.carbpol.2019.115710>.
- (27) Wojda, S. J.; Marozas, I. A.; Anseth, K. S.; Yaszemski, M. J.; Donahue, S. W. Thiol-Ene Hydrogels for Local Delivery of PTH for Bone Regeneration in Critical Size Defects. *J. Orthop. Res.* **2020**, *38* (3), 536–544. <https://doi.org/10.1002/jor.24502>.
- (28) Hegedűs, O.; Juriga, D.; Sipos, E.; Voniatis, C.; Juhász, Á.; Idrissi, A.; Zrínyi, M.; Varga, G.; Jedlovsky-Hajdú, A.; Nagy, K. S. Free Thiol Groups on Poly(Aspartamide) Based Hydrogels Facilitate Tooth-Derived Progenitor Cell Proliferation and Differentiation. *PLOS ONE* **2019**, *14* (12), e0226363. <https://doi.org/10.1371/journal.pone.0226363>.
- (29) Kalantari, M.; Ghosh, T.; Liu, Y.; Zhang, J.; Zou, J.; Lei, C.; Yu, C. Highly Thiolated Dendritic Mesoporous Silica Nanoparticles with High-Content Gold as Nanozymes: The Nano-Gold Size Matters. *ACS Appl. Mater. Interfaces* **2019**, *11* (14), 13264–13272. <https://doi.org/10.1021/acsami.9b01527>.

- (30) Halder, M.; Bhatia, Y.; Singh, Y. Self-Assembled Di- and Tripeptide Gels for the Passive Entrapment and PH-Responsive, Sustained Release of an Antidiabetic Drug, Glimepiride. *Biomater. Sci.* **2022**, *10* (9), 2248–2262. <https://doi.org/10.1039/D2BM00344A>.
- (31) Chauhan, N.; Gupta, P.; Arora, L.; Pal, D.; Singh, Y. Dexamethasone-Loaded, Injectable Pullulan-Poly(Ethylene Glycol) Hydrogels for Bone Tissue Regeneration in Chronic Inflammatory Conditions. *Mater. Sci. Eng. C* **2021**, *130*, 112463. <https://doi.org/10.1016/j.msec.2021.112463>.
- (32) Pinna, A.; Torki Baghbaderani, M.; Vigil Hernández, V.; Naruphontjirakul, P.; Li, S.; McFarlane, T.; Hachim, D.; Stevens, M. M.; Porter, A. E.; Jones, J. R. Nanoceria Provides Antioxidant and Osteogenic Properties to Mesoporous Silica Nanoparticles for Osteoporosis Treatment. *Acta Biomater.* **2021**, *122*, 365–376. <https://doi.org/10.1016/j.actbio.2020.12.029>.
- (33) Liang, C.-C.; Park, A. Y.; Guan, J.-L. In Vitro Scratch Assay: A Convenient and Inexpensive Method for Analysis of Cell Migration in Vitro. *Nat. Protoc.* **2007**, *2* (2), 329–333. <https://doi.org/10.1038/nprot.2007.30>.
- (34) Nazir, F.; Ashraf, I.; Iqbal, M.; Ahmad, T.; Anjum, S. 6-Deoxy-Aminocellulose Derivatives Embedded Soft Gelatin Methacryloyl (GelMA) Hydrogels for Improved Wound Healing Applications: In Vitro and in Vivo Studies. *Int. J. Biol. Macromol.* **2021**, *185*, 419–433. <https://doi.org/10.1016/j.ijbiomac.2021.06.112>.
- (35) Spampinato, V.; Parracino, M. A.; La Spina, R.; Rossi, F.; Ceccone, G. Surface Analysis of Gold Nanoparticles Functionalized with Thiol-Modified Glucose SAMs for Biosensor Applications. *Front. Chem.* **2016**, *4*. <https://doi.org/10.3389/fchem.2016.00008>.
- (36) Li, Y.; Song, F.; Cheng, L.; Qian, J.; Chen, Q. Functionalized Large-Pore Mesoporous Silica Microparticles for Gefitinib and Doxorubicin Codelivery. *Mater. Basel Switz.* **2019**, *12* (5), 766. <https://doi.org/10.3390/ma12050766>.
- (37) AbouAitah, K.; Swiderska-Sroda, A.; Farghali, A. A.; Wojnarowicz, J.; Stefanek, A.; Gierlotka, S.; Opalinska, A.; Allayeh, A. K.; Ciach, T.; Lojkowski, W. Folic Acid-Conjugated Mesoporous Silica Particles as Nanocarriers of Natural Prodrugs for Cancer Targeting and Antioxidant Action. *Oncotarget* **2018**, *9* (41), 26466–26490. <https://doi.org/10.18632/oncotarget.25470>.
- (38) Chen, M.; Li, Y.; Huang, X.; Gu, Y.; Li, S.; Yin, P.; Zhang, L.; Tang, P. Skeleton-Vasculature Chain Reaction: A Novel Insight into the Mystery of Homeostasis. *Bone Res.* **2021**, *9* (1), 21. <https://doi.org/10.1038/s41413-021-00138-0>.
- (39) Kanniyappan, H.; Venkatesan, M.; Panji, J.; Ramasamy, M.; Muthuvijayan, V. Evaluating the Inherent Osteogenic and Angiogenic Potential of Mesoporous Silica Nanoparticles to Augment Vascularized Bone Tissue Formation. *Microporous Mesoporous Mater.* **2021**, *311*, 110687. <https://doi.org/10.1016/j.micromeso.2020.110687>.

- (40) Gkioni, K.; Leeuwenburgh, S. C. G.; Douglas, T. E. L.; Mikos, A. G.; Jansen, J. A. Mineralization of Hydrogels for Bone Regeneration. *Tissue Eng. Part B Rev.* **2010**, *16* (6), 577–585. <https://doi.org/10.1089/ten.teb.2010.0462>.
- (41) Wu, X.; Walsh, K.; Hoff, B. L.; Camci-Unal, G. Mineralization of Biomaterials for Bone Tissue Engineering. *Bioengineering* **2020**, *7* (4), 132. <https://doi.org/10.3390/bioengineering7040132>.
- (42) Zhou, X.; Feng, W.; Qiu, K.; Chen, L.; Wang, W.; Nie, W.; Mo, X.; He, C. BMP-2 Derived Peptide and Dexamethasone Incorporated Mesoporous Silica Nanoparticles for Enhanced Osteogenic Differentiation of Bone Mesenchymal Stem Cells. *ACS Appl. Mater. Interfaces* **2015**, *7* (29), 15777–15789. <https://doi.org/10.1021/acsami.5b02636>.
- (43) Yin, Y.; Huang, Q.; Yang, M.; Xiao, J.; Wu, H.; Liu, Y.; Li, Q.; Huang, W.; Lei, G.; Zhou, K. MgO Nanoparticles Protect against Titanium Particle-Induced Osteolysis in a Mouse Model Because of Their Positive Immunomodulatory Effect. *ACS Biomater. Sci. Eng.* **2020**, *6* (5), 3005–3014. <https://doi.org/10.1021/acsbiomaterials.9b01852>.
- (44) Lo, Y.-C.; Chang, Y.-H.; Wei, B.-L.; Huang, Y.-L.; Chiou, W.-F. Betulinic Acid Stimulates the Differentiation and Mineralization of Osteoblastic MC3T3-E1 Cells: Involvement of BMP/Runx2 and β -Catenin Signals. *J. Agric. Food Chem.* **2010**, *58* (11), 6643–6649. <https://doi.org/10.1021/jf904158k>.
- (45) Tu, M.-G.; Chen, Y.-W.; Shie, M.-Y. Macrophage-Mediated Osteogenesis Activation in Co-Culture with Osteoblast on Calcium Silicate Cement. *J. Mater. Sci. Mater. Med.* **2015**, *26* (12), 276. <https://doi.org/10.1007/s10856-015-5607-z>.
- (46) Mladenović, Ž.; Johansson, A.; Willman, B.; Shahabi, K.; Björn, E.; Ransjö, M. Soluble Silica Inhibits Osteoclast Formation and Bone Resorption in Vitro. *Acta Biomater.* **2014**, *10* (1), 406–418. <https://doi.org/10.1016/j.actbio.2013.08.039>.
- (47) Nah, H.; Lee, D.; Lee, J. S.; Lee, S. J.; Heo, D. N.; Lee, Y.-H.; Bang, J. B.; Hwang, Y.-S.; Moon, H.-J.; Kwon, I. K. Strategy to Inhibit Effective Differentiation of RANKL-Induced Osteoclasts Using Vitamin D-Conjugated Gold Nanoparticles. *Appl. Surf. Sci.* **2020**, *527*, 146765. <https://doi.org/10.1016/j.apsusc.2020.146765>.
- (48) Aryal A.C, S.; Miyai, K.; Izu, Y.; Hayata, T.; Notomi, T.; Noda, M.; Ezura, Y. Nck Influences Preosteoblastic/Osteoblastic Migration and Bone Mass. *Proc. Natl. Acad. Sci.* **2015**, *112* (50), 15432–15437. <https://doi.org/10.1073/pnas.1518253112>.
- (49) Lamalice, L.; Le Boeuf, F.; Huot, J. Endothelial Cell Migration During Angiogenesis. *Circ. Res.* **2007**, *100* (6), 782–794. <https://doi.org/10.1161/01.RES.0000259593.07661.1e>.

CHAPTER - 5

Conclusions and perspectives

5.1. Summary of the thesis

The aim of this thesis was to explore nanomaterial for drug delivery, wound healing, and bone regeneration. Nanomaterials have distinct physical and chemical properties, which make them suitable as drug cargo and scaffolds for tissue regeneration. The nanomaterials investigated earlier for such applications have been associated with several limitations, like polymeric nanoparticles exhibit less drug retention and permeation across ocular barriers, biomimetic activity of cerium oxide is size dependent and mesoporous silica nanoparticles have no antioxidant potential of their own. Functional nanoparticles can be modified chemically and imparted with new properties to achieve desirable effects. Therefore, our aim was to develop nanomaterials with improved safety and effectiveness to overcome those limitations.

This thesis is organized into five chapters. **Chapter 1** is introductory and includes a brief overview on ocular infections, wound healing, and bone disorders. It also includes an exhaustive literature survey on the nanomaterials being developed for such applications along with the identification of existing knowledge gaps. This chapter also includes specific objectives of the thesis, hypothesis statement, and organization of the thesis.

In **Chapter 2**, we have reported the development and evaluation of ciprofloxacin-loaded polymeric nanoparticles of chitosan/lecithin (CL NPs) for the treatment of ocular bacterial infections. The intrinsic antibacterial property of chitosan along with that of ciprofloxacin creates an additive effect and improved antimicrobial action. The addition of lecithin helps in the prolonged residence and enhanced corneal permeability. High drug loading was achieved, and the polymer matrix showed slow degradation, which resulted in the sustained release of ciprofloxacin. Nanoparticles exhibited excellent antibacterial properties against *P. aeruginosa* and *S. aureus* without compromising the cytocompatibility towards mammalian cells. As required for any drug carrier intended for ocular delivery, nanoparticles were found to have good mucoadhesive property. The drug delivery system investigated can be effectively explored for the prolonged release of ciprofloxacin while evading the anatomical barriers present in ocular tissues.

Chapter 3 investigates the development of functionalized, silica ceria nanocomposite (FSC), as an antibiotic-free system, to treat biofilms present in chronic wounds. The therapeutic nanocomposite was engineered in a manner to utilize the surface area of MSN for uniform distribution of CNP, resulting in a drug-free and size-independent antibacterial nanomaterial. The nanocomposite was thoroughly characterized for its physical and chemical

properties. Owing to the incorporation of cerium and cationic charge, nanocomposite possessed excellent biocatalytic, biomimetic, and antibacterial activities. The cell culture studies revealed that the functionalized nanocomposite promotes wound healing via cell proliferation and migration. Overall, the functionalized nanocomposite is a suitable candidate for restoring stalled healing in chronic wounds.

The aim of **Chapter 4** was to develop a therapeutic nanomaterial comprising of thiolated mesoporous silica nanoparticles for the treatment of osteoporosis. The presence of thiol groups imparted antioxidant and cell adhesion properties to mesoporous silica nanoparticles, which is not inherent to these nanomaterials. The functionalized nanomaterial showed osteogenicity and promoted bone regeneration by stimulating the expression of various osteogenic genes and proteins. Mesoporous silica nanoparticles were able to scavenge reactive oxygen species effectively and protected the cells against oxidative stress-induced damage. The nanomaterial aided cell migration and angiogenesis in cell culture. Overall, a drug-free nanomaterial was developed, which shows a strong potential in bone regeneration and osteoporosis.

This section, which is **Chapter 5**, provides the conclusions and perspective on the work done in comparison to the existing literature.

5.1.1 Contribution to the existing knowledge

A major aim of this study was to explore the potential of functional nanomaterial for addressing the challenges associated with the materials being developed for drug delivery and tissue regeneration.

Ocular drug delivery is one of the most challenging areas owing to the nature of ocular tissue. Various nanoformulations have been designed and investigated for drug delivery to achieve high drug bioavailability. However, the major focus of these preparations available in the market has been to utilize the nanomaterial as drug carrier only, with much less focus on developing functional nanomaterials, which is a key knowledge gap in the field. To address this gap, we have developed a nanoparticulate system from bioactive polymers having intrinsic antimicrobial and mucoadhesive properties, and loaded it with ciprofloxacin to treat bacterial ocular infections. Our nanoparticulate system exhibited high drug loading and sustained release, which resulted in excellent antibacterial properties. It also showed good mucoadhesive property, which is likely to enhance drug retention in eye.

Nanomaterials, such as inorganic, metal, and carbon nanoparticles have been immensely explored for wound healing and tissue regeneration. One such material is cerium oxide nanoparticles, which is well documented for its therapeutic value but these properties has been found to be size-dependent. Another well explored inorganic nanomaterial is mesoporous silica nanoparticles, which have been exclusively used as drug carrier but lack intrinsic antibacterial properties. Composite nanomaterial offers the advantage of integrating two materials and creating a nanomaterial with improved and enhanced effects. We have

developed a nanocomposite of cerium and silica nanoparticles to address the challenge associated with their use. In this nanocomposite, surface chemistry and frameworks in mesoporous silica nanoparticles were utilized to incorporate cerium oxide nanoparticles. Our nanocomposite was able to retain the original properties and show improved action when compared to the constituting nanomaterials. We were able to develop a drug-free and size-independent nanocomposite, which possessed excellent antibacterial and antioxidant properties, with good biocompatibility and potential application in wound healing.

Osteoporosis is a chronic bone disorder, which has been conventionally managed by using a cocktail of anti-resorptive and osteogenic drugs. Besides causing peripheral toxicity, these drugs fail to address the prooxidative stress, an important factor identified in the disease progression. To address this challenge in the field, we have developed thiolated mesoporous silica nanoparticles to promote osteogenesis. Mesoporous silica nanoparticles are known to promote osteogenesis but they lack antioxidant properties, which are very much required for such applications. Taking inspiration from the body's natural thiol-based anti-oxidative system, free thiols were functionalized on the surface of mesoporous silica nanoparticles to obtain thiolated mesoporous nanoparticles. As envisaged, it promoted osteogenesis, provided protection from oxidative stress, and showed improved cell adhesion, which can be employed in bone regeneration applications.

The overall gain of this study is, we developed functional nanomaterial which show promising potential for treatment of biofilm infected wounds and osteoporosis. To treat bacterial ocular infections, a synergic therapeutic effect was achieved with use of antibacterial nanoparticles.

5.1.2. Future perspectives

The antibacterial, polymeric nanoemulsion prepared for the ocular drug delivery has shown promising results. In this work, we have used a standard antibiotic to treat the bacterial infection but it is well known that the prolonged use of antibiotics results in antimicrobial resistant strains and renders them ineffective. As our carrier system itself has a decent intrinsic antimicrobial property, some modifications can be done to make it a drug-free, therapeutic nanoemulsion with improved antimicrobial activities. Also, this material needs further optimization to minimize batch-to-batch variation and testing in animal models to check the effectiveness in real microenvironment present in ocular tissues. If similar results are obtained in *in vivo* studies, it can be evaluated further in order to develop a functional nanomaterial for effective and viable treatment of bacterial ocular infections. Similarly, cationized silica cerium composite showed excellent antioxidant, antibacterial, and wound healing properties but it needs to be evaluated against resistant bacterial strains, which are responsible for altering normal wound healing. The effectiveness of this nanocomposite needs to be investigated in the simulated environment of chronic wounds. It is also possible to develop a delivery system for this nanocomposite, such as transdermal patches. The nanocomposite can be loaded into

reservoir-based transdermal patches for sustained release or applied topically on the wound site. The thiolated mesoporous silica nanoparticles can be used as a complementary medicine along with the standard treatment available for osteoporosis. However, for its clinical translation, a mode of delivery needs to be developed. The injectability of nanoparticles needs to be investigated so that these can be directly injected at the site of action to achieve enhanced localized, therapeutic effects with minimal peripheral toxicity.

APPENDIX

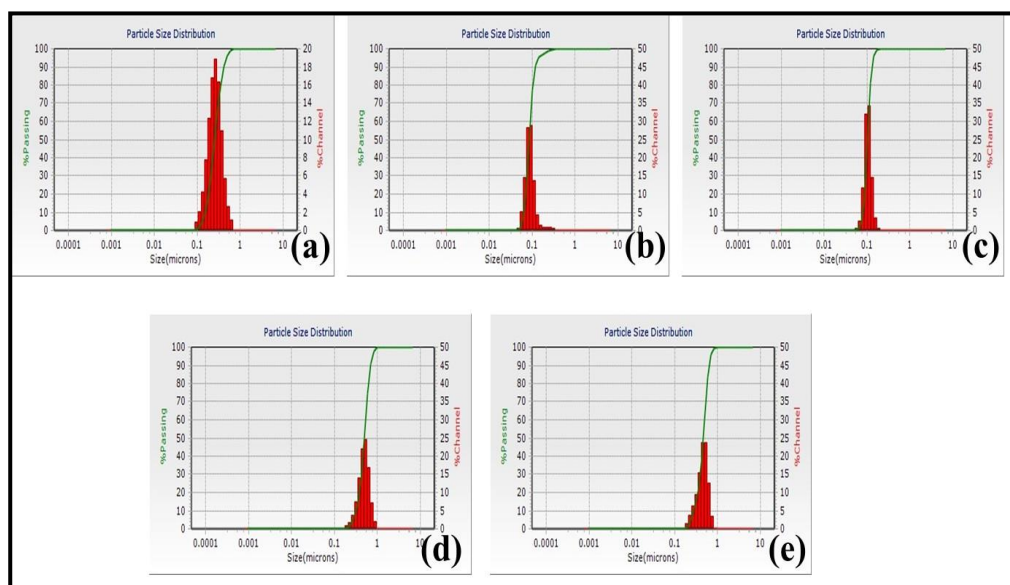


Figure A1. Particle size distribution ($n = 3$) using DLS. (a) MSN. (b) CNP. (c) FCNP. (d) SC. (e) FSC.

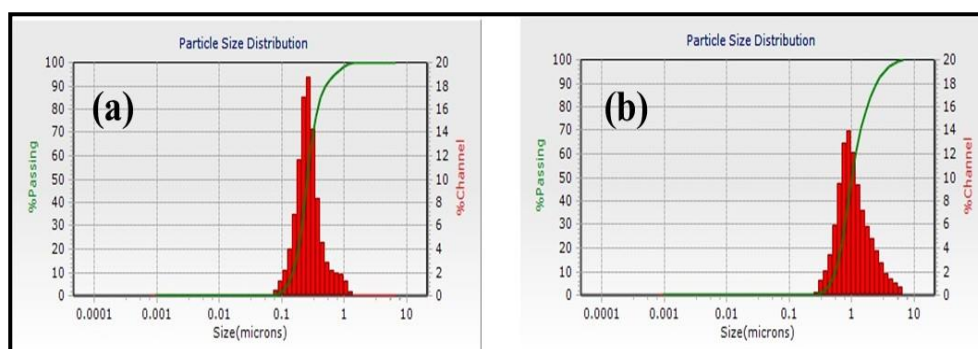


Figure A2. FSC nanocomposite of different sizes. (a) 257 nm. (b) 911 nm.

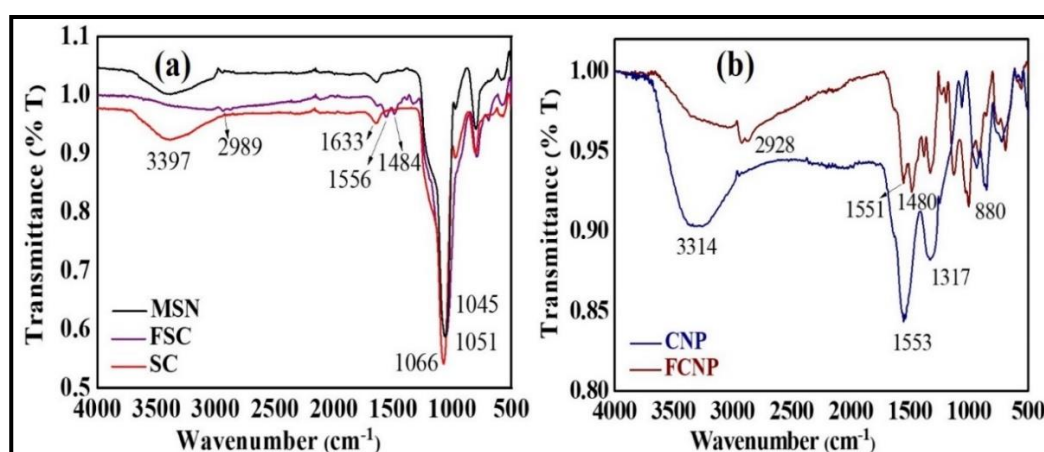


Figure A3. FT-IR spectra. (a) MSN, SC, and FSC. (b) CNP and FCNP.

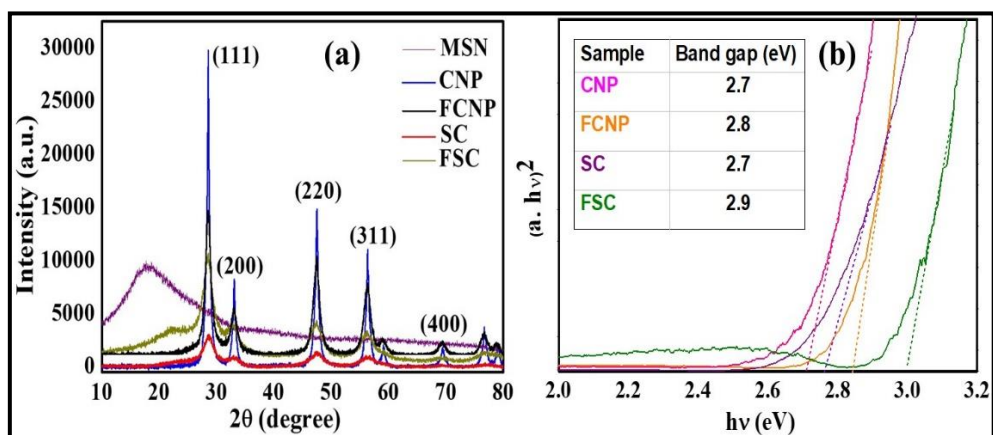


Figure A4. (a) PXRD patterns of CNP, SC, and MSN. (b) Band gap energy of CNP, FCNP, SC, and FSC.

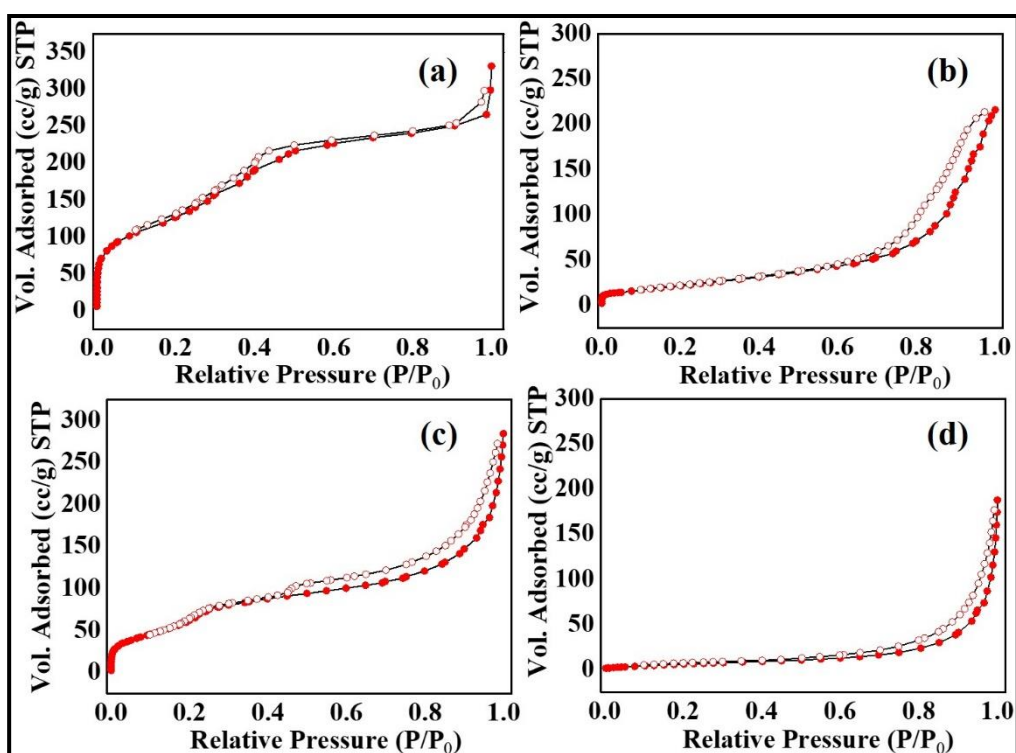


Figure A5. N_2 adsorption-desorption isotherms. (a) MSN. (b) CNP. (c) SC. (d) FSC.

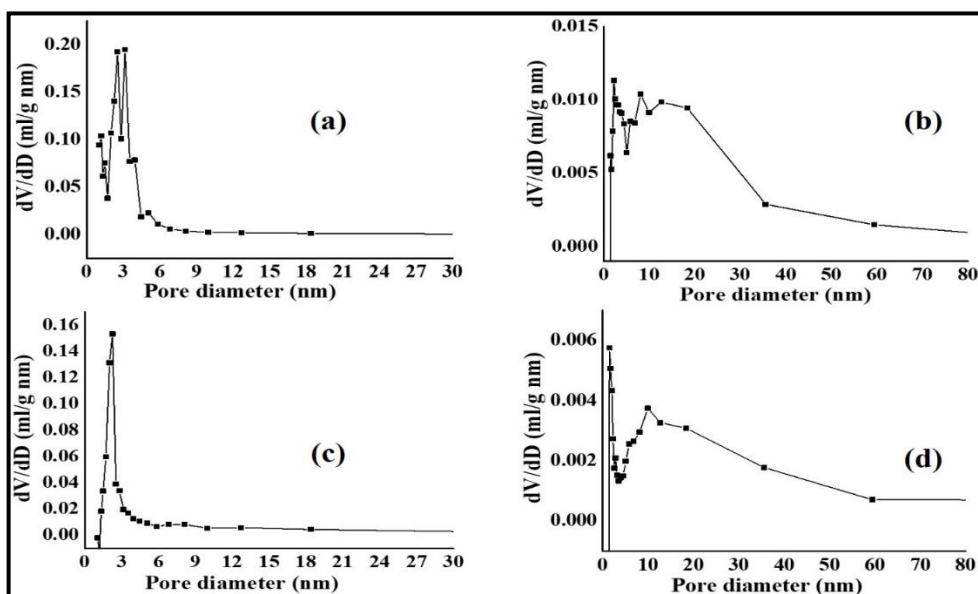


Figure A6. BJH pore size distribution curves. (a) MSN. (b) CNP. (c) SC. (d) FSC.

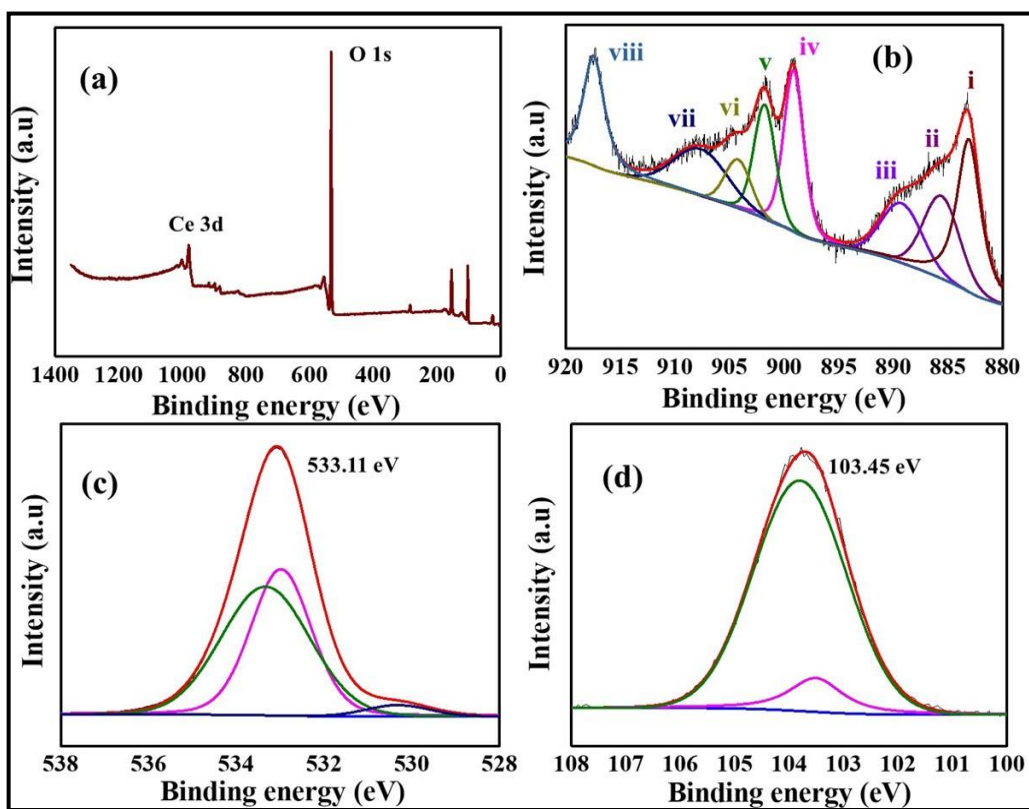


Figure A7. XPS spectra of SC. (a) Survey spectrum. (b) Ce 3d. (c) O 1s and (d) Si 2p.

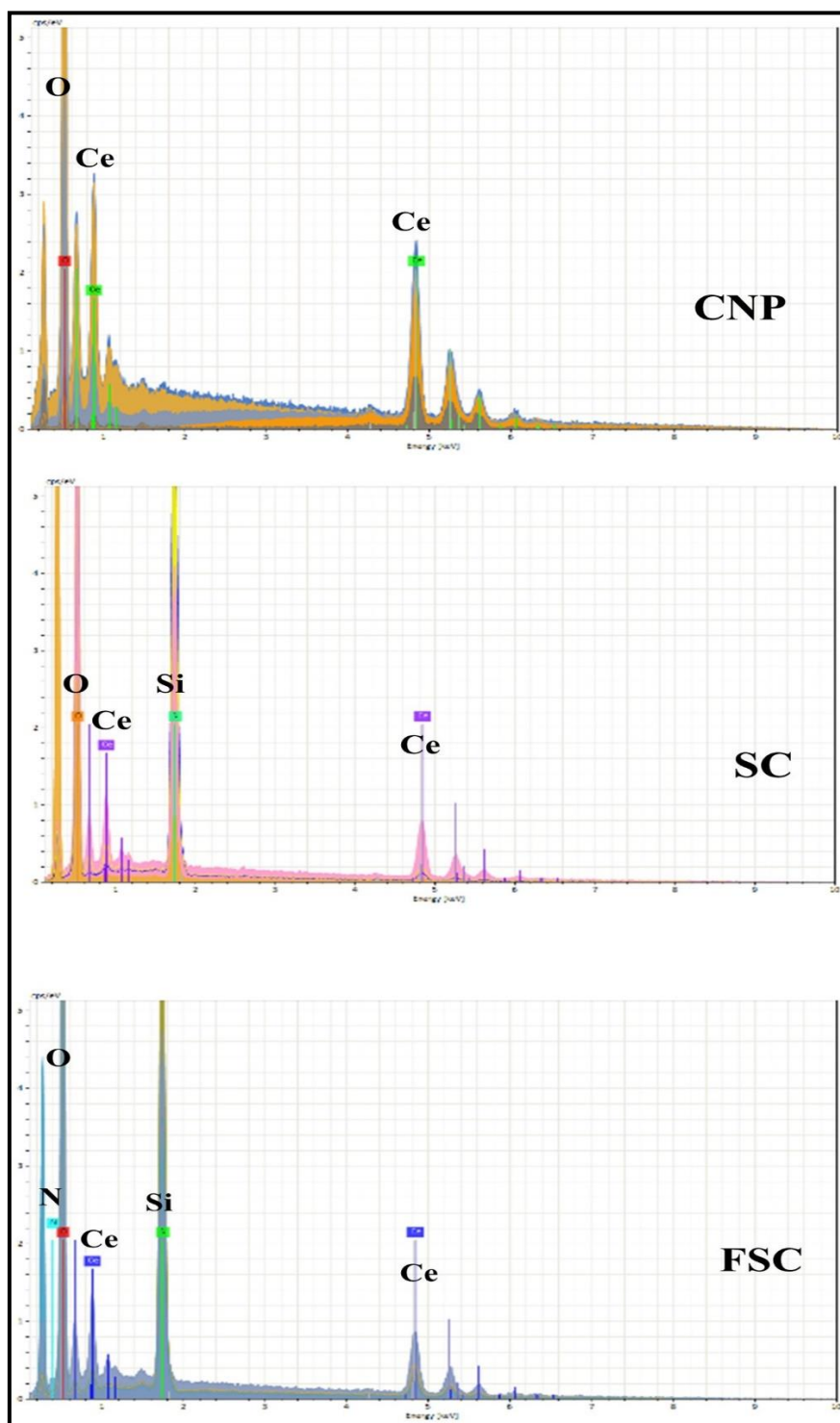


Figure A8. EDX spectra of CNP, SC, and FSC.

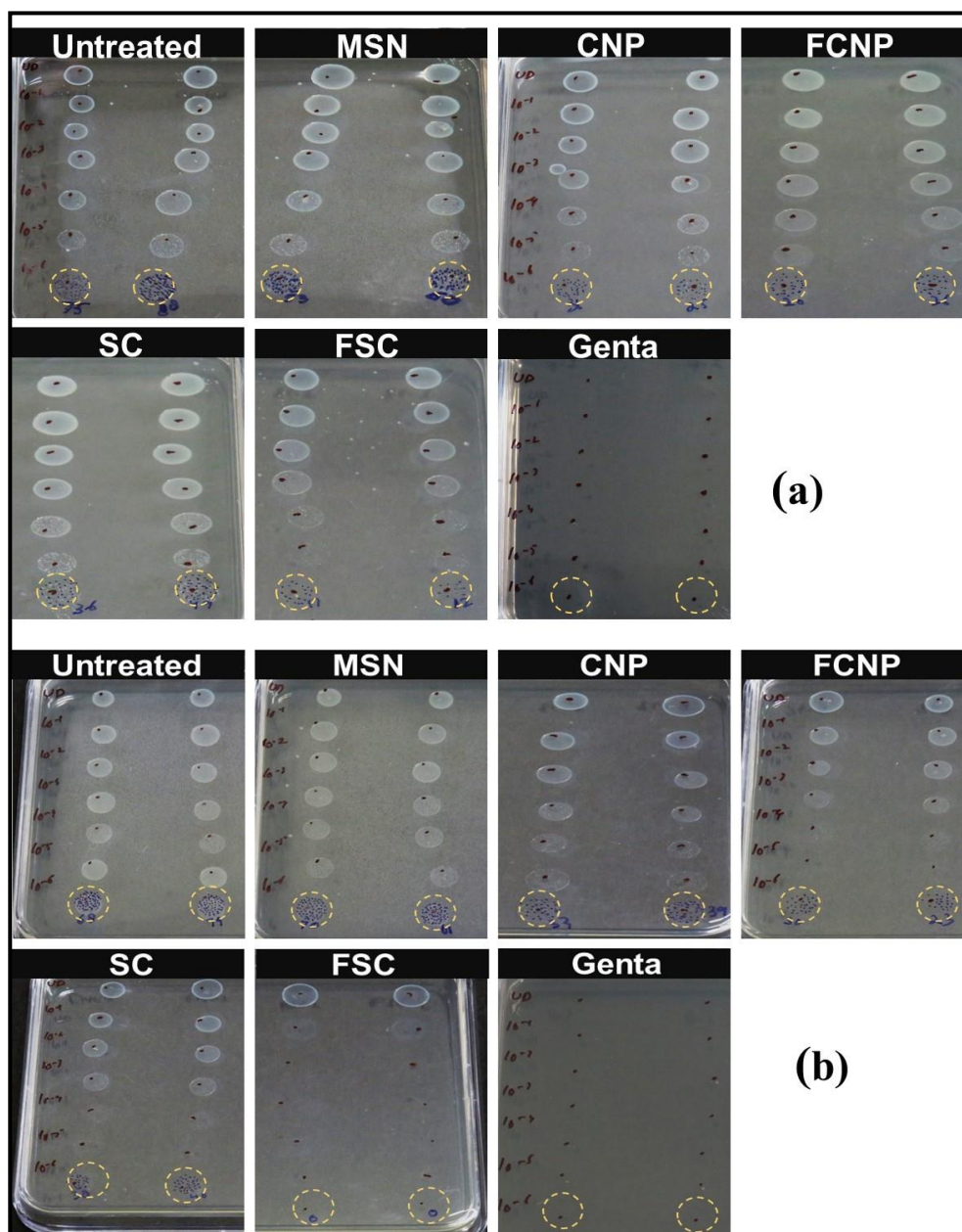


Figure A9. Images of bacterial colonies on agar plates. (a) *E. coli* in 24 h. (b) *S. aureus* in 12 h.

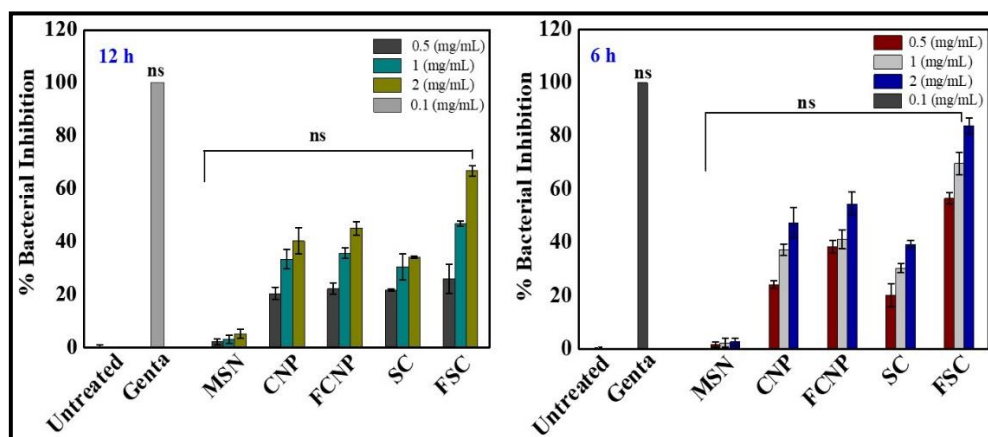


Figure A10. Inhibition of bacterial growth. (a) *E. coli* in 12 h. (b) *S. aureus* in 6 h. The ns represents the non-significant difference.

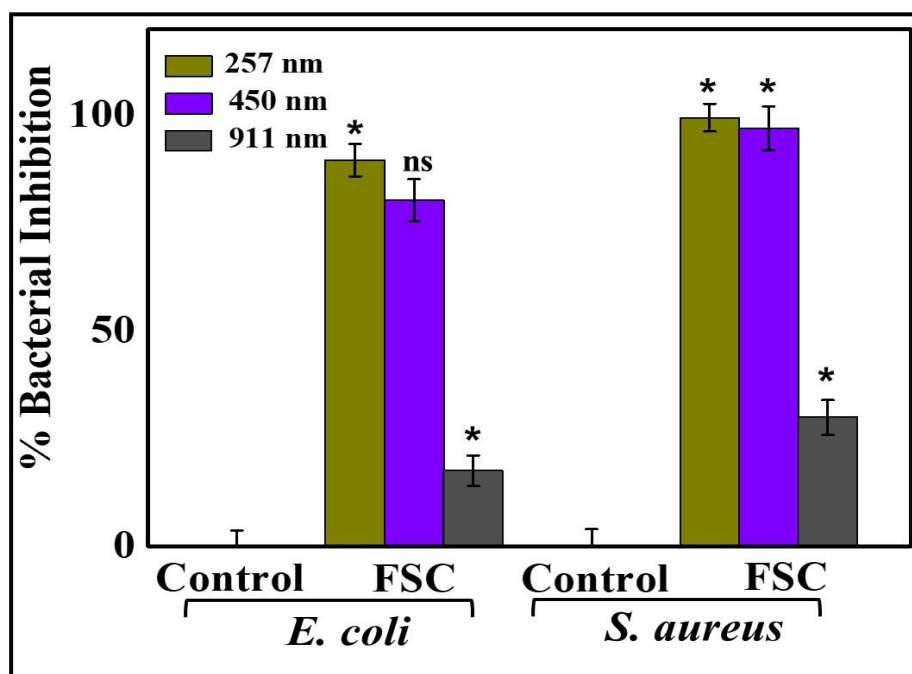


Figure A11. Antibacterial activity exhibited by FSC nanocomposites of different size against *E. coli* and *S. aureus*. * $p < 0.05$ represents the statistically significant difference and ns indicates non-significant difference.

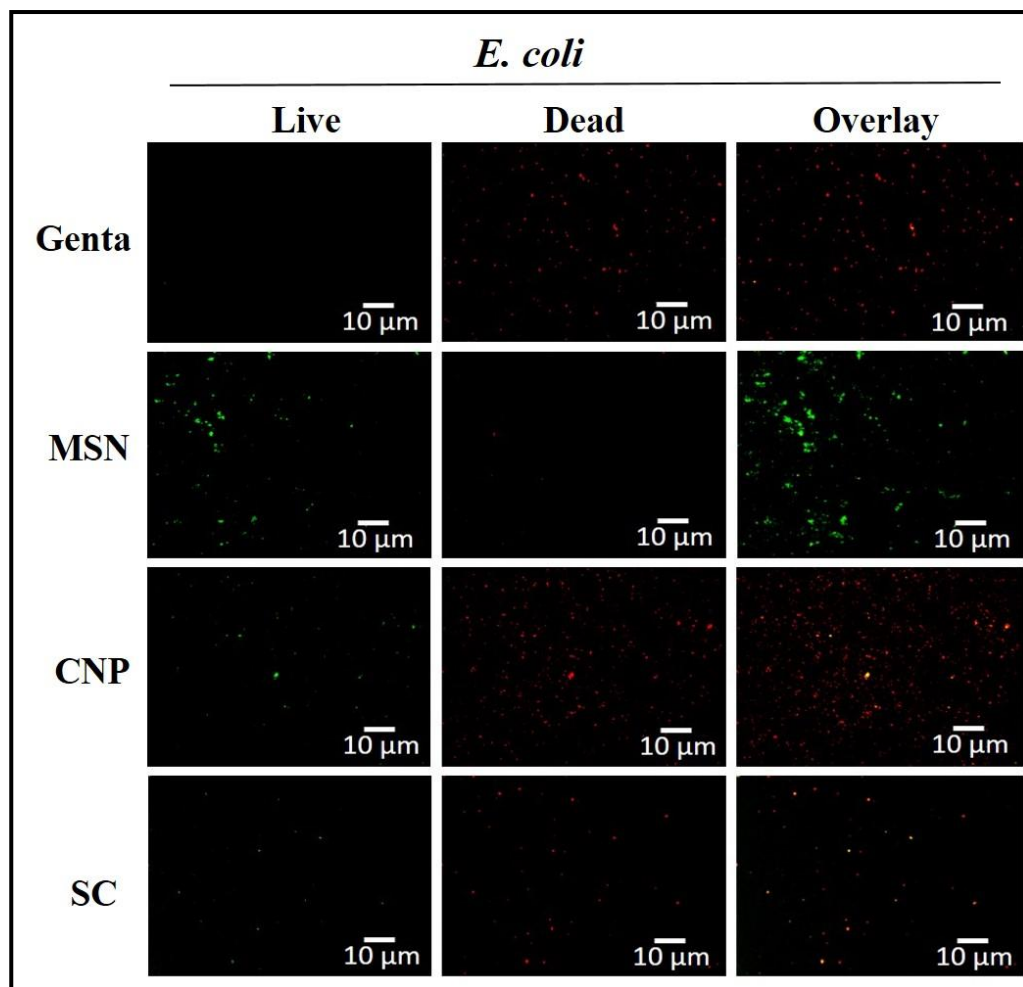


Figure A12. Fluorescence microscopic images of gentamicin (Genta), MSN, CNP, and SC-treated bacterial suspension of *E. coli*. Scale bar: 10 μm .

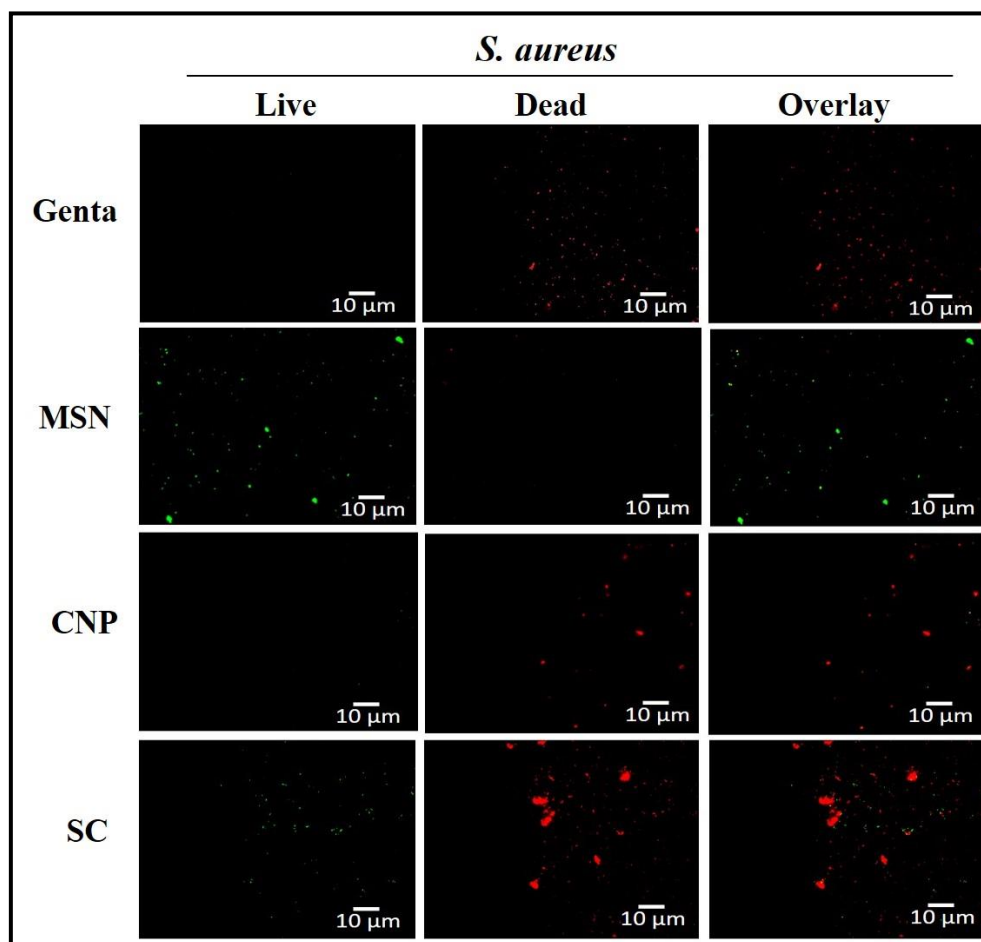


Figure A13. Fluorescence microscopic images of gentamicin (Genta), MSN, CNP, and SC-treated bacterial suspension of *S. aureus*. Scale bar: 10 μm .

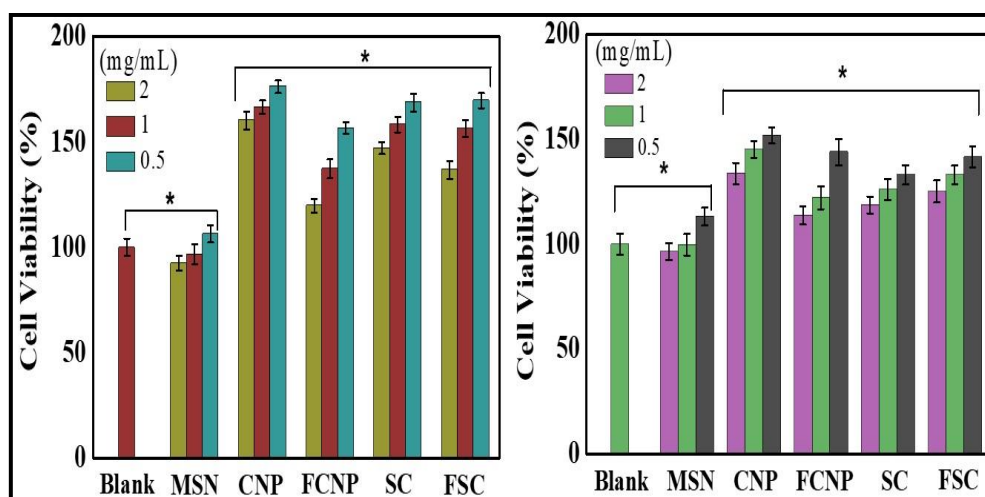


Figure A14. Cell viability assay of untreated (blank) and MSN, CNP, FCNP, SC and FSC extract-treated L929 cells for 72 h. (a) MTT. (b) CCK 8. * $p < 0.05$ represents the statistically significant difference.

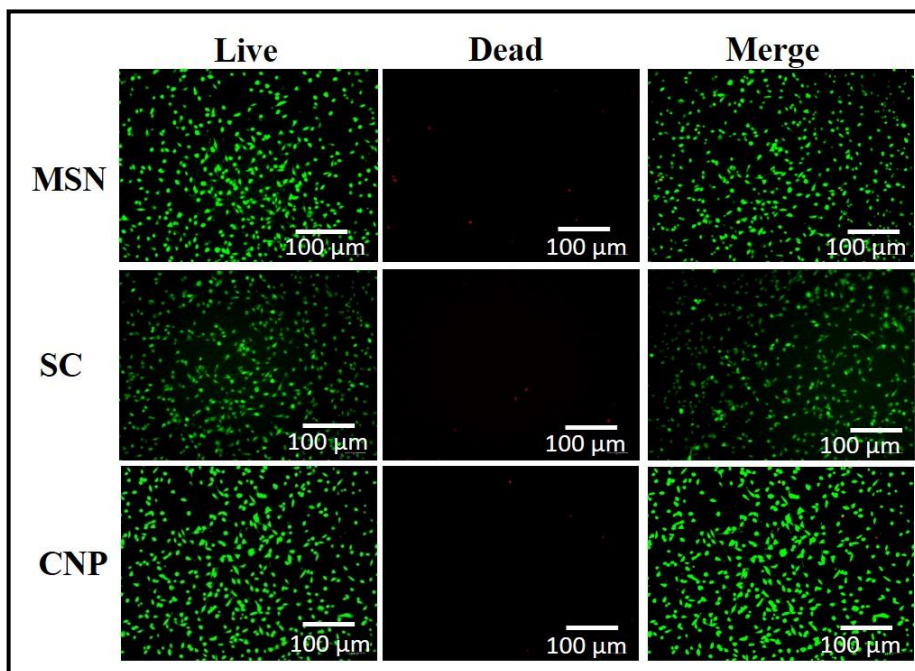


Figure A15. Fluorescence microscopic images of MSN, SC and CNP conditioned media-treated L929 cells. Scale bar: 100 μm .

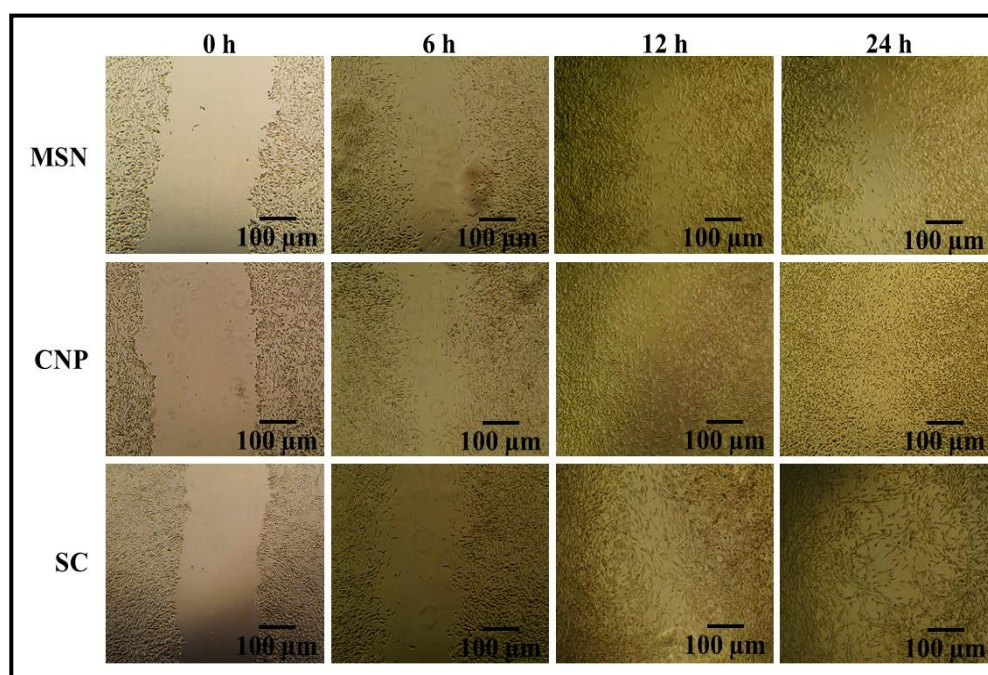


Figure A16. Scratch assay. Microscopic images of MSN, CNP and SC extract-treated cells at the time interval of 0, 6, 12 and 24 h. Scale bar: 100 μm .

Table A1. Physical properties of nanoparticles (MSN, CNP) and nanocomposites (SC, FSC).

MSN	479	0.42
CNP	87	0.32
SC	436	0.36
FSC	29	0.19

Table A2. Ratio of Ce³⁺/Ce⁴⁺ estimated using Ce 3d XPS spectrum of FSC.

Peaks	Binding energy (eV)	Area
i	882.34	14170
ii	885.13	9925
iii	888.49	9859
iv	898.19	8663
v	900.80	8143
vi	903.65	8457
vii	907.68	7654
viii	916.71	7820
ii, iv, vi	Ce ³⁺	9015
i, iii, v, vii, viii	Ce ⁴⁺	9529.2
	Ce ³⁺ / Ce ⁴⁺	0.94
	Ce ³⁺ / (Ce ³⁺ + Ce ⁴⁺) ×100	48%

Protocol for RNA Isolation. For RNA isolation, cells were harvested at time interval of 7 and 14 days and trypsinized. The cells were collected after centrifugation and thoroughly washed with PBS. Next, 400 µL of trizol solution was added and incubated for 5 min at RT. Chloroform (80 µL) was added and again incubated for 5 min. The separation of aqueous and organic layer was done by centrifugation at 12000g, 4 °C for 15 min. RNA was carefully aspirated out and transferred to a new tube. To precipitate RNA, 200 µL of propanol was added and incubated for 10 min at RT. RNA pellet was washed with 75% ethanol and air dried. The amount of RNA isolated was quantified using a NANODROP (Thermo Fisher Scientific).

Protocol for cDNA Synthesis. cDNA synthesis from the isolated RNA was done using iScriptTM cDNA synthesis kit (Bio-Rad). To prepare 1 µg of cDNA, 5x iScript Reaction Mix (4 µL), isolated RNA samples (1 µg), and iScript Reverse Transcriptase (1 µL) were taken in nuclease-free water, and volume made up to 20 µL. The reaction mixture was transferred to VeritiTM 96-well Thermal Cycler (Applied Biosystems, Thermo Fisher Scientific), with priming for 5 min at 20 °C, reverse transcription at 46 °C for 20 min, and RT inactivation at 95 °C for 1 min.

Protocol for Quantitative Real-Time PCR (RT-PCR). For gene analysis, the PowerUp SYBR Green Master Mix microamp optical 8-Tube strip (0.2 mL, Applied Biosystems, Life Technologies) was used. The reaction mixture (9 µL) was prepared by mixing SYBR Master Mix (3.75 µL), forward and reverse primers (0.5 µL each), 100 ng cDNA (1 µL), and nuclease-free water (q.s). The real-time PCR was done using an Applied Biosystems QuantStudio3 real-time PCR.

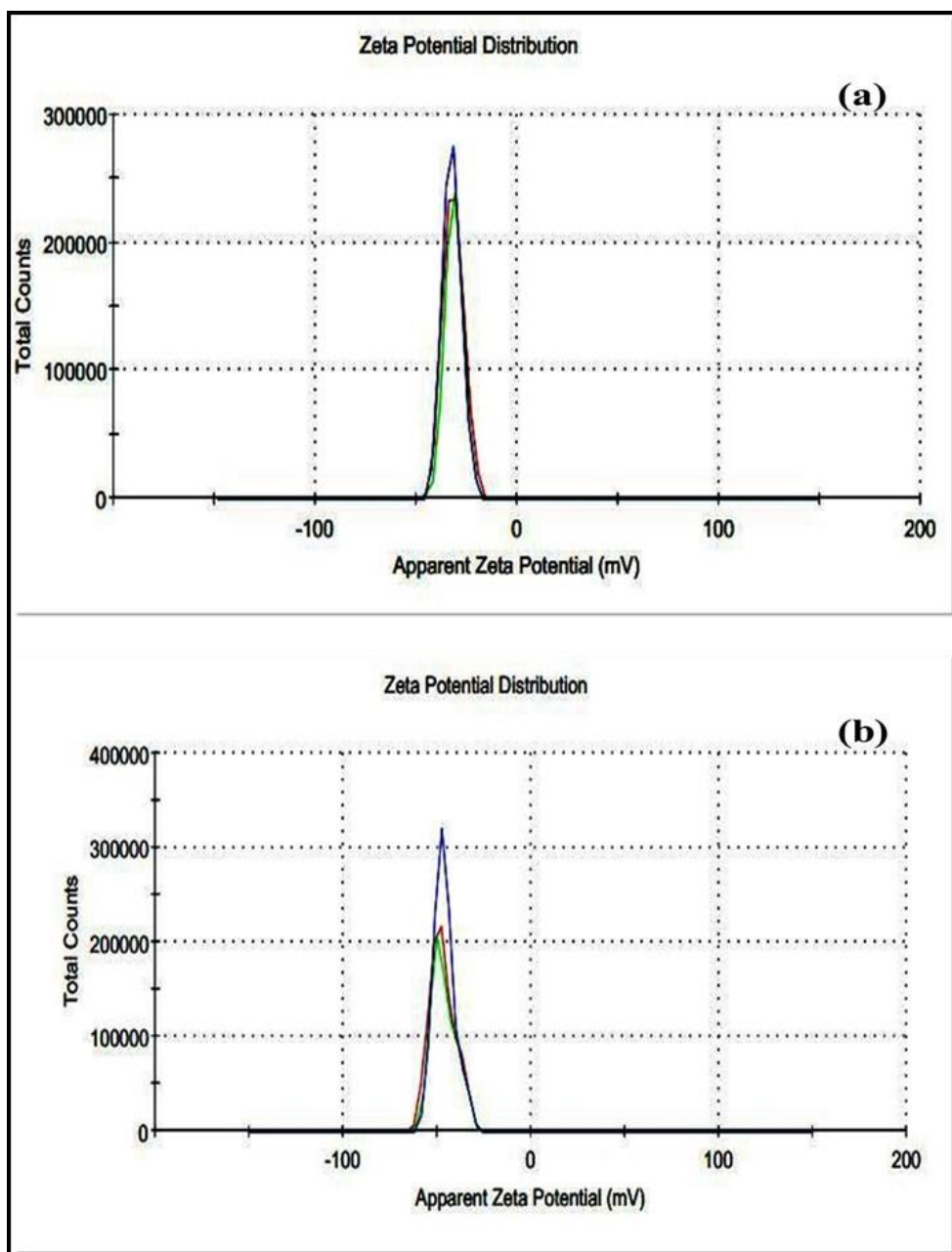


Figure A17. Zeta potential measurements. (a) MSN. (b) MSN-SH.

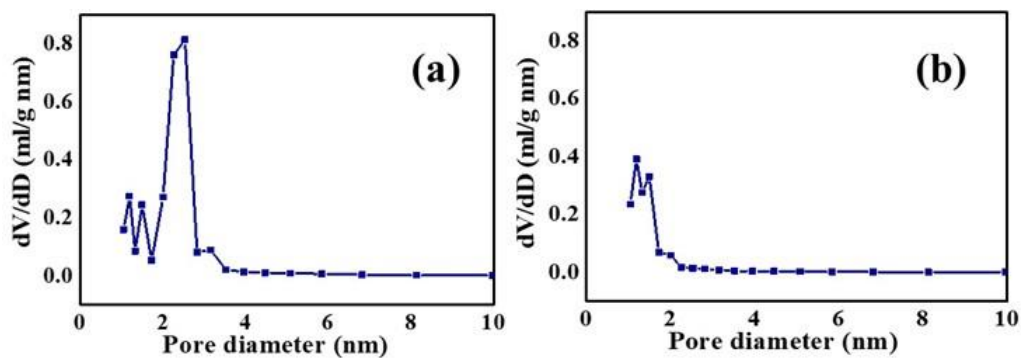


Figure A18. Barrett-Joyner-Halenda (BJH) pore size distribution. (a) MSN. (b) MSN-SH.

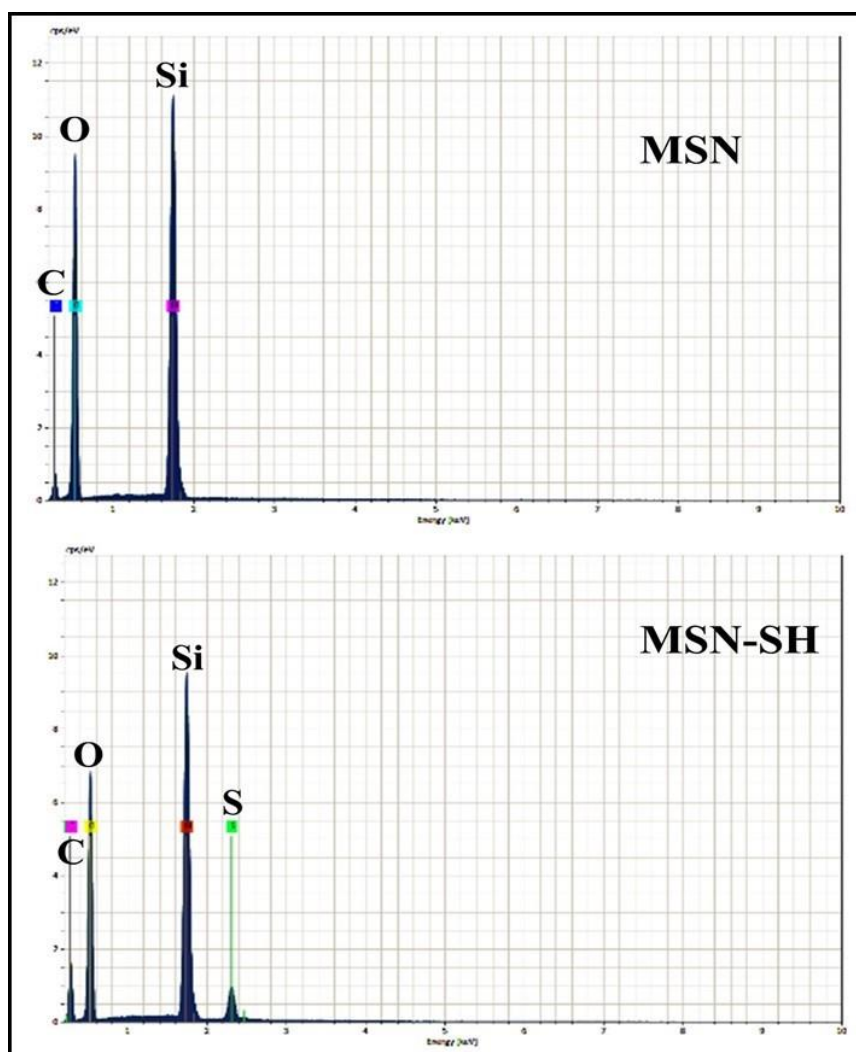


Figure A19. Energy dispersive X-ray spectroscopy (EDX) spectra of MSN and MSN-SH.

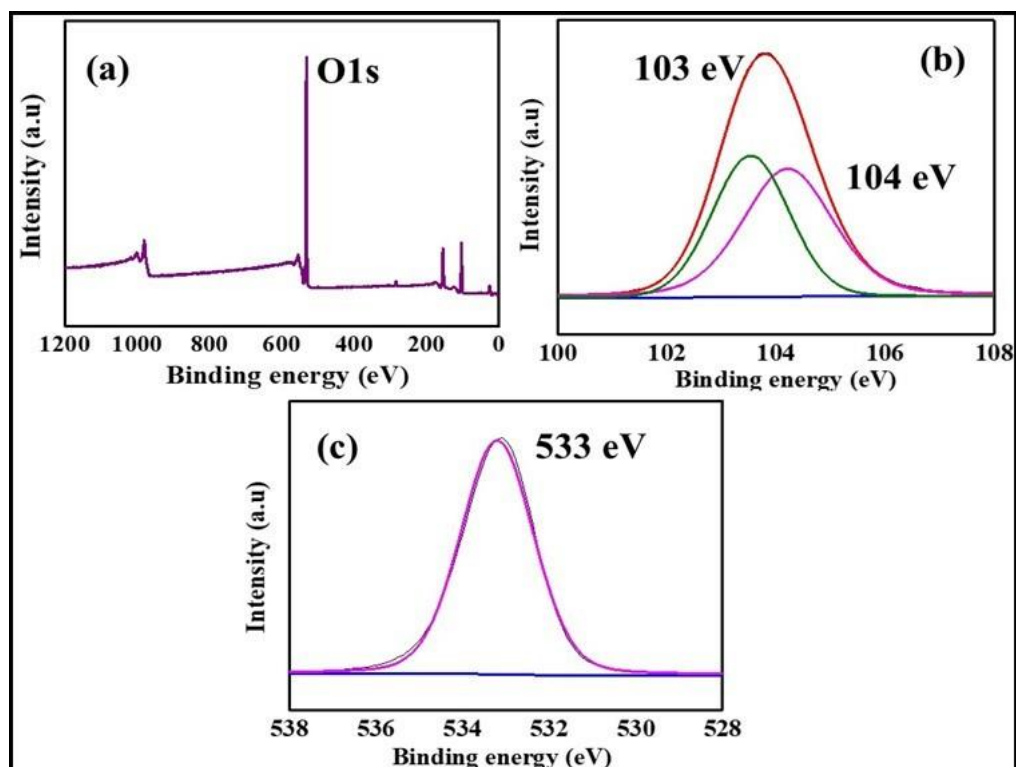


Figure A20. X-ray photoelectron spectroscopy (XPS) spectra. (a) Survey scan. (b) Si 2p. (c) O 1s.

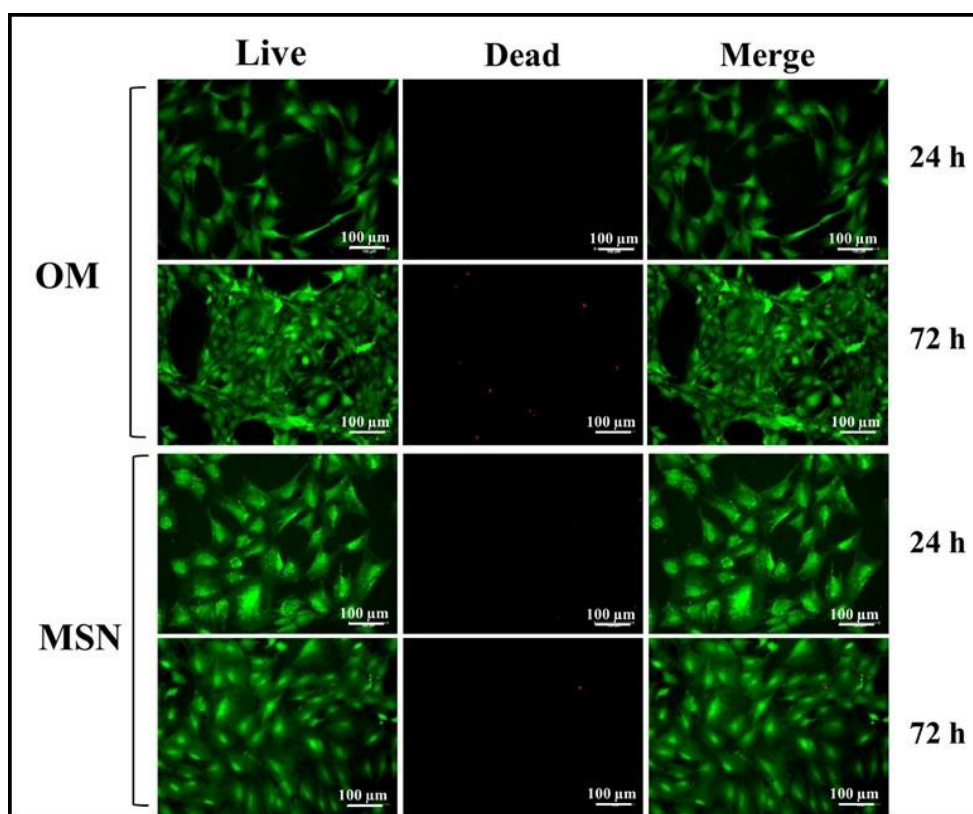


Figure A21. Fluorescence images of live (green) and dead (red) MC3T3 cells treated with osteogenic media (OM) and MSN. Scale bar: 100 μm

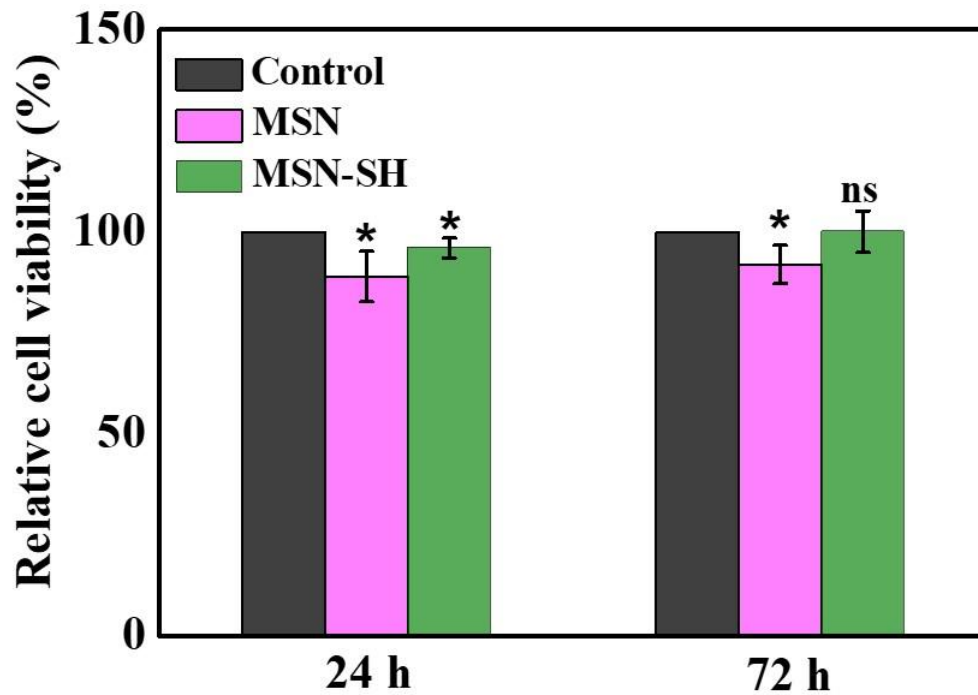


Figure A22. Relative cell viabilities of untreated HUVEC cells (control) and cells treated with MSN and MSN-SH. * $p < 0.05$ represents the statistical significance and ns indicates non-significant difference.

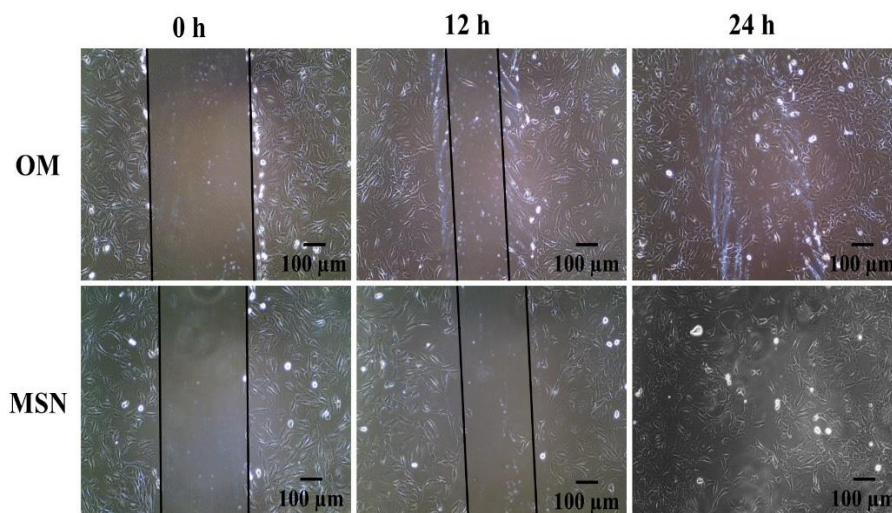


Figure A23. Migration assay using MC3T3 cells treated with osteogenic media (OM) and MSN. Scale bar: 100 μm .

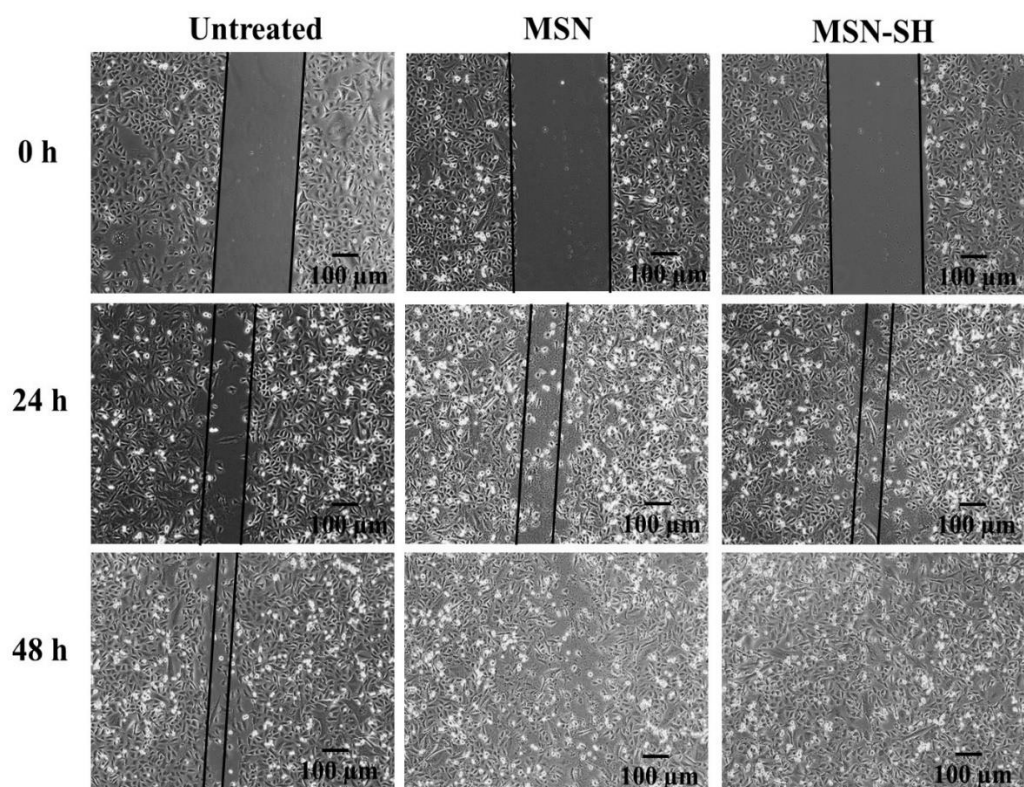


Figure A24. Migration assay using untreated HUVEC cells (control) and cells treated with MSN and MSN-SH. Scale bar: 100 µm.

Table A3. Primer sequences used in real-time PCR.

GAPDH FP	5'-AGGTCGGTGGAACGGATTTG-3'
GAPDH RP	5'-GGGGTCGTTGATGGCAACA-3'
ALP FP	5'-CCAACCTCTTTTGTGCCAGAGA-3'
ALP RP	5'-GGCTACATTGGTGTTGAGCTTTT-3'
RUNX2 FP	5'-TCCACCACGCCGCTGTCT-3'
RUNX2_RP	5'-TCAGTGAGGGATGAAATGCT-3'
OCN FP	5'-CTGACCTCACAGATCCCAAGC-3'
OCN RP	5'-TGGTCTGATAGCTCGTCACAAG-3'
OPN FP	5'-CTTGCTTGGGTTTGCAGTCTT-3'
OPN RP	5'-GGTCGTAGTTAGTCCCTCAGA-3'